

On the Universality of Mass Inflation Inside Black  
Holes

by

Jim Shung Fai Chan

A thesis  
presented to the University of Waterloo  
in fulfilment of the  
thesis requirement for the degree of  
Doctor of Philosophy  
in  
Applied Mathematics

Waterloo, Ontario, Canada, 1998

©Jim Shung Fai Chan 1998



National Library  
of Canada

Acquisitions and  
Bibliographic Services

395 Wellington Street  
Ottawa ON K1A 0N4  
Canada

Bibliothèque nationale  
du Canada

Acquisitions et  
services bibliographiques

395, rue Wellington  
Ottawa ON K1A 0N4  
Canada

*Your file* *Votre référence*

*Our file* *Notre référence*

The author has granted a non-exclusive licence allowing the National Library of Canada to reproduce, loan, distribute or sell copies of this thesis in microform, paper or electronic formats.

The author retains ownership of the copyright in this thesis. Neither the thesis nor substantial extracts from it may be printed or otherwise reproduced without the author's permission.

L'auteur a accordé une licence non exclusive permettant à la Bibliothèque nationale du Canada de reproduire, prêter, distribuer ou vendre des copies de cette thèse sous la forme de microfiche/film, de reproduction sur papier ou sur format électronique.

L'auteur conserve la propriété du droit d'auteur qui protège cette thèse. Ni la thèse ni des extraits substantiels de celle-ci ne doivent être imprimés ou autrement reproduits sans son autorisation.

0-612-30593-7

The University of Waterloo requires the signatures of all persons using or photocopying this thesis. Please sign below, and give address and date.

## Abstract

The Cauchy horizon of the Reissner-Nordström black hole has been shown to be unstable under the perturbation of infalling and outgoing fluxes of radiation. Its behavior is characterized by an exponentially increasing mass function inside the hole. In this thesis I investigate the interiors of various black holes which arise as solutions of different low-energy candidates for quantum gravity theories. The spacetimes I consider include  $(1 + 1)$ -dimensional dilaton spacetimes, the  $(2 + 1)$ -dimensional black hole, a black string in  $3 + 1$  dimensions and Schwarzschild-anti-de Sitter spacetime. I find that mass inflation is a process in which the divergence of the inner mass function strongly depends on the attenuating behavior of the late time radiation. I calculate the radiation falloff rates in different black hole backgrounds, both analytically and numerically, and investigate the circumstances which are conducive to mass inflation. In certain cases the falloff can be so strong that the inner mass function is not divergent at the Cauchy horizon under the perturbation of the ingoing and outgoing radiation.

## Acknowledgements

I would like to thank Dr. Robert Mann for his enthusiastic supervision during all those years. The discussions with him are proved to be inspiring and fruitful. It is his physical insights that make the equations vivid and interesting, his encouragement and support made this work possible. I owe grateful thanks to him for the comments and linguistic corrections during the revisions of this thesis.

I thank the Natural Sciences and Engineering Research Council of Canada for the two postgraduate scholarships. I am also grateful for the financial support from the Department of Applied Mathematics and for the research assistantships from Dr. Mann.

The numerical simulations presented in this thesis were done by using MATLAB and Maple V.

## Trademarks

**MATLAB** is a registered trademark of The MathWorks, Inc.

**Maple** and **Maple V** are the trademarks of Waterloo Maple Software.

To My Sister Connie and Her Family

# Contents

<b>1</b>	<b>Introduction</b>	<b>1</b>
1.1	Spacetime Metrics . . . . .	3
1.2	Spacetime Structure . . . . .	8
1.3	Instability of the Cauchy Horizon . . . . .	14
1.4	Outline of the Thesis . . . . .	20
<b>2</b>	<b>Review of Mass Inflation</b>	<b>24</b>
2.1	Background Spacetime . . . . .	25
2.2	Continuous Cross-Flow Model . . . . .	31
2.3	Thin-Shell Model . . . . .	38
<b>3</b>	<b>Mass Inflation In 1 + 1 Dimensions</b>	<b>45</b>
3.1	First Dilaton Background . . . . .	48
3.2	Second Dilaton Background . . . . .	57
3.3	Zero Surface Gravity at Cauchy Horizon . . . . .	62

<b>4</b>	<b>Scalar Waves in <math>D + 1</math> Dimensions</b>	<b>73</b>
4.1	General Setup . . . . .	75
4.2	Waves in Schwarzschild-like Background . . . . .	84
<b>5</b>	<b>(1 + 1)-Dimensional Dilaton Gravity Revisited</b>	<b>101</b>
5.1	Waves in the Second Dilaton Background . . . . .	104
5.2	Mass Inflation in the Second Background . . . . .	118
<b>6</b>	<b>Mass Inflation In 2 + 1 Dimensions</b>	<b>125</b>
6.1	Radiation Falloff . . . . .	131
6.2	Mass Inflation Calculation . . . . .	142
6.3	Radiation Outside a Spinning 3D Black Hole . . . . .	147
6.4	A Spinoff . . . . .	155
<b>7</b>	<b>Schwarzschild-Anti-de Sitter Background</b>	<b>161</b>
<b>8</b>	<b>Conclusion</b>	<b>177</b>
<b>A</b>	<b>Vocabulary</b>	<b>182</b>
	<b>Bibliography</b>	<b>185</b>

# List of Figures

1.1	The conformal structure of the Schwarzschild spacetime. An explanation of the symbols $i^+$ , $i^0$ , etc. can be found in Appendix A. . . . .	9
1.2	Conformal diagram for the Kerr spacetime with $\theta = 0$ . . . . .	12
1.3	The world lines of two observers, one on each side of the event horizon. . . . .	15
2.1	Conformal diagram for the Reissner-Nordström spacetime with $M^2 > q^2$ . . . . .	27
2.2	Reissner-Nordström background perturbed by cross-flowing streams of radiation. The streams of scattered radiation come from the asymmetries of a collapsing star. . . . .	35
2.3	The $45^\circ$ line S represents an outgoing thin null shell on this conformal diagram for the charged Vaidya background. . . . .	40
3.1	A null line S divides the spacetime into regions I and II. . . . .	51
3.2	A sample graph of $\mathcal{M}(X)$ in the first solution. . . . .	55
3.3	A sample graph of $\mathcal{M}(X)$ in the second solution. . . . .	60
3.4	Conformal diagram for an extremal Reissner-Nordström black hole. . . . .	72

4.1	Potential for the Schwarzschild background. . . . .	79
4.2	The potential $V$ in figure 4.1, but in a semi-log scale. . . . .	80
4.3	The potential in figure 4.1, but in a log-log scale. Only positive $\rho$ is shown in this graph. . . . .	81
4.4	The decay of a scalar wave in Schwarzschild background with $l = 1$ . . . . .	85
4.5	The decay of a scalar wave in Schwarzschild background with $l = 0$ . . . . .	86
4.6	The decay of a scalar wave in Schwarzschild background with $l = 0$ . In this case, the observation of the decay is made at a point close to the event horizon. . . . .	88
5.1	Two sample potentials $V(\rho)$ for the scalar wave in the second dilaton spacetime. . . . .	110
5.2	Scalar wave decay behavior in the second dilaton spacetime with $\xi = 10, Q = 1$ . . . . .	111
5.3	Scalar wave decay behavior in the second dilaton spacetime with i) $\xi = 10, Q = 5$ , and ii) $\xi = 1, Q = 1$ . . . . .	112
5.4	Scalar wave decay behavior in the second dilaton spacetime with $\xi \leq 1/4$ . . . . .	113
5.5	Scalar wave decay behavior in the second dilaton spacetime with $\xi = 10, Q = 1$ . This diagram is similar to figure 5.2 but the observation is made near the event horizon of the black hole. . . . .	115
5.6	Scalar wave falloff in the triple-horizon geometry. The initial impulse is at $x = -15$ and the observation is made at $x = -10$ ( $\rho = 20$ ). . . . .	121

5.7	Scalar wave falloff in another triple-horizon black hole. Mass inflation is expected in this background because the surface gravity $\kappa_-$ is much larger than that of the black hole background associated to figure 5.6.	124
6.1	Causal structure of the 3D Black Hole. . . . .	130
6.2	Exponential falloff for a conformal scalar wave using the Dirichlet boundary condition. . . . .	139
6.3	Exponentially decaying scalar waves using the Neumann condition.	140
6.4	The graph of potential function (6.34) with $\lambda = 0.02$ and $V_0 = 1$ . . .	141
6.5	Potential function $V(\rho)$ of two spinning 3D black hole backgrounds with (i) $ \Lambda  J^2/M^2 = 10^{-3}$ and (ii) $ \Lambda  J^2/M^2 = 0.8$ . . . . .	152
6.6	Exponentially decaying behavior of $ V(\rho) $ near the black hole event horizon . . . . .	153
6.7	Exponential decay of the conformally invariant scalar waves in the spinning 3D black hole background. . . . .	154
6.8	Exponentially decaying wave in the black string spacetime . . . . .	160
7.1	Potential $V$ for the SAdS background. The six potentials are generated with $R_b = 2$ and (a) $\Lambda = -10^{-4}, l = 2$ , (b) $\Lambda = -10^{-4}, l = 1$ , (c) $\Lambda = -10^{-4}, l = 0$ , (A) $\Lambda = -10^{-2}, l = 2$ , (B) $\Lambda = -10^{-2}, l = 1$ , (C) $\Lambda = -10^{-2}, l = 0$ . . . . .	165
7.2	Scalar wave of $l = 0$ decays away in the SAdS background with $\Lambda = -10^{-4}$ . Dirichlet condition is used at $\rho = 0$ . . . . .	167
7.3	Scalar wave falloff pattern of $l = 0$ using $\Lambda = -10^{-4}$ and Neumann condition at $\rho = 0$ . . . . .	168

7.4	Scalar wave falloff pattern of $l = 0$ using $\Lambda = -10^{-4}$ and Dirichlet condition at $\rho = 0$ . The observation in this case is close to the event horizon. . . . .	169
7.5	Loglog graph of the scalar wave decay behavior in the SAdS background with $\Lambda = -10^{-4}$ and $l = 1$ . Dirichlet condition is used in this case. . . . .	170
7.6	Similar graph to figure 7.5 but using the Neumann condition ( $\Lambda = -10^{-4}$ and $l = 1$ ). . . . .	171
7.7	Semilog graph of the scalar wave decay behavior in the SAdS background using $\Lambda = -10^{-2}$ , $l = 0$ and the Dirichlet condition. . . . .	173
7.8	Conformally invariant scalar wave decay behavior using $\Lambda = -10^{-2}$ , $l = 0$ and the Neumann condition. . . . .	174
7.9	Semilog graph of the scalar wave decay behavior using $\Lambda = -10^{-2}$ , $l = 2$ and the Dirichlet condition. . . . .	175
7.10	The simulation for this semilog graph uses the same inputs as the one in figure 7.9 but Neumann boundary condition replaces the Dirichlet condition in this case. . . . .	176

# List of Tables

6.1	The exponential falloff rate $\alpha$ , which is found by graphical method, can be greater than the surface gravity $\kappa_-$ in the rotating 3D black holes. . . . .	156
-----	--	-----

# Chapter 1

## Introduction

The first nontrivial and most important exact solution of Einstein's equations was found by Karl Schwarzschild in 1916 [1], [2](p. 118). This solution represents a spherically symmetric vacuum spacetime. The spacetime is interpretable as either the exterior spacetime of a spherically symmetric object in vacuum or the spacetime of a fully gravitationally collapsed spherical object, i.e. a black hole. However the existence of black holes remained unproven because they cannot be observed directly. Nevertheless astronomers are able to collect suggestive evidence for their existence by using modern observational techniques [3, 4]. For example, a research team used the images from the repaired Hubble Space Telescope to study a dark celestial object at the center of the giant elliptical galaxy M87 in the Virgo constellation [3]. Astronomers in the team concluded that the object is a black hole after measuring the speed of a gas disk orbiting around the dark object. They argued that a stellar object having sufficient mass to keep the gas moving at such high speed could not remain in equilibrium, and would necessarily undergo gravitational collapse, leading to a black hole.

Although Schwarzschild's solution is indisputably important in the study of Einstein's General Relativity, this solution only represents the vacuum spacetime of a spherical object, or approximates the vacuum spacetime of a nearly spherical object. In practice, astronomers can only hope to detect a black hole by observing nearby objects with which it is in mutual orbit, like companion stars or gas disks. In this situation, the black hole at the center cannot be the Schwarzschild black hole because the spacetime is no longer spherically symmetric. However a solution representing a spacetime with axial symmetry is known due to the effort of Kerr [5]. The Kerr solution can be interpreted as describing a rotating black hole [6](p. 161).

The importance of black holes in understanding gravitational theory cannot be underestimated. Apart from their possible astrophysical relevance as noted briefly above, they raise important questions which impact upon some of our most fundamental concepts in physics, including thermodynamics [7], causality [8], conservation laws [9], and the development of a quantum theory of gravity [10]. This thesis is concerned with some specific aspects of black hole physics: namely the relationships between their interior structure and the asymptotic properties of the spacetimes in which they reside. To set the stage for this investigation we shall, in Section 1.1, discuss the Einstein equations after introducing the spacetime metric. This mathematical object defines the geometry of a spacetime and is used to construct the Einstein tensor  $G_{ab}$ . In this chapter, we shall consider only the Schwarzschild and Kerr spacetimes. The structure of these spacetimes will be discussed in Section 1.2. We shall find that the interior of a Kerr black hole has several objectionable properties. One of these properties is that it is unstable. We shall look at this instability problem closely in Section 1.3. This instability problem has initiated a series of investigations about the internal structure of the Kerr black hole. Recently theorists

discovered a phenomenon called *mass inflation* which could occur inside the Kerr black hole. In this thesis we shall study mass inflation inside several black holes which are solutions to different theories of gravity. In Section 1.4, we shall outline the approach and content of this thesis.

## 1.1 Spacetime Metrics

General Relativity envisages the gravitational force as a physical result of a “distortion” of spacetime. In this context one needs a geometrical way to describe the spacetime. Spacetime refers to the continuum of space and time, concepts which were treated separately in the prerelativity era prior to 1905. This geometrical description is facilitated by using a metric. In the most general case, a metric in an arbitrary coordinate system  $\{x^c\}$  can be expressed as

$$ds^2 = g_{ab} dx^a dx^b, \quad (1.1)$$

where Einstein’s summation notation is used and the indices run from 1 to 4 in 3+1 spacetime dimensions. The metric components  $g_{ab}$ , which satisfy the equation  $g_{ab} = g_{ba}$ , are functions of  $x^c$  in general. For example, the simplest (3 + 1)-dimensional spacetime metric in Relativity can be written as

$$ds^2 = -c^2 dt^2 + dx^2 + dy^2 + dz^2 \quad (1.2)$$

in Cartesian coordinates or as

$$ds^2 = \begin{bmatrix} dt & dr & d\theta & d\phi \end{bmatrix} \begin{bmatrix} -c^2 & 0 & 0 & 0 \\ 0 & 1 & 0 & 0 \\ 0 & 0 & r^2 & 0 \\ 0 & 0 & 0 & r^2 \sin^2(\theta) \end{bmatrix} \begin{bmatrix} dt \\ dr \\ d\theta \\ d\phi \end{bmatrix} \quad (1.3)$$

in spherical coordinates. The constant  $c$  is the speed of light in vacuum. Either metric (1.2) or (1.3) represents the same spacetime. The spacetime metric is not positive definite. That is to say if we consider a matrix with components  $g_{ab}$ , like the one in (1.3), the determinant of this matrix is not positive. In fact, the symmetric matrix representing a spacetime metric has only one negative eigenvalue. The metric that has only one negative eigenvalue is called Lorentzian.

The Einstein equations were discovered in 1915 and read

$$G_{ab} = \frac{8\pi G}{c^2} T_{ab} . \quad (1.4)$$

The symmetric tensor  $G_{ab}$  is the Einstein tensor and  $T_{ab}$  is the stress-energy-momentum tensor. The constant  $G$  in (1.4) is the gravitational constant and  $c$  is the speed of light in vacuum. These constants will be set to unity in the rest of this thesis without loss of generality [2](p. xi). Despite the simple appearance of equation (1.4), it represents a set of six independent, non-linear, second order partial differential equations in  $3 + 1$  spacetime dimensions. (In fact there are ten different equations in (1.4) but we always have the freedom to choose the coordinate system which yields 4 degrees of freedom in  $3 + 1$  dimensions. Thus there are six independent equations in (1.4).) These differential equations determine the components of the spacetime metric.

The Einstein tensor  $G_{ab}$  in (1.4) is constructed from the spacetime metric in a non-linear way. It is defined as

$$G_{ab} \equiv R_{ab} - \frac{1}{2} R g_{ab} , \quad (1.5)$$

where the tensor  $R_{ab}$  is the Ricci tensor and  $R$  is the Ricci scalar. They are related to one another via the definition

$$R \equiv R_{ab} g^{ab} . \quad (1.6)$$

The tensor  $g^{ab}$  is the inverse of the metric tensor  $g_{ab}$ . The metric tensor and its inverse are used to map covariant tensors to their contravariant counterparts or vice versa. In this thesis, the Ricci tensor is defined as

$$R_{ab} \equiv R^c{}_{acb} , \quad (1.7)$$

$$R^d{}_{acb} \equiv \partial_c \Gamma_{ab}{}^d - \partial_b \Gamma_{ac}{}^d + \Gamma_{ce}{}^d \Gamma_{ab}{}^e - \Gamma_{be}{}^d \Gamma_{ac}{}^e . \quad (1.8)$$

The operation  $\partial_c$  is the usual partial derivative with respect to the “ $c^{\text{th}}$ ” coordinate  $x^c$ . The quantity  $R^d{}_{acb}$  is the Riemann curvature tensor, and the Christoffel symbol (of the second kind)  $\Gamma_{ab}{}^c$  is defined as

$$\Gamma_{ab}{}^c \equiv \frac{1}{2} g^{cd} ( \partial_a g_{bd} + \partial_b g_{da} - \partial_d g_{ab} ) . \quad (1.9)$$

As a result, the Ricci scalar and tensor are constructed from non-linear combinations of the metric tensor and its first and second partial derivatives. Therefore the Einstein equations are a system of second order, non-linear partial differential equations in the metric components.

As the name suggests, the Riemann curvature tensor describes the local curvature of a spacetime. If all the components of this tensor vanish everywhere in a spacetime, the spacetime is called “flat” (or Minkowski). The concept of flatness is not coordinate-dependent because the Riemann tensor components transform from one coordinate system to another one as follows:

$$\tilde{R}^d{}_{abc} = \frac{\partial \hat{x}^d}{\partial \tilde{x}^i} \frac{\partial \tilde{x}^i}{\partial \hat{x}^a} \frac{\partial \tilde{x}^j}{\partial \hat{x}^b} \frac{\partial \tilde{x}^k}{\partial \hat{x}^c} \tilde{R}^l{}_{ijk} . \quad (1.10)$$

The Riemann tensor components on the left of the above equation are written in the coordinate system  $\{\hat{x}^a\}$  and those on the right are written in another coordinate system  $\{\tilde{x}^i\}$ . It is understood that we can write  $\tilde{x}^i = \tilde{x}^i(\hat{x})$  or  $\hat{x}^a = \hat{x}^a(\tilde{x})$ . Therefore if all the components of the Riemann tensor vanish everywhere in one coordinate

system, the components of this tensor will be zero in other coordinate systems. If a spacetime is not flat, one also can describe its curvature in a coordinate-independent way, for example, using scalars which are invariant under any change of coordinates. Thus curvature scalars like the Ricci scalar or the Kretschmann scalar

$$K \equiv R_{abcd} R^{abcd} \quad (1.11)$$

can be used to describe the spacetime curvature [11].

The Schwarzschild spacetime mentioned at the beginning of this chapter can be described by the metric

$$ds^2 = - \left( 1 - \frac{2M}{r} \right) dt^2 + \left( 1 - \frac{2M}{r} \right)^{-1} dr^2 + r^2 d\theta^2 + r^2 \sin^2(\theta) d\phi^2 . \quad (1.12)$$

This metric satisfies the Einstein equations (1.4) with  $T_{ab} = 0$ . The constant  $M$  in the metric is an integration constant which is interpreted as the mass of a spherically symmetric object in vacuum [1], [2](p. 124), [6](p. 149), and is assumed to be positive.

A more general solution satisfying the vacuum Einstein equations (i.e.  $T_{ab} = 0$ ) is the Kerr spacetime which is given by the metric

$$\begin{aligned} ds^2 = & - \left( 1 - \frac{2Mr}{\Sigma} \right) dt^2 + \left( 1 - \frac{2Mr}{\Sigma} + \frac{a^2}{\Sigma} \sin^2(\theta) \right)^{-1} dr^2 \\ & + \Sigma d\theta^2 + \left( r^2 + a^2 + \frac{2a^2 M r}{\Sigma} \sin^2(\theta) \right) \sin^2(\theta) d\phi^2 \\ & - \frac{4aMr}{\Sigma} \sin^2(\theta) dt d\phi , \end{aligned} \quad (1.13)$$

where  $\Sigma = r^2 + a^2 \cos^2(\theta)$ . As mentioned before, the Kerr metric represents a spacetime which generalizes the Schwarzschild spacetime with axial symmetry replacing spherical symmetry. In other words, the Kerr solution can represent the spacetime of a rotating black hole. Thus one might expect that the constant  $a$  in the metric

above is a parameter associated with angular momentum. Indeed, we can interpret  $a M$  as the angular momentum of the rotating black hole [5], [2](p. 314). When  $a$  equals zero, the Kerr metric (1.13) reduces to the Schwarzschild metric (1.12).

Let us return to the Schwarzschild spacetime. The metric (1.12) becomes singular when  $\theta = 0$ ,  $\theta = \pi$ ,  $r = 0$  and  $r = 2 M$ . The first two are coordinate singularities because the coordinate system fails to be one-to-one along the polar axis. At the last two “points”, some of the metric components become unbounded. Therefore it is natural to assume that the range of  $r$  is  $2 M < r < \infty$  for the metric (1.12).

The line  $r = 0$  in the Schwarzschild spacetime is not simply a coordinate singularity. Instead it is a spacetime singularity [2](p. 153) because the spacetime curvature is unbounded there. This singularity cannot be removed by *any* coordinate transformation. One way to show this is to compute the Kretschmann scalar which is  $48 M^2/r^6$  in the Schwarzschild spacetime. Since this scalar diverges at  $r = 0$ , the spacetime has arbitrarily large curvature near  $r = 0$ . This confirms the claim that the point  $r = 0$  in 3-space is a curvature singularity of the Schwarzschild solution.

Finally, the fact that the Kretschmann scalar does not diverge at  $r = 2 M$  suggests that the divergence in the metric components at  $r = 2 M$  is a result of a poor choice of coordinates. We can show this by transforming the metric (1.12) from the coordinate system  $\{t, r, \theta, \phi\}$  to another coordinate system. For example, consider the coordinates [12], [2](p. 153)

$$U = - \exp\left(\frac{r-t}{4M}\right) \sqrt{\frac{r}{2M} - 1}, \quad (1.14)$$

$$V = \exp\left(\frac{r+t}{4M}\right) \sqrt{\frac{r}{2M} - 1}. \quad (1.15)$$

For  $t \in \mathbb{R}$  and  $r \in (2 M, \infty)$ , the coordinate  $U$  belongs to  $\mathbb{R}^-$  and  $V \in \mathbb{R}^+$ . In the

new coordinate system  $\{U, V, \theta, \phi\}$ , the Schwarzschild metric (1.12) becomes

$$ds^2 = -\frac{32 M^3}{r} \exp\left(-\frac{r}{2M}\right) dU dV + r^2 d\theta^2 + r^2 \sin^2(\theta) d\phi^2 . \quad (1.16)$$

where  $r$  is a function of  $UV$  defined implicitly by the equation

$$UV = \left(1 - \frac{r}{2M}\right) \exp\left(\frac{r}{2M}\right) . \quad (1.17)$$

The equation (1.17) is well-behaved for all  $r \in \mathbb{R}$  and the metric (1.16) has no divergent components at  $r = 2M$ . (It is not difficult to see that the components of the inverse metric  $g^{ab}$  are also finite at  $r = 2M$ .) In other words,  $r = 2M$  is simply a coordinate singularity in the metric (1.12). Since  $r = 0$  is a spacetime singularity, as mentioned earlier, we can consider  $0 < r < \infty$  in the new metric (1.16).

## 1.2 Spacetime Structure

We can visualize the structure of the Schwarzschild spacetime by considering its *conformal diagram* [13]. Such diagrams allow us to represent the full infinite spacetime in a finite-sized diagram whilst preserving the relationships between null geodesics. (See Appendix A for the explanation of geodesics.) Hence they allow us to straightforwardly consider how light propagates in a given spacetime. This knowledge in turn allows us to understand the causal relationship between points in the spacetime, and hence its causal structure.

In the case of the Schwarzschild spacetime, we ignore the coordinates  $\theta$  and  $\phi$ , and introduce new coordinates  $T$  and  $X$  which are defined implicitly by

$$U = \tan(T - X) , \quad (1.18)$$

$$V = \tan(T + X) . \quad (1.19)$$

The coordinates  $U$  and  $V$  are those in the metric (1.16). Under this transformation the “point”  $r = \infty$  is mapped to the lines  $T - X = -\pi/2$  and  $T + X = \pi/2$  on  $X$ - $T$ -plane via  $U = -\infty$  and  $V = \infty$ , respectively. Moreover the hypersurface  $r = 2M$  is now located at  $T = \pm X$ . The line  $r = 0$  in the spacetime corresponds to the line  $UV = 1$  on the  $U$ - $V$ -plane. It is straightforward to show that this line is mapped to the lines  $T = \pm\pi/4$  on the  $X$ - $T$ -plane. As a result, we can depict the region  $0 < r < \infty$  in the spacetime described by (1.16) (which is equivalent to (1.12)), on figure 1.1. We have the line  $r = 0$  in two places of the diagram, namely the top and the bottom of it because of the symmetry in time in the Schwarzschild metric.

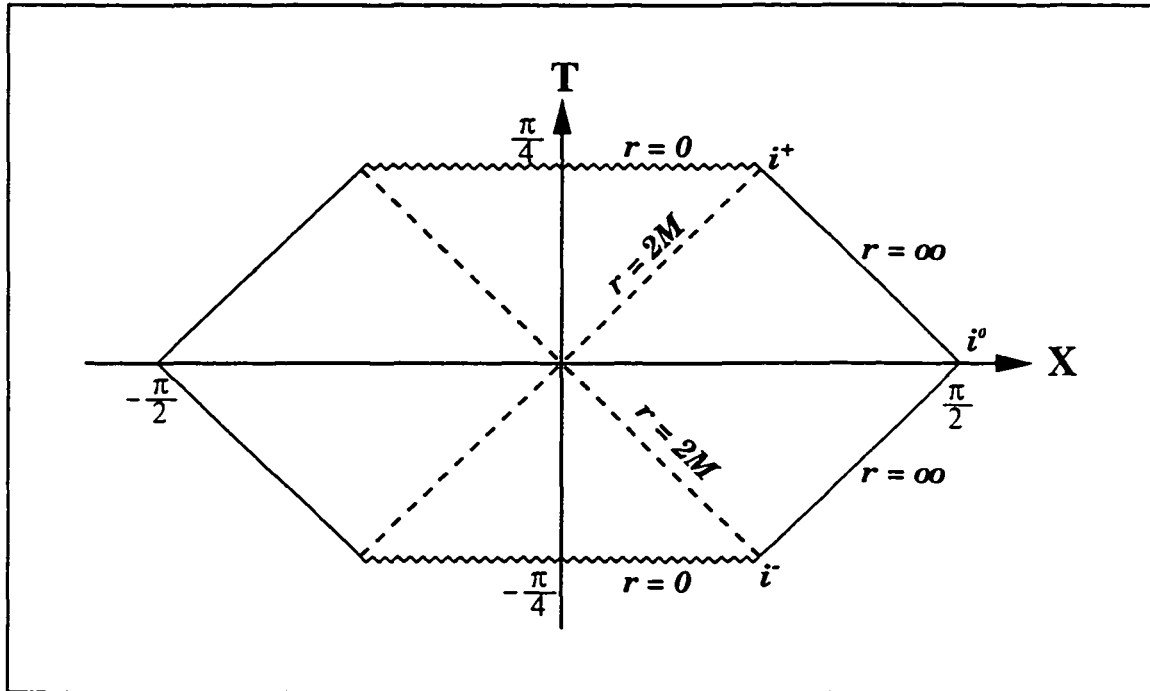


Figure 1.1: The conformal structure of the Schwarzschild spacetime. An explanation of the symbols  $i^+$ ,  $i^0$ , etc. can be found in Appendix A.

Let us consider the metric (1.2) which is the usual flat spacetime in the Cartesian

coordinates. Light travels in this spacetime in straight lines at a speed of  $c$ . That is to say a photon's coordinates  $(x, y, z)$  obey the equation

$$0 = -c^2 + \left(\frac{dx}{dt}\right)^2 + \left(\frac{dy}{dt}\right)^2 + \left(\frac{dz}{dt}\right)^2 . \quad (1.20)$$

In other words, for a light ray, one must have  $ds/dt = 0$ . If we consider a ray of light in the Schwarzschild spacetime at a fixed direction, i.e. for constant  $\theta$  and  $\phi$ , the trajectory of the ray will be given by either  $U = \text{constant}$  or  $V = \text{constant}$ , according to the alternative form of the Schwarzschild metric (1.16). This explains why  $U$  and  $V$  are sometimes called lightlike coordinates. Any 45-degree line on figure 1.1 represents a beam of light because of the equations (1.18) and (1.19). On the other hand, a material particle in the Schwarzschild spacetime will trace a path whose tangent slope is everywhere greater than unity in magnitude on figure 1.1 because it moves at a speed less than  $c$  in 3-space. This provides a simple way to classify the causal relationship between two points on the diagram. A diagram such as figure 1.1 is called a Penrose diagram [13], [6](p. 154).

Consider an observer at a finite distance  $r > 2M$ . At a given fixed instant (which may be taken to be  $T = 0$  without loss of generality because the spacetime is static) this observer will be located somewhere between  $0 < X < \pi/2$  along the  $X$ -axis in figure 1.1. As  $t$  increases for the observer, a path in the conformal diagram is traced out. Such a path is called the world line of the observer, and extends upward in the direction of the flow of time. On a conformal diagram, if the slope of a given world line is always greater than unity in magnitude, the line is timelike. If the slope of a curve on a conformal diagram has magnitude 1, the curve is lightlike; if its magnitude is always less than unity, the curve is spacelike. All known massive objects have timelike world lines.

For a freely falling observer remaining outside  $r = 2M$  as  $t$  tends to infinity,

the world line approaches the “point”  $i^+$  in the diagram. However an observer wandering into the region  $r < 2M$  can never leave this region because his or her world line will always have a slope whose magnitude is greater than one. The lightlike hypersurface  $r = 2M$  is called event horizon because any event that takes place inside it cannot be observed by any exterior observer. No signal can pass through this hypersurface from  $r < 2M$  to  $r > 2M$ . The event horizon defines the boundary of a black hole. If a spherical star of mass  $M$  has *all* its material concentrated within its Schwarzschild radius  $R_b = 2M$ , it becomes a black hole. This can happen when the star is so massive that its gravitational pull eventually dominates the internal outward pressures of the star. This leads to a decrease in the radius of the star. Once the star’s radius shrinks to its Schwarzschild value, it is impossible for the implosion to be reversed or stopped. This process is called gravitational collapse, first described by Oppenheimer and Snyder [14].

According to figure 1.1, an observer entering the Schwarzschild black hole is not only trapped inside the hole forever but will unavoidably run into the spacetime singularity at  $r = 0$ . Since the Kretschmann scalar diverges at  $r = 0$ , there is an infinite spacetime curvature there. The observer will be crushed by tremendous tidal forces near the singularity. In the case of a collapsing star, its constituent material will experience unbounded tidal forces near the singularity.

We can similarly construct a Penrose diagram for the Kerr metric (1.13): it is shown in figure 1.2 [6](p. 165). However this diagram is valid only for  $\theta = 0$ . Note that in addition to the boundary of the black hole (event horizon)  $r = r_+$  which is a lightlike hypersurface, there is another important lightlike hypersurface  $r = r_-$ , where

$$r_{\pm} = M \pm \sqrt{M^2 - a^2} \tag{1.21}$$

and  $M > a$  for physical celestial objects [15](p. 231). As with the Schwarzschild black hole any straight line of slope  $\pm 1$  on this Penrose diagram represents the path of a light ray.

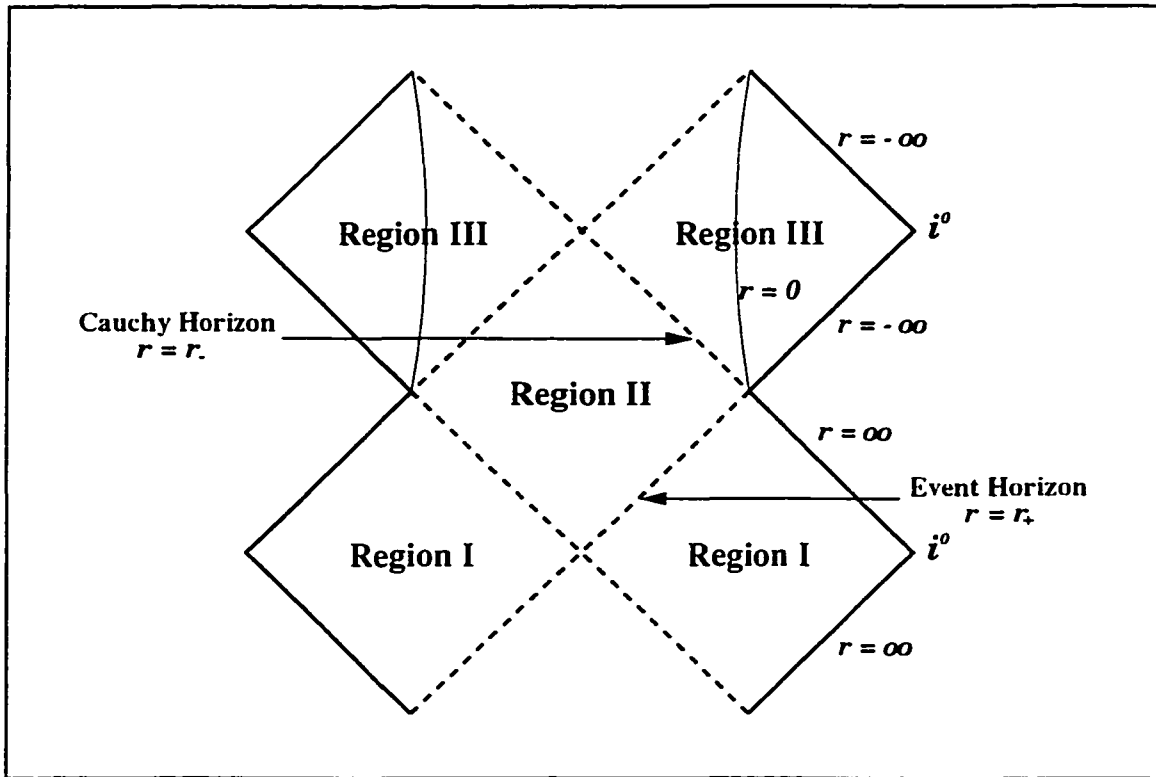


Figure 1.2: Conformal diagram for the Kerr spacetime with  $\theta = 0$ .

The other lightlike hypersurface  $r = r_-$  has the following interesting property. In figure 1.2, it is not difficult to see that for any point causally preceding the hypersurface  $r = r_-$  (that is below the line  $r = r_-$ ), its past lightcone is always confined to regions I and II. In other words, every past directed, non-spacelike curve passing through such a point will intersect a spacelike Cauchy surface in regions I and II. Therefore we can formulate a well-posed Cauchy problem in regions I and

II. However for any point inside the hypersurface  $r = r_-$ , some of its past directed, non-spacelike curves cannot intersect any Cauchy surface in regions I and II. In other words, any field at that point depends upon some data outside of regions I and II. In this sense, the future predictability of physical law breaks down at  $r = r_-$  because a well-posed Cauchy problem cannot be formulated properly in regions I and II. We call this lightlike hypersurface a Cauchy horizon. The definition of a Cauchy horizon can be found in Appendix A.

The Kerr spacetime has a singularity on the equatorial plane  $\theta = \pi/2$  at  $r = 0$  which is enclosed by the Cauchy horizon. One can show that this is a curvature singularity by calculating the Kretschmann scalar. The scalar diverges when  $\Sigma$  in (1.13) vanishes. This singularity is not a point in 3-space; rather it is a ring on the equatorial plane in 3-space [2](p. 315). Thus the coordinate  $r$  is not really a radial coordinate. The hypersurface  $r = 0$  in figure 1.2 is not shown as a singularity because the diagram is drawn for  $\theta = 0$ . Since  $r = 0$  away from the equatorial plane is not a spacetime singularity, one can extend the spacetime beyond  $r = 0$  in the diagram. We might interpret the region  $r < 0$  as another universe which is asymptotically flat at large  $|r|$  [2](p. 316).

The interior of the Kerr black hole also admits closed timelike curves near the ring singularity [6](p. 162). A spacetime that admits closed timelike curves is believed to be unphysical because it implies that an observer in such spacetime could visit his or her own past while traveling forward in time.

In fact, the Kerr spacetime is not the only black hole spacetime that has event and Cauchy horizons. When a spherically symmetric black hole carries a nonzero electric charge, its spacetime has a causal structure similar to that of the Kerr spacetime. This electrically charged Schwarzschild solution is called Reissner-Nordström solution [16], [6](p. 158). The presence of charge renders the Reissner-Nordström

solution less widely applicable to astrophysical situations because celestial bodies are electrically neutral in general. Nevertheless this spacetime is useful in the study of black hole physics because its causal structure is similar to that of the Kerr spacetime but is mathematically simpler than the Kerr metric. When a rotating star is electrically charged, the spacetime becomes a Kerr-Newman spacetime which also has two horizons [17].

### 1.3 Instability of the Cauchy Horizon

It follows from the Singularity Theorems [18], [6](p. 263) that a spacetime singularity unavoidably arises whenever a black hole is formed. However the Singularity Theorems do not shed any light on the nature and location of these singularities. As discussed previously, the Kerr black hole exhibits a curvature singularity only at  $r = 0$  on the equatorial plane. There is no sign of any physical singularity at the Cauchy horizon in this dual-horizon black hole. However the Cauchy horizons in those dual-horizon black holes are found to be unstable [19](p. 222). A brief discussion will illustrate why this is so.

As discussed in the previous section, the world line of a freely falling observer remaining outside a Schwarzschild black hole eventually approaches the point  $i^+$ . This is also true for observers remaining outside the Kerr and Reissner-Nordström black hole event horizons. The curve  $\Gamma_+$  in figure 1.3 represents the world line of an observer located at  $\theta = 0$  outside a Kerr black hole. This curve has a finite length in figure 1.3 but represents an infinite passage of time because the point  $B$  represents the limit  $t \rightarrow \infty$  for all timelike geodesics outside the black hole. We shall refer to observers with world lines extending to the point  $B$  in figure 1.3 as *immortal*.

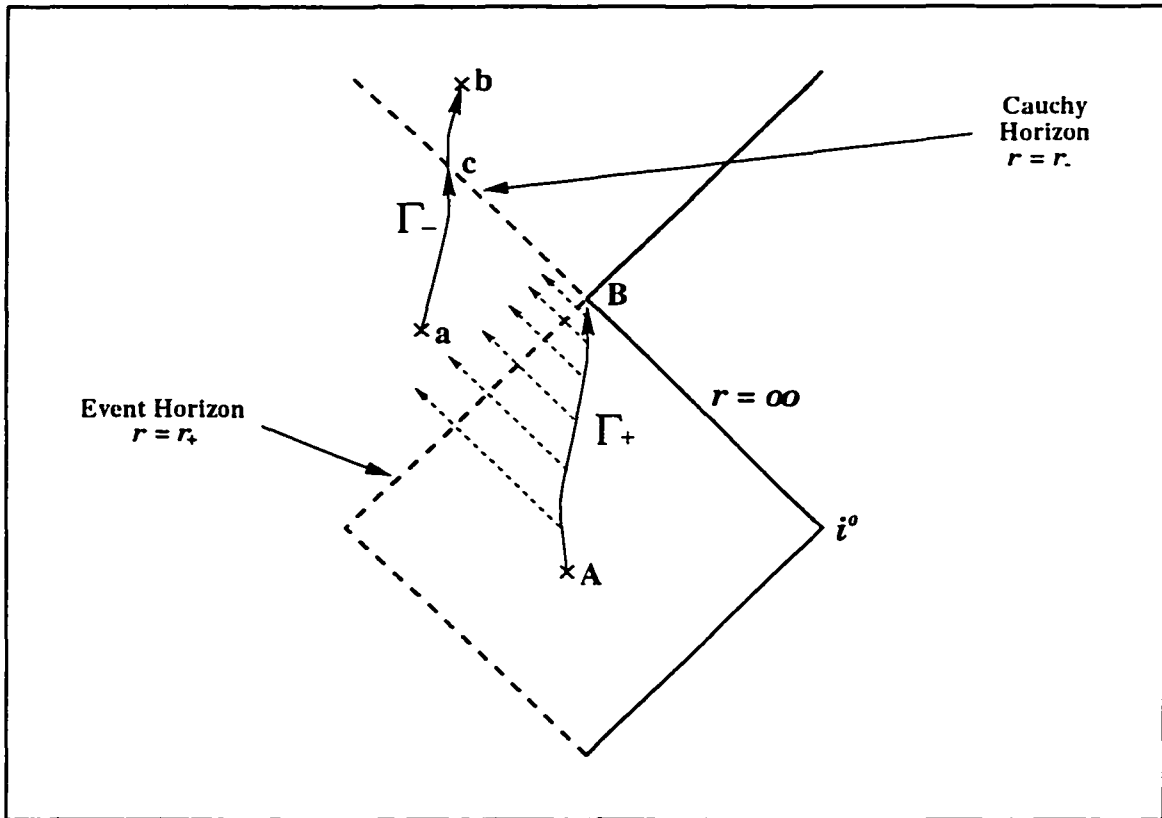


Figure 1.3: The world lines of two observers, one on each side of the event horizon.

Figure 1.3 also shows another observer with world line  $\Gamma_-$  inside the black hole. This observer's world line joins a point a, where  $r_- < r < r_+$ , to another point b ( $r < r_-$ ) through the point c which is at the Cauchy horizon  $r = r_-$ . Unlike the curve  $\Gamma_+$ , the world line  $\Gamma_-$  of this observer represents only a finite lapse of time. In other words, this observer takes a finite amount of time to go from point a to b, or just to point c.

If the immortal observer with world line  $\Gamma_+$  throws just one photon into the black hole every year, there will be infinitely many photons thrown into the hole. These photons are represented by the dotted lines of slope minus one in the diagram. On the other hand, the observer with the world line  $\Gamma_-$  will receive these photons one by one. However, the frequency of reception of the photons increases while the interior observer approaches the point c. Although the external observer emits infinitely many photons in an infinite time, the internal one will receive them in finite time because the time to reach point c is finite. As a result, the photon reception rate diverges when the internal observer moves towards the Cauchy horizon. If each photon has the same energy, the photon energy density in the neighborhood of the Cauchy horizon becomes unbounded. In this sense, the Cauchy horizon is a place where a spacetime singularity might arise. Although the divergent energy density at the Cauchy horizon is a consequence of pouring an infinite energy into the black hole (infinite number of photons of the same energy), it is possible to obtain a divergent energy density at the horizon by putting a finite amount of energy into the black hole. We shall see this effect in the thesis. Since mass-energy gives rise to spacetime curvature, theorists conjectured that the infinite energy density at the Cauchy horizon would destroy the horizon by turning it into a spacetime singularity. The lightlike hypersurface would become a spacelike curvature singularity like the one inside the Schwarzschild black hole. In this way, the loss of predictability

problem mentioned in the last section would be eliminated [2](p. 318).

Needless to say, an immortal being could do something more interesting than throwing photons into a black hole forever. The setup of eternally emitted photons mentioned above is just illustrative. However nature has a mechanism that tends to keep black holes irradiated for arbitrarily long periods of time. ( Here we refer to a physical black hole. The Kerr and Reissner-Nordström black holes should be excluded because they require exact symmetry, namely axial or spherical symmetry. In reality, one will not expect any celestial body to be perfectly spherical or axially symmetric. However, many celestial objects are very close to being symmetric. Therefore we can consider the asymmetries as perturbations to the black hole spacetime which possesses exact symmetry. )

We expect that the exterior of an aging, electrically neutral and sufficiently massive star that undergoes gravitational collapse will settle down to a Kerr black hole [2](p. 312). Any asymmetries it initially has will be washed out during the process. These asymmetries decay and induce gravitational radiation [20] which will propagate throughout the exterior of the star. Similar to electromagnetic radiation, gravitational radiation propagates at the speed of light [21](p. 255) and can play the same role as the electromagnetic radiation in triggering instability at the Cauchy horizon. Although the flux of gravitational radiation originates from the collapsing star, it does not all go outward and leave the star behind. Some of it interacts with the gravitational field created by the star and is scattered backward. Consequently the asymmetries of the star induce a flux of radiation which will irradiate the Cauchy horizon after the black hole is formed. This stream of gravitational radiation flows into the black hole forever due to continual scattering, although its intensity decreases. The decrease in amplitude is at a rate inversely proportional to some power of time. Thus the presence of the asymmetries during the collapse

induces a decaying but everlasting flux of radiation which irradiates the black hole. Eventually these fluxes are focused along the Cauchy horizon. Both numerical and analytic investigations using the Reissner-Nordström background [22, 23] show that radiation fields diverge at this lightlike hypersurface.

The presence of an infinite radiation density at the Cauchy horizon is not sufficient to conclude that the spacetime curvature diverges there because all considerations of this process thus far have assumed the validity of a background spacetime, which is the Reissner-Nordström spacetime. (Recall that this spacetime is non-singular at the Cauchy horizon.) However it is widely believed that if we take the back-reaction of the divergent stress-energy tensor into account, the Cauchy horizon would turn into a spacetime singularity. In order to do this one must solve the Einstein equations with the infalling radiation as a source. This was first done by Hiscock [24] who modeled the effect of the back reaction by using the Reissner-Nordström-Vaidya spacetime [25]. This black hole spacetime is similar to the Reissner-Nordström spacetime but the black hole is irradiated. Hiscock showed that the Ricci scalar and Kretschmann scalar remain finite at the Cauchy horizon but that a freely falling observer crossing the Cauchy horizon experiences an infinite tidal force. Hiscock concluded that the back reaction on the Reissner-Nordström geometry turns the Cauchy horizon into a so-called *whimper singularity* [24]. This is a singularity in which all the curvature scalars are finite and the components of the Riemann tensor are bounded in some non-parallel propagated frames; however there exists at least one curve to the singularity along which the Riemann tensor components are unbounded in a parallel propagated frame [26](p. 160). Whimper singularities are expected to be unstable, and can be turned into curvature scalar singularities under the slightest perturbation [27].

We have seen that the inclusion of infalling radiation in the Reissner-Nordström

background induces only a mild whimper singularity at the Cauchy horizon. Poisson and Israel [28] recently showed that a much stronger spacetime singularity is found when outgoing radiation is put in the Reissner-Nordström-Vaidya background. Such a singularity is characterized by a divergence of an internal mass parameter inside the black hole. This phenomenon, which yields a scalar curvature singularity at the Cauchy horizon, is called *mass inflation*. Despite the mass becoming unbounded, observers outside the black hole cannot detect this catastrophe because it occurs inside the event horizon.

After Poisson and Israel had discovered the mass inflation phenomenon, Ori demonstrated the phenomenon by using a simpler model [29]. Due to the simplicity of the model, he was able to compute the tidal distortion at the Cauchy horizon. It turned out to be finite, and he argued that the mass inflation singularity is weak enough for the continuation of spacetime beyond the Cauchy horizon. This viewpoint is completely different from that of Hiscock [24] and Poisson-Israel [28]. On the other hand, Yurtsever [30] and Gnedins [31] suggested that the Cauchy horizon of the Reissner-Nordström black hole corresponds to a strong spacelike singularity under generic perturbation. This is again different from the point of view in [28, 32]. These authors claimed that the Cauchy horizon will become a lightlike singularity under the mass inflation process. However Gnedins' result was shown to be incorrect [33, 34]. Moreover the argument by Yurtsever that null singularities cannot be generic was also shown to be wrong [35]. Thus we believe that the Cauchy horizon will become a lightlike singularity when it is perturbed.

## 1.4 Outline of the Thesis

With the preceding considerations in mind, we shall focus on the mechanism of mass inflation in this thesis, towards three specific ends.

First we shall consider the circumstances under which the phenomenon of mass inflation can take place in spacetimes other than the prototypical Reissner-Nordström background mentioned above. Since the very existence of a Cauchy horizon raises fundamental questions about the predictability of physical theory, it is important to understand the extent to which mass inflation is a generic process. Some of the black hole spacetimes considered in this thesis have different asymptotic properties than the Reissner-Nordström case, whereas others arise as solutions to gravitational theories other than General Relativity, e.g. string theory and its generalizations to dilaton gravity. Moreover these theories predict dual-horizon black holes which have very different properties than the Reissner-Nordström case. Indeed, it turns out that the inner mass parameters of some black holes do not diverge in some cases. However the mass inflation mechanism does have some basic features which are shared by different black hole backgrounds.

The second goal is to examine how the spacetime geometry affects the specific details of the mass inflation phenomenon. Originally Poisson and Israel showed that the inner mass parameter  $m_{in}$  diverges as

$$m_{in}(v) \sim e^{\kappa v} \frac{d}{dv} \delta m(v), \quad (1.22)$$

when the advanced time  $v$  goes to infinity [28]. The positive constant  $\kappa$  is the surface gravity at the Cauchy horizon (defined in Appendix A) and the mass-energy of the radiation influx  $\delta m$  is inversely proportional to some power of  $v$  in the Reissner-Nordström background. Hence the term  $\exp(\kappa v)$  always dominates the decaying

$\delta m$ . In some of the spacetimes mentioned above, the surface gravity  $\kappa$  at the Cauchy horizon vanishes, and it is interesting to understand the phenomenon in this case. We find that under certain conditions mass inflation can still occur, but the rate of divergence differs from the prototypical Reissner-Nordström case.

Finally, we consider how differing spacetime geometries affect the influx of radiation. By studying wave propagation in different spacetime backgrounds, we find that an inverse power-law decay of  $\delta m$  is not always valid. Indeed, this decay rate is particularly sensitive to the asymptotic properties of the spacetime. In some cases, for example, instead of an inverse power decay,  $\delta m$  can die out at an exponential rate. In this case, the terms  $\exp(\kappa v)$  and  $\delta m(v)$  compete in equation (1.22). It is evident that the increasing term  $\exp(\kappa v)$  does not always dominate the decaying  $\delta m$ , and so mass inflation can be stopped. As we shall see in Chapter 7, the radiation decay rate in a  $(3 + 1)$ -dimensional, asymptotically anti-de Sitter black hole spacetime is not governed by any simple law.

In Chapter 2, we shall review mass inflation at a more technical level. The Reissner-Nordström-Vaidya spacetime will be discussed, followed by the mass inflation calculations in this background. In addition to the method used by Poisson and Israel, another simpler method introduced by Ori [29] will be explained as well. All the mass inflation calculations after Chapter 2 make use of this method.

After the readers are familiar with the phenomenon, we shall move on to Chapter 3 in which mass inflation in two  $(1 + 1)$ -dimensional spacetimes is studied. These spacetimes come from a dilaton theory of gravity which was originally proposed for studying quantum gravity. Although the dimension of these spacetimes is different, we shall see that mass inflation can take place in a similar fashion as in the Reissner-Nordström-Vaidya spacetime. These  $(1 + 1)$ -dimensional black holes not only serve as toy models for testing mass inflation in theories other than General Relativity,

but also provide examples with zero surface gravity at the Cauchy horizon. The consequence of a vanishing surface gravity will also be examined.

We turn next to a consideration of the behavior of the decaying term  $\delta m$ . In Chapter 4, we shall consider scalar waves in asymptotically flat spacetimes with an arbitrary number of (odd) dimensions. Scalar waves are considered because other waves with higher spin, like gravitational waves, obey wave equations similar to the one for scalar waves [36], [37](p. 244), [38]. Although the main results of this chapter have been obtained before, the method employed to determine the falloff rate differs from that used previously. Furthermore, the analytic results obtained in this chapter provide us with a cross-check of the numerical approach we take in studying scalar waves. This numerical approach will be used in subsequent chapters in studying the radiation falloff rates in other spacetimes.

In Chapter 5 the methods outlined in Section 4.1 will be used to revisit the  $(1 + 1)$ -dimensional black holes considered in chapter 3. We first check if the use of an inverse power falloff of  $\delta m$  in Chapter 3 is appropriate. We find that only one of the two dilaton black hole backgrounds induces this kind of falloff in the scalar waves. Waves in the second dilaton black hole background decay away at an exponential rate. This conclusion is supported by both analytic and numeric investigations. The effect of this exponential radiation falloff on mass inflation will be discussed.

We shall study mass inflation in  $2 + 1$  dimensions in Chapter 6. This 3D black hole spacetime is a solution to the Einstein equations in  $2 + 1$  dimensions. This black hole spacetime is indeed a  $(2 + 1)$ -dimensional anti-de Sitter space with identification. The black hole background allows an exact mass inflation calculation even when the hole is rotating because the metric is simpler in  $2 + 1$  dimensions. The appropriate radiation falloff rate in the background will also be calculated an-

alytically and numerically. In this case, the scalar waves do not decay away at an inverse power rate. The correct radiation falloff rate will then be used in the mass inflation calculation. In this chapter, we shall also consider a spacetime which comes from a  $(3 + 1)$ -dimensional string theory. However, this spacetime does not represent a black hole; it is interpretable as an infinite black string. We shall only briefly discuss the radiation and mass inflation problems in this case because this spacetime is similar to the 3D black hole spacetime.

Chapter 7 is devoted to a study of radiation falloff in a  $(3 + 1)$ -dimensional Schwarzschild-anti-de Sitter spacetime. The motivation for this study arises from the desire to obtain a comparison with both the asymptotically flat Schwarzschild case and the anti-de Sitter 3D black hole. We shall see that the late time behavior of the waves can be much more complicated than that described for either of these latter two cases, and a wide range of falloff behavior is possible depending on the relative magnitudes of the mass and cosmological constant. Any computation of mass inflation in such a spacetime will necessarily have to take this falloff behavior into account.

The last chapter of this thesis will summarize the results in the previous chapters. Conclusions will be drawn and the direction for future research will be discussed.

## Chapter 2

# Review of Mass Inflation

The mass inflation phenomenon can be demonstrated in various ways [28, 29, 39, 40]. It also takes place in many other theories of gravity [41, 42, 43, 44, 45, 46, 47]. In this chapter, however, we shall study the mechanism by using the continuous cross-flow model which is used by Poisson and Israel in their original paper. Ori's thin-shell model will also be discussed because it gives an exact mass inflation formula due to its simplicity. This model is important for our purposes because it forms the basis for the mass inflation calculations in the thesis.

Since Poisson and Israel discovered the phenomenon in a Reissner-Nordström background which is irradiated by fluxes of ingoing and outgoing radiation, we shall review this spacetime geometry in Section 2.1 before we study their method of calculation in Section 2.2. Finally we shall look at Ori's thin-shell model in Section 2.3.

## 2.1 Background Spacetime

The Reissner-Nordström solution represents the spacetime of a static and spherically symmetric black hole with an electric charge. Thus the spacetime is filled with an electromagnetic field. Because of this, the stress-energy tensor in the Einstein equations (1.4) is no longer zero; it equals the stress-energy tensor  $\hat{T}_{ab}$  associated with the Maxwell tensor. If we employ a metric which implies spherical symmetry in 3-space, i.e.

$$ds^2 = g_{tt}(t, r) dt^2 + 2 g_{tr}(t, r) dt dr + g_{rr}(t, r) dr^2 + r^2 [d\theta^2 + \sin^2(\theta) d\phi^2] . \quad (2.1)$$

the Maxwell tensor becomes

$$F_{ab} = \frac{q}{r^2} \sqrt{-g_{tt} g_{rr} + g_{tr}^2} \begin{bmatrix} 0 & -1 & 0 & 0 \\ 1 & 0 & 0 & 0 \\ 0 & 0 & 0 & 0 \\ 0 & 0 & 0 & 0 \end{bmatrix} . \quad (2.2)$$

where the indices  $a$  and  $b$  run from 1 to 4. The electromagnetic field tensor (2.2) satisfies the sourceless Maxwell's equations  $\nabla_{[a} F_{bc]} = 0$  and  $\nabla^b F_{ab} = 4\pi j_a = 0$ . The constant  $q$  above represents an electric charge. It is not difficult to show that the stress-energy tensor for the electric field reads

$$\hat{T}_{ab} = \frac{1}{4\pi} \left[ F_{ac} F_b{}^c - \frac{1}{4} F_{cd} F^{cd} g_{ab} \right] = \frac{q^2}{8\pi r^4} \begin{bmatrix} -g_{tt} & -g_{tr} & 0 & 0 \\ -g_{tr} & -g_{rr} & 0 & 0 \\ 0 & 0 & r^2 & 0 \\ 0 & 0 & 0 & r^2 \sin^2(\theta) \end{bmatrix} . \quad (2.3)$$

The solution to the Einstein equations with the stress-energy tensor  $\hat{T}_{ab}$  above

is the Reissner-Nordström metric which reads

$$ds^2 = -N(r) dt^2 + \frac{dr^2}{N(r)} + r^2 d\Omega^2, \quad (2.4)$$

$$N(r) = 1 - \frac{2M}{r} + \frac{q^2}{r^2}. \quad (2.5)$$

The function  $N$  is called lapse function which describes how the spacelike hypersurfaces of constant  $t$  evolve. The derivative of this function measures the gravitational force on a sphere  $r = \text{constant}$ . We introduce the surface gravity  $\kappa$  which is given by  $\kappa = |N'(r)/2|$  in this case. Further explanation for the lapse function and the surface gravity can be found in Appendix A. The term  $d\Omega^2$  above equals  $d\theta^2 + \sin^2(\theta) d\phi^2$ . If the electric charge  $q$  is zero, this metric reduces to the Schwarzschild metric (1.12). Thus it is obvious that the positive constant  $M$  is the mass of this spherical black hole [16], [6](p. 156). This metric has singularities at  $\theta = 0$ ,  $\theta = \pi$ ,  $r = r_{\pm}$  and  $r = 0$ , where

$$r_{\pm} = M \pm M \sqrt{1 - \frac{q^2}{M^2}} \quad (2.6)$$

so that  $N(r_{\pm}) = 0$ . We have assumed that  $M^2 > q^2$  for physical reasons. (It is difficult for astrophysical bodies to maintain substantial electric charge  $|q| \geq M$  without being neutralized [2](p. 314).) The first two singularities at  $\theta = 0$  and  $\theta = \pi$  are coordinate singularities. The other singularities at radii  $r = r_{\pm}$  are also coordinate singularities [6](p. 157). They are analogous to the coordinate singularity at  $r = 2M$  in the Schwarzschild metric (1.12). Finally, the point  $r = 0$  in 3-space is a spacetime singularity because the Kretschmann scalar in this spacetime equals

$$K = \frac{8}{r^8} (6M^2 r^2 - 12M q^2 r + 7q^4). \quad (2.7)$$

Since this curvature scalar diverges at  $r = 0$ , the line  $r = 0$  in the spacetime is

a curvature singularity. The conformal diagram for this dual-horizon black hole is given in figure 2.1.

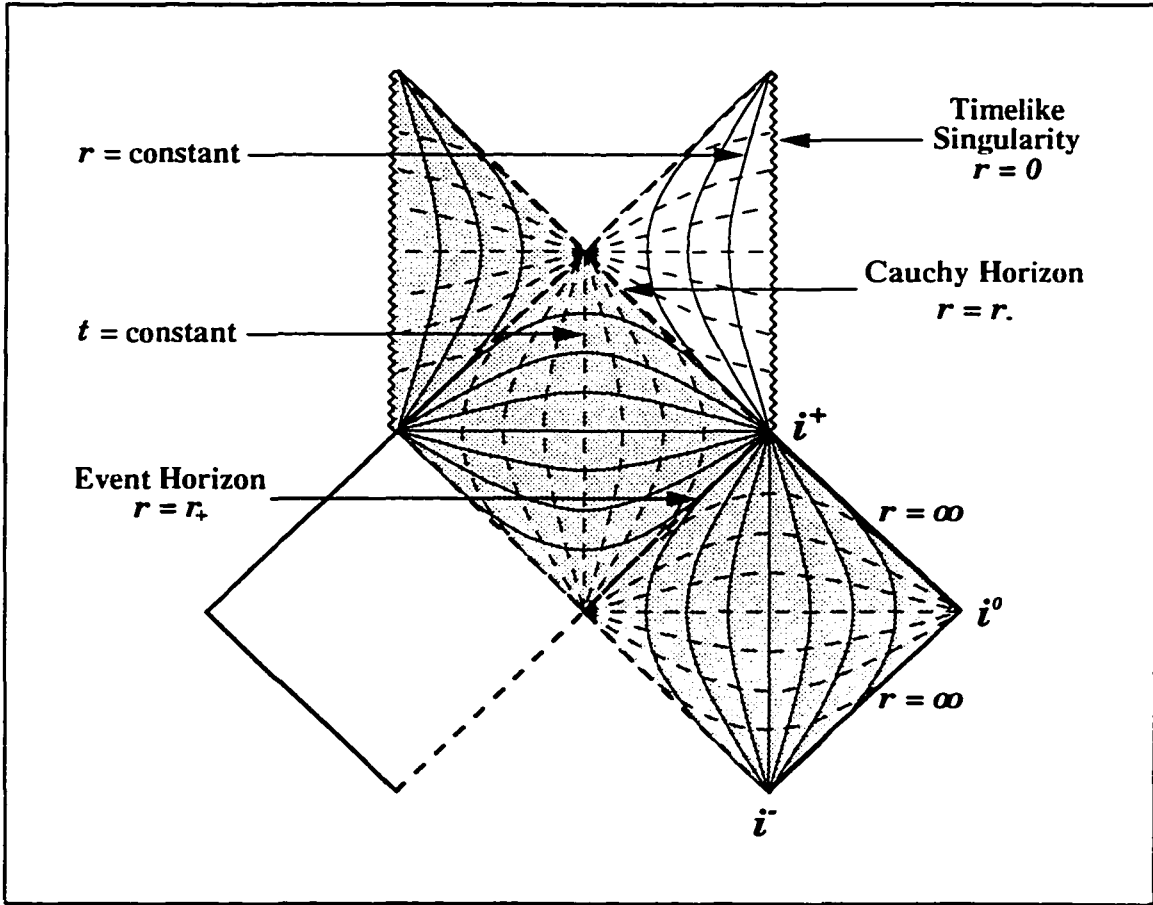


Figure 2.1: Conformal diagram for the Reissner-Nordström spacetime with  $M^2 > q^2$

If we define the “tortoise coordinate”  $\rho$  as [48](p. 665)

$$\rho \equiv \int \frac{dr}{N(r)}, \quad (2.8)$$

the spacetime metric can be written as

$$ds^2 = -N(r) [dt^2 - d\rho^2] + r^2 d\Omega^2. \quad (2.9)$$

This coordinate tends to positive infinity when  $r \rightarrow \infty$ , and it goes to negative infinity when  $r$  approaches to  $r_+$ . By introducing an advanced time  $v$  and retarded time  $u$ , which are defined as

$$v \equiv t + \rho , \quad (2.10)$$

$$u \equiv t - \rho \quad (2.11)$$

so that  $u < t < v$  for positive  $\rho$ , the metric (2.9) admits another form

$$ds^2 = -N(r) dv du + r^2 d\Omega^2 \quad (2.12)$$

or the Eddington-Finkelstein metric forms [2](p. 153)

$$ds^2 = -N(r) dv^2 + 2 dv dr + r^2 d\Omega^2 , \quad (2.13)$$

$$ds^2 = -N(r) du^2 - 2 du dr + r^2 d\Omega^2 . \quad (2.14)$$

From these, we see that the coordinates  $v$  and  $u$  are null because in any fixed direction, i.e. when  $\theta$  and  $\phi$  are constant,  $ds^2$  vanishes for constant  $v$  or  $u$ . Furthermore, at constant  $v$ ,  $\rho$  decreases while the time increases. On the other hand, at constant  $u$ , the tortoise coordinate  $\rho$  increases when  $t$  grows. For these reasons,  $v$  and  $u$  are called ingoing and outgoing null coordinates, respectively. Notice that all forms of the Reissner-Nordström metric above have the coordinate singularities at  $\theta = 0$  and  $\theta = \pi$ , and the spacetime singularity at  $r = 0$ . The hypersurfaces  $r = r_{\pm}$  are not coordinate singularities in the Eddington-Finkelstein metrics because  $g_{ab}$  and  $g^{ab}$  are bounded at  $r = r_{\pm}$  [6](p. 150). However the metrics (2.4), (2.9) and (2.12) are still singular at  $r = r_{\pm}$ .

Since the metric (2.13) is non-singular at  $r = r_{\pm}$ , the coordinate  $r$  has a range  $0 < r < \infty$  for all values of  $v \in \mathbb{R}$ . This portion of the Reissner-Nordström spacetime is represented by the shaded area in figure 2.1. As we can see in the diagram, the Cauchy horizon is located at  $v \rightarrow \infty$ .

We now consider an irradiated Reissner-Nordström black hole. When the hole is showered by infalling radiation, the spacetime is no longer stationary. We introduce a coordinate system  $\{v, r, \theta, \phi\}$  with a metric

$$ds^2 = -N_{in}(v, r) dv^2 + 2 dv dr + r^2 d\Omega^2 . \quad (2.15)$$

The coordinate  $v$  is an ingoing null coordinate as the one we have seen before [49]. When there is infalling radiation in the spacetime, the stress-energy tensor becomes  $T_{ab} = \hat{T}_{ab} + \tilde{T}_{ab}$ . The additional term  $\tilde{T}_{ab}$  describes the radiation [50]. We can express this tensor as

$$\tilde{T}_{ab} = \rho_{in} l_a l_b , \quad (2.16)$$

$$l_a = -\partial_a v = -\delta^1_a , \quad (2.17)$$

where  $x^1$  is the coordinate  $v$ . The function  $\rho_{in}$  is the energy density of the radiation. It was mentioned in Chapter 1 that the ingoing radiation is infinitely blueshifted near the Cauchy horizon; thus we are interested in the high frequency radiation whose wavelength is small relative to the scale of spacetime curvature. This justifies the use of the Isaacson's effective stress-energy tensor for the gravitational radiation [50] which is simply (2.16). It is straightforward to show that the solution to the Einstein equations is [25, 50]

$$N_{in}(v, r) = 1 - \frac{2 m_{in}(v)}{r} + \frac{q^2}{r^2} , \quad (2.18)$$

$$\frac{d}{dv} m_{in}(v) = 4 \pi r^2 \rho_{in} . \quad (2.19)$$

One can show that equation (2.19) is consistent with the conservation law  $\nabla^a T_{ab} = 0$  [2](p. 69). This solution is called the charged Vaidya solution because it is the electrically charged version of the Vaidya solution. (The Vaidya solution represents a Schwarzschild black hole being irradiated by ingoing radiation [25, 49].)

The function  $m_{in}$  in equations (2.18) and (2.19) is interpretable as the mass of the irradiated black hole. This interpretation becomes obvious when  $m_{in}$  is constant because it is then simply the mass of a Reissner-Nordström black hole. When  $m_{in}$  is  $v$ -dependent, the spacetime becomes non-stationary but it is still asymptotically flat. The asymptotic flatness induces a notion of gravitating mass as follows. The vector  $\xi^\alpha = \langle 1, 0, 0, 0 \rangle$  in the coordinate system  $\{v, r, \theta, \phi\}$  is the generator of an asymptotic time translation symmetry in this charged Vaidya spacetime. In other words,  $\xi^\alpha$  satisfies the condition  $\mathcal{L}_\xi g_{ab} \rightarrow 0$  when  $r \rightarrow \infty$  [2](p. 283) because the Lie derivative  $\mathcal{L}_\xi$  of the metric components  $g_{ab}$  equals  $\partial_v g_{ab}$  [2](p. 439). The energy  $\mathcal{E}$  of the spacetime is then given by [2](p. 291)

$$\mathcal{E} = -\frac{1}{8\pi} \lim_{r \rightarrow \infty} \int_0^{2\pi} \int_0^\pi \epsilon_{34ab} \nabla^a \xi^b dx^2 dx^3 . \quad (2.20)$$

where the term  $\epsilon_{abcd}$  is the Levi-Civita tensor, and  $x^3 = \theta$  and  $x^4 = \phi$ . By using Maple V's *tensor package*, it is straightforward to show that

$$-\frac{1}{8\pi} \int_0^{2\pi} \int_0^\pi \epsilon_{34ab} \nabla^a \xi^b dx^2 dx^3 = m_{in} - \frac{q^2}{r} . \quad (2.21)$$

Therefore  $\mathcal{E}$  equals  $m_{in}$ , and this justifies the claim that  $m_{in}$  is the mass of the irradiated black hole.

We now consider a charged spherical object which emits radiation. That is to say there is outgoing radiation in the Reissner-Nordström background. In this case, the stress-energy tensor for the outgoing radiation becomes

$$\tilde{T}_{ab} = \rho_{out} n_a n_b , \quad (2.22)$$

$$n_a = -\partial_a u = -\delta^1_a \quad (2.23)$$

in a coordinate system  $\{u, r, \theta, \phi\}$  with a metric

$$ds^2 = -N_{out}(u, r) du^2 - 2 du dr + r^2 d\Omega^2 . \quad (2.24)$$

Analogous to  $v$  in the metric (2.15), the coordinate  $u$  is an outgoing null coordinate in the metric above. The solution to the Einstein equations with  $T_{ab} = \hat{T}_{ab} + \tilde{T}_{ab}$  reads

$$N_{out}(u, r) = 1 - \frac{2 m_{out}(u)}{r} + \frac{q^2}{r^2} , \quad (2.25)$$

$$\frac{d}{du} m_{out}(u) = -4 \pi r^2 \rho_{out} . \quad (2.26)$$

We interpret the function  $m_{out}$  as the mass of the central object by using the equation (2.20). This interpretation is consistent with the fact that  $m_{out}$  is decreasing, which is evident from the right side of (2.26), when the object is radiating.

## 2.2 Continuous Cross-Flow Model

The continuous cross-flow model devised by Poisson and Israel [28] requires the presence of continuous fluxes of both incoming and outgoing radiation. These two streams of radiation are manipulated in such a way that they cross each other near the Cauchy horizon of the Reissner-Nordström black hole background. When there is either ingoing or outgoing radiation in the spacetime, the metric solution has a simple form as shown in the last section. For the cross-flowing configuration, however, it is not easy to solve the field equation for the metric. Poisson and Israel attack this problem as follows [28].

Since the spacetime is assumed to be spherical, they write the metric as

$$ds^2 = \bar{g}_{\mu\nu} dx^\mu dx^\nu + r^2 d\Omega^2 , \quad (2.27)$$

where the Greek indices run from 1 to 2 and the function  $r$  depends upon  $x^\mu$ . One

can show that the four-dimensional Einstein tensor  $G_{ab}$  can be split into [28]

$$G_{\mu\nu} = -\frac{1}{r^2} \left\{ 2r \bar{\nabla}_\mu \bar{\nabla}_\nu r + \bar{g}_{\mu\nu} \left[ 1 - (\bar{\nabla}r)^2 - 2r \bar{\nabla}^2 r \right] \right\} . \quad (2.28)$$

$$G_{\theta\theta} = r \bar{\nabla}^2 r - \frac{r^2 \bar{R}}{2} , \quad (2.29)$$

$$G_{\phi\phi} = \frac{1}{\sin^2(\theta)} \left[ r \bar{\nabla}^2 r - \frac{r^2 \bar{R}}{2} \right] . \quad (2.30)$$

The operator  $\bar{\nabla}$  denotes the covariant derivative and  $\bar{R}$  the Ricci scalar associated with the two-dimensional Lorentzian metric  $\bar{g}_{\mu\nu}$ .

We notice that the metric (2.27) is equivalent to (2.1) in the previous section. In the coordinate system for (2.1), the stress-energy tensor for the electromagnetic field is given by (2.3). Therefore the electromagnetic part of the stress-energy tensor in the coordinate system  $\{x^\mu, \theta, \phi\}$  is simply

$$\hat{T}_{ab} = \frac{q^2}{8\pi r^4} \left[ -\bar{g}_{\mu\nu} \delta^\mu_a \delta^\nu_b + r^2 \delta^3_a \delta^3_b + r^2 \sin^2(\theta) \delta^4_a \delta^4_b \right] . \quad (2.31)$$

For the cross-flowing radiation, Poisson and Israel write the radiation part of the stress-energy tensor as

$$\bar{T}_{ab} = \frac{1}{4\pi r^2} [L_i(V) l_a l_b + L_o(U) n_a n_b] , \quad (2.32)$$

$$l_a = -\partial_a V , \quad (2.33)$$

$$n_a = -\partial_a U . \quad (2.34)$$

The functions  $L_i$  and  $L_o$  represent the luminosities of the ingoing and outgoing radiation, respectively [28]. The coordinates  $\{U, V\}$  in (2.32) are some arbitrary outgoing and ingoing null coordinates whose relationship to the coordinates  $x^\mu$  will be defined later. Equation (2.32) says that the stress-energy tensor for the cross-flowing radiation is a superposition of the stress-energy tensor for ingoing radiation and that for outgoing radiation. Isaacson [50] showed that for polychromatic radiation, the stress-energy tensor is simply a superposition of the stress-energy tensors

of each monochromatic mode of the radiation. Therefore we assume that there is no interaction between the two streams of radiation.

Since the total stress-energy tensor  $T_{ab}$  must be conserved, the sum of the divergences of  $\hat{T}_{ab}$  and  $\bar{T}_{ab}$  vanishes. We know that the electromagnetic part of the stress-energy tensor obeys the conservation law; the radiation part  $\bar{T}_{ab}$  thus inherits the divergence-free property from  $T_{ab}$ . This four-dimensional conservation law  $\nabla^a \bar{T}_{ab} = 0$  reduces to

$$\bar{\nabla}^\nu \left( r^2 \bar{T}_{\mu\nu} \right) = 0 . \quad (2.35)$$

Equation (2.35) represents the usual 4-dimensional divergence-free property of  $\bar{T}_{ab}$  but is expressed in terms of the 2-dimensional metric  $\bar{g}_{\mu\nu}$ .

It is convenient to work with the scalar functions  $f(x^\mu)$ ,  $\kappa(x^\mu)$  and  $m(x^\mu)$  [28]. These functions are invariant and related through the equations

$$f(x^\mu) \equiv \bar{g}^{\mu\nu} \partial_\mu r \partial_\nu r = 1 - \frac{2m(x^\mu)}{r} + \frac{q^2}{r^2} , \quad (2.36)$$

$$\kappa(x^\mu) \equiv -\frac{1}{2} \partial_r f = -\frac{m(x^\mu)}{r^2} + \frac{q^2}{r^3} . \quad (2.37)$$

It is obvious that the function  $m$  is the mass of the black hole if we turn off either  $L_i$  or  $L_o$  in  $\bar{T}_{ab}$ . In terms of these functions, the field equations become [28]

$$\bar{\nabla}_{\mu\nu} r + \kappa \bar{g}_{\mu\nu} = -4\pi r \bar{T}_{\mu\nu} , \quad (2.38)$$

$$\bar{R} - 2 \partial_r \kappa = 0 . \quad (2.39)$$

The solution of these equations describes a Reissner-Nordström black hole background in the presence of ingoing and outgoing radiation described by the stress-energy tensor (2.32).

By using the definition of  $f$ , one can manipulate equations (2.38) and (2.39) and obtain [28]

$$\bar{\nabla}^2 m = -(4\pi)^2 r^3 \bar{T}_{\mu\nu} \bar{T}^{\mu\nu} . \quad (2.40)$$

In a double null coordinate system, the 2-metric can be written as

$$\bar{g}_{\mu\nu} dx^\mu dx^\nu = -2e^{2\sigma} dU dV , \quad (2.41)$$

and equation (2.40) becomes

$$-2e^{-2\sigma} \partial_U \partial_V m = -\frac{2}{r} e^{-4\sigma} L_i(V) L_o(U) . \quad (2.42)$$

For a well-posed problem, we expect that the value of  $m(U, V)$  on a characteristic surface described by the equations  $U = U_o$  and  $V = V_o$  is given a priori. As a result the mass function  $m(U, V)$  can be integrated as

$$\begin{aligned} m(U, V) &= m(U, V_o) + m(U_o, V) - m(U_o, V_o) \\ &+ \int_{U_o}^U \int_{V_o}^V \frac{L_i(\mathcal{V}) L_o(\mathcal{U})}{r(\mathcal{U}, \mathcal{V}) \exp(2\sigma(\mathcal{U}, \mathcal{V}))} d\mathcal{V} d\mathcal{U} . \end{aligned} \quad (2.43)$$

The spacetime of the model constructed by Poisson and Israel is shown in figure 2.2. It is covered by the coordinates  $\{U, V, \theta, \phi\}$  but  $\theta$  and  $\phi$  are suppressed in the diagram. The interior of the Reissner-Nordström black hole is perturbed by two streams of radiation. The ingoing stream is turned on at  $V = V_i$  and is turned off at  $V = V_f$ . The outgoing stream is switched on during the interval  $U_i \leq U \leq U_f$ . These two fluxes cross each other in a region between the event and Cauchy horizons. We denote the radiation-free region before  $U = U_i$  and  $V = V_i$  by region I. The region before  $U = U_i$  but after  $V = V_f$  is called region II. Finally, region III is the sector when  $U > U_f$  and  $V > V_f$ . These three regions are radiation-free and they are patches of the usual Reissner-Nordström spacetime.

Since the radiation is supposed to be electrically neutral, the electric charge  $q$  is the same everywhere in figure 2.2. This is not true for the mass though. Region I is a portion of the Reissner-Nordström spacetime with a constant mass  $M_1$ . Similarly region II and region III have constant masses of  $M_2$  and  $M_3$ , respectively. In

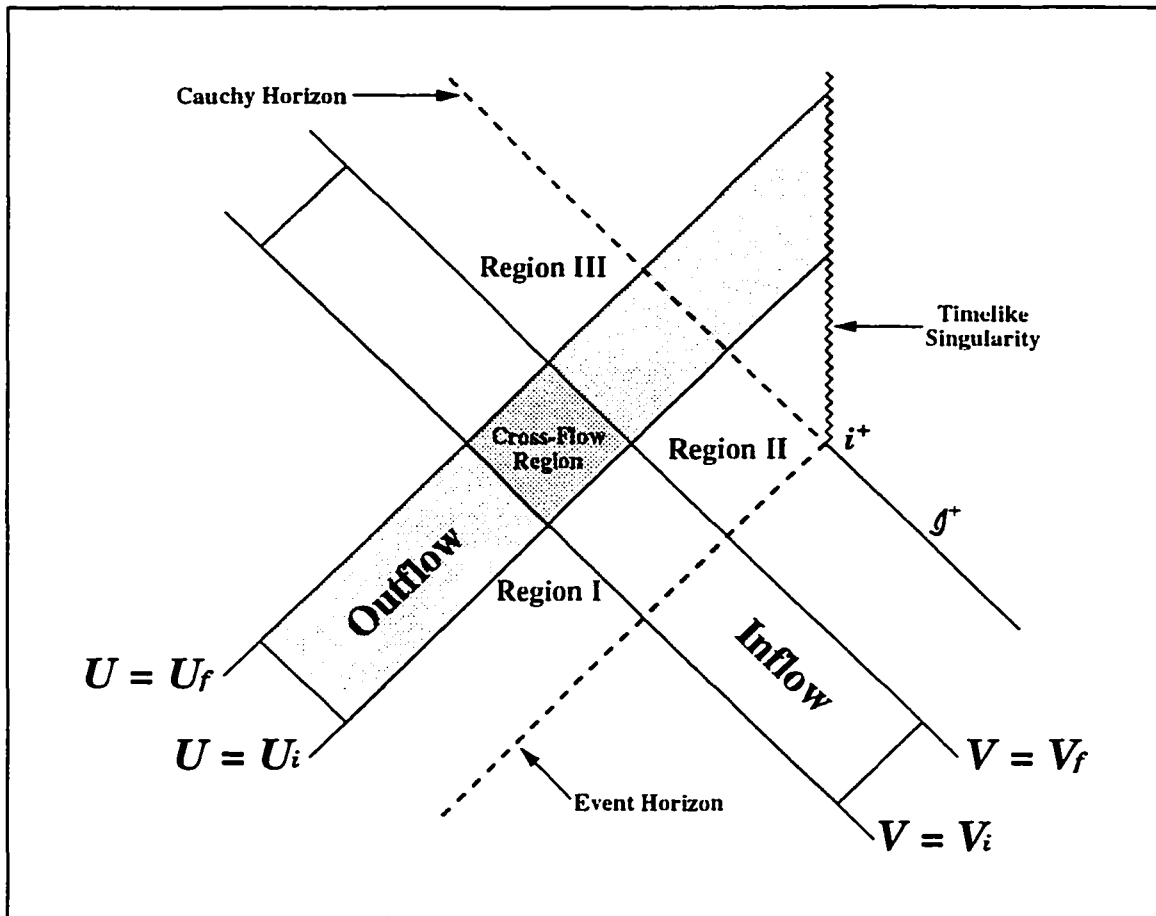


Figure 2.2: Reissner-Nordström background perturbed by cross-flowing streams of radiation. The streams of scattered radiation come from the asymmetries of a collapsing star.

the inflow region between regions I and II, the spacetime is the charged Vaidya spacetime with infalling radiation. We denote the mass parameter in this region by  $m_i(V)$ . This is analogous to  $m_{in}(v)$  in equation (2.18). In the outflow region outside the cross-flow region, we denote the mass parameter as  $m_o(U)$  because this region is a portion of the charged Vaidya spacetime with outgoing radiation which is described by equations (2.24) to (2.26). However since the outflow stream is inside the black hole, we must switch the sign of  $u$  in order to have an increasing mass parameter  $\bar{m}_{out}(u) = m_{out}(-u)$  [28]. The mass parameter in the cross-flow region is denoted by  $m_X(U, V)$  which is given by equation (2.43).

Since the null coordinates  $\{U, V\}$  are arbitrary, we can choose them to be

$$V = -\exp(-\kappa_2 v) , \quad (2.44)$$

$$U = -\exp(-\kappa_1 u) , \quad (2.45)$$

where  $v$  and  $u$  are the advanced and retarded times. Now we can easily associate the null coordinates in the cross-flowing region to those in the pure inflow or pure outflow regions. The Cauchy horizon is now located along the line  $V = 0$  because the surface gravity  $\kappa_2$  at the inner horizon in region II is positive and  $v \rightarrow \infty$  at the horizon. The other positive constant  $\kappa_1$  is also the surface gravity at the inner horizon. However it is the inner horizon of the *extended* region I which is not shown in figure 2.2. In other words,  $\kappa_1$  is the same as  $\kappa_2$  except the mass  $M_1$  replaces  $M_2$ . In terms of the retarded and advanced times, the two mass parameters  $m_i(V)$  and  $m_o(U)$  are related to  $m_{in}(v)$  in

$$ds^2 = - \left[ 1 - \frac{2m_{in}(v)}{r} + \frac{q^2}{r^2} \right] dv^2 + 2 dv dr + r^2 d\Omega^2 \quad (2.46)$$

and  $\bar{m}_{out}(u)$  in

$$ds^2 = - \left[ 1 - \frac{2\bar{m}_{out}(u)}{r} + \frac{q^2}{r^2} \right] du^2 + 2 du dr + r^2 d\Omega^2 \quad (2.47)$$

as

$$m_{in}(v) = m_i(-\exp(-\kappa_2 v)) , \quad (2.48)$$

$$\tilde{m}_{out}(u) = m_o(-\exp(-\kappa_1 u)) . \quad (2.49)$$

Therefore the luminosity functions  $L_i$  and  $L_o$  can be written as

$$L_i(-e^{-\kappa_2 v}) = \frac{dm_{in}(v)}{dv} \left( \frac{dv}{dV} \right)^2 = \frac{1}{\kappa_2^2} \exp(2\kappa_2 v) \frac{dm_{in}(v)}{dv} . \quad (2.50)$$

$$L_o(-e^{-\kappa_1 u}) = \frac{d\tilde{m}_{out}(u)}{du} \left( \frac{du}{dU} \right)^2 = \frac{1}{\kappa_1^2} \exp(2\kappa_1 u) \frac{d\tilde{m}_{out}(u)}{du} . \quad (2.51)$$

In order to sew these patches of spacetime together continuously, all the mass parameters must obey the following conditions:

$$m_i(V_i) = m_o(U_i) = m_X(U_i, V_i) = M_1 , \quad (2.52)$$

$$m_i(V_f) = M_2 , \quad (2.53)$$

$$m_X(U_f, V_f) = M_3 . \quad (2.54)$$

$$m_X(U, V_i) = m_o(U) , \quad (2.55)$$

$$m_X(U_i, V) = m_i(V) . \quad (2.56)$$

As a result, equation (2.43) for the cross-flow region can be written as

$$m_X(U, V) = m_o(U) + m_i(V) - M_1 + \int_{U_i}^U dU L_o(U) \int_{V_i}^V \frac{L_i(V) dV}{r(U, V) \exp(2\sigma(U, V))} \quad (2.57)$$

for  $U \in (U_i, U_f)$  and  $V \in (V_i, V_f)$ . The luminosity  $L_i$  is given by equation (2.50). The advanced time  $v$  relates to  $V$  by equation (2.44). Since the term  $dm_{in}/dv$ , according to the result by Price [20], decreases at a rate  $1/v^p$ , where  $p$  is a positive integer, the luminosity  $L_i(V)$  reads

$$L_i(V) \propto \frac{1}{V^2} [\ln(-V)]^{-p} \quad (2.58)$$

which diverges at the Cauchy horizon  $V = 0$ . The integer  $p \geq 12$  comes from the late time radiation falloff rate measured in advanced time  $v$  [28]. Poisson and Israel showed that the term  $r \exp(2\sigma)$  is finite while the inflow approaching the Cauchy horizon. They argued that the  $\mathcal{V}$  integration in (2.57) must be unbounded when  $V_f$  goes to zero. That is to say  $m_X$  diverges when the ingoing stream approaches to the Cauchy horizon [28]. Thus Poisson and Israel concluded that the mass in region III diverges due to the divergent mass in the cross-flow region. This inflating mass parameter is expected to seal the Cauchy horizon by turning it into a spacetime singularity. However the divergence of the mass parameter cannot be detected by the observers outside the black hole because no signal can escape from the event horizon.

### 2.3 Thin-Shell Model

Although Poisson and Israel showed that the inner mass parameter increases without bound at the Cauchy horizon, their approach is mathematically complicated. By realizing that the mass inflation mechanism relies little on the quantity of the outgoing radiation, Ori came up with a simpler model shortly after the discovery of the phenomenon. The new model allows a better estimation of the rate of growth of the mass parameter. He constructed his model by replacing the continuous stream of outflowing radiation by an outgoing thin null shell. That is to say his model describes an outgoing null shell in a Reissner-Nordström black hole which is also irradiated by ingoing radial radiation [29].

In order to construct this configuration, Ori matched two patches of the charged Vaidya solution along a null line  $S$  between the event and Cauchy horizons. This is shown in figure 2.3. Regions I and II are two different copies of the charged

Vaidya solution for ingoing radiation (2.15) with different mass parameters  $m_1$  and  $m_2$ , respectively. The difference in  $m_1$  and  $m_2$  implies that the null line S can be interpreted as representing a thin shell of outgoing radiation. In other words, the discontinuity in the spacetime along S represents the presence of a thin shell. By using Price's result for late time radiation [20],  $m_1$  can be assumed to be

$$m_1(v_1) = M - \delta m(v_1) , \quad (2.59)$$

$$\delta m(v) = \frac{h}{v^{p-1}} , \quad (2.60)$$

where  $M$ ,  $h$  and  $p$  are positive constants and  $v_1$  is the advanced time in region I. The integer exponent  $p$  determines the decay rate of the ingoing radiation and it is greater than or equal to 12 for gravitational radiation. The constant  $h$  is arbitrary but the other constant  $M$  is interpretable as the final mass of the black hole measured by an observer at spatial infinity. This is obvious because when the advanced time  $v_1$  goes to infinity, the exterior mass of the black hole  $m_1$  tends to  $M$ . Moreover, since the metric of region I reads

$$ds^2 = -N_1(v_1, r) dv_1^2 + 2 dv_1 dr + r^2 d\Omega^2 . \quad (2.61)$$

$$N_1(v_1, r) = 1 - \frac{2m_1(v_1)}{r} + \frac{q^2}{r^2} , \quad (2.62)$$

the Cauchy horizon is given by

$$r_- = M \left( 1 - \sqrt{1 - \frac{q^2}{M^2}} \right) . \quad (2.63)$$

On the other hand, the geometry of region II is described by the metric

$$ds^2 = -N_2(v_2, r) dv_2^2 + 2 dv_2 dr + r^2 d\Omega^2 , \quad (2.64)$$

$$N_2(v_2, r) = 1 - \frac{2m_2(v_2)}{r} + \frac{q^2}{r^2} , \quad (2.65)$$

$$m_2(v_2) = m_1(v_1) + \Delta m(v_2) , \quad (2.66)$$

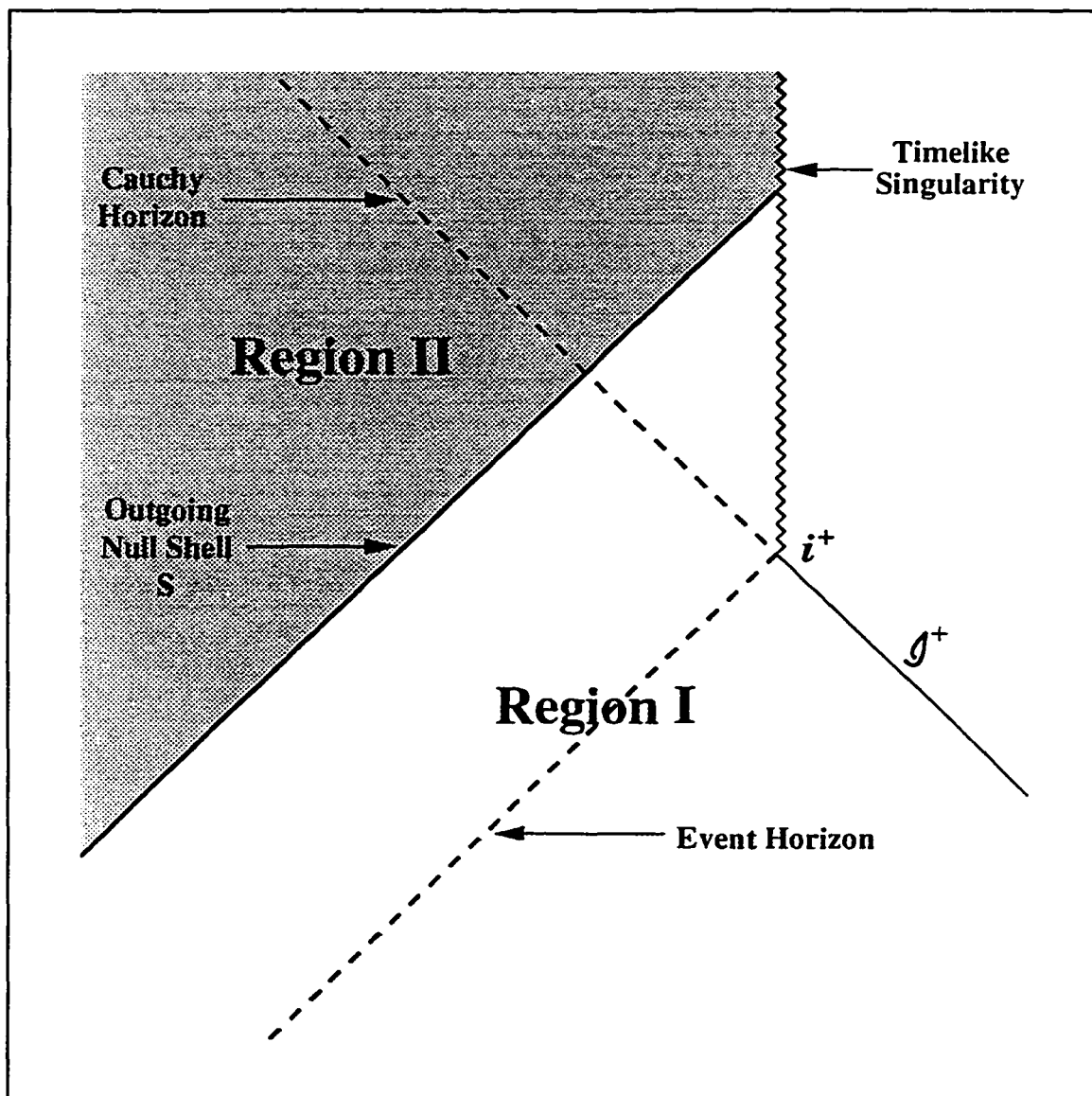


Figure 2.3: The 45° line  $S$  represents an outgoing thin null shell on this conformal diagram for the charged Vaidya background.

where  $\Delta m$  is the mass-energy of the outgoing null shell S. Ori showed that the mass parameter  $m_2$  increases without bound when S approaches the Cauchy horizon.

This can be shown in the following way. The shell's null generators can be parameterized by an affine parameter  $\lambda$  so that they are characterized by the radius  $r = R(\lambda)$  and advanced time  $v(\lambda)$ . Without loss of generality, this parameter is assumed to be negative outside the Cauchy horizon and equal zero at the horizon. The function  $R(\lambda)$  has the same value when the shell is observed from either region I or region II because the surface element  $r^2 d\Omega^2$  is the same in both regions. This is not the case for the advanced time  $v$ . In general, regions I and II have their own advanced time coordinates  $v_1$  and  $v_2$ , respectively. Therefore the advanced time associated with the shell is divided into  $v_1(\lambda)$  and  $v_2(\lambda)$  for regions I and II.

In order for S to be null, we must have the null condition

$$\frac{\dot{R}(\lambda)}{\dot{v}_i(\lambda)} = \frac{1}{2} N_i(v_i(\lambda), R(\lambda)) , \quad (2.67)$$

where the subscript  $i$  is either 1 or 2 for regions I or II, respectively. In the rest of this section, the overdot denotes derivative with respect to  $\lambda$ . We introduce a function  $\mathcal{M}$  which is defined as

$$\mathcal{M}(r) \equiv \frac{r}{2} + \frac{q^2}{2r} \quad (2.68)$$

whereby  $N_i(v_i, R)$  can be written as

$$N_i(v_i, R) = \frac{2}{R} [\mathcal{M}(R) - m_i(v_i)] . \quad (2.69)$$

Notice that  $\mathcal{M}$  is the same in both regions and has the same dimensions as mass.

The null generator must satisfy the equation

$$\ddot{v}_i(\lambda) = -\frac{1}{2} N_i'(v_i(\lambda), R(\lambda)) [\dot{v}_i(\lambda)]^2 \quad (2.70)$$

which is one of the Euler-Lagrange equations for geodesics. The primes in the equation above denote partial derivatives with respect to the spatial variable  $R$ . We can rewrite equation (2.70) as

$$\ddot{v}_i(\lambda) = -\frac{1}{R(\lambda)} \left[ \mathcal{M}'(R(\lambda)) - \frac{1}{2} N_i(v_i(\lambda), R(\lambda)) \right] [\dot{v}_i(\lambda)]^2 . \quad (2.71)$$

Ori introduced a function  $z_i(\lambda)$  which is important in the rest of the calculation. This function is defined as [29]

$$z_i(\lambda) \equiv \frac{R(\lambda)}{\dot{v}_i(\lambda)} . \quad (2.72)$$

We multiply this function by  $\dot{R}$  and simplify it by using the equations (2.67) and (2.69). We then obtain

$$z_i(\lambda) \dot{R}(\lambda) = \mathcal{M}(R(\lambda)) - m_i(v_i(\lambda)) . \quad (2.73)$$

On the other hand, if we differentiate this function with respect to  $\lambda$ , we have

$$\dot{z}_i(\lambda) = \mathcal{M}'(R(\lambda)) \quad (2.74)$$

after using equations (2.67) and (2.71). As a result, if we know the function  $R$ , the spacetime in both regions can be determined by the following set of equations:

$$z_i(\lambda) = Z_i + \int_0^\lambda \mathcal{M}'(R(\zeta)) d\zeta , \quad (2.75)$$

$$v_i(\lambda) = \int^\lambda \frac{R(\zeta)}{z_i(\zeta)} d\zeta , \quad (2.76)$$

$$m_i(v_i(\lambda)) = \mathcal{M}(R(\lambda)) - z_i(\lambda) \dot{R}(\lambda) . \quad (2.77)$$

The integration constants  $Z_i$  are as yet unknown. There is no integration constant for the integral of  $v$  because it is irrelevant in the rest of the calculation.

Let us compute the two integration constants  $Z_1$  and  $Z_2$ . When  $\lambda$  is close to zero, the shell is in the exterior neighborhood of the Cauchy horizon which is given

by  $\lambda = 0$ . In this case it follows from (2.75) that  $z_i$  can be approximated as

$$z_i(\lambda) \approx Z_i + \mathcal{M}'(r_-) \lambda = Z_i - \kappa_- r_- \lambda, \quad (2.78)$$

where

$$\kappa_- = -\frac{1}{r_-} \mathcal{M}'(r_-) = \frac{1}{r_-^2} \sqrt{M^2 - q^2} \quad (2.79)$$

is the surface gravity at the Cauchy horizon  $r_-$ . By using this approximation, equation (2.76) can be approximated as

$$v_i(\lambda) \approx \int^\lambda \frac{r_-}{Z_i - \kappa_- r_- \zeta} d\zeta = -\frac{1}{\kappa_-} \ln\left(\frac{Z_i}{\kappa_- r_-} - \lambda\right) \quad (2.80)$$

in a small neighborhood of  $\lambda = 0$ . Because the advanced time  $v_1$  in region I goes to positive infinity at the Cauchy horizon ( $\lambda = 0$ ), we conclude that  $Z_1 = 0$  according to (2.80). Consequently we obtain

$$\lambda \approx -\exp(-\kappa_- v_1) \quad (2.81)$$

in a small neighborhood of the exterior of the Cauchy horizon.

Since  $\Delta m = m_2 - m_1$  and  $m_i$  are given by equation (2.77), the mass of the null shell S reads

$$\Delta m(v_1(\lambda)) = -Z_2 \dot{R}(\lambda) \quad (2.82)$$

by using equation (2.75). Inside the black hole,  $\dot{R}$  must be negative and we conclude that  $Z_2$  must be positive in order to have a positive mass-energy for the shell. The specific value of  $Z_2$ , however, is not important in the calculation.

We now calculate the radial function  $R$ . The condition (2.67) for the null shell in region I can be written as

$$\frac{d\tilde{R}(v_1)}{dv_1} = \frac{1}{2} \left\{ 1 - \frac{2m_1(v_1)}{\tilde{R}(v_1)} + \frac{q^2}{[\tilde{R}(v_1)]^2} \right\}. \quad (2.83)$$

The tilde is used to denote the functional dependence on  $v_1$  instead of  $\lambda$  in  $R$ , that is  $\tilde{R}(v_1(\lambda)) = R(\lambda)$ . As mentioned before, the exterior mass parameter  $m_1$  is given by (2.59). We observe that equation (2.83) is an ordinary differential equation in  $\tilde{R}$  which has a series solution in  $v_1$  [43]. It is not difficult to show that the asymptotic expansion of the solution  $\tilde{R}$  at  $r_-$  reads

$$\tilde{R}(v) = r_- + \frac{1}{\kappa_- r_-} \delta m(v) - \frac{1}{\kappa_-^2 r_-} \frac{d}{dv} \delta m(v) + O\left(\frac{d^2}{dv^2} \delta m(v)\right). \quad (2.84)$$

Finally we recall that the mass-energy of the outgoing null shell is given by equation (2.82). According to the expansion (2.84),  $\dot{R}(\lambda)$  has a leading order term of

$$\dot{R}(\lambda) = \frac{d\tilde{R}(v_1)}{dv_1} \dot{v}_1(\lambda) \approx - \frac{(p-1)h}{\kappa_-^2 r_-} \frac{\exp(\kappa_- v_1)}{v_1^p}, \quad (2.85)$$

where equations (2.60) and (2.81) have been used. It follows from equations (2.82) and (2.85) that

$$\Delta m(v_1) \approx \frac{(p-1)h Z_2}{\kappa_-^2 r_-} \frac{\exp(\kappa_- v_1)}{v_1^p}. \quad (2.86)$$

Thus  $\Delta m$  diverges when  $v_1$  goes to infinity because the exponential growth is dominant compared to the inverse power attenuation of  $1/v_1^p$ . In other words, when the shell S approaches the Cauchy horizon ( $v_1 \rightarrow \infty$ ), its mass increases without bound. Consequently the inner mass parameter  $m_2$  also diverges while S approaches the horizon. Furthermore, as a portion of the charged Vaidya spacetime, region II has a zero Ricci scalar but its Kretschmann scalar reads

$$R_{abcd} R^{abcd} = \frac{8}{r^8} \left[ 6 m_2^2(v_2) r^2 - 12 m_2(v_2) q^2 r + 7 q^4 \right]. \quad (2.87)$$

This implies that the spacetime has a scalar curvature singularity at the Cauchy horizon induced by the divergence of the inner mass parameter  $m_2$ .

## Chapter 3

# Mass Inflation In $1 + 1$ Dimensions

Investigation of lower dimensional theories of gravity could be interesting and encouraging because these theories provide an alternative arena for studying the physics of gravity. This might deepen our understanding of the generic features of gravity. Such theories have been particularly useful in elucidating the basic features of classical gravity [51], in developing models for exploring the back-reaction problem in black hole radiation [52], and in constructing simple model theories of quantum gravity [53]. The computational aspects of problems in lower dimensional theories of gravity are more tractable than those in  $3 + 1$  dimensions, often affording a greater measure of conceptual insight. An example of this is the search for an exact solution to the Dirac equation for massive spinor particles in  $(1 + 1)$ -dimensional vacuum background which allows an explicit demonstration (albeit in a very simplified context) of the equality of the vacuum expectation value of the stress energy outside of a black hole for both scalars and spinors [54, 55]. Similar calculations can only be done approximately in  $3 + 1$  dimensions though. Other examples include studies of the generic properties of black hole solutions [51], black

hole radiation [52, 55, 54], cosmology [56], singularities [57] and quantum gravity [53].

Note that in (1+1)-dimensional spacetimes, the metric tensor  $g_{ab}$  has only three different components. The two degrees of coordinate freedom reduce the number of unknown metric components to just one. However the first obstacle to be overcome in making use of any (1 + 1)-dimensional theory of gravity is that the Einstein tensor  $G_{ab}$  is identically zero in 1 + 1 dimensions for *all* metric tensors  $g_{ab}$ . Hence the Einstein equations in 1 + 1 dimensions imply a zero stress-energy tensor. In this sense, the Einstein equations have no dynamical content in 1 + 1 dimensions.

In order to cope with this difficulty, several theories of gravity in two dimensions have been proposed. One of them is the non-critical string-inspired dilaton theory using the low-energy string effective action in 1 + 1 dimensions [58]. Different models with different parameters can be proposed using this theory. Many classical solutions of this theory have been found. Because these models are mathematically simple, they are useful as toy models in the investigation of the problems about perturbative renormalizability [59], black hole evaporation [52] and black hole thermodynamics [58]. This low energy string effective action has the form

$$S = \int d^2x \sqrt{-g} e^{-2\phi} \left[ R + \gamma (\nabla\phi)^2 - \frac{1}{4} e^{\epsilon\phi} F_{ab} F^{ab} + V(\phi) \right], \quad (3.1)$$

where the indices run from 1 to 2. In this action,  $R$  is the Ricci scalar,  $F_{ab}$  is the Maxwell tensor and  $\phi$  is the scalar dilaton field. The constants  $\gamma$  and  $\epsilon$  are coupling parameters and  $V$  is the potential function of the dilaton field.

This form of the action is related to the (3+1)-dimensional spherically symmetric gravity in the following way. Pure gravity in 3 + 1 dimensions corresponds to the action

$$S^{(4)} = \int d^4x \sqrt{-g^{(4)}} R^{(4)}, \quad (3.2)$$

where  $g^{(4)}$  and  $R^{(4)}$  are the determinant of the metric and the Ricci scalar in 3 + 1 dimensions, respectively. If we rewrite this action using a metric of the form

$$ds^2 = g^{(2)}_{\mu\nu} dx^\mu dx^\nu + e^{-2\psi} d\Omega^2, \quad (3.3)$$

where  $\mu$  and  $\nu$  run from 1 to 2, we obtain

$$\begin{aligned} S^{(4)} = & \int d^2x \sqrt{-g^{(2)}} e^{-2\psi} \left[ R^{(2)} + 2 (\nabla\psi)^2 + 2e^{2\psi} \right] \\ & + 4 \int d^2x \sqrt{-g^{(2)}} \nabla^\mu \left( e^{-2\psi} \nabla_\mu \psi \right), \end{aligned} \quad (3.4)$$

where  $\nabla$  is the covariant derivative operator with respect to the two-dimensional metric  $g^{(2)}_{\mu\nu}$ . The quantity  $g^{(2)}$  is the determinant of  $g^{(2)}_{\mu\nu}$  and  $R^{(2)}$  is the Ricci scalar for  $g^{(2)}_{\mu\nu}$ . This action, apart from the total derivative which is often discarded, is of the same form as equation (3.1).

If we prescribe the potential function as

$$V(\phi) = \sum_{n=0}^k a_n e^{2n\phi}, \quad (3.5)$$

where  $k$  is some positive integer and the  $a_n$  are some coupling constants, the action (3.1) can be written as

$$\begin{aligned} S = & \int d^2x \sqrt{-g} e^{-2\phi} \left[ R + \gamma (\nabla\phi)^2 - \frac{1}{4} F_{ab} F^{ab} + Q^2 + \sigma e^{2\phi} \right] \\ & + \int d^2x \sqrt{-g} \left[ \sum_{n=2}^k a_n e^{2(n-1)\phi} - 8\pi \mathcal{L}_M \right]. \end{aligned} \quad (3.6)$$

In this form, we have chosen  $\epsilon = 0$  and have denoted  $a_0$  and  $a_1$  in (3.5) by  $Q^2$  and  $\sigma$ . The last term  $8\pi \mathcal{L}_M$  in (3.6) does not come from the action (3.1). This additional term is added by hand in order to include a matter contribution. The symbol  $\mathcal{L}_M$  denotes the matter Lagrangian which has the property that  $\delta\mathcal{L}_M/\delta g_{ab} = \sqrt{-g} T^{ab}$ , where  $T^{ab}$  is the stress-energy-momentum tensor. In the rest of this chapter we shall choose  $T^{ab}$  to be the stress-energy tensor of a null fluid as that in Ori's model.

A choice of the values of the parameters  $\gamma$ ,  $Q$ ,  $\sigma$ , and  $a_n$  is tantamount to a particular choice of theory. In the next two sections, we shall consider two distinct choices of the parameters. Each of these choices leads to a set of field equations whose solution is interpretable as a multi-horizon black hole spacetime.

Our goal in this chapter is to study mass inflation in black holes with several horizons within the event horizon. We first study mass inflation with non-zero surface gravity at the Cauchy horizon in the two dilaton background spacetimes in Sections 3.1 and 3.2. After these, we turn our attention to vanishing surface gravity in Section 3.3 in which the mass inflation mechanism will be challenged.

### 3.1 First Dilaton Background

By varying the vector potential in the Maxwell tensor, and also varying the dilaton field and the metric tensor, the action (3.6) gives the following field equations [58]:

$$0 = \nabla_b (e^{-2\phi} F_a{}^b) , \quad (3.7)$$

$$0 = R + \gamma \nabla^2 \phi - \gamma (\nabla \phi)^2 - \frac{1}{4} F^2 + Q^2 - \sum_{n=2}^k (n-1) a_n e^{2n\phi} . \quad (3.8)$$

$$\begin{aligned} 8\pi e^{2\phi} T_{ab} = & 2 \nabla_{ab} \phi - 2 \nabla^2 \phi g_{ab} + (\gamma - 4) \left[ \nabla_a \phi \nabla_b \phi - \frac{1}{2} (\nabla \phi)^2 g_{ab} \right] \\ & + 2 (\nabla \phi)^2 g_{ab} - \frac{1}{2} \left[ F_{ac} F_b{}^c - \frac{1}{4} F^2 g_{ab} \right] \\ & - \frac{1}{2} \left[ Q^2 + \sigma e^{2\phi} + \sum_{n=2}^k a_n e^{2n\phi} \right] g_{ab} . \end{aligned} \quad (3.9)$$

In the Eddington-Finkelstein metric

$$ds^2 = 2 dv dx - N(v, x) dv^2 , \quad (3.10)$$

when  $\gamma = \sigma = 2$  and  $Q = 0$ , these field equations admit the solution [58, 44]

$$F_{12} = f = \frac{q}{(x - x_o)^2}, \quad (3.11)$$

$$\phi = -\ln|x - x_o|, \quad (3.12)$$

$$N(v, x) = \frac{\mathcal{M}(x) - m(v)}{x - x_o}, \quad (3.13)$$

$$\mathcal{M}(x) = (x - x_o) \left[ 1 + \frac{q^2}{4(x - x_o)^2} - \frac{1}{2} \sum_{n=2}^k \frac{a_n}{2n - 3} (x - x_o)^{2-2n} \right] \quad (3.14)$$

with the use of stress-energy tensor

$$T_{ab} = \hat{\rho} l_a l_b. \quad (3.15)$$

The coordinates  $x^1$  and  $x^2$  are  $v$  and  $x$  respectively. The energy density  $\hat{\rho}$  relates to the function  $m$  through the equation

$$8\pi \hat{\rho} = \frac{dm(v)}{dv}. \quad (3.16)$$

Similar to the definition (2.17) in the last chapter, the null vector  $l_a$  in (3.15) is defined as  $l_a \equiv -\delta^1_a$ . This metric can represent a black hole spacetime [58]. This is easy to see when the energy density vanishes. In this case, the function  $m$  becomes a constant, say  $M$ . One can manipulate the coupling parameters so that  $\mathcal{M}$  equals  $M$  at some finite  $x$ . This defines the event horizon of a black hole. Because the lapse function  $N$  tends to 1 when  $|x|$  approaches infinity, this metric can be interpreted as an asymptotically flat black hole spacetime. In the rest of this thesis, this interpretation of the spacetime is understood.

Due to the presence of the parameters  $a_n$ , the function  $\mathcal{M}$  is a polynomial of degree  $2k - 2$  in  $1/(x - x_o)$ . Thus the black hole spacetime allows a multi-horizon

structure for specific values of  $a_n$ . Moreover this asymptotically flat spacetime is singular at  $x = x_o$ . This point is a spacetime singularity because for any metric of the form (3.10), the Ricci scalar equals  $-\partial_{xx}N(v, x)$ . The divergence of the Ricci scalar at  $x = x_o$  suggests that we could divide the  $x$ - $v$ -plane into two separate sets along  $x = x_o$ . Each of them is interpreted as an asymptotically flat universe with a one-way-collapse solution (3.11) to (3.14). In this thesis, we shall focus on the universe  $x > x_o$  for simplicity. The calculation for the left one is analogous to that for the right universe.

Since the stress-energy tensor (3.15) describes infalling radiation in the spacetime. (this is similar to the stress tensor (2.16),) this black hole is irradiated by infalling radiation which has an energy density of  $\hat{\rho}$ . When  $\hat{\rho}$  vanishes, the function  $m(v)$  becomes a constant which is the ADM mass of the black hole [60. 44]. When  $m$  is  $v$ -dependent, it is the mass of the black hole measured by an observer at null infinity. The constants  $q$  and  $x_o$  in the solution are integration constants corresponding to the electric charge of the hole and the choice of the spatial coordinate's origin, respectively. The constant  $x_o$  will be chosen to be zero in the rest of this section without loss of generality.

Consider the matching of two patches of solution (3.11) to (3.14) along an outgoing null line  $S$  as shown in figure 3.1. This matching scheme is identical to the one used by Ori and is explained in Section 2.3 of the last chapter. This construction of the spacetime describes, in addition to influx, a null particle propagating outward between the Cauchy and event horizons. The two spacetime sectors in regions I and II share the same electric charge  $q$  and potential parameters  $a_n$  but the spacetime in region I is characterized by a mass parameter of  $m_1$ , whereas region II is distinguished by another mass parameter  $m_2$ , which is different from  $m_1$ .

According to the metric (3.10), any outgoing null line satisfies the autonomous

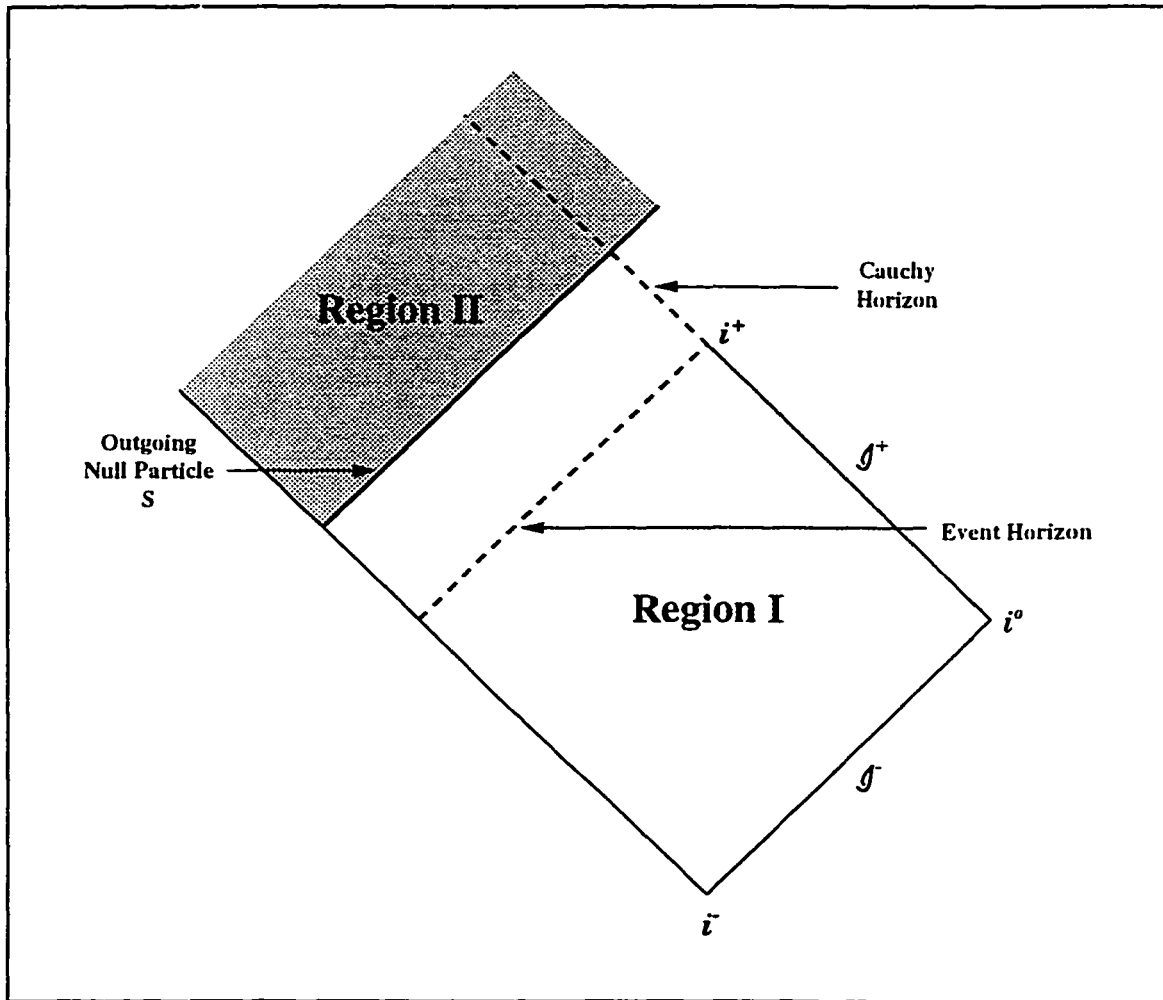


Figure 3.1: A null line  $S$  divides the spacetime into regions I and II.

differential equation

$$\frac{\dot{x}(\lambda)}{\dot{v}(\lambda)} = \frac{1}{2} N(v(\lambda), x(\lambda)) , \quad (3.17)$$

where  $\lambda$  is an affine parameter and the overdot denotes derivative with respect to  $\lambda$ . This equation is analogous to (2.67). We denote the value of the  $x$  coordinate of the outgoing null line  $S$  by a function  $X(\lambda)$  and choose the parameter  $\lambda$  to be zero at the Cauchy horizon and negative outside it.

One of the Euler-Lagrange equations for geodesics implies that the null generators for  $S$  satisfy the equation

$$\ddot{v}_i(\lambda) = -\frac{1}{2} \left[ \frac{\dot{v}_i(\lambda)}{X(\lambda)} \right]^2 [X(\lambda) \mathcal{M}'(X(\lambda)) - \mathcal{M}(X(\lambda)) + m_i(v_i(\lambda))] . \quad (3.18)$$

(One can show that the other Euler-Lagrange equation for the geodesics can be obtained by differentiating equation (3.17) with respect to  $\lambda$ .) We have used an overdot to denote the derivative with respect to  $\lambda$  and prime for the derivative with respect to  $X$ . In analogy with equation (2.72), we define

$$z_i(\lambda) \equiv \frac{X(\lambda)}{\dot{v}_i(\lambda)} \quad (3.19)$$

so that we obtain the equations

$$2 z_i(\lambda) \dot{X}(\lambda) = \mathcal{M}(X(\lambda)) - m_i(v_i(\lambda)) , \quad (3.20)$$

$$\dot{z}_i(\lambda) = \frac{1}{2} \mathcal{M}'(X(\lambda)) \quad (3.21)$$

after using (3.13), (3.17) and (3.18). We observe that this pair of equations is analogous to the pair (2.73) and (2.74). The function  $X$  is defined along the boundary between the regions I and II which are characterized by the functions  $m_i$  and  $v_i$ . The index  $i$  is either 1 or 2 for regions I or II accordingly. It follows from (3.19) to

(3.21) that

$$z_i(\lambda) = Z_i + \frac{1}{2} \int_0^\lambda \mathcal{M}'(X(\zeta)) d\zeta . \quad (3.22)$$

$$v_i(\lambda) = \int^\lambda \frac{X(\zeta)}{z_i(\zeta)} d\zeta , \quad (3.23)$$

$$m_i(v_i(\lambda)) = \mathcal{M}(X(\lambda)) - 2 z_i(\lambda) \dot{X}(\lambda) . \quad (3.24)$$

These three equations are the counterparts of those in (2.75) to (2.77). They are similar to those three in on page 42 because of the resemblance in the lapse functions  $N$ . They will determine the evolution of the spacetime once the boundary function  $X$  is known.

By using the equations (3.22) and (3.24), the “mass” of the null particle is given by

$$\Delta m(\lambda) \equiv m_2(v_2(\lambda)) - m_1(v_1(\lambda)) = 2(Z_1 - Z_2) \dot{X}(\lambda) . \quad (3.25)$$

We also define a constant

$$M \equiv m_1(v_1(\lambda)) + \delta m(v_1(\lambda)) \quad (3.26)$$

as the mass of the black hole observed in region I after the hole has absorbed all the infalling radiation of mass-energy  $\delta m$ . This equation is identical to (2.59) in which the  $\delta m$  is given by (2.60). For this (1 + 1)-dimensional spacetime, we assume that the radiation also decays at the rate

$$\delta m(v_1) = \frac{h}{v_1^{p-1}} \quad (3.27)$$

at late time, where  $h$  and  $p$  are positive constants. This ansatz is expected to be correct because the lapse function in this spacetime reads

$$N = 1 - \frac{m}{x} + O\left(\frac{1}{x^2}\right) \quad (3.28)$$

which is structurally similar to the lapse function of the Schwarzschild solution. Therefore we have reason to believe that waves propagate in a similar way in the two backgrounds. The detailed justification of (3.27) will be postponed until Chapter 5.

Equation (3.22) has an approximate solution

$$z_i(\lambda) \approx Z_i - \kappa_- X_- \lambda \quad (3.29)$$

in the neighborhood of  $\lambda = 0$ . The constant  $X_-$  denotes the position of the Cauchy horizon which corresponds to  $X(\lambda = 0)$ . This approximation is the counterpart of (2.78) in Ori's mass inflation calculation. The surface gravity  $\kappa_-$  at the Cauchy horizon is defined as

$$\kappa_- \equiv -\frac{1}{2} \frac{d}{dx} \left[ \frac{\mathcal{M}(x) - M}{x} \right] \Big|_{x=X_-} = -\frac{\mathcal{M}'(X_-)}{2X_-}. \quad (3.30)$$

This constant is always positive if  $\mathcal{M}'(X_-) \neq 0$  because the slope of the graph of  $\mathcal{M}(X)$  at  $X_-$  is negative as shown in figure 3.2. The other case where  $\kappa_- = 0$  will be studied in the last section of this chapter.

According to equations (3.23) and (3.29), in the neighborhood of  $\lambda = 0$ , we can approximate  $v_i$  as

$$v_i(\lambda) \approx \int^\lambda \frac{X_-}{Z_i - \kappa_- X_- \zeta} d\zeta = -\frac{1}{\kappa_-} \ln \left( \frac{Z_i}{\kappa_- X_-} - \lambda \right). \quad (3.31)$$

Since the Cauchy horizon corresponds to the limit  $v_1 \rightarrow \infty$ , we infer that  $Z_1$  must be zero. This also implies that  $Z_2 > 0$  in order to have a positive  $\Delta m$  in (3.25) because  $\dot{X}$  must be negative inside the black hole of the right universe.

Given the condition (3.17) for the null generators, we can write  $X$  as an asymptotic series in  $v_1$ . This condition in region I reads

$$\frac{\dot{X}(\lambda)}{\dot{v}_1(\lambda)} = \frac{1}{2} \frac{\mathcal{M}(X(\lambda)) - m_1(v_1(\lambda))}{X(\lambda)}, \quad (3.32)$$

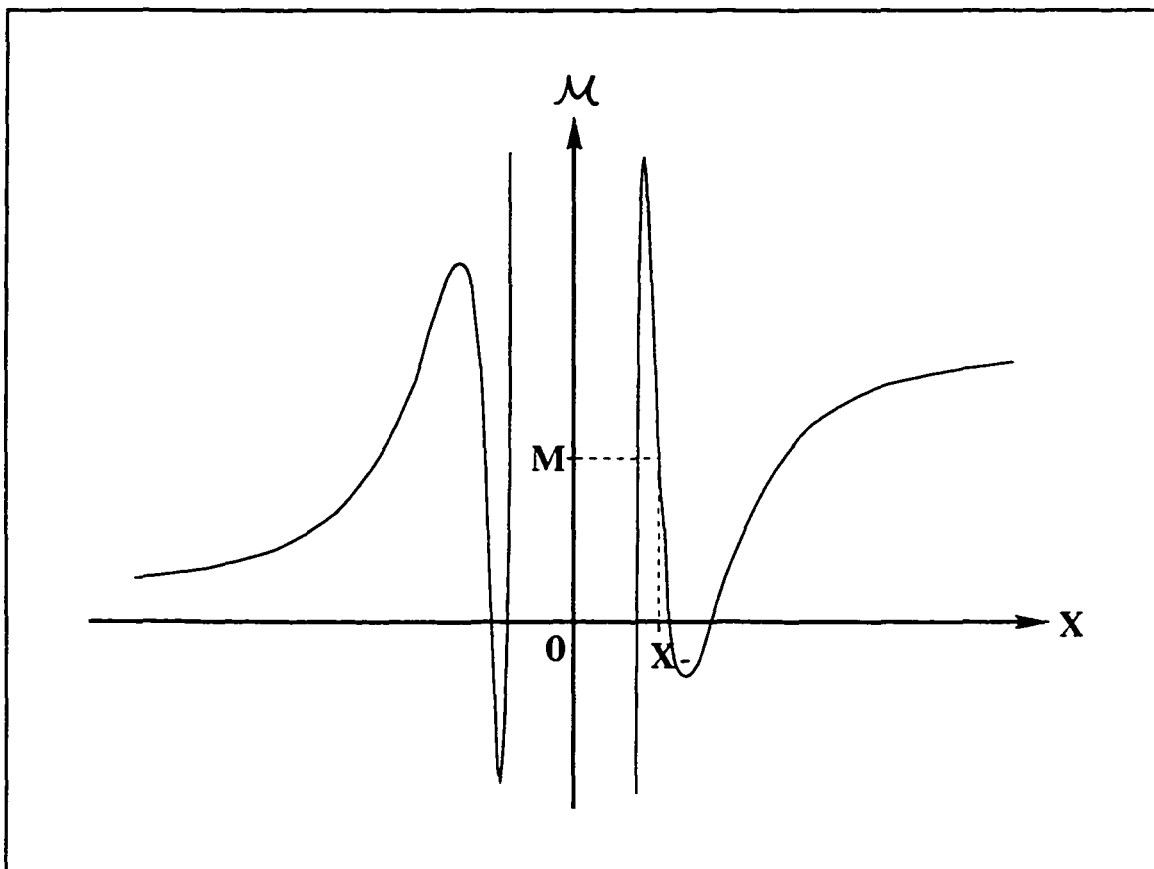


Figure 3.2: A sample graph of  $\mathcal{M}(X)$  in the first solution.

where equation (3.13) has been used. By using (3.26), the equation above can be written as

$$\delta m(v_1) = \frac{d}{dv_1} \tilde{X}^2(v_1) + M - \mathcal{M}(\tilde{X}(v_1)) \quad (3.33)$$

which is an ordinary differential equation for  $\tilde{X}(v_1)$ . The function  $\tilde{X}(v_1)$  is related to  $X(\lambda)$  via the equation  $\tilde{X}(v_1(\lambda)) = X(\lambda)$ . If we let

$$\tilde{X}(v_1) = X_- + \epsilon(v_1), \quad (3.34)$$

the function  $\mathcal{M}(\tilde{X}(v_1))$  can be expanded in a Taylor series as

$$\mathcal{M}(\tilde{X}(v)) = \mathcal{M}(X_-) + \mathcal{M}'(X_-)\epsilon(v) + \sum_{n=2}^{\infty} \frac{\mathcal{M}^{(n)}(X_-)}{n!} \epsilon^n(v) \quad (3.35)$$

when  $\epsilon$  is small enough, because  $\mathcal{M}$  is a polynomial in  $1/X$ . In the vicinity of  $X_-$ , the condition  $0 < \epsilon \ll 1$  holds. After putting this expansion into (3.33), we obtain

$$\delta m(v_1) = 2\tilde{X}(v_1)\epsilon'(v_1) - \mathcal{M}'(X_-)\epsilon(v_1) - \sum_{n=2}^{\infty} \frac{\mathcal{M}^{(n)}(X_-)}{n!} \epsilon^n(v_1) \quad (3.36)$$

because  $\mathcal{M}(X_-) = M$ . This differential equation can be solved by expressing  $\epsilon$  as a series in  $1/v_1$ , thus  $\tilde{X}$  has an asymptotic series in  $v_1$ . For the first order approximation, we have  $\delta m \approx -\mathcal{M}'(X_-)\epsilon$  which yields

$$\epsilon(v_1) \approx \frac{\delta m(v_1)}{2\kappa_- X_-}. \quad (3.37)$$

As a result, equation (3.34) becomes

$$\tilde{X}(v_1) = X_- + \frac{1}{2\kappa_- X_-} \delta m(v_1) + O\left(\frac{d}{dv_1} \delta m\right). \quad (3.38)$$

In region I, the advanced time  $v_1$  can be approximated as

$$v_1(\lambda) \approx -\frac{1}{\kappa_-} \ln|\lambda| \quad (3.39)$$

in some negative neighborhood of  $\lambda = 0$ . By using equations (3.38) and (3.39), we obtain

$$\dot{X}(\lambda) = \frac{d\bar{X}}{dv_1} \dot{v}_1(\lambda) \approx -\frac{1}{2\kappa_-^2 X_- \lambda} \frac{d}{dv_1} \delta m . \quad (3.40)$$

Therefore equations (3.25), (3.27) and (3.40) yield

$$\Delta m(\lambda) \approx -\frac{(p-1)hZ_2}{\kappa_-^2 X_- \lambda v_1^p(\lambda)} \quad (3.41)$$

which can be written as

$$\Delta m \approx \frac{(p-1)hZ_2}{\kappa_-^2 X_-} \frac{\exp(\kappa_- v_1)}{v_1^p} . \quad (3.42)$$

This expression for the mass-energy of the null particle S is identical to (2.86) and it induces mass inflation in the inner region of the black hole. When the particle S approaches the Cauchy horizon,  $v_1$  goes to infinity and triggers an exponential increase in  $\Delta m$  because  $\kappa_-$  is positive. Although  $\Delta m$  is attenuated by the term  $v_1^{-p}$ , it does not halt the inflation because  $v_1^p$  grows slower than the exponential term  $\exp(\kappa_- v_1)$ . Therefore the inner mass parameter  $m_2 = m_1 + \Delta m$  diverges at the Cauchy horizon as well.

## 3.2 Second Dilaton Background

We now consider another model in the dilaton theory in 1 + 1 dimensions. The action (3.6), when  $\gamma = 4$ ,  $\sigma = 0$  and the parameter  $Q$  is set to some positive constant, gives the field equations [58, 44]

$$0 = \nabla_b (e^{-2\phi} F_a^b) , \quad (3.43)$$

$$0 = R + 4\nabla^2\phi - 4(\nabla\phi)^2 - \frac{1}{4}F^2 + Q^2 - \sum_{n=2}^k (n-1) a_n e^{2n\phi} , \quad (3.44)$$

$$\begin{aligned}
8\pi e^{2\phi} T_{ab} &= 2\nabla_{ab}\phi - 2\nabla^2\phi g_{ab} + 2(\nabla\phi)^2 g_{ab} - \frac{1}{2}Q^2 g_{ab} \\
&\quad - \frac{1}{2}\left[F_{ac}F_b{}^c - \frac{1}{4}F^2 g_{ab}\right] - \frac{1}{2}g_{ab}\sum_{n=2}^k a_n e^{2n\phi}. \quad (3.45)
\end{aligned}$$

If the stress-energy tensor (3.15) is used, these field equations have a solution [44]

$$F_{12} = f \equiv q e^{2\phi}, \quad (3.46)$$

$$\phi = -\frac{Q}{2}(x - x_o), \quad (3.47)$$

$$N(v, x) = \frac{2}{Q} [\mathcal{M}(x) - m(v)] e^{2\phi}. \quad (3.48)$$

$$\mathcal{M}(x) = \frac{Q}{2} e^{-2\phi} \left[ 1 + \frac{q^2}{2Q^2} e^{4\phi} - \frac{1}{Q^2} \sum_{n=2}^k \frac{a_n}{n-1} e^{2n\phi} \right] \quad (3.49)$$

in the coordinate system (3.10). The constant  $q$  represents an electric charge and  $x_o$  represents the freedom in the choice of origin of the spatial coordinate. We can ensure that this solution represents a black hole spacetime by choosing the parameters  $Q$ ,  $q$  and  $a_n$  appropriately. The function  $m(v)$ , which satisfies the differential equation (3.16), is the mass of the black hole [60]. Since the stress-energy tensor (3.15) represents the ingoing radiation, this black hole (with possibly multiple horizons) is also irradiated. This spacetime is also asymptotically flat as  $x \rightarrow \infty$  but is singular when  $x$  goes to  $-\infty$ .

Consider the matching of two patches of solution (3.46) to (3.49) along an outgoing null line  $S$ . This is similar to the matching scheme we have seen in the last section. This time we define the function  $z$  as

$$z(\lambda) \equiv \frac{\exp(-2\phi(X(\lambda)))}{\dot{v}(\lambda)}. \quad (3.50)$$

The Euler-Lagrange equation for geodesics in this case reads

$$\ddot{v}(\lambda) = -\frac{[\dot{v}(\lambda)]^2}{Q} [\mathcal{M}'(X(\lambda)) - Q \mathcal{M}(X(\lambda)) + Q m(v(\lambda))] e^{2\phi(X(\lambda))} \quad (3.51)$$

along the null line S as shown in figure 3.1. The variable  $\lambda$  is the affine parameter of the null particle and it increases to zero at the Cauchy horizon. The function  $X$  equals the coordinate  $x$  along S. As a result the set of equations analogous to (3.22) to (3.24) can be obtained and reads

$$z_i(\lambda) = Z_i + \frac{1}{Q} \int_0^\lambda \mathcal{M}'(X(\zeta)) d\zeta . \quad (3.52)$$

$$v_i(\lambda) = \int^\lambda \frac{\exp(-2\phi(X(\zeta)))}{z_i(\zeta)} d\zeta , \quad (3.53)$$

$$m_i(v_i(\lambda)) = \mathcal{M}(X(\lambda)) - Q z_i(\lambda) \dot{X}(\lambda) . \quad (3.54)$$

Again we have used the subscripts 1 and 2 to distinguish the quantities  $m$ ,  $v$ ,  $z$  and  $Z$  in regions I and II. Equation (3.52) is found by calculating  $\dot{z}_i$  with the use of (3.17), (3.47), (3.48) and (3.51). We use the definition of  $z$  in (3.50) to derive (3.53). Finally by using the equations (3.17) and (3.48), we obtain equation (3.54) when we compute  $z_i \dot{X}$ .

In this case, equations (3.52) and (3.54) give the mass-energy of the null particle S as

$$\Delta m(\lambda) \equiv m_2(\lambda) - m_1(\lambda) = Q (Z_1 - Z_2) \dot{X}(\lambda) . \quad (3.55)$$

Similar to the approximation in the last section, equation (3.52) can be approximated as

$$z_i(\lambda) \approx Z_i - \kappa_- e^{-2\phi(X_-)} \lambda , \quad (3.56)$$

where the surface gravity  $\kappa_-$  reads

$$\kappa_- \equiv -\frac{1}{Q} \mathcal{M}'(X_-) e^{2\phi(X_-)} . \quad (3.57)$$

As is shown in figure 3.3,  $\mathcal{M}(X)$  at the Cauchy horizon  $X_-$  equals  $M$  and it has a negative slope there. This implies that  $\kappa_-$  is always positive. For the moment we shall consider the case  $\mathcal{M}'(X_-) \neq 0$ ; the other possibility will be investigated in the next section.

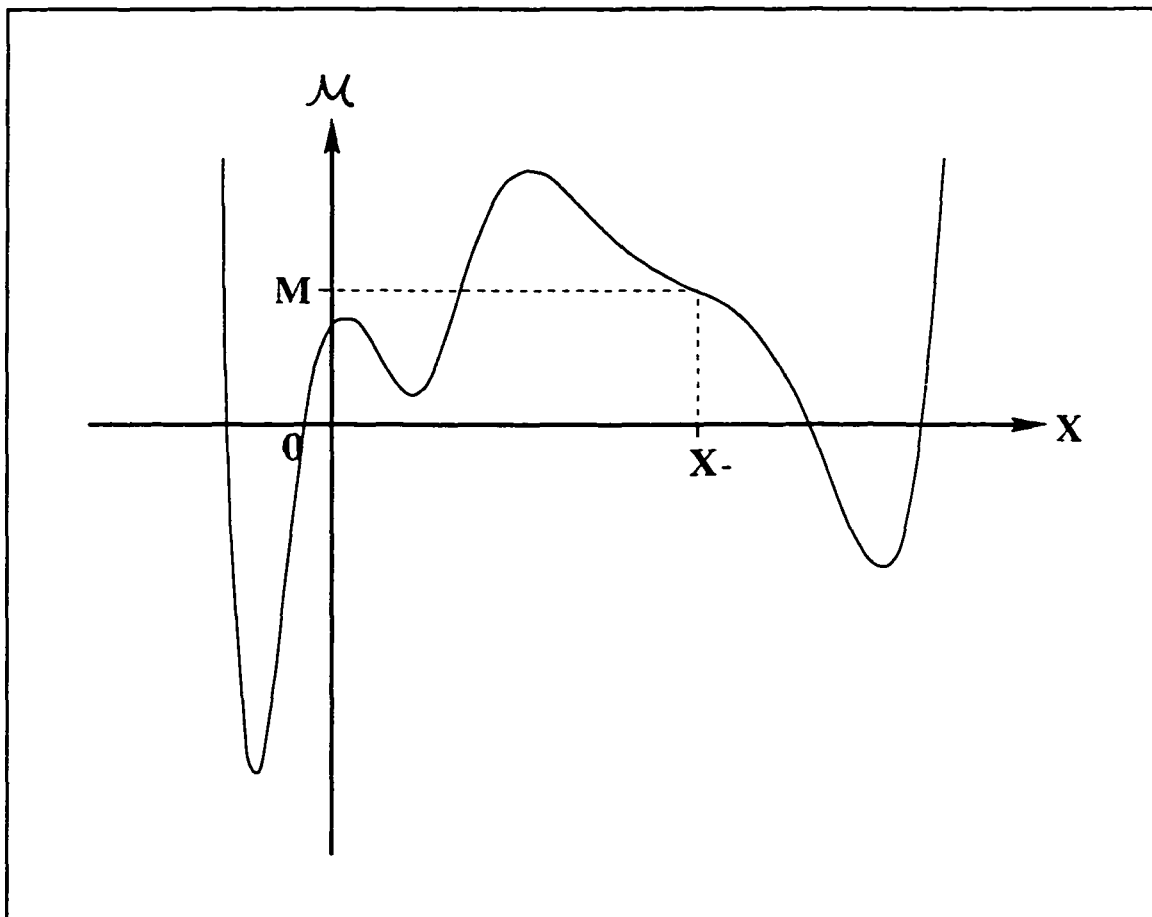


Figure 3.3: A sample graph of  $\mathcal{M}(X)$  in the second solution.

Since  $Z_1$  must be zero for the reason as that given in the previous section,  $Z_2$  is positive in order for  $S$  to have a positive energy. Moreover equation (3.53) in region

I can be approximated as

$$v_1(\lambda) \approx -\frac{1}{\kappa_-} \int^\lambda e^{2\phi(X_-) - 2\phi(X(\zeta))} \frac{d\zeta}{\zeta} \approx -\frac{1}{\kappa_-} \ln|\lambda| \quad (3.58)$$

in some neighborhood of  $\lambda = 0$ . On the other hand, when  $|\lambda| \ll 1$ ,  $z_2 \approx Z_2$  which implies

$$v_2(\lambda) \approx \int^\lambda e^{-2\phi(X_-)}/Z_2 d\zeta = e^{-2\phi(X_-)} \frac{\lambda}{Z_2}. \quad (3.59)$$

We now compute the function  $X$ . If we define a function  $\tilde{X}(v_1(\lambda)) = X(\lambda)$  and expand  $\tilde{X}$  at  $X_-$  by using the null condition (3.17), we obtain

$$\tilde{X}(v_1) = X_- + \frac{\exp(2\phi(X_-))}{Q \kappa_-} \delta m(v_1) + O\left(\frac{d}{dv_1} \delta m\right). \quad (3.60)$$

This expansion for  $\tilde{X}$  around the Cauchy horizon  $X_-$  allows us to write

$$\dot{X}(\lambda) \approx -\frac{\exp(2\phi(X_-))}{Q \kappa_-^2 \lambda} \frac{d}{dv_1} \delta m(v_1). \quad (3.61)$$

Because this (1 + 1)-dimensional spacetime is also asymptotically flat, we adopt the radiation falloff rate

$$\delta m(v) = \frac{h}{v^{p-1}} \quad (3.62)$$

which is the same as equation (3.27) in the previous section and equation (2.60) in the Reissner-Nordström background. When  $\lambda$  tends to zero from below, we find that  $\Delta m$  approximately equals

$$\Delta m(\lambda) \approx -\frac{(p-1) h Z_2 \exp(2\phi(X_-))}{\kappa_-^2 \lambda v_1^p(\lambda)}. \quad (3.63)$$

We replace  $\lambda$  by  $v_2$  using (3.59), and approximate the inner mass parameter  $m_2(v_2)$  near the Cauchy horizon as

$$m_2(v_2) \approx M - \frac{h \kappa_-^{p-1}}{|\ln|Z_2 \exp(2\phi(X_-)) v_2||^{p-1}} - \frac{(p-1) h \kappa_-^{p-2}}{v_2 |\ln|Z_2 \exp(2\phi(X_-)) v_2||^p}. \quad (3.64)$$

We conclude that in the case  $\mathcal{M}'(X_-) < 0$ , the mass in region II of this (1 + 1)-dimensional dilaton black hole spacetime becomes unbounded near the Cauchy horizon where  $v_2 = 0$ .

The divergence of the inner mass parameters in these dilaton black hole spacetimes is expected to induce a curvature singularity at the Cauchy horizon. We recall that the Ricci scalar for the spacetime of the form (3.10) is proportional to the second derivative of  $N(v, x)$  with respect to  $x$ . It is clear that the mass functions survive after differentiating the lapse functions (3.13) and (3.48) twice with respect to  $x$ . As a result, the divergence of the inner mass parameter at the Cauchy horizon is tantamount to the presence of the scalar curvature singularity there.

### 3.3 Zero Surface Gravity at Cauchy Horizon

In the last two sections, we have found that mass inflation occurs in the (1 + 1)-dimensional spacetimes (3.10, 3.13, 3.14) and (3.10, 3.48, 3.49). However, since the lapse functions we studied are polynomials of some function of  $x$  with degree greater than 2, it is possible for the surface gravity at the Cauchy horizon to be zero for certain values of the coupling parameters. This corresponds to the case when  $\mathcal{M}'(X)$  equals zero at  $X = X_-$ , according to equations (3.30) and (3.57). More generally, it is possible for the first  $n$  derivatives of  $\mathcal{M}(X)$  to be zero at the Cauchy horizon in the two dilaton solutions, where  $n$  is some positive integer. Such configurations will introduce qualitatively different behavior near the horizon.

Since  $\mathcal{M}(X)$  is a polynomial of some functions of  $x$  in both solutions, it has some finite order derivatives which are non-zero at the Cauchy horizon  $X = X_-$ . Thus we suppose there exists a positive integer  $b \geq 1$  such that for every integer  $n \in [1, b]$ , we have  $\mathcal{M}^{(n)}(X_-) = 0$  but  $\mathcal{M}^{(b+1)}(X_-) \neq 0$ . In the last two sections,

we have seen the consequence of having  $b = 0$ , namely  $\kappa_- \neq 0$ . Furthermore we also have the condition  $\mathcal{M}(X_-) = M$  as before, where  $M$  is the asymptotic mass of the black hole in region I.

In the first dilaton solution, the lapse function with constant mass can be expressed as

$$\tilde{N}(x) \equiv N|_{m=M} = \frac{\mathcal{M}(x) - M}{x} = (x - X_+)(x - X_-)^{b+1} P(x), \quad (3.65)$$

where  $X_+ > X_- > 0$  is the location of the event horizon. The function  $P$  represents the zeroes correspond to the horizons within the second (Cauchy) horizon or other complex roots of  $\tilde{N}(x)$ . The detail of this function is not important to us except for the property that it is positive definite for all  $x \geq X_-$ . It is clear from equation (3.65) that  $\tilde{N}^{(n)}(X_-) = 0$  when  $n$  is less than or equal to  $b$ . This is consistent with the definition of  $b$  which is introduced in the last paragraph. This equation also implies that  $\tilde{N}^{(b+1)}(X_-) \neq 0$ .

For the second dilaton solution, we have

$$\begin{aligned} \tilde{N}(x) &\equiv N|_{m=M} = \frac{2}{Q} [\mathcal{M}(x) - M] e^{2\phi(x)} \\ &= [e^{-2\phi(x)} - e^{-2\phi(X_+)}] [e^{-2\phi(x)} - e^{-2\phi(X_-)}]^{b+1} P(e^{-2\phi(x)}). \end{aligned} \quad (3.66)$$

Although we used  $P$  to represent the function corresponding to all other roots of  $\tilde{N}$ , the one in (3.66) is different from the one in equation (3.65). Nevertheless it is also positive definite for all  $x \geq X_-$ . The integer  $b$  given here yields the same properties on the lapse function as the one in (3.65).

After differentiating the lapse function  $\tilde{N}(x)$  in (3.65)  $b+1$  times and evaluating the result at  $X_-$ , we obtain the equation

$$\frac{\mathcal{M}^{(b+1)}(X_-)}{X_-} = (b+1)!(X_- - X_+)P(X_-). \quad (3.67)$$

The version of this equation for the second dilaton background solution reads

$$\begin{aligned} & \frac{2}{Q} \mathcal{M}^{(b+1)}(X_-) e^{2\phi(X_-)} \\ = & (b+1)! Q^{b+1} \frac{\exp(-2\phi(X_-)) - \exp(-2\phi(X_+))}{\exp(2(b+1)\phi(X_-))} P(e^{-2\phi(X_-)}) . \end{aligned} \quad (3.68)$$

Since we assume  $X_+ > X_-$ , we conclude that  $\mathcal{M}^{(b+1)}(X_-)$  must be negative for both solutions. This is true because  $P$  is positive at the Cauchy horizon and  $\exp(-2\phi)$  is an increasing function in the second solution.

In the case when the first  $b$  derivatives of  $\mathcal{M}$  at  $X_-$  vanish, equation (3.36) for the first dilaton solution becomes

$$\delta m(v_1) = 2 [X_- + \epsilon(v_1)] \epsilon'(v_1) - \frac{\mathcal{M}^{(b+1)}(X_-)}{(b+1)!} \epsilon^{b+1}(v_1) + \dots \quad (3.69)$$

One can show that this non-linear differential equation in  $\epsilon$  has a solution

$$\epsilon(v) = \left(\frac{k}{v}\right)^{1/b} + O\left(\frac{1}{v^{2/b}}\right) . \quad (3.70)$$

$$k = -\frac{2(b+1)! X_-}{b \mathcal{M}^{(b+1)}(X_-)} > 0 . \quad (3.71)$$

Unlike the case  $\mathcal{M}'(X_-) \neq 0$ , the leading order term of  $\epsilon$  is independent of the decay rate of the late time radiation  $\delta m$ . Equation (3.70) is deduced with the assumption that  $\delta m$  is proportional to  $v^{1-p}$ , where  $p \geq 4$  is a positive integer. The reason for  $p$  being at least 4 will be given in Chapter 4. Equation (3.70) indicates some of the qualitative differences between the cases of non-vanishing and vanishing surface gravity. For the second solution, it is not difficult to show that the analogue of (3.69) reads

$$\delta m(v_1) = Q e^{-2\phi(X_-)} e^{-2\phi(\epsilon(v_1))} \epsilon'(v_1) - \frac{\mathcal{M}^{(b+1)}(X_-)}{(b+1)!} \epsilon^{b+1}(v_1) + \dots . \quad (3.72)$$

where  $\epsilon(v_1) = \tilde{X}(v_1) - X_-$ . This equation has a solution

$$\tilde{X}(v_1) = X_- + \left(\frac{k}{v_1}\right)^{1/b} + O\left(\frac{1}{v_1^{2/b}}\right), \quad (3.73)$$

$$k = -\frac{(b+1)! Q \exp(-2\phi(X_-))}{b \mathcal{M}^{(b+1)}(X_-)} > 0. \quad (3.74)$$

We observe that the term  $\delta m$  also plays no role in the leading order term in (3.73). As before, we have assumed that  $\delta m$  dies off at a rate of  $O(1/v^{p-1})$ . This assumption can be relaxed to include any  $\delta m$  which decays faster than  $1/v^{(1/b+1)}$ .

When  $\mathcal{M}'(X_-) = 0$ ,  $\kappa_- = 0$  and the approximations in both (3.29) and (3.56) become poor because  $z_i$  is just a constant. In order to improve the approximation, we have to go back to the equations (3.22) and (3.52) and revise the approximation. These two equations share a common property that

$$\dot{z}_1(\lambda) \propto \mathcal{M}'(X(\lambda)). \quad (3.75)$$

By expanding  $X$  at  $X_-$ ,  $\dot{z}$  has an expansion

$$\dot{z}_1(\lambda) \propto \frac{\mathcal{M}^{(b+1)}(X_-)}{b!} \epsilon^b(\lambda) + \frac{\mathcal{M}^{(b+2)}(X_-)}{(b+1)!} \epsilon^{b+1}(\lambda) + O(\epsilon^{b+2}(\lambda)). \quad (3.76)$$

Thus we have

$$\dot{z}_1(\lambda) \approx -\left(1 + \frac{1}{b}\right) X_- \frac{1}{v_1(\lambda)} + \frac{\mathcal{M}^{(b+2)}(X_-)}{2(b+1)!} \left[\frac{k}{v_1(\lambda)}\right]^{1+1/b} \quad (3.77)$$

for the first solution and

$$\dot{z}_1(\lambda) \approx -\left(1 + \frac{1}{b}\right) e^{-2\phi(X_-)} \frac{1}{v_1(\lambda)} + \frac{\mathcal{M}^{(b+2)}(X_-)}{Q(b+1)!} \left[\frac{k}{v_1(\lambda)}\right]^{1+1/b} \quad (3.78)$$

for the second one. On the other hand, in the first solution the definition of the function  $z$  implies

$$z_1(\lambda) \approx \frac{X_-}{\dot{v}_1(\lambda)} + \left[\frac{k}{v_1(\lambda)}\right]^{1/b} \frac{1}{\dot{v}_1(\lambda)} \quad (3.79)$$

in the neighborhood of  $X_-$ . Similarly equation (3.50) of the second solution yields

$$z_1(\lambda) \approx \frac{\exp(-2\phi(X_-))}{\dot{v}_1(\lambda)} + Q e^{-2\phi(X_-)} \left[ \frac{k}{v_1(\lambda)} \right]^{1/b} \frac{1}{\dot{v}_1(\lambda)}. \quad (3.80)$$

After combining equations (3.77) and (3.79) for the first dilaton background solution or equations (3.78) and (3.80) for the second solution, we obtain a differential equation for  $v_1(\lambda)$ . It is not difficult to show that in both backgrounds we have a solution

$$v_1(\lambda) \propto \lambda^{-b} + O(\lambda^{1-b}). \quad (3.81)$$

This equation in turn implies that

$$X(\lambda) = X_- + O(\lambda). \quad (3.82)$$

According to the equations (3.25) and (3.55), the mass-energy of the outgoing null particle S is proportional to the derivative of  $X$  with respect to  $\lambda$ . When the surface gravity vanishes, the mass-energy of S becomes

$$\Delta m(\lambda) \propto 1 + O(\lambda). \quad (3.83)$$

We now see that the inner mass parameter

$$m_2(\lambda) = m_1(\lambda) + \Delta m(\lambda) \quad (3.84)$$

is bounded when S approaches the Cauchy horizon where  $\lambda = 0$ . In other words, there is no mass inflation near the Cauchy horizon when the surface gravity at the horizon vanishes.

This result should not surprise anyone because the mass inflation mechanism for non-vanishing surface gravity strongly depends on the fact that  $v_1$  is logarithmic in  $\lambda$  (equations (3.39) and (3.58)). For example, we can see that the logarithmic terms

in (3.64) enable the divergence of the inner mass parameter  $m_2$  when  $v_2$  approaches zero. This logarithmic behavior of  $v_1$  is the result of having the leading order term of  $z_1$  to be proportional to  $\lambda$ . Thus deviation from the linear behavior of  $z_1$  in  $\lambda$  is expected to alter the mass inflation mechanism. This result is true for both dilaton solutions in 1 + 1 dimensions. In contrast to that of the non-zero surface gravity case, the dominant part of the inner mass parameter with zero surface gravity is independent of the radiation residual mass  $\delta m$ .

It is worth noting that although the lapse functions are very different in the two dilaton backgrounds, the mass inflation calculations in both spacetimes resemble one another. Moreover the result of the calculations, namely the inner mass parameters, are similar in the two cases as well. This similarity has much to do with the use of the same radiation residual mass  $\delta m$ . Recall that in both dilaton spacetimes, we assume that  $\delta m$  has the form (3.27) even though the lapse functions are different. In Chapter 5, we shall see that this ansatz is not the most natural choice for the second dilaton background. After using a more reasonable  $\delta m$  in the second solution and recalculating the inner mass parameter, we shall see that the mass parameter behaves differently. Indeed the role of  $\delta m$  in the mass inflation mechanism is so important that a change in the power of the inverse power falloff ansatz could alter the conclusion. We shall demonstrate this point by considering the following in the vanishing surface gravity geometry.

In the zero surface gravity calculation, we assumed that the radiation residual mass  $\delta m(v)$  dies out at a rate faster than  $1/v^{(1+1/b)}$ . This leads to an  $\epsilon$  of order  $O(v^{-1/b})$  for both dilaton solutions. In equation (3.69), this assumption implies that the left side of the equation plays no role in the dominant part of  $\epsilon$ . For the second dilaton background, the null condition yields (3.72), and we can see that  $\delta m$  also plays no role in this background. For simplicity, we shall use the first dilaton

solution to show the resurrection of mass inflation.

We let  $\delta m$  to be proportional to  $1/v^{(1+1/b)}$  which is the critical falloff rate for mass inflation when the surface gravity vanishes. Although this rate might not be physical, we employ it only for demonstration purposes. The use of this residual mass at critical decaying rate yields a first order approximation equation

$$\delta m(v) = 2 X_- \epsilon'(v) - \frac{\mathcal{M}^{(b+1)}(X_-)}{(b+1)!} \epsilon^{b+1}(v) \quad (3.85)$$

which is similar to (3.69). In this case, the term  $\delta m$  in (3.85) cannot be ignored in the first order approximation. For concreteness, we write

$$\delta m(v) = \frac{h}{v^{1+1/b}}. \quad (3.86)$$

where  $h$  is a positive constant. It is not difficult to show that the solution for (3.85) reads

$$\epsilon(v) = \left( \frac{K}{v} \right)^{1/b}. \quad (3.87)$$

where the coefficient  $K > 0$  satisfies the algebraic equation

$$(k - K) K^{1/b} = \frac{h (b+1)!}{\mathcal{M}^{(b+1)}(X_-)}. \quad (3.88)$$

The constant  $k$  in this equation is simply the one in (3.71). When  $h$  in (3.88) vanishes,  $K$  equals  $k$  and (3.87) reduces to (3.70). At the beginning of this section, we have shown that  $\mathcal{M}^{(b+1)}(X_-)$  is negative which implies that

$$K > k > 0. \quad (3.89)$$

By using the equations (3.19) and (3.22), we obtain the equation

$$\frac{1}{\dot{v}(\lambda)} = - \left( 1 + \frac{1}{b} \right) \frac{K}{k} \int_0^\lambda \frac{d\zeta}{v(\zeta)} \quad (3.90)$$

for the leading order approximation. This equation has a solution

$$v(\lambda) = [C \lambda]^{-(\alpha+1)} . \quad (3.91)$$

The integration constant  $C$  must be negative so that the term inside the square brackets above is always positive outside the Cauchy horizon. On the other hand, the other constant  $\alpha$  satisfies the equation

$$\alpha + 1 = \frac{\frac{k}{K} \frac{b}{b+1}}{1 - \frac{k}{K} \frac{b}{b+1}} > 0 . \quad (3.92)$$

The term  $\alpha + 1$  is positive because  $b$  is a positive integer and  $k < K$ . This agrees with the fact that  $v$  in (3.91) tends to positive infinity when  $\lambda$  goes to zero from below. Finally with the help of (3.91) we can express  $\epsilon$  in (3.87) in terms of  $\lambda$  and obtain

$$\epsilon(v(\lambda)) = K^{1/b} (C \lambda)^{(\alpha+1)/b} . \quad (3.93)$$

By using equation (3.92), it is straightforward to show that

$$\frac{\alpha + 1}{b} = \left[ \frac{K}{k} + b \left( \frac{K}{k} - 1 \right) \right]^{-1} < 1 . \quad (3.94)$$

This equation implies mass inflation at the Cauchy horizon because the mass-energy of the null particle S is given by  $-2Z_2 \dot{X}(\lambda)$ . Recall that the function  $\epsilon$  is the difference between  $X(\lambda)$  and  $X_-$ . Therefore differentiating  $X$  with respect to  $\lambda$  is equivalent to calculating  $\dot{\epsilon}(\lambda)$ . Since  $(\alpha + 1)/b$  is less than unity according to (3.94), we conclude that  $\dot{\epsilon}(\lambda)$  must be divergent as  $\lambda \rightarrow 0^-$ . This implies the divergence of  $\Delta m$  and  $m_2$  when S approaches the Cauchy horizon.

In this calculation for vanishing surface gravity at the Cauchy horizon, we have learned two important lessons. We now understand that the detailed geometry of the black hole could affect the mass inflation mechanism. This is similar to the case

in the Reissner-Nordström-de Sitter background in 3 + 1 dimensions [61]. Merely having a Cauchy horizon and cross-flowing radiation do not guarantee the phenomenon. The question of how the lapse function behaves at the horizon should be taken into account in the analysis. Secondly the role played by the residual radiation mass  $\delta m$  deserves further investigation. In the previous calculation, we have witnessed a competition between the falloff of the residual mass and a growing term due to the geometry of the spacetime. If  $\delta m$  shrinks too fast, mass inflation simply does not occur which gives regularity of spacetime at the Cauchy horizon. On the other hand, when the attenuation from the residual mass is weak enough, the phenomenon resumes and produces a scalar curvature singularity at the hypersurface.

The two (1 + 1)-dimensional spacetimes studied in this chapter are not the only spacetimes with vanishing surface gravity at the Cauchy horizon. In 3 + 1 dimensions, the extremal Reissner-Nordström black hole also has zero surface gravity at the Cauchy horizon. In this case, the metric is given by equations (2.4) and (2.5) with  $q^2 = M^2$ . The conformal diagram for this extremal Reissner-Nordström black hole is shown in figure 3.4 [6](p. 160). Since the lapse function can be rewritten as

$$N(\tau) = \left(1 - \frac{M}{\tau}\right)^2, \quad (3.95)$$

it is clear that the surface gravity  $\kappa = -N'(\tau)/2$  vanishes at the Cauchy horizon  $\tau = M$ . Although this spacetime has a property of zero surface gravity at the Cauchy horizon, we shall not use it as a background spacetime for demonstrating the mass inflation phenomenon. In order to carry out a mass inflation calculation, we must turn the static Reissner-Nordström spacetime into a charged Vaidya spacetime

near the Cauchy horizon. This charged Vaidya spacetime has a mass parameter

$$m(v) = M_e - \delta m(v) . \quad (3.96)$$

Since we would like to have a vanishing surface gravity at the Cauchy horizon, we must have  $q^2 = M_e^2$ . That is to say  $m \rightarrow M_e = |q|$  as  $v$  goes to infinity. Since the mass  $m$  is an increasing function, at any finite advanced time  $v$ , we have  $m < |q|$ . This inequality says that the spacetime is not a black hole spacetime at any finite time; rather it is a naked singularity spacetime [2](p. 315). In other words, in order to have  $\kappa = 0$  at the Cauchy horizon of a Reissner-Nordström spacetime with constant  $q$ , one must begin with a naked singularity spacetime, i.e. with no black hole! Indeed one can construct a black hole spacetime with zero surface gravity at the Cauchy horizon by introducing a charge current in the spacetime. However the problem will become too complicated for demonstrating mass inflation. The two spacetimes studied in this chapter do not have the naked singularity problem because the Cauchy horizons are always *inside* the event horizons.

In the next section we shall leave the problem of mass inflation temporarily and consider the falloff behavior of  $\delta m$  in a more elegant fashion.

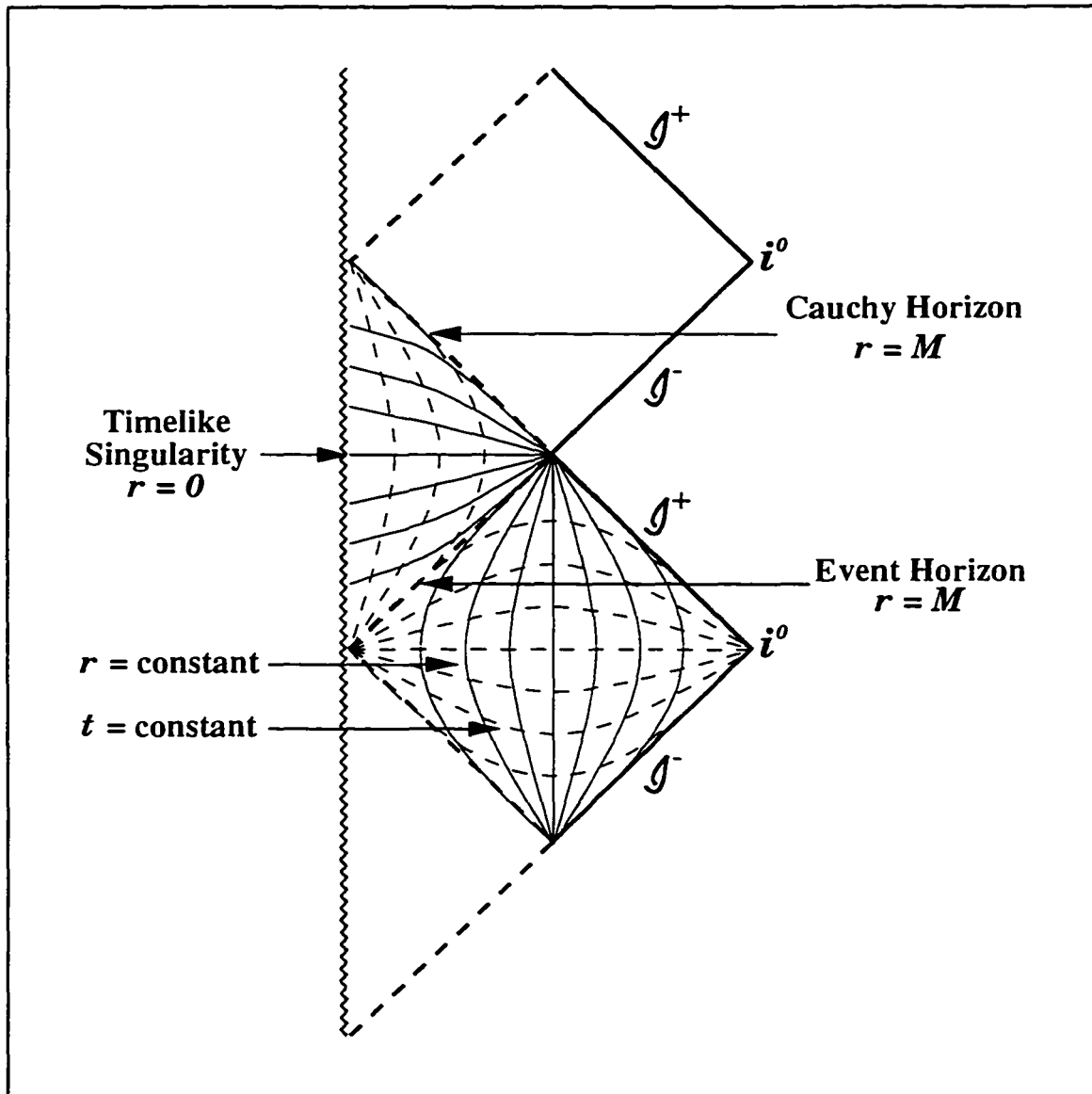


Figure 3.4: Conformal diagram for an extremal Reissner-Nordström black hole.

## Chapter 4

# Scalar Waves in $D + 1$ Dimensions

In the last chapter we have seen that mass inflation takes place in (1+1)-dimensional dilaton spacetimes. This is true at least in the case when the surface gravity at the Cauchy horizon is non-vanishing. However when the surface gravity of the inner horizon vanishes, the mechanism can change radically.

In the investigation, we have taken for granted that the late time radiation falloff rate obeys an inverse power law so that

$$\frac{d}{dv}m(v) \sim \frac{1}{v^p} . \quad (4.1)$$

The rate of change of the mass is decreasing because  $p$  is a positive integer and  $v$  increases with time. This result was first discovered by Richard Price in the early seventies when he studied perturbations near a Schwarzschild black hole [20]. The number  $p$  is determined by the mode of the radiation, namely  $p = 2(2l + 2)$ , where  $l$  is the mode of the spherical harmonics. As was mentioned in Chapter 1, the presence of the radiation is a consequence of the gravitational perturbation which originates from the spacetime asymmetry. The gravitational wave which

corresponds to  $l = 2$  implies that  $p = 12$  in  $3 + 1$  dimensions. In the last chapter, we chose  $p \geq 4$  instead of 12 because the  $(1 + 1)$ -dimensional spacetime has no rotational degrees of freedom. This accounts for the use of  $l = 0$  in  $1 + 1$  dimensions.

Since the two solutions of the dilaton black holes in  $1 + 1$  dimensions are also asymptotically flat, we employed the radiation falloff rate (4.1) for the exterior mass in the last chapter. Asymptotic flatness was believed to be relevant because the late time behavior of the radiation at a point is dominated by the waves that have traveled a large distance. A brief explanation of this can be found in [38].

In Section 3.3, we have seen that the radiation falloff rate can affect the result of mass inflation calculations. This is the case at least when the surface gravity at the Cauchy horizon becomes zero. It is thus important to ensure that the use of equation (4.1) in the calculation is reasonable. The purpose of this chapter is to investigate the circumstances under which this is the case for a general class of asymptotically flat spacetimes. The results we obtain confirm those obtained previously in more restricted contexts by Price [20] and by Ching et. al. [38]. However the analytic methods used in this chapter are quite different from those in the literature. Furthermore, they provide a cross-check for the numerical methods used. These methods will be employed in later chapters for spacetimes which are not asymptotically flat.

Before we justify the use of (4.1) as the late time radiation decay in  $(1 + 1)$ -dimensional dilaton spacetimes, let us consider a wave propagation problem in this chapter. In Section 4.1, we shall formulate the wave propagation problem in  $D + 1$  dimensions mathematically. This formulation provides the basis for analytic study and numeric simulation in the rest of this thesis. Since Price's inverse power falloff rate for the late time radiation is important in the mass inflation calculation, we shall give a review of this falloff rate in Section 4.2. However the demonstration of

the inverse power decay will be done in a Schwarzschild-like black hole in  $D + 1$  dimensions, where  $D$  is an odd integer.

## 4.1 General Setup

We shall study the scalar wave equation in arbitrary dimensions because black holes in  $2 + 1$  dimensions will be considered later in this thesis. Strictly speaking we should consider the wave equation of a spin-2 field which is an appropriate description for the gravitational radiation. A massless scalar wave is studied in this thesis as an analogue of the gravitational wave because the field equation for the scalar wave not only captures the essential features of the spin-2 wave [23]. [37](p. 244) but is mathematically simpler than that for the spin-2 wave [62. 63]. Moreover, by using the scalar wave equation, the results obtained in this chapter are directly comparable to those in [20, 38]. For the number of spatial dimensions  $D$  being a positive integer greater than or equal to 1, the scalar wave equation in  $D + 1$  dimensions reads

$$\nabla^2 \Psi = \xi R \Psi \quad (4.2)$$

where  $\xi$  is an arbitrary constant. If this constant equals to  $(D - 1)/(4D)$ , equation (4.2) will be conformally invariant [2](p. 447).

We simplify the problem by considering static, spherically symmetric  $(D + 1)$ -dimensional spacetimes which have metrics of the form

$$ds^2 = -N(r) dt^2 + \frac{dr^2}{N(r)} + r^2 d\Omega_{D-1}^2. \quad (4.3)$$

The function  $N$  is the lapse function of the spacetime and  $d\Omega_{D-1}^2$  is the metric of a  $(D - 1)$ -dimensional unit sphere. This metric (4.3) is sufficient for the discussion

in the rest of the thesis. Further simplification can be made if we assume

$$\Psi = r^{(1-D)/2} \psi(t, r) Y_l^D . \quad (4.4)$$

The parameter  $l$  only admits non-negative integer values because the functions  $Y_l^D$  are the  $D$ -dimensional spherical harmonics which satisfy the equation

$$\hat{L}^2 [Y_l^D] = -l(l + D - 2) Y_l^D . \quad (4.5)$$

The product  $-l(l + D - 2)$  is the eigenvalue of the operator  $\hat{L}^2$  which is the angular derivative operator. In fact, equation (4.5) can be derived from the scalar equation  $\nabla^2 (r^l Y_l^D) = 0$  in  $D$ -dimensional *Euclidean* space. It is straightforward to show that equation (4.2) reduces to the following equation after the use of the aforementioned simplifications:

$$-\partial_{tt}\psi(t, r) + N(r) \partial_r [N(r) \partial_r \psi(t, r)] - N(r) V_c(r) \psi(t, r) = 0 . \quad (4.6)$$

The function  $V_c(r)$  in (4.6) is defined as

$$\begin{aligned} V_c(r) \equiv & \xi R + \frac{D-1}{2r} \frac{d}{dr} N(r) + \frac{(D-3)(D-1)}{4r^2} [N(r) - 1] \\ & + \frac{(2l + D - 3)(2l + D - 1)}{4r^2} \end{aligned} \quad (4.7)$$

in which the Ricci scalar in  $D + 1$  dimensions with metric (4.3) is given by

$$R = \frac{1}{r^{D-1}} \frac{d^2}{dr^2} \left\{ r^{D-1} [1 - N(r)] \right\} . \quad (4.8)$$

One can rewrite the wave equation (4.6) as

$$-\partial_{tt}\psi(t, r) + N(r) \mathcal{L}[\psi(t, r)] = 0 \quad (4.9)$$

with the help of the spatial differential operator

$$\mathcal{L} \equiv \partial_r [N(r) \partial_r] - V_c(r) . \quad (4.10)$$

Alternatively if we introduce the tortoise coordinate

$$\rho \equiv \int \frac{dr}{N(r)}. \quad (4.11)$$

equation (4.6) can be written as

$$\partial_{tt}\psi(t, \rho) - \partial_{\rho\rho}\psi(t, \rho) + V(\rho)\psi(t, \rho) = 0. \quad (4.12)$$

The function  $V$  which is defined as

$$V(\rho) \equiv N(\tau(\rho)) V_c(\tau(\rho)) \quad (4.13)$$

plays the role of a potential which is induced by the background spacetime geometry. Although the potential  $V$ , when it is written in terms of  $\rho$ , can be very complicated, equation (4.12) has the familiar form of a potential scattering problem. By using the retarded time  $u = t - \rho$  and advanced time  $v = t + \rho$ , equation (4.12) admits another form

$$\partial_{uv}\psi(u, v) = -\frac{1}{4} N(\tau(u, v)) V_c(\tau(u, v)) \psi(u, v). \quad (4.14)$$

In this thesis, we shall solve the scalar wave equation (4.2) by using either equation (4.9), (4.12) or (4.14), or a combination of these equations.

In the case of the Schwarzschild background, the graph of  $V$  has a sharp peak (see figure 4.1) which can be thought of as a barrier. Since the lapse function for the Schwarzschild spacetime is given by  $N(r) = 1 - 2M/r$ , we have

$$\rho = \tau + 2M \ln \left| \frac{r}{2M} - 1 \right| \quad (4.15)$$

which spans the whole real line for  $2M < r < \infty$ . By using the equation (4.7), we obtain

$$V = N(r) V_c(r) = \left( 1 - \frac{2M}{r} \right) \left[ \frac{l(l+1)}{r^2} + \frac{2M}{r^3} \right]. \quad (4.16)$$

This potential tends to zero when  $\rho$  goes to negative infinity ( $r \rightarrow 2M$ ) and positive infinity ( $r \rightarrow \infty$ ) but it has a peak at finite distance. Figures 4.2 and 4.3 show the same potential barrier but in differing length scales. The barrier in figure 4.2 is shown in a *semi-log* scale which reveals the fact that  $V$  goes to zero exponentially as  $\rho \rightarrow -\infty$ . It is interpreted this way because a straight line on a graph in this scale represents exponential growing or shrinking. On this graph, the straight line has a slope of about  $300/1400 \approx 0.21 \approx 0.5 \log(e)$ . This number can be explained as the following. First of all, figures 4.1 to 4.3 are drawn by using the value  $M = 1$ . When  $\rho$  tends to negative infinity (this is equivalent to  $r \rightarrow 2M$  from above),  $V$  goes to zero due to the decrease of the factor  $N(r)$ . By using the equation (4.15), we can write  $N = 2M \exp((\rho - r)/(2M)) / r$  which tends to  $\exp(\rho/(2M) - 1)$  when  $r \rightarrow 2M$ . Therefore the potential  $V$  should increase at a rate  $\exp(\rho/(2M))$  near  $r = 2M$ . By converting this rate into  $10^{\log(e)\rho/(2M)}$ , we can see that the graph represents the exponential increase of  $V$  correctly.

On the other hand, the straight line with negative slope in figure 4.3 implies that when  $\rho \rightarrow \infty$ ,  $V$  tends to zero at a rate inversely proportional to some power of  $\rho$ . Note that this straight line has a different interpretation because figure 4.3 is in a *log-log* scale. According to the graph, the slope is roughly  $-5/2.5$  which implies that  $V \sim 10^{-2 \log(\rho)}$  at large distance. This is consistent with equation (4.16) because  $V = O(1/r^2)$  at large  $r$  and  $\rho \approx r$  for large  $r$ .

Equation (4.12) can be integrated numerically by using the finite difference method [64](p. 2). We first discretize the D'Alembert operator  $\partial_{tt} - \partial_{\rho\rho}$  as

$$\begin{aligned}
 (\partial_{tt} - \partial_{\rho\rho})\psi(t, \rho) \mapsto & \frac{\psi(t - \Delta t, \rho) - 2\psi(t, \rho) + \psi(t + \Delta t, \rho)}{(\Delta t)^2} \\
 & - \frac{\psi(t, \rho - \Delta\rho) - 2\psi(t, \rho) + \psi(t, \rho + \Delta\rho)}{(\Delta\rho)^2} \\
 & + O((\Delta t)^2) + O((\Delta\rho)^2)
 \end{aligned} \tag{4.17}$$

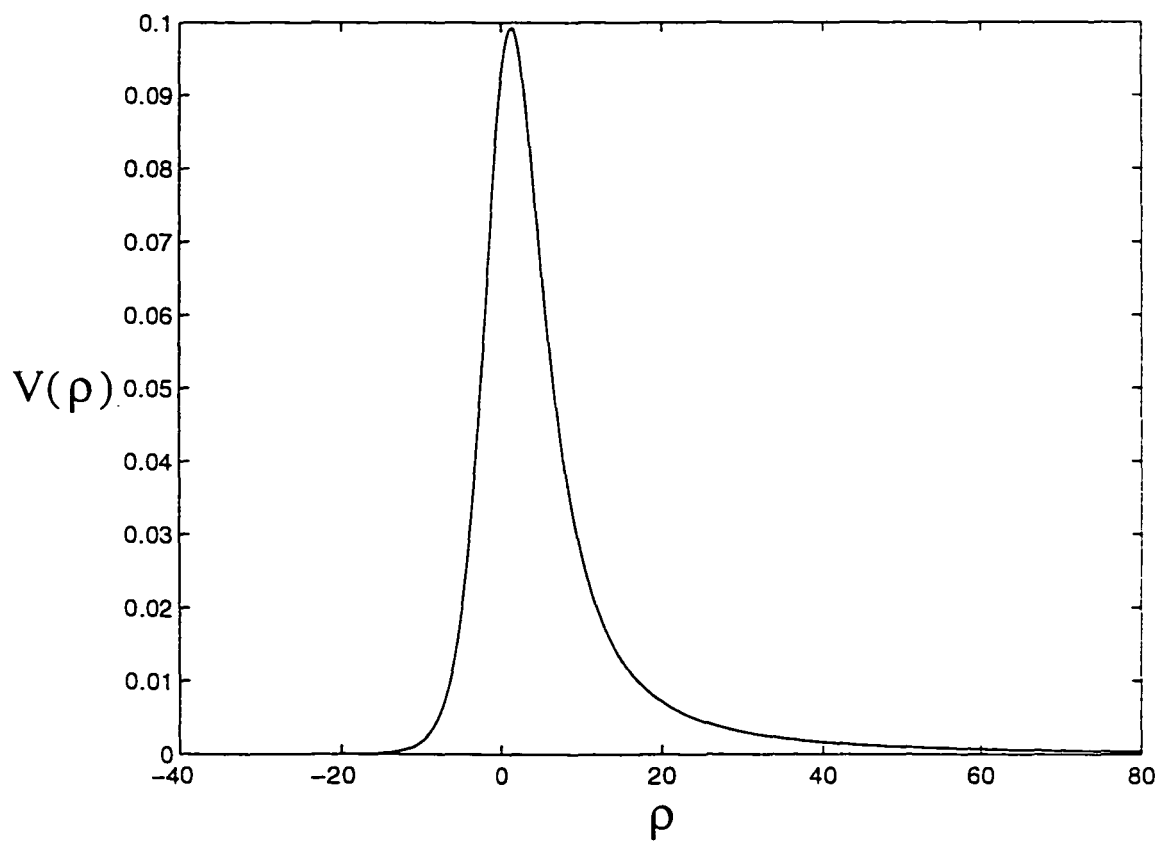


Figure 4.1: Potential for the Schwarzschild background.

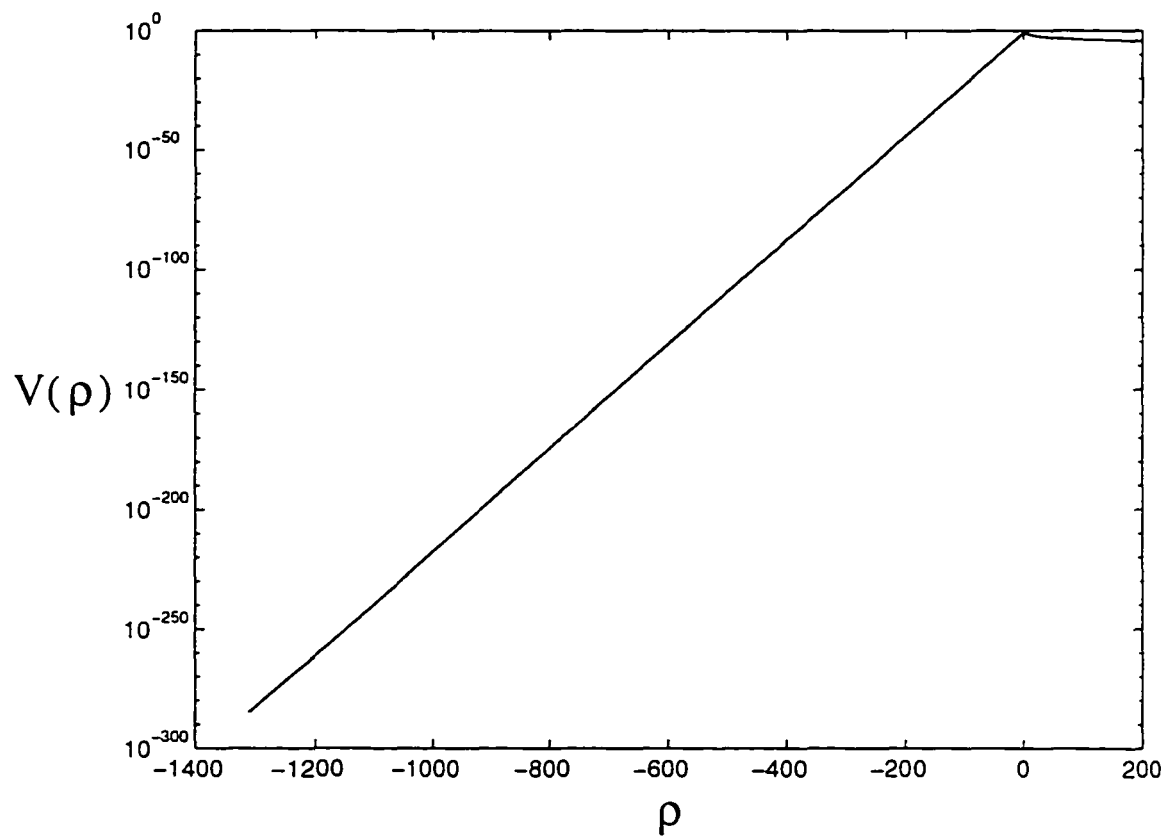


Figure 4.2: The potential  $V$  in figure 4.1, but in a semi-log scale.

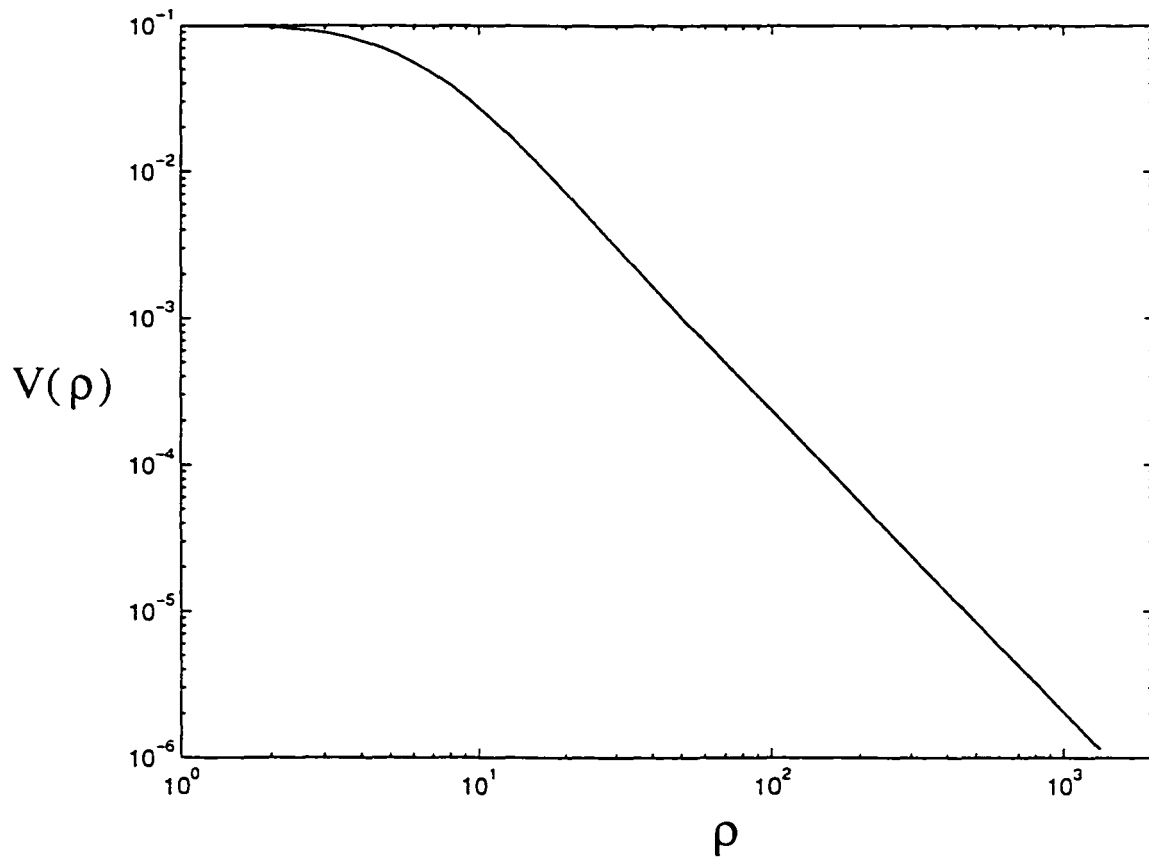


Figure 4.3: The potential in figure 4.1, but in a log-log scale. Only positive  $\rho$  is shown in this graph.

by using Taylor's theorem. In order to formulate a well-posed Cauchy problem, we must include the initial conditions on the field  $\psi$  as part of the problem. For simplicity we choose these conditions to be

$$\psi(t = 0, \rho) = 0 \quad (4.18)$$

$$\partial_t \psi(t = 0, \rho) = u(\rho) \quad (4.19)$$

in the rest of the thesis. In this thesis we shall employ a Gaussian distribution with finite support for  $u(\rho)$ . We shall see, in the Green's function approach, that the time response of the field  $\psi$  is dictated by the Green's function. The initial conditions turn out to be some scaling factors which are time-independent. Since we are only interested in the late time response of the wave, the details of the initial condition are not important to us.

Discretizing condition (4.19) yields

$$\frac{\psi(\Delta t, \rho) - \psi(-\Delta t, \rho)}{2 \Delta t} = u(\rho) + O(\Delta t^2) . \quad (4.20)$$

After dividing the upper half of the  $\rho$ - $t$ -plane into meshes of size  $\Delta\rho \times \Delta t$ , we define the following:

$$\psi(m \Delta t, n \Delta\rho) \equiv \psi_{m,n} , \quad (4.21)$$

$$V(n \Delta\rho) \equiv V_n , \quad (4.22)$$

$$u(n \Delta\rho) \equiv u_n , \quad (4.23)$$

where  $m \in \mathbb{Z}^+$  and  $n \in \mathbb{Z}$ . The mesh size has to satisfy the condition  $\Delta\rho \geq \Delta t$  so that the numerical rate of propagation of data is never smaller than its analytical counterpart [64](p. 53). The discretization of the Cauchy problem above then

implies

$$\psi_{-1,n} = -\Delta t u_n, \quad (4.24)$$

$$\psi_{0,n} = 0, \quad (4.25)$$

$$\psi_{m+1,n} = \left[ 2 - 2 \frac{\Delta t^2}{\Delta \rho^2} - \Delta t^2 V_n \right] \psi_{m,n} - \psi_{m-1,n} + \frac{\Delta t^2}{\Delta \rho^2} [\psi_{m,n-1} + \psi_{m,n+1}]. \quad (4.26)$$

As a result, we can follow the evolution of the field  $\psi$  from the time  $t = 0$  to arbitrarily late times, within the capability of the computer.

In the case when the black hole geometry is asymptotically flat, the tortoise coordinate  $\rho$  goes from negative infinity to positive infinity. Our Cauchy problem is similar to the infinite string problem in which the initial data propagates towards the left and right indefinitely. The initial data does not propagate in both directions indefinitely when the background is asymptotically anti-de Sitter. In this type of black hole spacetime, the tortoise coordinate goes from minus infinity to zero in the exterior region of the black hole. (It is possible for the tortoise coordinate to be semi-infinite even when the spacetime is not asymptotically anti-de Sitter [65, 66].) In this case, the right-propagating data cannot travel in the positive direction forever. In analogy with the semi-infinite vibrating string problem, a boundary condition at spatial infinity (i.e.  $\rho = 0$ ) is needed in order to formulate the problem appropriately. There are two types of boundary condition that are widely used in the anti-de Sitter backgrounds: the Dirichlet and Neumann conditions [67]. In our case, the former reads

$$\psi(t, \rho = 0) = 0 \quad (4.27)$$

while the latter is simply

$$\partial_\rho \psi(t, \rho = 0) = 0. \quad (4.28)$$

We shall employ either one of these conditions for our analytic and numeric computations whenever a boundary condition at spatial infinity is needed.

## 4.2 Waves in Schwarzschild-like Background

In this section we shall study the behavior of radiation falloff in asymptotically flat background spacetimes which resemble the Schwarzschild spacetime. As we have seen in the previous chapters, the radiation falloff rate in late time is important in the mass inflation calculation. In particular, it is the inverse power rate of radiation attenuation that makes mass inflation possible. We shall present the results of the numerical calculation first because this will give the readers a better idea of how the radiation decays at an inverse power rate, and what the late time radiation is.

Figure 4.4 shows a sample of an inverse power decay for a scalar wave in the Schwarzschild background of mass  $M$ . We solve the wave equation (4.12) numerically using the scheme discussed in the previous section. The compact initial Gaussian impulse is centered at a distance  $r = 10 M$  (or  $\rho = 12.76 M$ ). For simplicity we choose  $l = 1$  for the spherical harmonic and mass  $M = 1$ . In fact the potential barrier shown in figures 4.1 to 4.3 is created by using these values of the parameters. Since the background is a Schwarzschild spacetime, the Ricci scalar vanishes and the choice of  $\xi$  becomes irrelevant. Figure 4.4 depicts how the magnitude of the scalar field  $\psi$  at a distance  $r = 20 M$  (i.e.  $\rho = 24.40 M$ ) evolves in time. We can see that the disturbance of the initial impulse (which is centered at  $r = 10 M$ ) takes about 10 units of time to reach the observation point  $r = 20 M$ . Prior to  $t = 200$  the field's intensity decreases and the decay is accompanied by oscillation of the quasi-normal modes [38]. After  $t = 200$  the scalar field dies out monotonically at a rate inversely proportional to time  $t$ . It is this portion of the

graph  $t \gg M$  that corresponds to the *late time radiation falloff*.

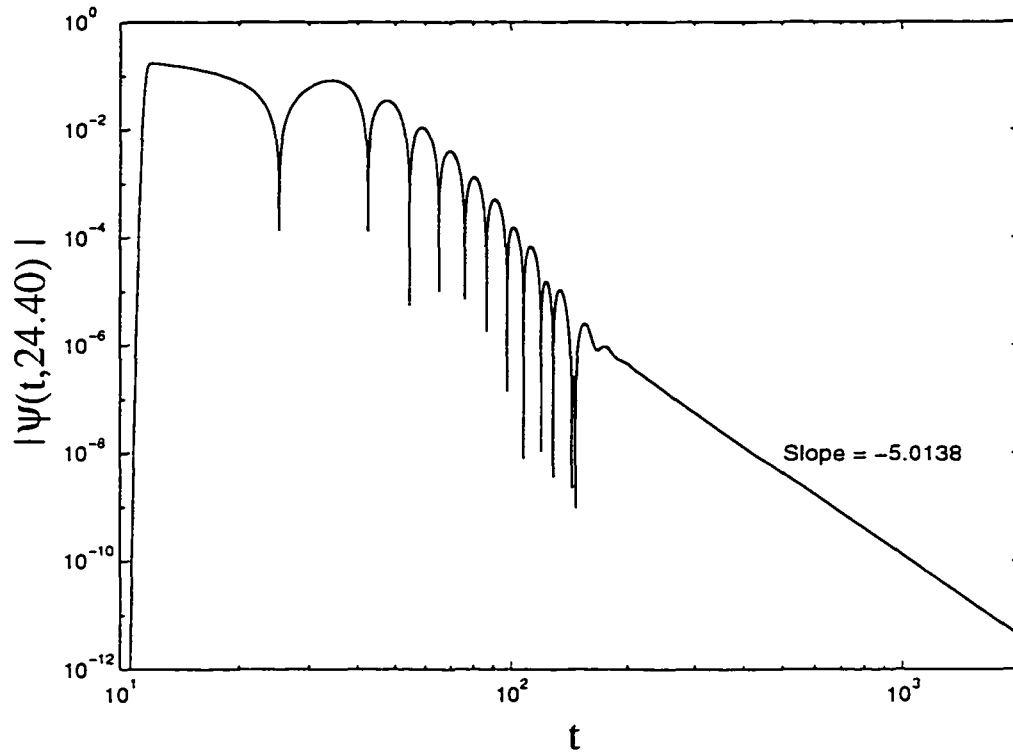


Figure 4.4: The decay of a scalar wave in Schwarzschild background with  $l = 1$ .

Indeed the “late time” is not really late after all. If we had a Schwarzschild black hole of 1000 solar masses and a scalar wave impulse was emitted at a distance  $r = 10 M$  which is about  $1.5 \times 10^4$  kilometers, figure 4.4 says that an observer at a distance  $20 M$  (about  $3 \times 10^4$  km) away would start seeing the monotonic decay of the wave at the time one second after the emission of the impulse. (The time scale in this case is given by  $1000 M_{\odot} \times G/c^3 \approx 0.0049$ , where  $M_{\odot}$  is a solar mass.) In other words, the quasi-normal ringing phenomenon lasts only about one second, followed by the late time inverse power falloff of the wave. By using the linear

regression technique, we find the slope of the straight line on the graph to be  $-5.01$ , in agreement with the analytic prediction of  $-(2l + 3)$  [20]. Figure 4.5 shows another decay of scalar wave which has a late time falloff rate of  $-3.02$ . This rate also agrees with the analytic prediction because this diagram is the ( $l = 0$ )-analogue of figure 4.4. (That is to say figure 4.5 corresponds to a simulation using  $l = 0$ .  $M = 1$ , initial impulse at  $r = 10 M$  and observation at  $r = 20 M$ .)

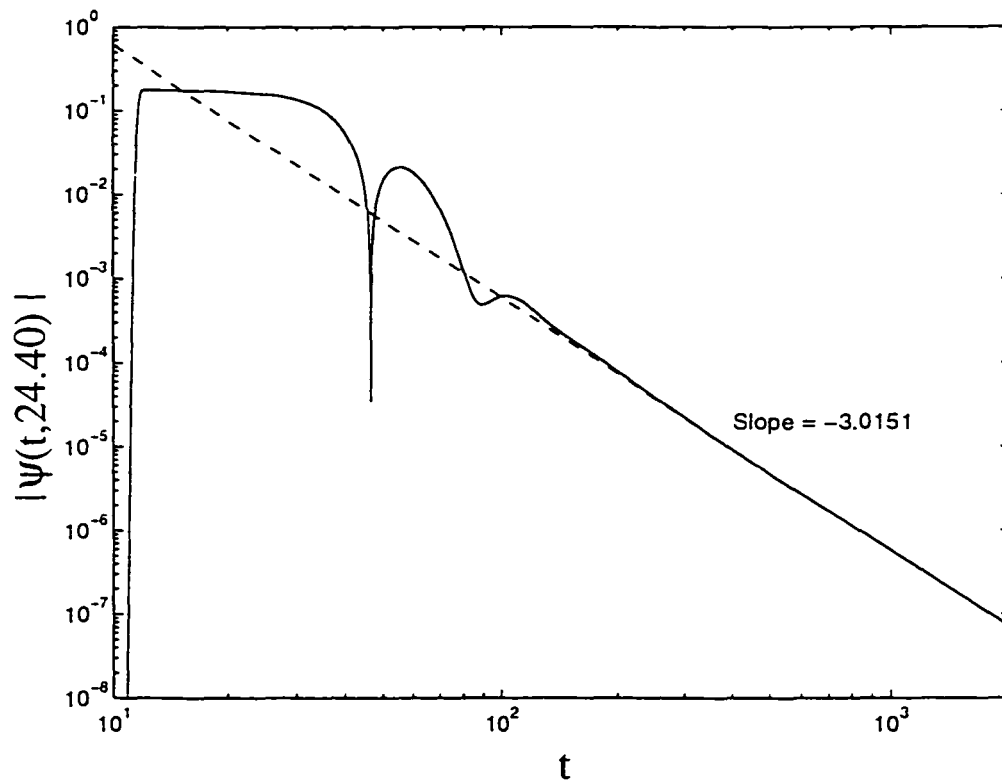


Figure 4.5: The decay of a scalar wave in Schwarzschild background with  $l = 0$ .

Figure 4.5 represents a case where the initial impulse is placed outside the peak of the potential barrier, and the observation is made further away from the barrier.

In the mass inflation process, the relevant decaying ingoing radiation must be found near the Cauchy horizon which is inside the black hole. However the result shown in figure 4.5 is obtained far away from the Schwarzschild black hole. Therefore it might be invalid to use the inverse power decay rate, which is obtained outside the event horizon, for the radiation inside the black hole. Figure 4.6 shows another numerical simulation in the Schwarzschild background with  $l = 0$ . The initial impulse is also placed at  $r = 10 M$  in this case but the observation is made at a distance  $r = 2.000002 M$  ( $\rho = -25.65 M$ ). In other words, the observer is very close to the event horizon of the black hole, and he or she is on the left side of the potential barrier. It is clear from the diagram that the late time radiation falloff also decreases at the inverse power rate  $-(2l + 3)$ . In other words, the gravitational red shift at the event horizon does not alter the falloff rate in the Schwarzschild background. Therefore it is valid to employ the inverse power rate for the radiation decay in the mass inflation calculation.

We are now ready to analytically demonstrate Price's inverse power radiation falloff rate. The method shown here is similar to those in [20, 68] but an asymptotic matching argument is used in this thesis. Let us consider a scalar wave in a  $(D + 1)$ -dimensional background which is asymptotically flat. For the remainder of this chapter we shall restrict ourselves to the case where the number of spatial dimensions  $D$  is odd. The motivation of this restriction is closely related to Huygen's Principle, which implies that the scalar wave obeying the equation  $\nabla^2 \Psi = 0$  always develops a tail when the number of spatial dimensions is even, regardless of whether or not the asymptotically flat background is sourceless [69](p. 291). The method used in this section cannot be applied to even spatial dimensions because the method makes use of the absence of radiation tails in the flat spacetime. This weakness of the method will be apparent when it is discussed in detail. Neverthe-

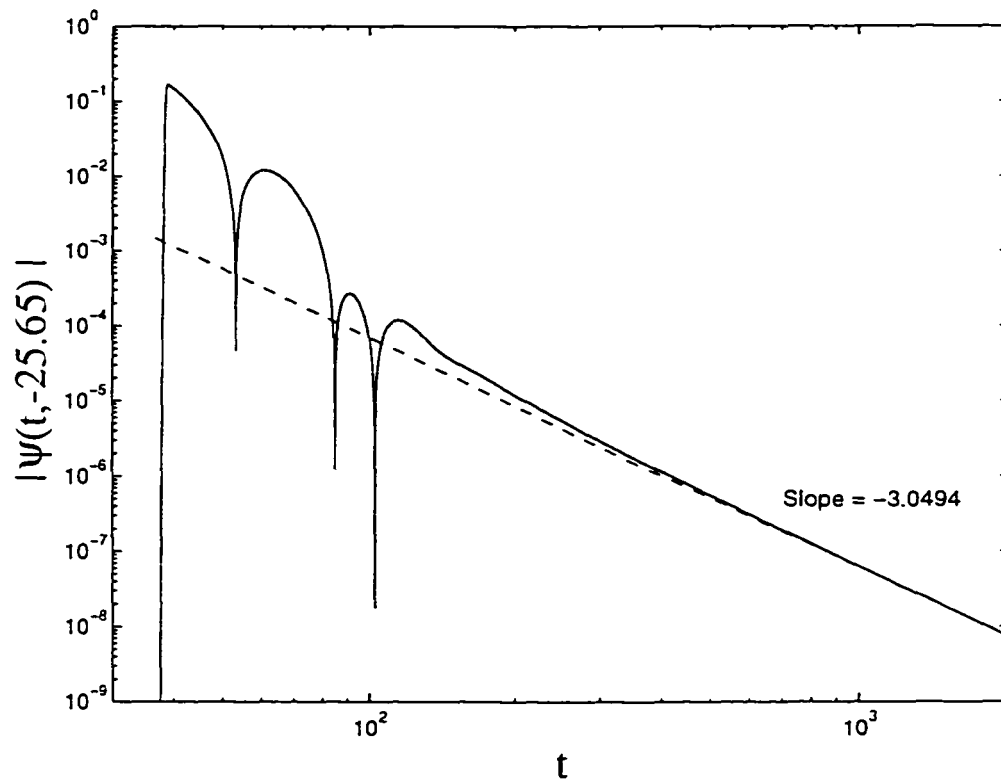


Figure 4.6: The decay of a scalar wave in Schwarzschild background with  $l = 0$ . In this case, the observation of the decay is made at a point close to the event horizon.

less, we shall study the radiation falloff and mass inflation in a  $(2 + 1)$ -dimensional black hole in a later chapter, and another method for calculating the radiation falloff rate will be discussed.

We consider a static, spherically symmetric spacetime with metric of the form (4.3). Inspired by the work of Ching et. al. [38, 70], the lapse function we shall study is generalized to the form

$$N(r) = 1 - \frac{m}{r^\alpha} \left( \ln \left| \frac{r}{R_o} \right| \right)^\beta. \quad (4.29)$$

The constants  $\alpha$  and  $\beta$  are integers, where  $\beta \geq 0$  but  $\alpha > 0$ . The other constant  $m$  is a positive real number. When we have  $\alpha = 1$ ,  $\beta = 0$  and  $D = 3$ , this lapse function reduces to the one in Schwarzschild spacetime of mass  $m/2$ . The constant  $R_o$  is a scale constant so that  $r/R_o$  is dimensionless. We suppose this lapse function represents a black hole spacetime for appropriate values of  $m$ ,  $\alpha$ ,  $\beta$  and  $R_o$ . We shall find the falloff pattern of the scalar wave in this black hole background. Although the form of (4.29) is more general than we need for this thesis, since our methods can cover this case we include it for completeness. By using this lapse function, we can compute the Ricci scalar (4.8), and then the potential function (4.7). The lapse function (4.29) gives a potential function

$$\begin{aligned} V_c(r) = & \frac{(2l + D - 3)(2l + D - 1)}{4r^2} \\ & + m \frac{4\xi(D - 1 - \alpha)(D - 2 - \alpha) - (D - 1)(D - 3 - 2\alpha)}{4} \frac{\sigma^\beta(r)}{r^{\alpha+2}} \\ & + m\beta \frac{2\xi(2D - 3 - 2\alpha) - D + 1}{2} \frac{\sigma^{\beta-1}(r)}{r^{\alpha+2}} \\ & + m\beta(\beta - 1)\xi \frac{\sigma^{\beta-2}(r)}{r^{\alpha+2}}, \end{aligned} \quad (4.30)$$

where  $\sigma(r) \equiv \ln|r/R_o|$ .

We first find the static solution  $\psi_S(r)$  of the wave equation (4.9). This is equivalent to looking for the solution of the equation  $\mathcal{L}[\psi_S(r)] = 0$ . This solution can

be expressed as a series; one can show that  $\psi_S(r)$  has the form

$$\psi_S(r) = r^{-\gamma} \sum_{j=0}^{\infty} \frac{a_j(r)}{r^{j\alpha}} + r^{\gamma+1} \sum_{j=0}^{\infty} \frac{c_j(r)}{r^{j\alpha}}, \quad (4.31)$$

where the constant  $\gamma \equiv l + (D - 3)/2$ . Notice that  $\gamma$  is an integer when the spatial dimension  $D$  is odd. Except when  $D = 1$  this integer is always positive for  $l \geq 0$ . Hence it is the first sum in the solution (4.31) that is physically relevant since it vanishes for large  $r$ . Therefore we choose it as the static solution, i.e.

$$\psi_S(r) = r^{-\gamma} \sum_{j=0}^{\infty} \frac{a_j(r)}{r^{j\alpha}}. \quad (4.32)$$

For the remainder of this chapter, we assume that  $D \geq 3$  so that this choice of  $\psi_S(r)$  is valid. The case when  $D = 1$  will be studied in the next chapter for the two solutions of the dilaton theory in  $1 + 1$  dimensions. The coefficients  $a_0(r)$  and  $c_0(r)$  in (4.31) are arbitrary constants but the other coefficients are polynomials in  $\sigma(r) = \ln|r/R_o|$ . Those coefficients  $a_1(r)$ ,  $c_1(r)$ ,  $a_2(r)$ ,  $c_2(r)$ , etc. can be generated

by the following equations.

$$\begin{aligned}
a_{j+1}(r) = & m \sigma^\beta(r) a_j(r) \\
& - \frac{m l (l + D - 2 - \alpha)}{2\gamma + 1} W(1 + (j + 1) \alpha, \sigma^\beta(r) a_j(r)) \\
& + \frac{m (l + \alpha) (l + D - 2)}{2\gamma + 1} W(2(\gamma + 1) + (j + 1) \alpha, \sigma^\beta(r) a_j(r)) \\
& - \frac{m \beta [l + \xi (2D - 3 - 2\alpha)]}{2\gamma + 1} W(1 + (j + 1) \alpha, \sigma^{\beta-1}(r) a_j(r)) \\
& - \frac{m \beta (l + D - 2)}{2\gamma + 1} W(2(\gamma + 1) + (j + 1) \alpha, \sigma^{\beta-1}(r) a_j(r)) \\
& - \frac{m \xi (D - 2 - \alpha) (D - 1 - \alpha)}{2\gamma + 1} W(1 + (j + 1) \alpha, \sigma^\beta(r) a_j(r)) \\
& + \frac{m \xi (D - 2 - \alpha)}{(2\gamma + 1) (D - 1 - \alpha)^{-1}} W(2(\gamma + 1) + (j + 1) \alpha, \sigma^\beta(r) a_j(r)) \\
& + \frac{m \xi \beta (2D - 3 - 2\alpha)}{2\gamma + 1} W(2(\gamma + 1) + (j + 1) \alpha, \sigma^{\beta-1}(r) a_j(r)) \\
& - \frac{m \beta (\beta - 1) \xi}{2\gamma + 1} W(1 + (j + 1) \alpha, \sigma^{\beta-2}(r) a_j(r)) \\
& + \frac{m \beta (\beta - 1) \xi}{2\gamma + 1} W(2(\gamma + 1) + (j + 1) \alpha, \sigma^{\beta-2}(r) a_j(r)) . \quad (4.33)
\end{aligned}$$

$$\begin{aligned}
c_{j+1}(\tau) = & m \sigma^\beta(\tau) c_j(\tau) \\
& + \frac{m(l+\alpha)(l+D-2)}{2\gamma+1} W(1+(j+1)\alpha, \sigma^\beta(\tau) c_j(\tau)) \\
& - \frac{ml(l+D-2-\alpha)}{2\gamma+1} W(-2\gamma+(j+1)\alpha, \sigma^\beta(\tau) c_j(\tau)) \\
& - \frac{m\beta(l+D-2)}{2\gamma+1} W(1+(j+1)\alpha, \sigma^{\beta-1}(\tau) c_j(\tau)) \\
& - \frac{m\beta[\xi(2D-3-2\alpha)+l]}{2\gamma+1} W(-2\gamma+(j+1)\alpha, \sigma^{\beta-1}(\tau) c_j(\tau)) \\
& + \frac{m\xi(D-2-\alpha)(D-1-\alpha)}{2\gamma+1} W(1+(j+1)\alpha, \sigma^\beta(\tau) c_j(\tau)) \\
& - \frac{m\xi(D-2-\alpha)(D-1-\alpha)}{2\gamma+1} W(-2\gamma+(j+1)\alpha, \sigma^\beta(\tau) c_j(\tau)) \\
& + \frac{m\xi\beta(2D-3-2\alpha)}{2\gamma+1} W(1+(j+1)\alpha, \sigma^{\beta-1}(\tau) c_j(\tau)) \\
& + \frac{m\beta(\beta-1)\xi}{2\gamma+1} W(1+(j+1)\alpha, \sigma^{\beta-2}(\tau) c_j(\tau)) \\
& - \frac{m\beta(\beta-1)\xi}{2\gamma+1} W(-2\gamma+(j+1)\alpha, \sigma^{\beta-2}(\tau) c_j(\tau)) . \tag{4.34}
\end{aligned}$$

The function  $W$  used above is defined as

$$W(s, f(\tau)) \equiv r^{s-1} \int_{\zeta^s}^{\tau} \frac{f(\zeta)}{\zeta^s} d\zeta . \tag{4.35}$$

where  $s$  is a real number and  $f$  is some function. This function  $W$  has a property that if  $f$  is a constant and  $s \neq 1$ , then  $W(s, f(\tau))$  equals a constant. When  $s$  is unity but  $f$  is again a constant,  $W(s, f(\tau))$  is proportional to  $\sigma(\tau) = \ln|r/R_0|$ . In the case when  $f(\tau)$  is no longer a constant but a polynomial of  $\sigma(\tau)$ , the function  $W$  gives another polynomial of  $\sigma(\tau)$ . The index  $j$  in equations (4.33) and (4.34) runs from zero to infinity. It is obvious that when the background is flat, i.e.  $m = 0$ , all  $a_j(\tau)$  and  $c_j(\tau)$  vanish except  $a_0$  and  $c_0$ . If  $m \neq 0$ , these coefficients are polynomials in  $\sigma(\tau)$ .

We follow the approach in the papers [20, 68] and let

$$\psi_I = \sum_{i=0}^{\infty} B_i(\tau) \left[ g^{(-i)}(u) + (-1)^i f^{(-i)}(v) \right] \quad (4.36)$$

be the form of the initial wave. The initial wave is the wave emitted by the central collapsing object at the onset of the gravitational collapse. In other words, this is the time when  $t \ll r$ . The functions  $g(u)$  and  $f(v)$  are as yet unknown. The term  $g^{(-i)}(u)$  represents  $i$  integrations of the function  $g(u)$  with respect to  $u$ ; similarly for  $f^{(-i)}(v)$ . Using (4.36), equation (4.14) becomes

$$\begin{aligned} 0 = & \frac{1}{2} N(\tau) \frac{d}{d\tau} B_0(\tau) \left[ g^{(1)}(u) - f^{(1)}(v) \right] \\ & - \frac{1}{4} N(\tau) \sum_{i=0}^{\infty} \left\{ \mathcal{L}[B_i(\tau)] - 2 \frac{d}{d\tau} B_{i+1}(\tau) \right\} \left[ g^{(-i)}(u) + (-1)^i f^{(-i)}(v) \right] . \end{aligned} \quad (4.37)$$

We determine the functions  $B_i(\tau)$  by setting the coefficients of the terms  $g^{(n)}(u) + (-1)^n f^{(n)}(v)$  in (4.37) to be zero. As a result, we obtain

$$B_0(\tau) = 1 , \quad (4.38)$$

$$B_{i+1}(\tau) = \frac{1}{2} N(\tau) \frac{d}{d\tau} B_i(\tau) - \frac{1}{2} \int V_c(\tau) B_i(\tau) d\tau , \quad (4.39)$$

where  $i = 0, 1, 2, \dots$ . We have set  $B_0(\tau) = \text{constant} = 1$  without loss of generality. The pair of equations above allow us to generate  $B_i(\tau)$  hierarchically in a straightforward manner.

We can split each  $B_i(\tau)$  into two parts, denoted by  $B_i^P(\tau)$  and  $B_i^T(\tau)$ . The term  $B_i^P(\tau)$  is defined as the  $m$ -independent portion of  $B_i(\tau)$ , while  $B_i^T(\tau)$  is the rest which is  $m$ -dependent. Physically speaking, the part  $B_i^P(\tau)$  represents the wave on the lightcone because it is the part that would have been generated if the background were flat ( $m = 0$ ). Price referred to this part as the primary wave which depends only on the mode of the spherical harmonics. The other part  $B_i^T(\tau)$  is called the tail of the wave because it is created by the presence of the spacetime

curvature ( $m \neq 0$ ) and is off the lightcone due to scattering. Given equations (4.38) and (4.39), one can show that the primary part of  $B_i(\tau)$  is simply

$$B_i^P(\tau) = \frac{\Gamma(\gamma + 1 + i)}{2^i i! \Gamma(\gamma + 1 - i)} \tau^i. \quad (4.40)$$

When  $D$  is odd,  $\gamma$  is an integer and the sequence  $\{B_i^P(\tau)\}_{i=0}^{\infty}$  truncates at  $i = \gamma + 1$ . In other words, there are a finite number of terms for the primary part of  $B_i(\tau)$  in odd spatial dimensions. However if  $D$  is even, the sequence constitutes infinitely many terms, thus the primary part of the initial wave  $\psi_I$  will have infinitely many terms in (4.36).

Let us consider the tail part of  $B_i(\tau)$ . Unlike the primary part,  $B_i^T(\tau)$  has no simple solution. Fortunately one can always generate  $B_i(\tau)$  recursively, and hence  $B_i^T(\tau)$ . It is worth noting that  $B_i^T(\tau)$  is of order  $O(\sigma^\beta(\tau)/\tau^{i+\alpha})$ . Moreover  $B_i^T(\tau)$  does not truncate itself, regardless of whether the number of spatial dimensions is odd or even. That is to say there are infinitely many terms in (4.36) corresponding to the tail part of the wave. As was mentioned above, in even spatial dimensions, there are also infinitely many terms for the primary part in (4.36). In this sense, the primary and tail parts of the wave are indistinguishable when  $D$  is an even integer. This will lead to a breakdown of this approach, and this is why we restrict ourselves to odd  $D$  in this chapter.

Since  $\gamma$  is an integer in odd spatial dimensions, it is convenient to define the functions  $G(u)$  and  $F(v)$  as

$$G(u) = g^{(-\gamma)}(u) \quad \text{and} \quad F(v) = f^{(-\gamma)}(v) \quad (4.41)$$

so that the initial wave can be expressed as  $\psi_I = \sum B_i(\tau) T_I^{\gamma-i}(u, v)$  where

$$T_I^{\gamma-i}(u, v) \equiv G^{(\gamma-i)}(u) + (-1)^i F^{(\gamma-i)}(v). \quad (4.42)$$

When the background is flat ( $m = 0$ ), only the first  $\gamma + 1$  terms of  $B_i^P(\tau)$  survive in  $B_i(\tau)$ . Because we expect that any outgoing radiation will propagate to spatial infinity without any scattering in a flat background, we must have

$$F^{(\gamma)}(v) = F^{(\gamma-1)}(v) = \dots = F^{(1)}(v) = F^{(0)}(v) = 0. \quad (4.43)$$

Recall that  $F(v)$  represents the scattered ingoing radiation [68] and the  $B_i^P(\tau)$  are non-zero only for  $0 \leq i \leq \gamma$ . Therefore having  $F(v) = 0$  ensures no ingoing wave in the flat background spacetime.

For concreteness, we suppose the scalar wave starts leaving the collapsing star at retarded time  $u = U_0$ ; that is to say the scalar field is zero before  $u = U_0$ . Continuity of the field at  $u = U_0$  requires that [20]

$$G^{(\gamma)}(U_0) = G^{(\gamma-1)}(U_0) = \dots = G^{(1)}(U_0) = G^{(0)}(U_0) = 0 \quad (4.44)$$

$$G^{(-1)}(u) = \int_{U_0}^u G^{(0)}(\zeta) d\zeta, \quad G^{(-2)}(u) = \int_{U_0}^u G^{(-1)}(\zeta) d\zeta, \quad \dots \quad (4.45)$$

We also assume that there is essentially no emission from the star after  $u = U_1 > U_0$  (due to gravitational red shift [20]). When the star possesses no initial static moment at the onset of collapse, i.e.  $\psi_S = 0$ , the outgoing primary part of the wave must be zero for all  $u \geq U_1 > U_0$  and we have

$$G^{(\gamma)}(u) = G^{(\gamma-1)}(u) = \dots = G^{(1)}(u) = G^{(0)}(u) = 0. \quad (4.46)$$

Only the first  $\gamma + 1$   $G$ 's vanish because the terms  $G(u)$  to  $G^{(\gamma)}(u)$  represent the primary wave and are responsible for the emission from the star. This condition further implies

$$G^{(-1)}(u) = \int_{U_0}^u G^{(0)}(\zeta) d\zeta = \int_{U_0}^{U_1} G^{(0)}(\zeta) d\zeta = \text{constant} \quad (4.47)$$

for all  $u \geq U_1$ . Therefore if there is no static moment before  $u = U_0$ , the scalar wave after time  $u = U_1$  is

$$\psi_{u \geq U_1} = \sum_{i=\gamma+1}^{\infty} B_i(\tau) T_I^{\gamma-i}(u, v), \quad (4.48)$$

where  $T_I^{-1}(u, v)$  is only a constant and  $B_i(\tau) = B_i^T(\tau)$  is of order  $O(\sigma^\beta(\tau)/\tau^{i+\alpha})$ . Consequently the first term of this solution which is time-independent is of order  $O(\sigma^\beta(\tau)/\tau^{\gamma+\alpha+1})$ . Physically, this says that the tail of the perturbation persists after the time  $u = U_1$ . The primary part of the wave has been “washed out” by the gravitational red shift before  $u = U_1$  [20].

The situation is more complicated if the collapsing object carries a static moment at the onset of the collapse because the static wave  $\psi_S(\tau)$  can also be divided into the primary and tail parts. In this case, we superimpose  $\psi_S(\tau)$  of (4.32) and  $\psi_I(\tau)$  of (4.36) together to form a new initial scalar wave. We also suppose that only the tail of the perturbation persists after the retarded time  $u = U_1$  [20]. For the superimposed initial wave this cutoff condition requires

$$G^{(0)}(u) = -\frac{2^\gamma \gamma!}{(2\gamma)!} a_0, \quad \forall u \geq U_1 \geq U_0 \quad (4.49)$$

which yields

$$G^{(\gamma)}(u) = G^{(\gamma-1)}(u) = \dots = G^{(1)}(u) = 0. \quad (4.50)$$

The restriction on  $G(u)$  above is different from the one in (4.46) because we want to ensure that the  $m$ -independent part of (4.32) can be canceled by the primary part of (4.36) properly after the time  $U_1$ , leaving the combined  $\psi_I$  to be  $m$ -dependent for  $u > U_1$ . As a result, the wave with initial static moment will become

$$\psi_{u \geq U_1} = \frac{1}{r^\gamma} \sum_{j=1}^{\infty} \frac{a_j(\tau)}{r^{j\alpha}} + \sum_{i=\gamma+1}^{\infty} B_i^T(\tau) T_I^{\gamma-i}(u, v). \quad (4.51)$$

One can show that the first sum in the equation above is of order  $O(\sigma^\beta(r)/r^{\gamma+\alpha})$  because the coefficient function  $a_1(r)$  is a polynomial in  $\sigma(r)$  with degree  $\beta$ . In the second sum, the term  $T_I^{-1}(u, v)$  is linear in  $u$  and the other term  $B_{\gamma+1}^T(r)$  is of order  $O(\sigma^\beta(r)/r^{\gamma+\alpha+1})$ .

Now we turn our attention to the scalar wave at late time. By late time, we mean  $t \gg r$ . For the late time wave  $\psi_L$ , we introduce another ansatz [68]

$$\psi_L = \sum_{i=0}^{\infty} C_i(r) T_L^i(u, v) . \quad (4.52)$$

$$T_L^i(u, v) \equiv I^{(i)}(u) + (-1)^i H^{(i)}(v) . \quad (4.53)$$

By substituting  $\psi = \psi_L$ , equation (4.14) becomes

$$\begin{aligned} 0 &= \frac{1}{4} N(r) \mathcal{L}[C_0(r)] T_L^0(u, v) \\ &+ \frac{1}{4} N(r) \sum_{i=0}^{\infty} \left\{ \mathcal{L}[C_{i+1}(r)] - 2 \frac{d}{dr} C_i(r) \right\} T_L^{i+1}(u, v) . \end{aligned} \quad (4.54)$$

Similar to what we did before, we set the coefficients of  $T_L^n(u, v)$  to be zero and obtain a set of equations

$$\mathcal{L}[C_0(r)] = 0 , \quad (4.55)$$

$$\mathcal{L}[C_{i+1}(r)] = 2 \frac{d}{dr} C_i(r) , \quad i = 0, 1, 2, \dots \quad (4.56)$$

Unlike the case for the initial wave  $\psi_I$ , recursive generation of the sequence of functions  $C_i(r)$  is not straightforward because it involves inverting the differential operator  $\mathcal{L}$ . We first solve for the zero order equation (4.55) and obtain a solution

$$C_0(r) = r^{\gamma+1} \sum_{j=0}^{\infty} \frac{c_j(r)}{r^{j\alpha}} . \quad (4.57)$$

The coefficient functions  $c_j(r)$  are those introduced in equation (4.31).

The other inhomogeneous differential equation (4.56) can be solved as a series solution. We can represent the solution as

$$C_i(r) = r^{\gamma+1+i} \sum_{j=0}^{\infty} \frac{c_j^i(r)}{r^{j\alpha}}, \quad (4.58)$$

where  $i = 0, 1, 2, \dots$ . When  $i = 0$ , it is understood that  $c_j^0(r) = c_j(r)$ . These coefficients  $c_j^i(r)$  can be calculated by using the recurrence relations

$$c_0^i(r) = c_0^i = \frac{2^i (2\gamma + 1)! (\gamma + i)!}{\gamma! (i)! (2\gamma + 1 + i)!} c_0, \quad (4.59)$$

$$\begin{aligned} c_{j+1}^{i+1}(r) = & m \sigma^\beta(r) c_j^{i+1}(r) \\ & + \frac{2\gamma}{2\gamma+1} W(-i + (j+1)\alpha, c_{j+1}^i(r)) \\ & + \frac{2(\gamma+1)}{2\gamma+1} W(-2\gamma-1-i+(j+1)\alpha, c_{j+1}^i(r)) \\ & + \frac{m(l+\alpha)(l+D-2)}{2\gamma+1} W(-i+(j+1)\alpha, \sigma^\beta(r) c_j^{i+1}(r)) \\ & - \frac{ml(l+D-2-\alpha)}{2\gamma+1} W(-2\gamma-1-i+(j+1)\alpha, \sigma^\beta(r) c_j^{i+1}(r)) \\ & - \frac{m\beta(l+D-2)}{2\gamma+1} W(-i+(j+1)\alpha, \sigma^{\beta-1}(r) c_j^{i+1}(r)) \\ & - \frac{m\beta l}{2\gamma+1} W(-2\gamma-1-i+(j+1)\alpha, \sigma^{\beta-1}(r) c_j^{i+1}(r)) \\ & - \frac{m\xi\beta(2D-3-2\alpha)}{2\gamma+1} W\left(-2\gamma-1-i+(j+1)\alpha, \frac{c_j^{i+1}(r)}{\sigma^{1-\beta}(r)}\right) \\ & + \frac{m\xi(D-2-\alpha)(D-1-\alpha)}{2\gamma+1} W(-i+(j+1)\alpha, \sigma^\beta(r) c_j^{i+1}(r)) \\ & - \frac{m\xi(D-2-\alpha)}{(2\gamma+1)(D-1-\alpha)^{-1}} W\left(-2\gamma-1-i+(j+1)\alpha, \frac{c_j^{i+1}(r)}{\sigma^{-\beta}(r)}\right) \\ & + \frac{m\xi\beta(2D-3-2\alpha)}{2\gamma+1} W(-i+(j+1)\alpha, \sigma^{\beta-1}(r) c_j^{i+1}(r)) \\ & - \frac{m\beta(\beta-1)\xi}{2\gamma+1} W(-2\gamma-1-i+(j+1)\alpha, \sigma^{\beta-2}(r) c_j^{i+1}(r)) \\ & + \frac{m\beta(\beta-1)\xi}{2\gamma+1} W(-i+(j+1)\alpha, \sigma^{\beta-2}(r) c_j^{i+1}(r)). \end{aligned} \quad (4.60)$$

Therefore we can compute all the coefficients  $c_j^i(\tau)$  by using the coefficients  $c_j(\tau)$  and the recurrence relations above. Since each coefficient  $c_0^i(\tau)$  is a constant instead of a polynomial in  $\sigma(\tau)$ , we can estimate the order of the late time wave  $\psi_L$  as

$$\psi_L = \sum_{i=0}^{\infty} O\left(r^{\gamma+1+i}\right) T_L^i(u, v) . \quad (4.61)$$

Finally we match the late time solution  $\psi_L$  to the initial solution  $\psi_I$  at some transient period where  $u, v$  and  $r$  are of the same order. Since the background is asymptotically flat, the tortoise coordinate  $\rho$  tends to  $r$  when  $r \rightarrow \infty$ : thus there exists a transient region so that  $\rho$  has an order similar to that of  $r$ . As a result, if  $t$  has the same order as  $r$ , the variables  $u, v$  and  $r$  must be in the same order in the transient region. The initial wave  $\psi_{u \geq U_1}$  in this period becomes

$$\begin{aligned} \psi_{u \geq U_1} &\sim O\left(\frac{\sigma^\beta(\tau)}{r^{\gamma+\alpha+1}}\right) , && \text{without initial static moment .} \\ \psi_{u \geq U_1} &\sim O\left(\frac{\sigma^\beta(\tau)}{r^{\gamma+\alpha}}\right) , && \text{with initial static moment .} \end{aligned}$$

In order to have consistent orders in the transient period, we must have

$$T_L^0(t, t) \sim O\left(\frac{(\ln|t|)^\beta}{t^{2\gamma+2+\alpha}}\right) \quad (4.62)$$

if there is no initial static moment. On the other hand the order of  $T_L^0$  must be

$$T_L^0(t, t) \sim O\left(\frac{(\ln|t|)^\beta}{t^{2\gamma+1+\alpha}}\right) \quad (4.63)$$

if there is a static moment at the onset of collapse. Equations (4.62) and (4.63) give the time response of  $\psi_L$  which is the scalar wave at late time. The inverse power falloff behavior modified by a logarithmic term was first noted by Ching *et al.* [70].

For a Schwarzschild background, we set  $D = 3$ ,  $\alpha = 1$  and  $\beta = 0$  and obtain  $\gamma = l$ , yielding the familiar inverse power decay rate according to equations (4.62)

and (4.63) [20, 68]. Since we have chosen the initial condition (4.18) in our numerical simulation, there is no initial static moment for the wave. Consequently the falloff in figure 4.4 has a power of  $-(2l + 3)$  instead of  $-(2l + 2)$ . This shows that the analysis presented in this section is consistent with the results in [20, 38, 68].

# Chapter 5

## (1 + 1)-Dimensional Dilaton Gravity Revisited

After the study of late time radiation falloff in a Schwarzschild-like background in the last chapter, we move on to the study of radiation falloff behavior in the (1 + 1)-dimensional dilaton spacetimes. For simplicity, we shall consider the static spacetimes, that is to say the masses of the two black holes in Chapter 3 are constant. The two metric solutions (the static versions) share the form

$$ds^2 = -N(x) dt^2 + \frac{dx^2}{N(x)} . \quad (5.1)$$

The first dilaton solution has a lapse function given by equations (3.13) and (3.14) which reads

$$N(x) = 1 - \frac{M}{x} + \frac{q^2}{4x^2} - \frac{1}{2} \sum_{n=2}^k \frac{a_n}{2n-3} x^{2-2n} . \quad (5.2)$$

The second dilaton spacetime's lapse function is given by (3.48) and (3.49) and its static version reads

$$N(x) = 1 - \frac{2M}{Q} e^{-Q(x-x_o)} + \frac{q^2}{2Q^2} e^{-2Q(x-x_o)} - \frac{1}{Q^2} \sum_{n=2}^k \frac{a_n}{n-1} e^{-nQ(x-x_o)} . \quad (5.3)$$

In these background spacetimes the scalar wave equation (4.2) becomes

$$\partial_{tt}\Psi - N(x)\partial_x[N(x)\partial_x\Psi] - \xi N(x)\frac{d^2}{dx^2}N(x)\Psi = 0. \quad (5.4)$$

Notice that the metric (5.1) does not need the transformation (4.4) to put (4.2) into the form (4.6). This is possible only when the spatial dimension is one: in this case there are no spherical harmonics in the spacetime. By using the tortoise coordinate

$$\rho \equiv \int \frac{dx}{N(x)}. \quad (5.5)$$

equation (5.4) above can be written as

$$\partial_{tt}\Psi - \partial_{\rho\rho}\Psi + V(\rho)\Psi = 0, \quad (5.6)$$

where the potential  $V$  is given by

$$V(\rho) = -\xi N(x(\rho))\left.\frac{d^2}{dx^2}N(x)\right|_{x=x(\rho)}. \quad (5.7)$$

Since we are only interested in the qualitative behavior of the wave, we simplify the two lapse functions into the form

$$N(x) = 1 - \frac{M}{x} \quad (5.8)$$

and

$$N(x) = 1 - e^{-Q(x-X_+)} \quad (5.9)$$

for the first and second dilaton solutions, respectively. This simplification allows exact analytic calculation for the scalar wave. The constant  $X_+$  denotes the position of the event horizon of the black hole which is represented by the metric (5.1)

with the lapse function (5.9). With these simplified lapse functions, the tortoise coordinates and the potential become

$$\rho = x + M \ln \left| \frac{x}{M} - 1 \right| . \quad (5.10)$$

$$V(\rho) = \left[ 1 - \frac{M}{x(\rho)} \right] \frac{2\xi M}{x^3(\rho)} \quad (5.11)$$

for the first solution and

$$\rho = \frac{1}{Q} \ln \left| e^{Q(x-X_+)} - 1 \right| , \quad (5.12)$$

$$V(\rho) = \xi Q^2 \frac{\exp(Q\rho)}{[1 + \exp(Q\rho)]^2} \quad (5.13)$$

for the second dilaton solution. These two tortoise coordinates extend over the whole real line for the exterior of the black holes.

The tortoise coordinate for the first dilaton solution has the same form as the one (4.15) in the Schwarzschild background. Generally if  $\xi$  is strictly positive, the potential (5.11) behaves like the one (4.16) with zero moment (i.e.  $l = 0$ ) in the Schwarzschild case. This allows us to immediately conclude that the late time radiation falloff outside the first dilaton black hole obeys an inverse power decay pattern if  $\xi > 0$ . We shall not consider the case  $\xi < 0$  because a negative potential implies that the wave outside the black hole gains energy from the spacetime but this is not physical.

For the second dilaton solution, the scalar field  $\Psi$  satisfies the partial differential equation

$$\partial_{tt}\Psi - \partial_{\rho\rho}\Psi + V_0 \frac{\exp(Q\rho)}{[1 + \exp(Q\rho)]^2} \Psi = 0 , \quad (5.14)$$

where  $V_0 = \xi Q^2$ . Once again, the case  $\xi \leq 0$  does not interest us. We shall devote the next section to finding the solution of this differential equation for  $V_0 > 0$  and

examining the falloff behavior of the scalar wave in this background. In Section 5.2 the mass inflation calculation will be re-examined by using the revised radiation falloff rate. We shall find that the inner mass parameter can be finite at the Cauchy horizon due to a stronger radiation attenuation in the second dilaton background spacetime.

## 5.1 Waves in the Second Dilaton Background

The procedure of finding the solution for equation (5.14) is as follows. We first write down the representation of the solution  $\Psi$  in terms of a Green's function. The rest of the problem then reduces to looking for the correct Green's function [69](p. 223). We shall Fourier transform the problem from the time domain to the frequency domain and obtain a new Green's function in the frequency space. Once we have solved for this Green's function, an inverse Fourier transformation will give the solution  $\Psi(t, \rho)$ .

We assume that there exists a Green's function

$$G(\rho, \zeta; t - \tau) = G(\zeta, \rho; t - \tau) \quad (5.15)$$

which is zero when  $t < \tau$ . We define a differential operator  $D$  as

$$D = \partial_{tt} - \partial_{\rho\rho} + V(\rho) \quad (5.16)$$

so that the Green's function corresponding to this operator has the property

$$DG(\rho, \zeta; t - \tau) = [\partial_{tt} - \partial_{\rho\rho} + V(\rho)] G(\rho, \zeta; t - \tau) = \delta(t - \tau) \delta(\rho - \zeta) . \quad (5.17)$$

The inner product between  $D\Psi(\tau, \zeta)$  and  $G(\rho, \zeta; t - \tau)$  then implies

$$\begin{aligned} \Psi(t, \rho) &= \int_0^\infty [G(\rho, \zeta; t - \tau) \partial_\zeta \Psi(\tau, \zeta) - \Psi(\tau, \zeta) \partial_\zeta G(\rho, \zeta; t - \tau)]_{\zeta=-\infty}^{\zeta=\infty} d\tau \\ &+ \int_{-\infty}^\infty [G(\rho, \zeta; t) \partial_t \Psi(0, \zeta) + \Psi(0, \zeta) \partial_t G(\rho, \zeta; t)] d\zeta . \end{aligned} \quad (5.18)$$

As a result, we have changed the question from finding  $\Psi(t, \rho)$  to searching for an appropriate Green's function  $G$ .

We now carry out a Fourier transformation and define

$$\tilde{G}(\rho, \zeta; \omega) \equiv \int_{-\infty}^{\infty} G(\rho, \zeta; t) e^{i\omega t} dt, \quad (5.19)$$

where  $\tilde{G}$  is the Green's function in the frequency domain. The inverse transformation is

$$G(\rho, \zeta; t) = \frac{1}{2\pi} \int_{-\infty}^{\infty} \tilde{G}(\rho, \zeta; \omega) e^{-i\omega t} d\omega. \quad (5.20)$$

In the frequency domain, equation (5.17) becomes

$$\tilde{D}\tilde{G}(\rho, \zeta; \omega) = [-\omega^2 - \partial_{\rho\rho} + V(\rho)] \tilde{G}(\rho, \zeta; \omega) = \delta(\rho - \zeta) \quad (5.21)$$

provided that  $G(\rho, \zeta; t)$  satisfies the conditions

$$\lim_{t \rightarrow \infty} G(\rho, \zeta; t) = \lim_{t \rightarrow \infty} \partial_t G(\rho, \zeta; t) = 0. \quad (5.22)$$

On physical grounds these assumptions are reasonable because any localized quantity is expected to be dispersed throughout the space by means of wave propagation. Mathematically, these assumptions are consistent with the Fourier transformability of the function  $G(\rho, \zeta; t)$  which must be absolutely integrable in  $t$  over  $\mathbb{R}$ . The Green's function in the frequency space can be represented as

$$\tilde{G}(\rho, \zeta; \omega) = \begin{cases} \frac{f(\zeta; \omega) g(\rho; \omega)}{W(\omega; g, f)} & \text{if } \zeta < \rho, \\ \frac{f(\rho; \omega) g(\zeta; \omega)}{W(\omega; g, f)} & \text{if } \rho < \zeta, \end{cases} \quad (5.23)$$

where the function  $W(\omega; g, f)$  is the Wronskian of two linearly independent functions  $g(\rho; \omega)$  and  $f(\rho; \omega)$ , that is

$$W(\omega; g, f) = g(\rho; \omega) \partial_{\rho} f(\rho; \omega) - f(\rho; \omega) \partial_{\rho} g(\rho; \omega). \quad (5.24)$$

These functions are two independent solutions of the equations

$$\tilde{D}f(\rho; \omega) = \tilde{D}g(\rho; \omega) = 0 . \quad (5.25)$$

Consequently the Wronskian  $W(\omega; g, f)$  is independent of  $\rho$ .

Let  $\tilde{\Psi}(\rho; \omega)$  be the Fourier transformation of the solution  $\Psi(t, \rho)$ . We impose boundary conditions on the functions  $f(\rho; \omega)$  and  $g(\rho; \omega)$  so that

$$f(\rho; \omega) \propto \tilde{\Psi}(\rho; \omega) \quad \text{and} \quad \partial_\rho f(\rho; \omega) \propto \partial_\rho \tilde{\Psi}(\rho; \omega) \quad (5.26)$$

as  $\rho \rightarrow -\infty$ . When  $\rho \rightarrow \infty$ , we require that

$$g(\rho; \omega) \propto \tilde{\Psi}(\rho; \omega) \quad \text{and} \quad \partial_\rho g(\rho; \omega) \propto \partial_\rho \tilde{\Psi}(\rho; \omega) . \quad (5.27)$$

On the right side of equation (5.18), after we have used the inverse Fourier transformation (5.20) in the first integral and interchanged the integrals with respect to  $d\omega$  and  $d\tau$ , the representation of  $\Psi(t, \rho)$  simply becomes

$$\Psi(t, \rho) = \int_{-\infty}^{\infty} [G(\rho, \zeta; t) \partial_t \Psi(0, \zeta) + \Psi(0, \zeta) \partial_t G(\rho, \zeta; t)] d\zeta . \quad (5.28)$$

Equation (5.23), (5.26) and (5.27) are used in order to remove the first integral in (5.18). We observe that the time response of the wave  $\Psi(t, \rho)$  comes entirely from the Green's function  $G(\rho, \zeta; t)$  and its derivative. As a result, the late time behavior of  $G$  determines that of the scalar wave.

There are two solutions for the differential equation  $\tilde{D}h(\rho; \omega) = 0$ , namely

$$h_1(\rho; \omega) = e^{-i\omega\rho} F(-\nu, 1 + \nu; 1 - \mu; z(\rho)) , \quad (5.29)$$

$$h_2(\rho; \omega) = e^{i\omega\rho} F(-\nu, 1 + \nu; 1 - \mu; 1 - z(\rho)) . \quad (5.30)$$

The function  $F$  is the hypergeometric function and  $z$  is defined as

$$z(\rho) \equiv \frac{\exp(Q\rho)}{1 + \exp(Q\rho)}. \quad (5.31)$$

The potential  $V$  in (5.13) can be written as  $V_0 z(1 - z)$ . The two parameters in the hypergeometric function are given by

$$\mu = i \frac{2\omega}{Q}, \quad (5.32)$$

$$\nu = -\frac{1}{2} + \frac{1}{2} \sqrt{1 - \frac{4V_0}{Q^2}}. \quad (5.33)$$

Because  $\rho \in \mathbb{R}$ ,  $z$  has a range of  $(0, 1)$  which guarantees absolute convergence in the hypergeometric function [71](p. 556). At the boundary  $\rho \rightarrow -\infty$  (the event horizon of the black hole) we employ the condition

$$f(\rho; \omega) = e^{-i\omega\rho} \quad \text{when} \quad \rho \rightarrow -\infty \quad (5.34)$$

as the ingoing wave condition [38]. At the other end, namely the spatial infinity, we use the condition

$$g(\rho; \omega) = e^{i\omega\rho} \quad \text{when} \quad \rho \rightarrow \infty \quad (5.35)$$

which represents an outgoing free wave because the spacetime is asymptotically flat. These boundary conditions simply mean that there are no waves coming from the black hole nor spatial infinity. The convention of  $-i$  for the ingoing wave and  $+i$  for the outgoing wave is determined by the convention of the (inverse) Fourier transformation (5.20). These boundary conditions determine the two functions  $f(\rho; \omega)$  and  $g(\rho; \omega)$  as

$$f(\rho; \omega) = h_1(\rho; \omega) = e^{-i\omega\rho} F(-\nu, 1 + \nu; 1 - \mu; z(\rho)), \quad (5.36)$$

$$g(\rho; \omega) = h_2(\rho; \omega) = e^{i\omega\rho} F(-\nu, 1 + \nu; 1 - \mu; 1 - z(\rho)). \quad (5.37)$$

One can show that the Wronskian of  $g$  and  $f$  is given by

$$\begin{aligned} W(\omega; g, f) &= -2i\omega F(z(\rho)) F(1 - z(\rho)) \\ &\quad + Q z(\rho) [1 - z(\rho)] F(z(\rho)) F'(1 - z(\rho)) \\ &\quad + Q z(\rho) [1 - z(\rho)] F(1 - z(\rho)) F'(z(\rho)) . \end{aligned} \quad (5.38)$$

where  $F(\cdot)$  is the shorthand notation of  $F(-\nu, 1 + \nu; 1 - \mu; \cdot)$  and the prime denotes differentiation of  $F(-\nu, 1 + \nu; 1 - \mu; z)$  with respect to the last argument  $z$ . Since the differential equation satisfied by  $f$  and  $g$  is a linear, homogeneous second order one, the Wronskian of  $g$  and  $f$  must be  $\rho$ -independent. In other words, the equation above is not sensitive to the value of  $\rho$  although individual terms in (5.38) depend upon this variable. We make use of this property and calculate the Wronskian (5.38) at  $\rho = 0$ . At this point,  $z(0) = 1 - z(0) = 1/2$ . With the help of the equalities [71](eqn. 15.1.26 and 15.2.4)

$$F\left(\frac{1}{2}\right) = F\left(-\nu, 1 + \nu; 1 - \mu; \frac{1}{2}\right) = \frac{\sqrt{\pi} 2^\mu \Gamma(1 - \mu)}{\Gamma([1 - \mu - \nu]/2) \Gamma([2 - \mu + \nu]/2)} . \quad (5.39)$$

$$\frac{d}{dz} F(a, b; c; z) = \frac{c-1}{z} [F(a, b; c-1; z) - F(a, b; c; z)] . \quad (5.40)$$

we obtain

$$W(\omega; g, f) = \frac{1}{2} F\left(\frac{1}{2}\right) \left[ Q F'\left(\frac{1}{2}\right) - 4i\omega F\left(\frac{1}{2}\right) \right] \quad (5.41)$$

for which the term inside the square bracket equals

$$Q F'\left(\frac{1}{2}\right) - 4i\omega F\left(\frac{1}{2}\right) = \frac{\sqrt{\pi} 2^{\mu+2} Q \Gamma(1 - \mu)}{\Gamma([- \mu - \nu]/2) \Gamma([1 - \mu + \nu]/2)} . \quad (5.42)$$

The inverse Fourier transformation is given by the equation (5.20). We evaluate this integral by analytically extending  $\omega$  to complex values and using Cauchy's residue theorem. The integration contour is chosen to be a large, closed semi-circle

on the lower half  $\omega$ -plane, with center at  $\omega = 0$ . By Jordan's lemma [72], the contribution from the arc of the large semi-circle goes to zero as the radius of the arc tends to infinity. The Green's function then becomes

$$G(\rho, \zeta; t) = i \sum \text{Res}\{\tilde{G}(\rho, \zeta; \omega) e^{-i\omega t}\} \quad (5.43)$$

because there is no branch cut in either  $f(\rho; \omega)$  or  $g(\rho; \omega)$  in this case [73](p. 160), [71](p. 255). This is different from the Schwarzschild case in which the function  $g(\rho; \omega)$  has a branch cut along the negative imaginary axis on the complex  $\omega$ -plane [38]. It is the presence of the branch cut that yields the inverse power radiation falloff rate in the Schwarzschild background. The term  $\text{Res}\{k(z)\}$  denotes the residue of the function  $k(z)$  at a pole. As a result, we conclude that  $G(\rho, \zeta; t)$ , and thus  $\Psi(t, \rho)$ , decays to zero exponentially because the poles always have negative imaginary parts.

We check this conclusion of exponential falloff by conducting several numerical simulations. Several sample graphs of the potential  $V(\rho)$  of (5.13) are given in figure 5.1. Figures 5.2 to 5.4 show the falloff response of the scalar wave in this (1 + 1)-dimensional dilaton spacetime. These graphs are generated with the event horizon at  $X_+ = -30$ . The initial impulse is located at  $x = -15$  and the observation is measured at  $x = -10$  (i.e.  $\rho = 20$ ). These graphs clearly show that the scalar wave dies out at an exponential rate.

We consider a case where  $X_+ = 30$ ,  $\xi = 10$ ,  $Q = 1$  and the initial impulse is placed at  $x = -15$  but the observation point is at  $\rho = -32.15$  (or  $x = -30 + 10^{-14}$ ). This case is comparable to the simulation associated with figure 5.2 because all the parameters save the observation point are the same in both cases. The observation point in this simulation is very close to the event horizon  $x = X_+$ , thus this simulation means to investigate the effect of gravitational redshift on

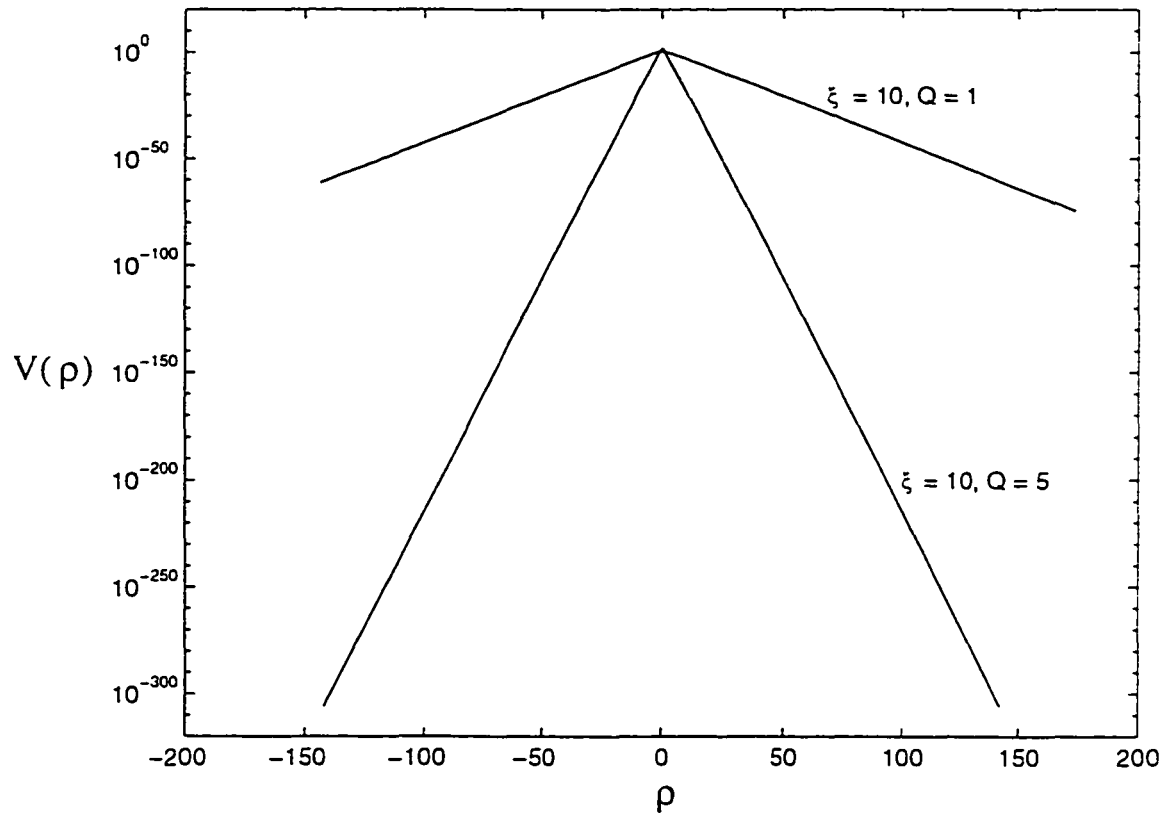


Figure 5.1: Two sample potentials  $V(\rho)$  for the scalar wave in the second dilaton spacetime.

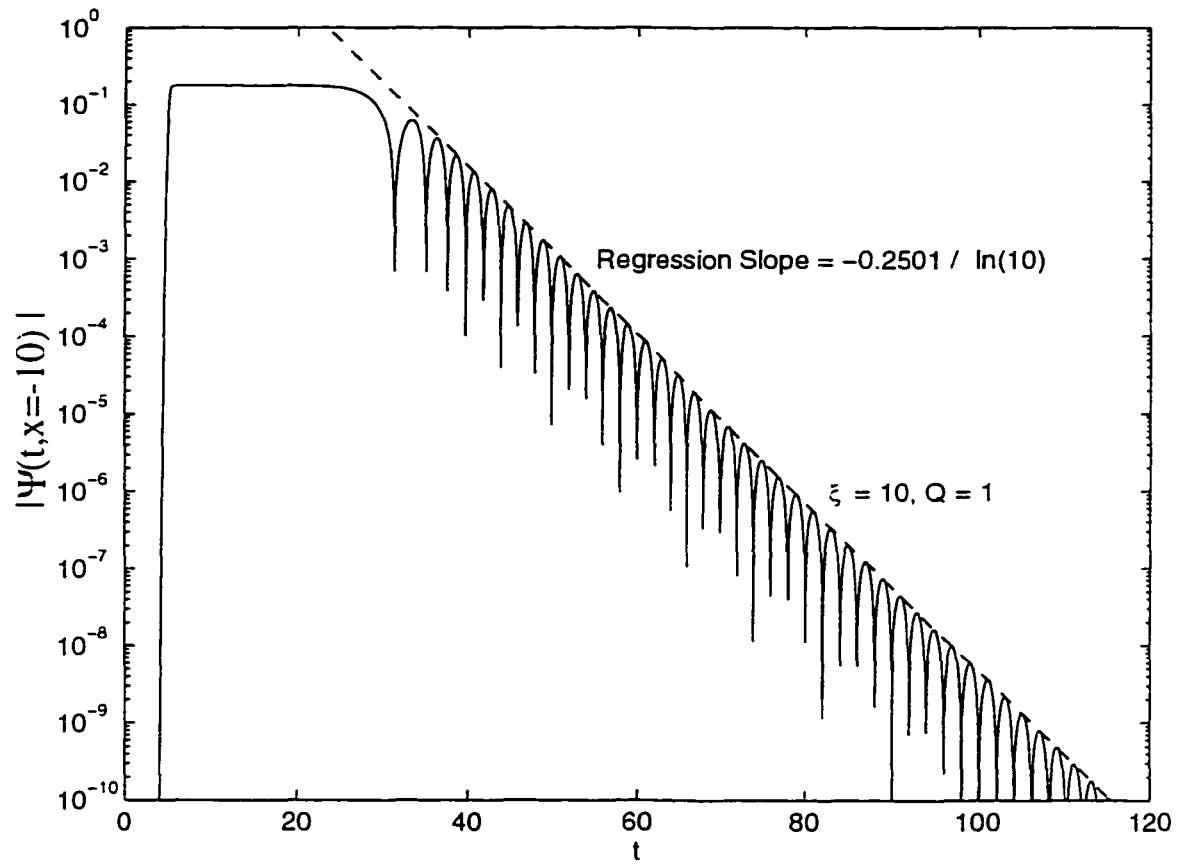


Figure 5.2: Scalar wave decay behavior in the second dilaton spacetime with  $\xi = 10$ .  
 $Q = 1$ .

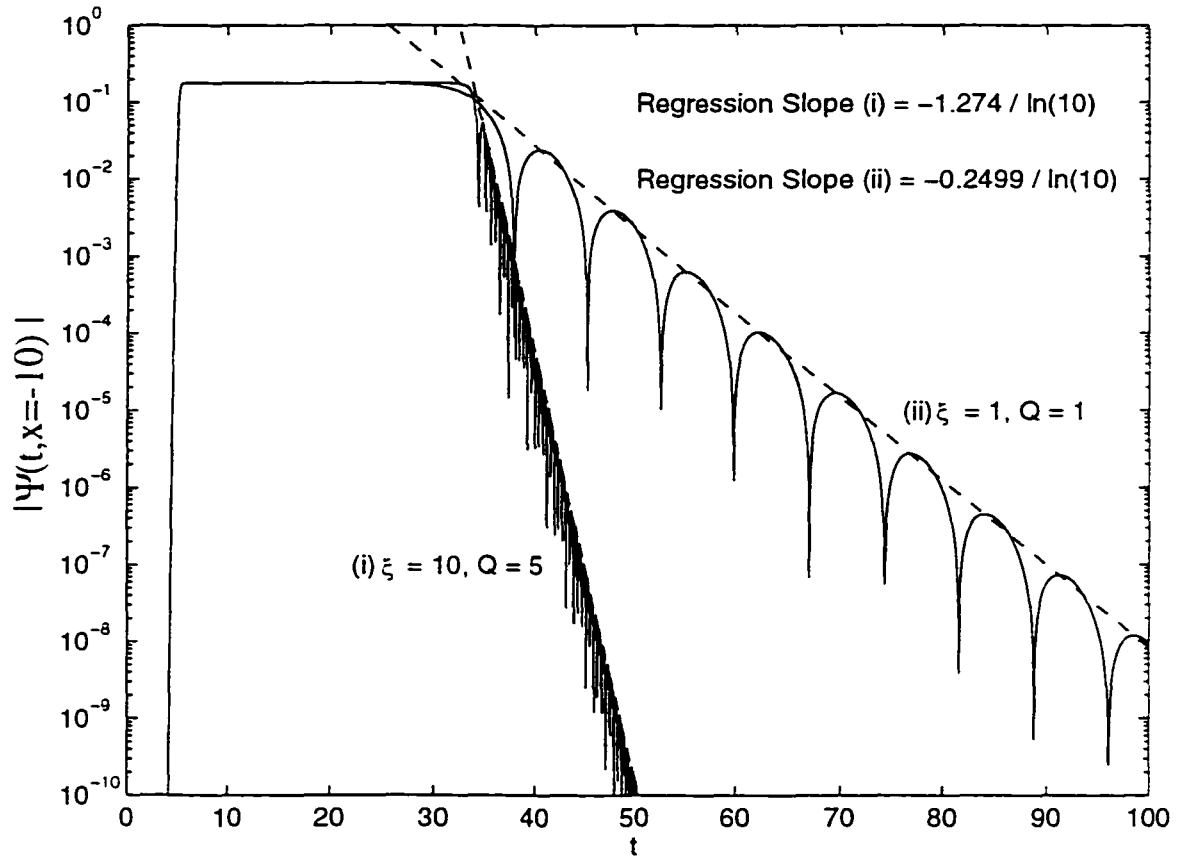


Figure 5.3: Scalar wave decay behavior in the second dilaton spacetime with i)  $\xi = 10, Q = 5$ , and ii)  $\xi = 1, Q = 1$ .

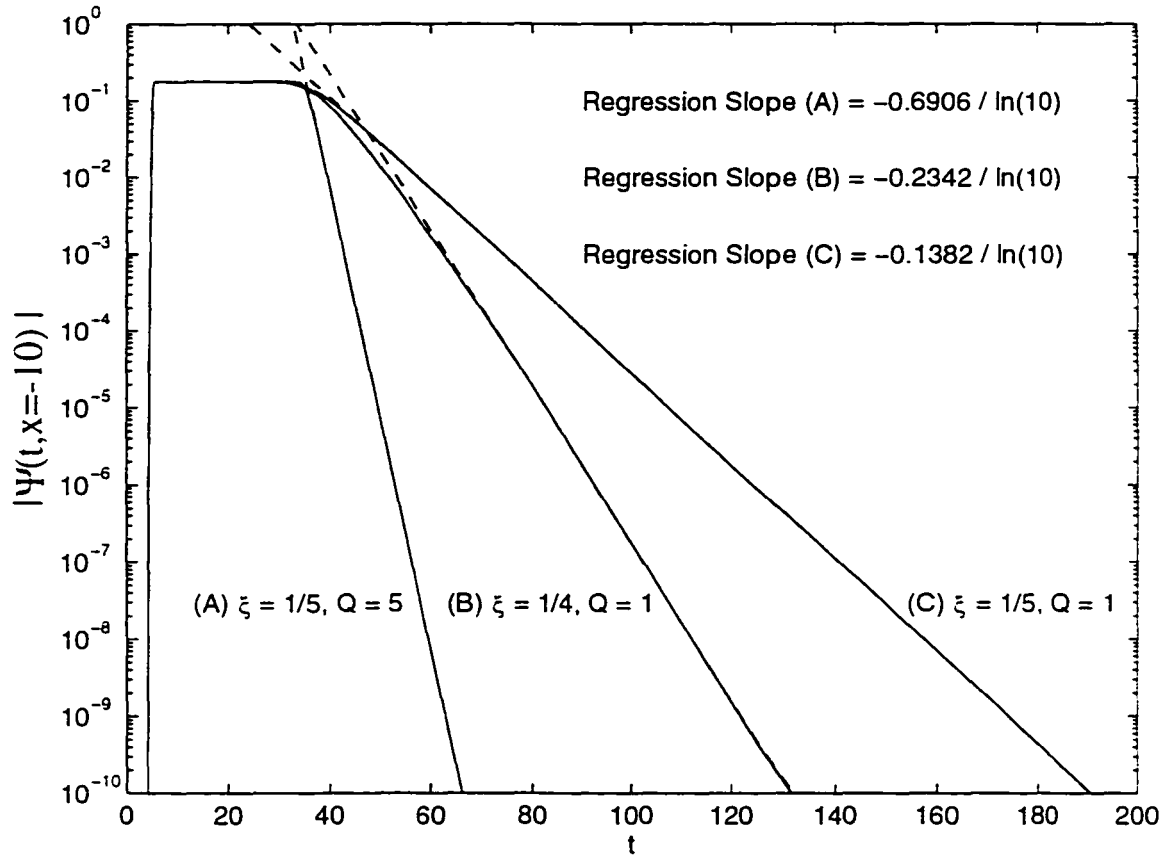


Figure 5.4: Scalar wave decay behavior in the second dilaton spacetime with  $\xi \leq 1/4$ .

the radiation falloff rate. Moreover the observer is located between the black hole and the peak of the potential function  $V$ . The result of this simulation is given in figure 5.5. It is obvious that the exponential falloff rate shown in figure 5.5 is the same as the rate in figure 5.2. Therefore it is valid to use the large-distance radiation falloff rate in the mass inflation calculation.

The exact exponential falloff rate in these graphs can be explained by the location of the poles in the Green's function  $\tilde{G}(\rho, \zeta; \omega)$ . On the lower half  $\omega$ -plane, there are infinitely many poles for the Green's function (5.23). They come from the roots of the Wronskian (5.41) in  $\omega$  which comes into play through the parameter  $\mu$ . According to the equations (5.39) and (5.42), these poles come from the four gamma functions and they are located at points such that

$$\frac{1}{2}(1 - \mu - \nu) = -k_1 . \quad (5.44)$$

$$\frac{1}{2}(2 - \mu + \nu) = -k_2 . \quad (5.45)$$

$$-\frac{1}{2}(\mu + \nu) = -k_3 . \quad (5.46)$$

$$\frac{1}{2}(1 - \mu + \nu) = -k_4 . \quad (5.47)$$

where  $k_1, k_2, k_3$  and  $k_4$  are non-negative integers.

The dominant exponential decay rate in the Green's function  $G(\rho, \zeta; t)$  is determined by the pole closest to the real axis on the lower half  $\omega$ -plane. On the lower half of this complex plane, we suppose

$$\omega = A - i|B| \quad (5.48)$$

so that

$$\mu = \frac{2|B|}{Q} + i \frac{2A}{Q} , \quad (5.49)$$

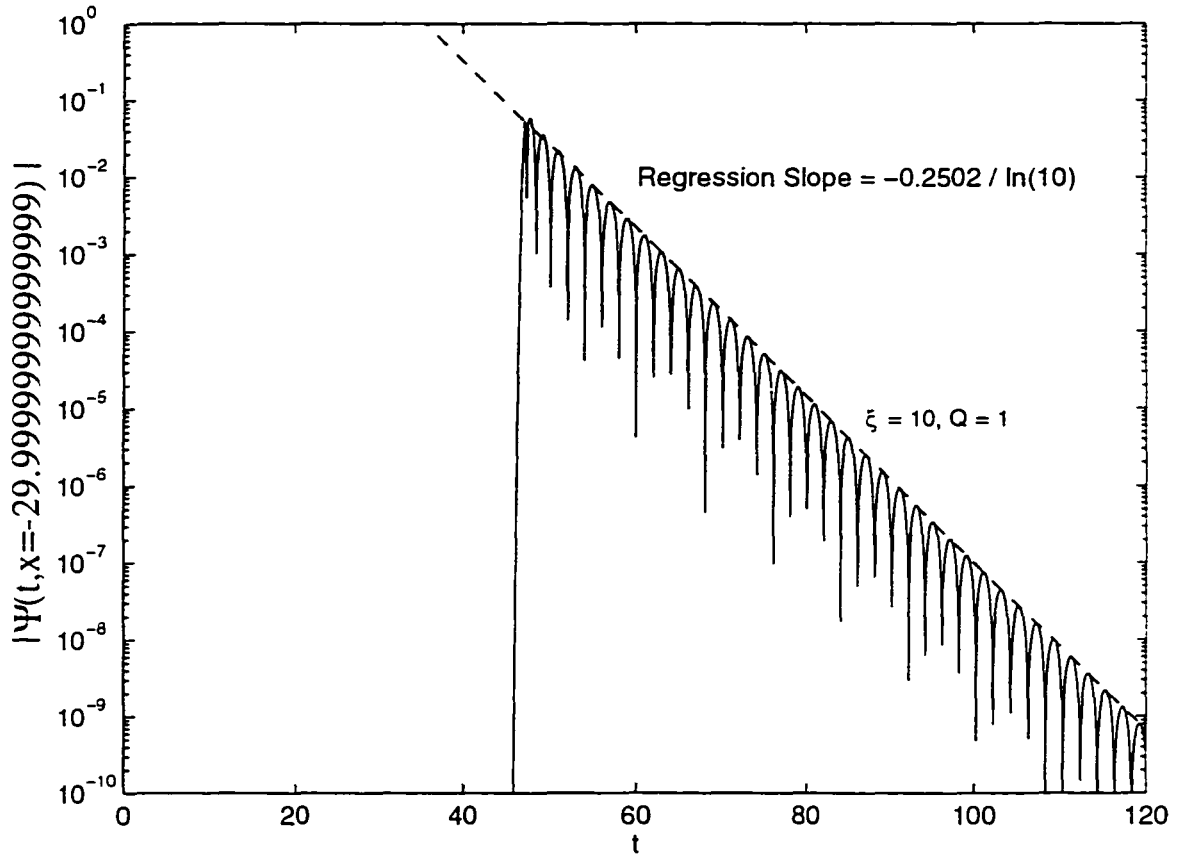


Figure 5.5: Scalar wave decay behavior in the second dilaton spacetime with  $\xi = 10$ ,  $Q = 1$ . This diagram is similar to figure 5.2 but the observation is made near the event horizon of the black hole.

where  $A, B \in \mathbb{R}$ . By using the equations (5.44) to (5.47), we conclude that

$$\begin{cases} A = -\frac{Q}{2} \operatorname{Im}(\nu) \\ |B| = \frac{Q}{2} [1 + 2k_1 - \operatorname{Re}(\nu)] \end{cases} \quad (5.50)$$

$$\begin{cases} A = \frac{Q}{2} \operatorname{Im}(\nu) \\ |B| = \frac{Q}{2} [2 + 2k_2 + \operatorname{Re}(\nu)] \end{cases} \quad (5.51)$$

$$\begin{cases} A = -\frac{Q}{2} \operatorname{Im}(\nu) \\ |B| = \frac{Q}{2} [2k_3 - \operatorname{Re}(\nu)] \end{cases} \quad (5.52)$$

$$\begin{cases} A = \frac{Q}{2} \operatorname{Im}(\nu) \\ |B| = \frac{Q}{2} [1 + 2k_4 + \operatorname{Re}(\nu)] \end{cases} \quad (5.53)$$

where  $\nu$  is given by

$$\nu = -\frac{1}{2} + \frac{1}{2} \sqrt{1 - 4\xi} . \quad (5.54)$$

These four sets of equations can be combined into two which are

$$\begin{cases} A = -\frac{Q}{2} \operatorname{Im}(\nu) \\ |B| = \frac{Q}{2} [k_1 - \operatorname{Re}(\nu)] \end{cases} \quad (5.55)$$

$$\begin{cases} A = \frac{Q}{2} \operatorname{Im}(\nu) \\ |B| = \frac{Q}{2} [1 + k_2 + \operatorname{Re}(\nu)] \end{cases} \quad (5.56)$$

Once again the integers  $k_1$  and  $k_2$  are non-negative.

It is clear that if the parameter  $\xi \leq 1/4$ , then  $\nu$  is real and the number  $A$  must be zero in (5.55) and (5.56). As a result of these purely imaginary poles in  $\omega$ , the

Green's function  $G(\rho, \zeta; t)$  in (5.43) does not have any oscillatory part and becomes monotonically decreasing in time. This property is passed to the scalar field as we have seen in figure 5.4. On the other hand, when  $\xi > 1/4$ , the poles in  $\omega$  have non-zero real parts which induce the oscillatory character in  $\Psi(t, \rho)$ .

Let us first consider the case  $\xi > 1/4$  more carefully. When  $\xi > 1/4$ , the real part of  $\nu$  is simply  $-1/2$ . If we compare the two equations for  $|B|$  in (5.55) and (5.56), the smallest possible  $|B|$ , which yields the  $\omega$  nearest to the  $\omega$ -real axis, comes from equation (5.55) with  $k_1 = 0$  or equation (5.56) with  $k_2 = 0$ . In any case,  $|B| = Q/4$  and the  $\omega$  that gives dominant exponential falloff rate is

$$\omega = \frac{Q}{4} \left( \pm \sqrt{4\xi - 1} - i \right). \quad (5.57)$$

This corresponds to the dominant exponential decay rate of  $\exp(-Q t/4)$  in  $\Psi$ . This agrees with what we found in figures 5.2 and 5.3.

If  $\xi \leq 1/4$  but  $\xi > 0$  (the latter condition comes from the positivity of the potential  $V$ ),  $\omega$  is always purely imaginary because

$$\text{Re}(\nu) = \nu = -\frac{1}{2} \left( 1 - \sqrt{1 - 4\xi} \right) \in \left( -\frac{1}{2}, 0 \right). \quad (5.58)$$

In this case, not both equations (5.55) and (5.56) give the same  $|B|$  that leads to dominant exponential decay. Only the equation (5.55) with  $k_1 = 0$  produces

$$\omega = -i \frac{Q}{4} \left( 1 - \sqrt{1 - 4\xi} \right) \quad (5.59)$$

which is the closest pole to the real axis on the lower half of the  $\omega$ -plane. Therefore the magnitude of the scalar wave decays monotonically in the exponential manner at a rate of  $\exp\left(-Q \left( 1 - \sqrt{1 - 4\xi} \right) t/4\right)$ . This also agrees with the numerical result as shown in figure 5.4.

## 5.2 Mass Inflation in the Second Background

With the correct late time radiation falloff rate in hand, we are ready to revise the mass inflation calculation and see how the exponential falloff modifies the mechanism in the second dilaton background. When the surface gravity at the Cauchy horizon is zero, we have seen that even an inverse power radiation falloff  $1/t^p$  (with  $p \geq 4$ ) does not trigger a divergence of the mass-energy of the null particle  $S$ . Thus it is not surprising that when the falloff rate is exponential, the inner mass parameter remains bounded.

In the case the surface gravity at the Cauchy horizon is non-zero, something interesting happens beneath the event horizon. First of all, the mass inflation calculation from equation (3.50) to (3.59) remains unaffected because these calculations deal with the geometrical aspect of the problem. In other words, the calculation does not involve the late time radiation falloff which manifested itself through the residual mass  $\delta m(v_1)$ . If the radiation dies out at a rate

$$\Psi(t, x) \sim e^{-\alpha t/2}, \quad (5.60)$$

where  $\alpha$  is some positive number, the residual mass  $\delta m(t)$  will satisfy the relation

$$\frac{d}{dt} \delta m(t) \sim e^{-\alpha t}. \quad (5.61)$$

As a result, we have to recalculate equation (3.60).

We introduce two functions  $\mathcal{F}$  and  $E$  which are related to  $\mathcal{M}$  as

$$\mathcal{M}(X(\lambda)) = \mathcal{F}\left(e^{-2\phi(X(\lambda))}\right) = \mathcal{F}(E(v_1(\lambda))) \quad (5.62)$$

so that the lapse function (3.48) along the null line  $S$  becomes

$$N = \frac{2}{Q E(v_1)} [\mathcal{F}(E(v_1)) - m_1(v_1)]. \quad (5.63)$$

The null condition (3.17) then gives

$$\frac{d}{dv_1} E = \mathcal{F}(E(v_1)) - m_1(v_1) = \mathcal{F}(E(v_1)) - M + \delta m(v_1) . \quad (5.64)$$

By defining  $E(v_1) = E_- + \epsilon(v_1)$  and expanding the function  $\mathcal{F}(E)$  at the point  $E_- \equiv \exp(-2\phi(X_-))$  in the equation above, we obtain

$$\epsilon'(v_1) = \delta m(v_1) + \mathcal{F}'(E_-) \epsilon(v_1) + O(\epsilon^2) \quad (5.65)$$

because  $\mathcal{F}(E_-) = M$ . Furthermore,  $\mathcal{F}'(E_-)$  is negative since the surface gravity, which is positive definite, at Cauchy horizon is

$$\kappa_- = -\frac{1}{Q} \mathcal{M}'(X_-) e^{2\phi(X_-)} = -\mathcal{F}'(E_-) . \quad (5.66)$$

The linearized version of equation (5.65) has a solution

$$\epsilon(v_1) = e^{-\kappa_- v_1} \int \delta m(v_1) e^{\kappa_- v_1} dv_1 . \quad (5.67)$$

Given  $\delta m$  is exponential in  $v_1$ , it is obvious that  $\epsilon(v_1)$  is also exponential at the same rate as  $\delta m$ . Finally because  $X$  relates to  $E$  through the equation

$$\bar{X}(v_1) = X_- + \frac{1}{Q} \ln \left| 1 + \frac{\epsilon(v_1)}{E_-} \right| , \quad (5.68)$$

the replacement for (3.60) is

$$\bar{X}(v_1) \approx X_- + \frac{1}{Q} e^{2\phi(X_-)} \beta \delta m(v_1) , \quad (5.69)$$

where  $\beta$  is a constant for  $\epsilon = \beta \delta m$ . After all equation (3.60) is not really replaced by a completely different equation.

As a result, the mass-energy of the null particle  $\Delta m(\lambda)$  becomes

$$\Delta m(\lambda) = -Q Z_2 \dot{X}(\lambda) = -h Z_2 e^{2\phi(X_-)} \left[ \frac{d}{dv_1} \delta m(v_1) \right] \frac{d}{d\lambda} v_1(\lambda) . \quad (5.70)$$

According to equations (3.58) and (5.61),  $\Delta m$  becomes

$$\Delta m(v_1) \sim e^{-\alpha v_1} e^{\kappa_- v_1} \quad (5.71)$$

in the neighborhood of the Cauchy horizon at which  $v_1 = \infty$ . It is clear that  $\Delta m$  does not necessary diverge at the Cauchy horizon if  $\alpha > \kappa_-$ ; in which case mass inflation does not occur at all. This is analogous to a case discussed in [61]. In fact, due to the multi-horizon structure of the black hole, one could manipulate the parameters  $q$  and  $a_n$  in equation (3.49) in such a way that  $\kappa_-$  is smaller than  $\alpha$ .

An example of such geometry is given by the following lapse function:

$$N(x) = 1 - \frac{2M}{Q} e^{2\phi(x)} + \frac{q^2 - 2a_2}{2Q^2} e^{4\phi(x)} - \frac{a_3}{2Q^2} e^{6\phi(x)}. \quad (5.72)$$

By choosing the  $q$  and  $a_n$  appropriately, this lapse function can be written as

$$N(x) = \left[ 1 - e^{-Q(x-X_+)} \right] \left[ 1 - \frac{1}{\gamma_2} e^{-Q(x-X_+)} \right] \left[ 1 - \frac{1}{\gamma_3} e^{-Q(x-X_+)} \right]. \quad (5.73)$$

where  $\gamma_2$  and  $\gamma_3$  are constants which satisfy the condition  $\gamma_3 > \gamma_2 > 1$ . This condition ensures that

$$X_+ > X_- = X_+ - \frac{1}{Q} \ln(\gamma_2) > X_3 = X_+ - \frac{1}{Q} \ln(\gamma_3). \quad (5.74)$$

The constants  $X_+$ ,  $X_-$  and  $X_3$  corresponds to the positions of the event horizon, Cauchy horizon and a third horizon, respectively. This geometry with  $\xi = 1$ ,  $Q = 1$ ,  $X_+ = -30$ ,  $\gamma_2 = 10$  and  $\gamma_3 = 10.5$  induces a late time radiation falloff rate of  $\exp(-0.24 t)$  which is evident from figure 5.6. On the other hand, the surface gravity at  $X_-$  is  $\kappa_- = Q(\gamma_2 - 1)(1 - \gamma_2/\gamma_3)/2 = 0.2143$ . Because this number is less than  $2 \times 0.24$ , we conclude that mass inflation cannot occur in this background due to the strong exponential attenuation from the radiation falloff. Therefore a spacetime that induces an exponentially shrinking wave can destroy the mass inflation mechanism.

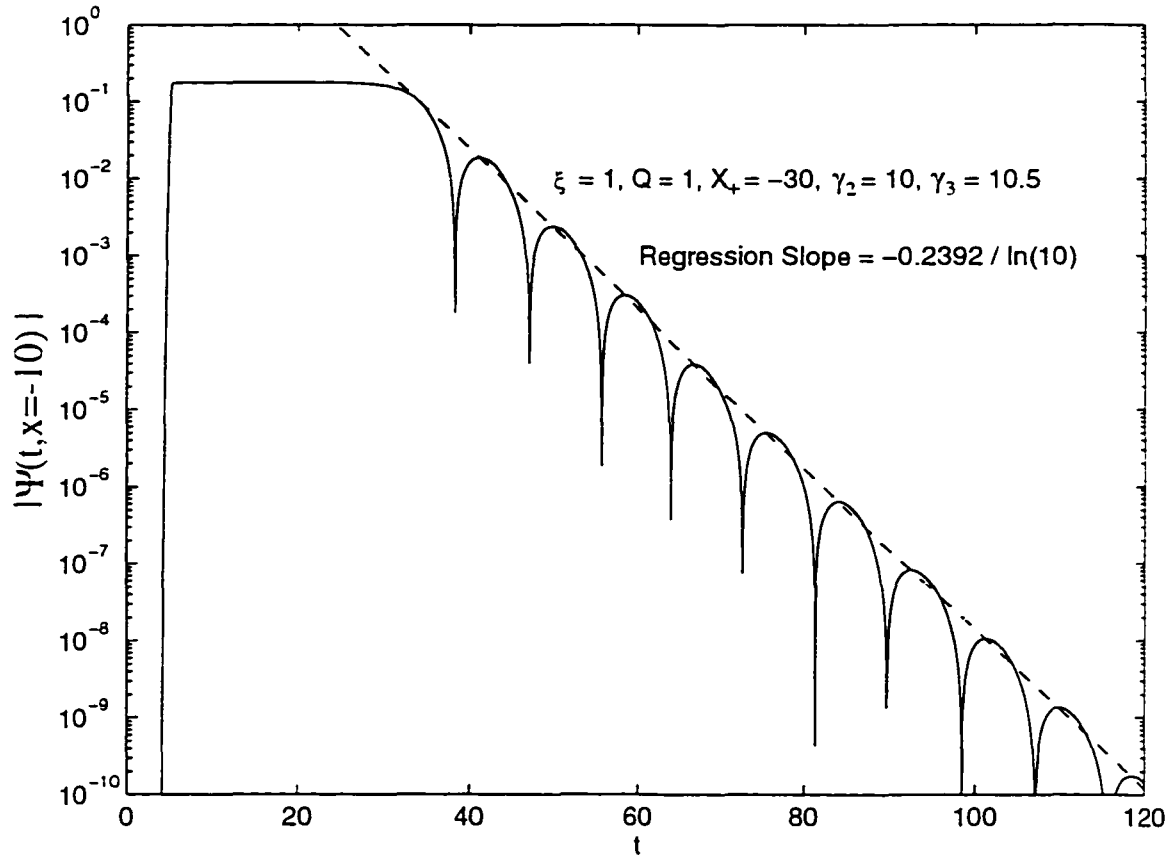


Figure 5.6: Scalar wave falloff in the triple-horizon geometry. The initial impulse is at  $x = -15$  and the observation is made at  $x = -10$  ( $\rho = 20$ ).

Nevertheless an exponential radiation falloff does not necessary stop the mass inflation. The case shown in figure 5.6 is an example where the radiation attenuation dominates. One can always find an example for the opposite situation. Indeed we can understand the competition between  $\kappa_-$  and  $\alpha$  with the help of the result for the single-horizon case. In the single-horizon case, the exponential decay rate of the radiation reads  $\exp(-\alpha t/2)$ , where  $\alpha = Q/2$  for  $\xi = 1 > 1/4$ . Recall that this result comes from the equation (5.57) of the last section. The constant  $Q$  plays an important role here because when we switch from the  $x$  coordinate to the  $\rho$  coordinate, it is the exponent of the tortoise coordinate according to equation (5.12). When the spacetime is determined by the lapse function (5.73), the tortoise coordinate reads

$$\begin{aligned} \rho(x) = & \frac{\gamma_2 \gamma_3}{Q (\gamma_2 - 1) (\gamma_3 - 1)} \ln \left| e^{Q(x-X_+)} - 1 \right| \\ & - \frac{\gamma_3}{Q (\gamma_2 - 1) (\gamma_3 - \gamma_2)} \ln \left| \gamma_2 e^{Q(x-X_+)} - 1 \right| \\ & + \frac{\gamma_2}{Q (\gamma_3 - 1) (\gamma_3 - \gamma_2)} \ln \left| \gamma_3 e^{Q(x-X_+)} - 1 \right|. \end{aligned} \quad (5.75)$$

In the triple-horizon example, the role of the  $Q$  in (5.12) is replaced by another constant  $Q (\gamma_2 - 1) (\gamma_3 - 1) / (\gamma_2 \gamma_3)$ . Thus the condition for suppressed mass inflation is expected to be

$$\alpha = \frac{1}{2} Q \frac{(\gamma_2 - 1) (\gamma_3 - 1)}{\gamma_2 \gamma_3} > \kappa_- = (\gamma_2 - 1) \left( 1 - \frac{\gamma_2}{\gamma_3} \right) \frac{Q}{2}. \quad (5.76)$$

The inequality above implies

$$\gamma_3 < 1 + \gamma_2 \quad (5.77)$$

which is satisfied by the case associated to figure 5.6 ( $\gamma_2 = 10$ ,  $\gamma_3 = 10.5$ ). On the other hand, if this condition is significantly violated, the surface gravity at the Cauchy horizon is expected to be greater than the exponent of the radiation falloff.

This is confirmed by another numerical test shown in figure 5.7. In this simulation, the inequality (5.77) is violated and the resultant falloff rate gives  $\alpha/2 = 0.24$ . However the surface gravity at the Cauchy horizon is 0.75 which is larger than  $\alpha$ . In this case, mass inflation occurs at the Cauchy horizon and produces a scalar curvature singularity there.

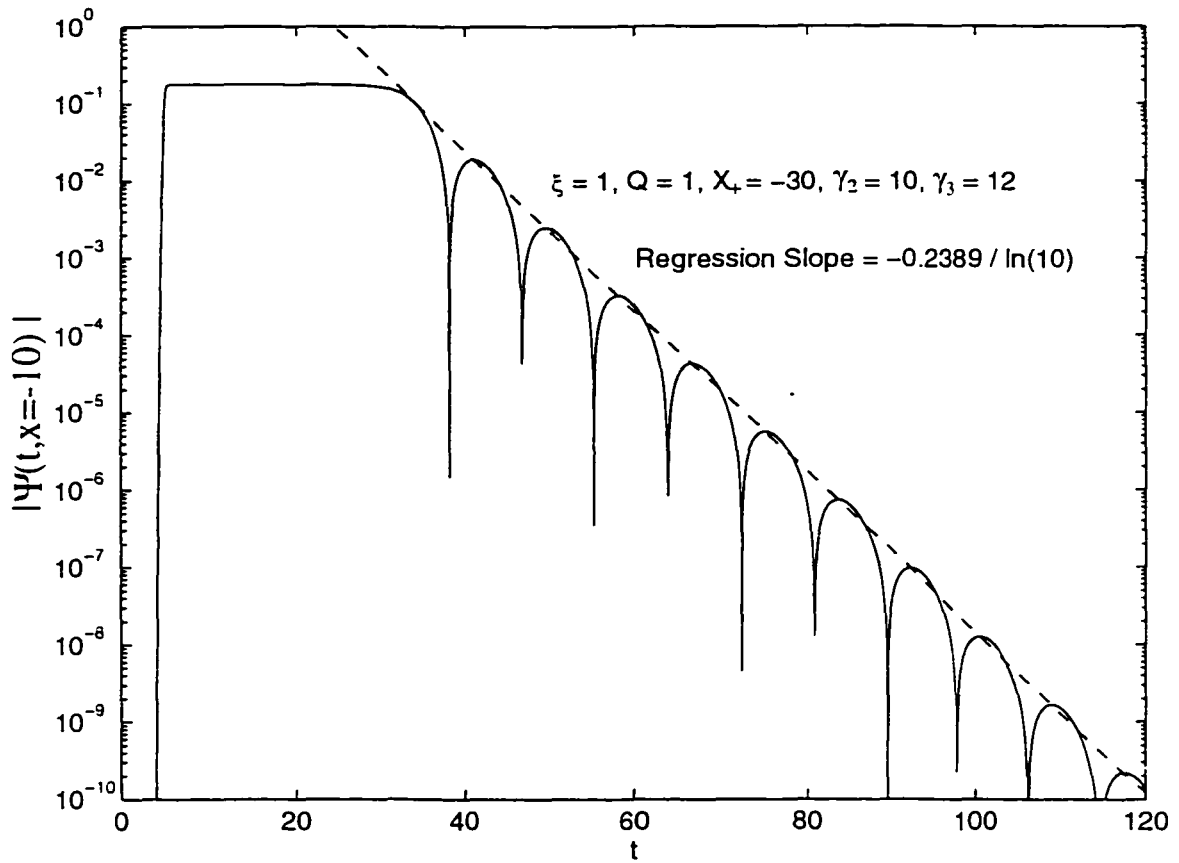


Figure 5.7: Scalar wave falloff in another triple-horizon black hole. Mass inflation is expected in this background because the surface gravity  $\kappa_-$  is much larger than that of the black hole background associated to figure 5.6.

# Chapter 6

## Mass Inflation In 2 + 1 Dimensions

So far we have only studied the asymptotically flat backgrounds in odd spatial dimensions. We now turn our attention to a (2+1)-dimensional black hole spacetime which is not asymptotically flat. This spacetime is interesting because the rotating version of it affords an exact mass inflation calculation [47] which is difficult to carry out in 3 + 1 dimensions [74, 75, 76].

The (2+1)-dimensional black hole spacetime, discovered by Bañados, Teitelboim and Zanelli [77, 78], is a spacetime satisfying the 3D vacuum Einstein equations with a negative cosmological constant ( $\Lambda < 0$ ), that is

$$G_{ab} + \Lambda g_{ab} = 0 . \quad (6.1)$$

The solution of the vacuum Einstein equations is given by

$$ds^2 = -N(r) dt^2 + \frac{dr^2}{N(r)} + r^2 \left[ N^\vartheta(r) dt + d\vartheta \right]^2 , \quad (6.2)$$

where

$$N(r) = -\Lambda r^2 - M + \frac{J^2}{4r^2} , \quad (6.3)$$

$$N^\vartheta(r) = -\frac{J}{2r^2} . \quad (6.4)$$

The variable  $\vartheta$  has a range  $0 \leq \vartheta < 2\pi$ . The constant  $M > 0$  is the quasi-local mass of the black hole and  $J$  is its angular momentum [79]. The black hole undergoes uniform rotation when  $J$  is a non-zero constant. The function  $N$  has two roots  $r = r_{\pm}$  when  $|J| < M/\sqrt{|\Lambda|}$ , where

$$r_{\pm}^2 \equiv \frac{M}{2|\Lambda|} \left( 1 \pm \sqrt{1 - |\Lambda| \frac{J^2}{M^2}} \right). \quad (6.5)$$

This spacetime is indeed a three dimensional anti-de Sitter spacetime with identification  $\vartheta \rightarrow \vartheta + 2\pi k$ , where  $k$  is an integer [77]. In other words, the Ricci scalar in this spacetime everywhere equals a negative constant ( $6\Lambda$ ). In particular, the curvature is finite at  $r = 0$ . The three dimensional anti-de Sitter spacetime can be embedded in a four-dimensional flat space

$$ds^2 = -du^2 - dv^2 + dx^2 + dy^2 \quad (6.6)$$

as a hyperboloid

$$-u^2 - v^2 + x^2 + y^2 = -l^2. \quad (6.7)$$

where  $l^2 = -1/\Lambda$  [6](p. 131). We can transform this anti-de Sitter spacetime to the 3D black hole spacetime (6.2) as follows [77]: When  $r > r_+$ , we transform the coordinates  $\{u, v, x, y\}$  into  $\{t, r, \vartheta\}$  by the equations

$$u = \sqrt{A(r)} \cosh(\tilde{\vartheta}), \quad (6.8)$$

$$v = \sqrt{B(r)} \sinh(\tilde{t}), \quad (6.9)$$

$$x = \sqrt{A(r)} \sinh(\tilde{\vartheta}), \quad (6.10)$$

$$y = \sqrt{B(r)} \cosh(\tilde{t}), \quad (6.11)$$

where

$$A(r) = l^2 \frac{r^2 - r_-^2}{r_+^2 - r_-^2}, \quad (6.12)$$

$$B(r) = l^2 \frac{r^2 - r_+^2}{r_+^2 - r_-^2}. \quad (6.13)$$

$$\bar{t} = \frac{r_+}{l^2} t - \frac{r_-}{l} \vartheta, \quad (6.14)$$

$$\bar{\vartheta} = -\frac{r_-}{l^2} t + \frac{r_+}{l} \vartheta. \quad (6.15)$$

In the region  $r_- < r < r_+$ , we have

$$u = \sqrt{A(r)} \cosh(\bar{\vartheta}), \quad (6.16)$$

$$v = -\sqrt{-B(r)} \cosh(\bar{t}). \quad (6.17)$$

$$x = \sqrt{A(r)} \sinh(\bar{\vartheta}), \quad (6.18)$$

$$y = -\sqrt{-B(r)} \sinh(\bar{t}). \quad (6.19)$$

and when  $0 < r < r_-$ , the transformation reads

$$u = \sqrt{-A(r)} \sinh(\bar{\vartheta}), \quad (6.20)$$

$$v = -\sqrt{-B(r)} \cosh(\bar{t}). \quad (6.21)$$

$$x = \sqrt{-A(r)} \cosh(\bar{\vartheta}). \quad (6.22)$$

$$y = -\sqrt{-B(r)} \sinh(\bar{t}). \quad (6.23)$$

The Killing vector

$$\xi = \frac{\partial}{\partial \vartheta} \quad (6.24)$$

in the 3D black hole spacetime (6.2) can be written as

$$\xi = \frac{\partial u}{\partial \vartheta} \frac{\partial}{\partial u} + \frac{\partial v}{\partial \vartheta} \frac{\partial}{\partial v} + \frac{\partial x}{\partial \vartheta} \frac{\partial}{\partial x} + \frac{\partial y}{\partial \vartheta} \frac{\partial}{\partial y} \quad (6.25)$$

which is simply [77]

$$\xi = \frac{r_+}{l} \left( x \frac{\partial}{\partial u} + u \frac{\partial}{\partial x} \right) - \frac{r_-}{l} \left( y \frac{\partial}{\partial v} + v \frac{\partial}{\partial y} \right). \quad (6.26)$$

It is straightforward to show that  $\xi \cdot \xi$  equals

$$\xi \cdot \xi = r^2 = r_-^2 + \frac{r_+^2 - r_-^2}{l^2} (u^2 - x^2) = r_+^2 - \frac{r_+^2 - r_-^2}{l^2} (v^2 - y^2). \quad (6.27)$$

In the original anti-de Sitter spacetime, the Killing vector  $\xi$  can be spacelike, null or timelike. This property is not manifest in the 3D black hole spacetime because  $r^2$  is not negative in (6.2). In fact, one identifies points in the original spacetime under a discrete isometry of the Lorentz group so that the Killing vector  $\xi$  is always spacelike in the 3D black hole spacetime. The identification is  $\vartheta \rightarrow \vartheta + 2\pi k$  [77]. Indeed the 3D black hole spacetime can be extended through “ $r = 0$ ” to another region in the anti-de Sitter space. Unfortunately the Killing vector not only becomes timelike in the extended region, it induces closed timelike curves in that region due to the identification  $\vartheta \rightarrow \vartheta + 2\pi k$ . As a result, causality is violated if we extend the 3D black hole spacetime to the region “ $r^2 < 0$ ”. Although the spacetime curvature is regular at  $r = 0$  in the 3D black hole, the causal structure starts becoming unphysical at  $r = 0$ . In this sense, Bañados, Teitelboim and Zanelli called  $r = 0$  a causal singularity [77]. It was subsequently shown by Mann and Ross that a collapsing cloud of dust in this black hole spacetime will have infinite density which induces diverging curvature at the center  $r = 0$  [80]. Moreover quantum considerations also show that  $r = 0$  is quantum mechanically unstable [67]. In this thesis, we shall adopt the point of view that equation (6.2) represents a black hole spacetime with “singularity” at  $r = 0$  [47].

Figure 6.1 shows the causal structure of this 3D black hole spacetime subject to the condition  $|J| < M/\sqrt{|\Lambda|}$  [77]. There are two horizons in this spacetime, namely

an outer one at  $r = r_+$  and an inner (Cauchy) horizon at  $r = r_-$ . Although this spacetime might be interpreted as having an infinite number of Cauchy horizons [6](p. 133), the Cauchy horizon we are referring to in this thesis is the one where  $r = r_-$ . The dual-horizon structure of this 3D black hole is a result of the non-zero angular momentum  $J$ . In other words, if the black hole is non-spinning, there is only one horizon - the event horizon. This is analogous to the relationship between Schwarzschild and Kerr black holes in 3 + 1 dimensions.

If we define new coordinates  $v$  and  $\theta$  as

$$v \equiv t + \int^r \frac{d\zeta}{N(\zeta)}, \quad (6.28)$$

$$\theta \equiv \vartheta - \int^r \frac{N^\vartheta(\zeta)}{N(\zeta)} d\zeta. \quad (6.29)$$

metric (6.2) becomes

$$ds^2 = - \left( |\Lambda| r^2 - M \right) dv^2 + 2 dv dr - J dv d\theta + r^2 d\theta^2. \quad (6.30)$$

In this coordinate system, it is clear that  $\partial_v$  and  $\partial_\theta$  are Killing vectors. As one approaches the Cauchy horizon from outside,  $r$  decreases and  $N(r)$  approaches zero from below. Thus by (6.28) the null coordinate  $v$  tends to positive infinity.

Before we present the mass inflation calculation, we consider the late time wave behavior in this 3D black hole background in the next section because the calculation depends upon how radiation dies off. In Section 6.1, we shall find that a scalar wave dies off in this background at an exponential rate. This conclusion is drawn from an exact analytic investigation using a static 3D black hole. The knowledge of the exponential radiation falloff will be used in Section 6.2 in which the mass inflation calculation will be discussed. We shall find that the inflation mechanism in this spacetime is very similar to those we discussed before, despite the fact that this spacetime is rotating and asymptotically non-flat. We shall also learn

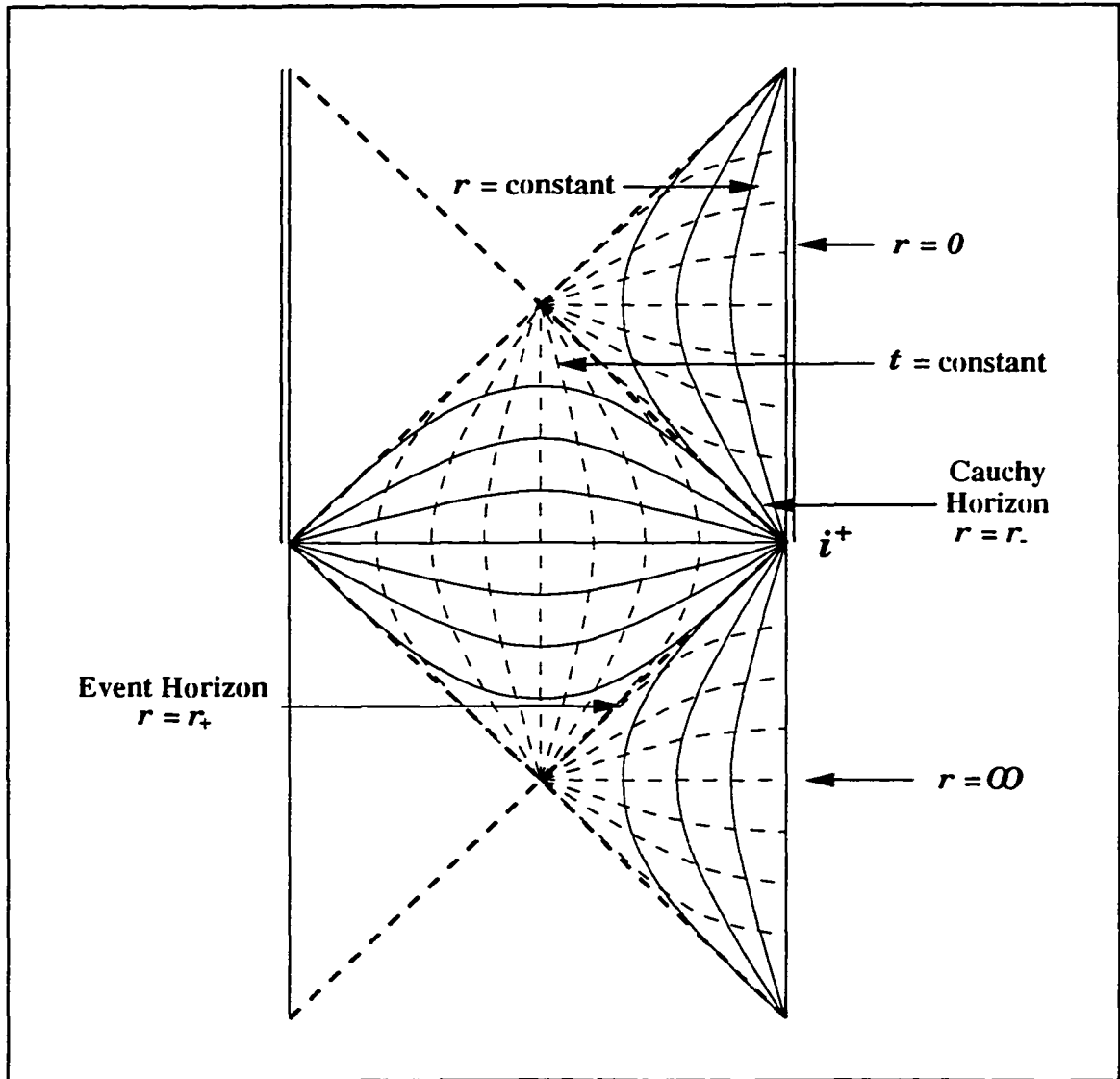


Figure 6.1: Causal structure of the 3D Black Hole.

that mass inflation can occur only when the radiation attenuation is weak enough because there is a competition in the inner mass parameter formula between the exponential blueshift related to the surface gravity at the Cauchy horizon and the exponential attenuation of the radiation intensity. This competition calls for a more detailed study of the radiation decay because the one given in Section 6.1 is not sufficient to determine the radiation falloff rate used in the mass inflation calculation in the non-static background. This detailed study is given in Section 6.3. In previous chapters, numerical simulations served as a check of the analytic calculation. However due to the complexity of the non-static spacetime structure in the present case, the numerical computation carried out in Section 6.3 will play an essential role in determining the radiation falloff rate. We shall find that it is possible for the mass inflation to be suppressed due to strong radiation attenuation. In the last section of this chapter, we shall consider a (3 + 1)-dimensional spacetime which could be considered as a close relative of this 3D black hole spacetime. However this spacetime comes from a string theory and it represents an infinite black string which is a one-dimensional “black object”. Radiation falloff and mass inflation in this spacetime will be discussed.

## 6.1 Radiation Falloff

When the angular momentum  $J$  equals zero, the 3D black hole metric (6.2) reduces to the same form as (4.3). Therefore the wave equation (4.2) in this static black hole spacetime can be reduced to (4.12) with

$$V_c(r) = \frac{3|\Lambda|}{4} (1 - 8\xi) + \frac{M + 4l^2}{4r^2} \quad (6.31)$$

after using the substitution (4.4). In this case, the tortoise coordinate  $\rho$  is given by

$$\rho \equiv \int \frac{dr}{N(r)} = \frac{1}{2\sqrt{|\Lambda|M}} \ln \left| \frac{\sqrt{|\Lambda|r - \sqrt{M}}}{\sqrt{|\Lambda|r + \sqrt{M}}} \right|. \quad (6.32)$$

For this non-rotating black hole, there is only one horizon which is at  $r = R_b = \sqrt{M/|\Lambda|}$ . When  $r$  goes from  $R_b$  to infinity, the tortoise coordinate has a range of  $(-\infty, 0)$ , i.e. this coordinate is semi-infinite in this geometry. We can write  $r$  in terms of  $\rho$  explicitly as

$$r = \sqrt{\frac{M}{|\Lambda|}} \frac{1 + \exp(2\sqrt{|\Lambda|M}\rho)}{1 - \exp(2\sqrt{|\Lambda|M}\rho)}. \quad (6.33)$$

For a conformally invariant wave in 2 + 1 dimensions, the parameter  $\xi$  in (4.2) equals 1/8 and the potential  $V = N V_e$  becomes

$$V(\rho) = V_0 \frac{\exp(\lambda\rho)}{[1 + \exp(\lambda\rho)]^2}. \quad (6.34)$$

For convenience, we have defined

$$V_0 \equiv |\Lambda|(M + 4l^2) > 0. \quad (6.35)$$

$$\lambda \equiv 2\sqrt{|\Lambda|M} > 0. \quad (6.36)$$

We have chosen to consider a conformal wave (i.e.  $\xi = 1/8$ ) because if the value of the parameter  $\xi$  is other than 1/8, the potential

$$V = N V_e = \frac{3\Lambda^2}{4}(1 - 8\xi)r^2 - \frac{\Lambda}{2}(2l^2 - M + 12\xi M) - \frac{M(M + 4l^2)}{4r^2} \quad (6.37)$$

becomes unbounded as  $r \rightarrow \infty$ . This divergence of  $V$  at a finite  $\rho$  ( $\rho \rightarrow 0$  as  $r \rightarrow \infty$ ) imposes a lot of difficulties in writing the code for the numeric calculation.

With the potential (6.34), the wave equation (4.12) is identical to (5.14) with  $\lambda$  in (6.34) being replaced by  $Q$ . Recall that the wave equation (5.14) comes from

the second (1 + 1)-dimensional dilaton spacetime. There is an important difference between the two cases, namely that  $\rho$  is semi-infinite instead of bi-infinite in this case, which complicates the calculation.

We shall solve the scalar wave equation by using the Green's function approach. The scalar field  $\Psi$  of (4.2) can be expressed as

$$\Psi = \frac{1}{\sqrt{r}} \psi(t, \rho) e^{iI\theta} . \quad (6.38)$$

The field  $\psi$  can be represented by a Green's function  $G$  as

$$\psi(t, \rho) = \int_{-\infty}^0 [G(\rho, \zeta; t) \partial_t \psi(0, \zeta) + \psi(0, \zeta) \partial_t G(\rho, \zeta; t)] d\zeta . \quad (6.39)$$

This Green's function in the time domain is related to another Green's function  $\tilde{G}$  in the frequency domain through the equation

$$G(\rho, \zeta; t) = \frac{1}{2\pi} \int_{-\infty}^{\infty} \tilde{G}(\rho, \zeta; \omega) e^{-i\omega t} d\omega . \quad (6.40)$$

The Green's function in the frequency space can be represented as

$$\tilde{G}(\rho, \zeta; \omega) = \begin{cases} \frac{f(\zeta; \omega) g(\rho; \omega)}{W(\omega; g, f)} & \text{if } \zeta < \rho . \\ \frac{f(\rho; \omega) g(\zeta; \omega)}{W(\omega; g, f)} & \text{if } \rho < \zeta . \end{cases} \quad (6.41)$$

where the function  $W(\omega; g, f)$  is the Wronskian defined in equation (5.24). Finally our original problem of the wave equation (4.12) with potential (6.34) relates to the Green's function via the two functions  $f$  and  $g$  which satisfy the equations

$$[\omega^2 + \partial_{\rho\rho} - V(\rho)] f(\rho; \omega) = 0 , \quad (6.42)$$

$$[\omega^2 + \partial_{\rho\rho} - V(\rho)] g(\rho; \omega) = 0 . \quad (6.43)$$

These functions are different because they satisfy different boundary conditions. namely

$$\begin{cases} f(\rho; \omega) \propto \bar{\psi}(\rho; \omega) \\ \partial_\rho f(\rho; \omega) \propto \partial_\rho \bar{\psi}(\rho; \omega) \end{cases} \quad \text{when } \rho \rightarrow -\infty . \quad (6.44)$$

$$\begin{cases} g(\rho; \omega) \propto \bar{\psi}(\rho; \omega) \\ \partial_\rho g(\rho; \omega) \propto \partial_\rho \bar{\psi}(\rho; \omega) \end{cases} \quad \text{when } \rho = 0 . \quad (6.45)$$

The function  $\bar{\psi}(\rho; \omega)$  is simply  $\psi(t, \rho)$  in the frequency space. As a result, if we know  $f$  and  $g$ , we know  $\Psi$ . As in the previous chapter, the time dependence of  $\Psi$  comes solely from the Green's function  $G$ . Thus knowing the time response of  $G$  is sufficient for us to infer the late time behavior of the scalar wave  $\Psi$ .

Although we have obtained the general solution of the differential equation

$$\left\{ \omega^2 + \partial_{\rho\rho} - V_0 \frac{\exp(\lambda\rho)}{[1 + \exp(\lambda\rho)]^2} \right\} h(\rho; \omega) = 0 \quad (6.46)$$

in the last chapter, namely equations (5.29) and (5.30), we shall write the solutions for this static 3D black hole differently as

$$h_\pm(\rho; \omega) = e^{\pm i\omega\rho} F(-\nu, 1 + \nu; 1 \pm \mu; z(\rho)) , \quad (6.47)$$

$$z(\rho) = \frac{\exp(\lambda\rho)}{1 + \exp(\lambda\rho)} . \quad (6.48)$$

$$\mu = i \frac{2\omega}{\lambda} , \quad (6.49)$$

$$\nu = -\frac{1}{2} + i \frac{l}{\sqrt{M}} . \quad (6.50)$$

The functions  $h_+$  and  $h_-$  satisfy the differential equation because  $h_-$  is simply  $h_1$  of (5.29) and  $h_+$  is the negative  $\omega$  version of  $h_-$ . Because  $\rho$  runs from minus infinity to zero,  $z$  in this case has a range of  $(0, 1/2)$  which also ensures the convergence in the hypergeometric function  $F$  [71](p. 556). Besides the obvious similarity between

the pair  $h_+$  and  $h_-$  over  $h_1$  and  $h_2$ , the other advantage of employing  $h_{\pm}$  is the simplicity of the Wronskian. One can show that

$$W(\omega; h_+, h_-) \equiv h_+(\rho; \omega) \partial_\rho h_-(\rho; \omega) - h_-(\rho; \omega) \partial_\rho h_+(\rho; \omega) = -2i\omega . \quad (6.51)$$

Thus the Wronskian vanishes at the point  $\omega = 0$  at which  $h_+ = h_-$ .

At the event horizon of the 3D black hole, we impose the ingoing wave condition

$$f(\rho; \omega) = e^{-i\omega\rho} \quad \text{when } \rho \rightarrow -\infty \quad (6.52)$$

as before (p. 107). This boundary condition determines the choice of  $f$  as

$$f(\rho; \omega) = h_-(\rho; \omega) . \quad (6.53)$$

The boundary condition at spatial infinity is more complicated than before because the black hole spacetime is an anti-de Sitter spacetime with identifications. In other words, waves in the  $\rho$ - $t$  coordinates cannot travel in the positive  $\rho$  direction indefinitely because spatial infinity ( $r = \infty$ ) corresponds to  $\rho = 0$ . We thus need a boundary condition at  $\rho = 0$ . Choosing the Dirichlet condition at  $\rho = 0$ , i.e.

$$\psi(t, \rho = 0) = 0 , \quad (6.54)$$

the function  $g(\rho; \omega)$  becomes

$$g(\rho; \omega) = h_+(\rho; \omega) - A h_-(\rho; \omega) , \quad (6.55)$$

where the coefficient  $A$  is defined as

$$A \equiv \frac{h_+(0; \omega)}{h_-(0; \omega)} . \quad (6.56)$$

When  $\rho$  vanishes,  $z$  equals one half and  $h_{\pm}(0; \omega)$  can be simplified [71](eqn. 15.1.26) so that

$$A = 2^{-2\mu} \frac{\Gamma(1 + \mu)}{\Gamma(1 - \mu)} \frac{\Gamma(1/2 - [\mu + \nu]/2)}{\Gamma(1 + [\mu + \nu]/2)} \frac{\Gamma(1 - [\mu - \nu]/2)}{\Gamma(1/2 + [\mu - \nu]/2)} . \quad (6.57)$$

We observe that  $A$  is unity when  $\omega$  equals zero. As a result,  $g$  vanishes at  $\omega = 0$  because  $h_+ = h_-$  at this frequency.

Had we chosen the Neumann condition instead of the Dirichlet condition for  $\psi$ , that is

$$\partial_\rho \psi(t, \rho)|_{\rho=0} = 0, \quad (6.58)$$

the function  $g(\rho, \omega)$  would simply become

$$g(\rho; \omega) = h_+(\rho; \omega) - B h_-(\rho; \omega). \quad (6.59)$$

where

$$\begin{aligned} B &\equiv \frac{\partial_\rho h_+(0; \omega)}{\partial_\rho h_-(0; \omega)} \\ &= 2^{-2\mu} \frac{\Gamma(1 + \mu)}{\Gamma(1 - \mu)} \frac{\Gamma(-[\mu + \nu]/2)}{\Gamma(1/2 + [\mu + \nu]/2)} \frac{\Gamma(1/2 - [\mu - \nu]/2)}{\Gamma([\mu - \nu]/2)}. \end{aligned} \quad (6.60)$$

Similar to the case of using the Dirichlet condition, we note that  $g$  becomes zero at the point  $\omega = 0$ . It is clear that the type of boundary condition at spatial infinity only affects the coefficient of  $h_-$  in  $g$ .

Now we combine everything and obtain

$$\tilde{G}(\rho, \zeta < \rho; \omega) = \frac{i}{2\omega} h_-(\zeta; \omega) [h_+(\rho; \omega) - A h_-(\rho; \omega)]. \quad (6.61)$$

Equation (6.61) above is the Green's function in the frequency space with the use of the Dirichlet boundary condition at spatial infinity. If the constant  $A$  in (6.61) is replaced by  $B$ , the equation will become the Green's function corresponding to the use of the Neumann condition at  $\rho = 0$ . The remainder of the problem is to bring the Green's function from the frequency domain back to the time domain because we are only interested in the time response of the radiation, especially at

the late time. The equation that transforms the Green's function is given by (5.20) in the previous chapter. The integral in this equation will be replaced by a contour integral on the complex  $\omega$ -plane. The contour of integration is chosen to be the standard large, closed semi-circle on the lower half  $\omega$ -plane. By Jordan's lemma, the contribution from the arc of the large semi-circle goes to zero as the radius of the arc tends to infinity. The Green's function then becomes

$$G(\rho, \zeta; t) = i \sum \text{Res} \left\{ \tilde{G}(\rho, \zeta; \omega) \exp(-i \omega t) \right\} \quad (6.62)$$

because there are no branch cuts in the Gamma functions [71](p. 255) and the hypergeometric functions [73](p. 160) in this case. The poles of the Green's function  $\tilde{G}(\rho, \zeta; \omega)$  within the contour come from the Gamma functions of the coefficient  $A$  or coefficient  $B$ , depending on which boundary condition is used at  $\rho = 0$ .

Let us consider the Dirichlet case first. The poles from the coefficient  $A$  correspond to

$$1 + \mu = -k_1, \quad (6.63)$$

$$\frac{1}{2} - \frac{\mu + \nu}{2} = -k_2, \quad (6.64)$$

$$1 - \frac{\mu - \nu}{2} = -k_3, \quad (6.65)$$

where  $k_1$ ,  $k_2$  and  $k_3$  are non-negative integers. The dominant exponential decay rate is determined by the pole closest to the real axis on the lower half  $\omega$ -plane. According to the three equations above, there are two such poles, namely

$$\omega = \pm \frac{l}{2\sqrt{M}} \lambda - i \frac{3}{4} \lambda. \quad (6.66)$$

As a result, the exponentially decaying Green's function  $G$  implies that  $\psi$  also decays in this manner at a rate of  $\exp(-3 \lambda t/4)$  when the Dirichlet condition is used at the boundary  $\rho = 0$ .

The next graph shows the numerical results using the potential (6.34). We used the same initial condition as the one in the numerical computation for the Schwarzschild case in Chapter 4. Since the background spacetime has a time-like spatial infinity in this case, we integrate equation (4.12) numerically with the Dirichlet boundary condition at  $r = \infty$  (i.e.  $\rho = 0$ .) Figure 6.2 illustrates the falloff behavior of the wave using different potentials. In the graph, the initial Gaussian impulse is located at twice the black hole radius ( $2 R_b$ ) and the observation is made at  $4 R_b$ . The straight line asymptotes of the ringing behavior on the semilog graph correspond to the exponential falloffs, numerically confirming that the wave exponentially decays in this static 3D black hole background at a rate  $\exp(-3 \lambda t/4)$ .

The change from the coefficient  $A$  to  $B$  in (6.61) for the Neumann condition at the spatial infinity causes the singular terms in  $\tilde{G}$  to be  $\Gamma(1 + \mu)$ ,  $\Gamma(-[\mu + \nu]/2)$  and  $\Gamma(1/2 - [\mu - \nu]/2)$ . These gamma functions imply the singularities at

$$\mu = -k_1 - 1 , \quad (6.67)$$

$$\mu = 2k_2 - \nu , \quad (6.68)$$

$$\mu = 2k_3 + 1 + \nu , \quad (6.69)$$

where  $k_1$ ,  $k_2$  and  $k_3$  are also non-negative integers. A quick inspection concludes that  $\psi$  dies out to zero at an exponential rate of  $\exp(-\lambda t/4)$  because the poles which are closest to the real  $\omega$ -axis are

$$\omega = \pm \frac{l}{2\sqrt{M}} \lambda - i \frac{\lambda}{4} . \quad (6.70)$$

Figure 6.3 illustrates the numerical results using the Neumann boundary condition at  $\rho = 0$ . It is clear from the graph that the scalar wave also exponentially decays when the Neumann condition is used. One can see that the falloff rate is

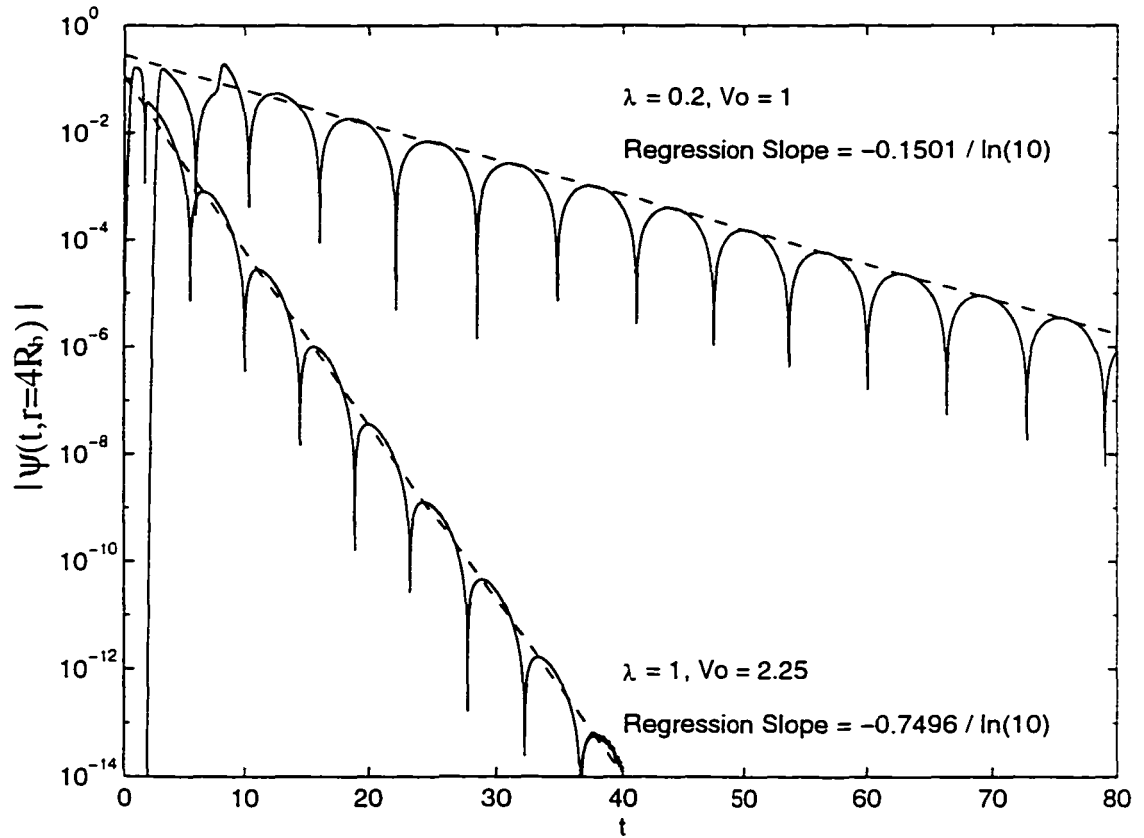


Figure 6.2: Exponential falloff for a conformal scalar wave using the Dirichlet boundary condition.

three times slower than that in the Dirichlet case because the dominant poles in this case are three times closer to the real  $\omega$ -axis than those in the Dirichlet case.

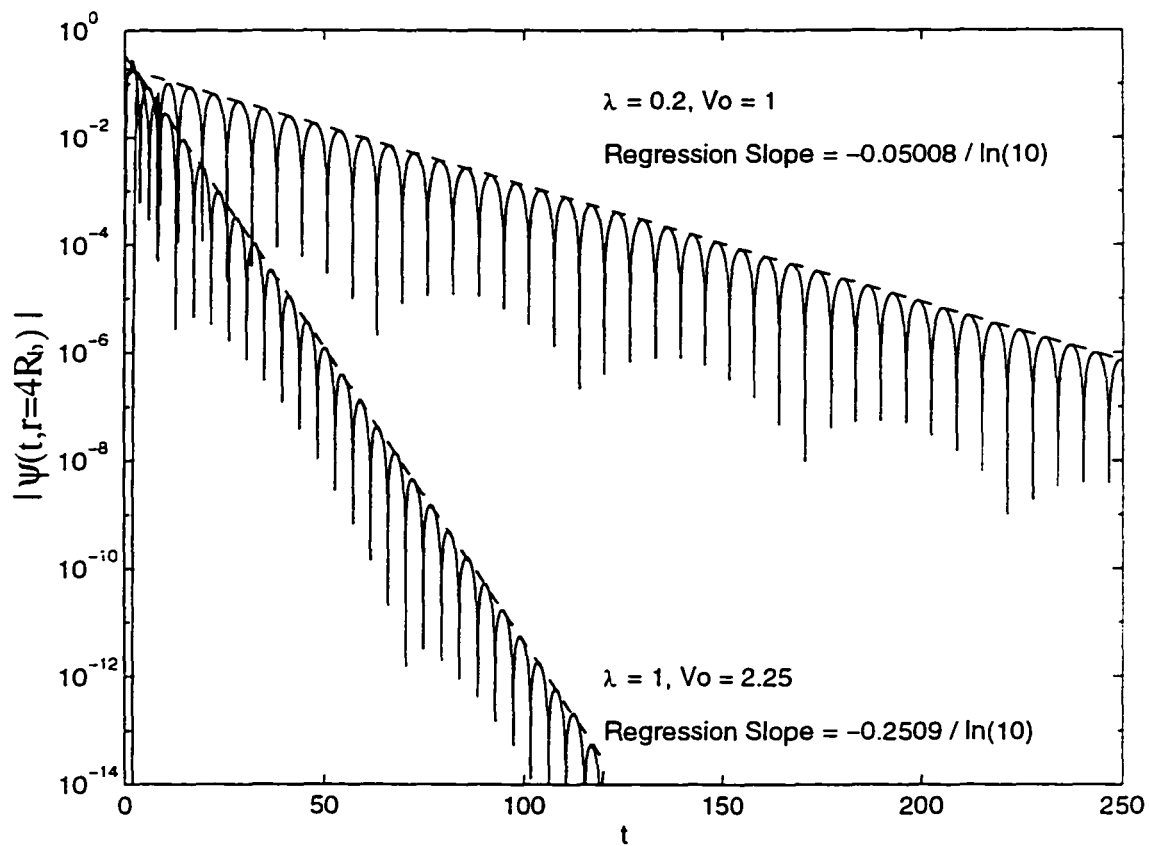


Figure 6.3: Exponentially decaying scalar waves using the Neumann condition.

In this 3D black hole spacetime, the potential  $V$  always has the absolute maximum  $V_0$  at  $\rho = 0$ , according to equation (6.34). This is evident from figure 6.4. Moreover there is no sharp peak in the potential. As a result, all observers are always on the left side of the potential maximum. This is different from the case

for the Schwarzschild background in which an observer could either be on the left or on the right of the potential maximum (sharp peak). Since in the 3D black hole background all observers are in a region in which the potential decreases in the decreasing- $\rho$  direction, they will observe similar falloff behavior for the radiation.



Figure 6.4: The graph of potential function (6.34) with  $\lambda = 0.02$  and  $V_0 = 1$ .

## 6.2 Mass Inflation Calculation

We now consider mass inflation in the rotating 3D black hole background. The stress-energy tensor of the null dust in this rotating background has the form

$$[T_{ab}] = \begin{bmatrix} \rho_{in} & 0 & 0 \\ 0 & 0 & 0 \\ 0 & 0 & 0 \end{bmatrix} \quad (6.71)$$

in the coordinate system  $\{v, r, \theta\}$ . Putting the stress-energy tensor (6.71) into the (2 + 1)-dimensional Einstein equations

$$G_{ab} + \Lambda g_{ab} = 8 \pi G T_{ab} . \quad (6.72)$$

we obtain an exact solution [47]

$$ds^2 = -\alpha(v, r) dv^2 + 2 dv dr - J dv d\theta + r^2 d\theta^2 . \quad (6.73)$$

where  $\alpha(v, r) = |\Lambda| r^2 - m(v)$ . The function  $m$  satisfies the equation

$$\frac{d}{dv} m(v) = 16 \pi G r \rho_{in} \quad (6.74)$$

because  $r \rho_{in}$  is a function of  $v$ , as may easily be shown from the conservation laws. As usual, we interpret  $m$  as the mass function of the spacetime described by (6.73) [79]. This metric is the (2 + 1)-dimensional rotating analogue of the Vaidya solution which is spherically symmetric.

We consider a pulse of outgoing radiation between the event and Cauchy horizons of the black hole spacetime (6.73) as in the mass inflation setup in the Vaidya-Reissner-Nordström background or the (1 + 1)-dimensional dilaton black hole backgrounds. However the pulse  $S$  in this case is a null ring in  $r$ - $\theta$  coordinates. We

denote the region enclosed by this ring as II and its complement as region I, characterized by the mass parameters  $m_2(v_2)$ , and  $m_1(v_1)$ , respectively. This setup is very close to the one depicted in figure 2.3 on page 40 or figure 3.1 on page 51. In other words, there is an outgoing null ring inside the 3D black hole which is irradiated by fluxes of ingoing radiation described by the stress-energy tensor (6.71). We match two patches of the solution (6.73) as before along the ring S which is found between the event and Cauchy horizons. Any null ray in this rotating black hole background satisfies the equation

$$-\alpha \dot{v}^2(\lambda) + 2\dot{v}(\lambda)\dot{r}(\lambda) - J\dot{v}(\lambda)\dot{\theta}(\lambda) + r^2(\lambda)\dot{\theta}^2(\lambda) = 0 \quad (6.75)$$

where  $\lambda$  is the affine parameter which is chosen to be zero at the Cauchy horizon and negative in region I. The overdot, once again, represents differentiation with respect to  $\lambda$ . The geodesic equations in this black hole spacetime are

$$2\ddot{v} = -\partial_r\alpha(v, r)\dot{v}^2 + 2r\dot{\theta}^2. \quad (6.76)$$

$$0 = \frac{d}{d\lambda} [-J\dot{v} + 2r^2\dot{\theta}]. \quad (6.77)$$

Equation (6.77) implies that

$$\dot{\theta}(\lambda) = \frac{J}{2r^2(\lambda)}\dot{v}(\lambda), \quad (6.78)$$

where we have set the constant of motion  $g(\partial_\theta, u)$  to zero. The vector  $u$  is the 3-velocity of the ring [2](p. 442).

By using (6.78), equation (6.76) can be written as

$$\frac{d}{d\lambda} \left[ \frac{2}{\dot{v}} \right] = \partial_r\mathcal{M}(r), \quad (6.79)$$

where  $\mathcal{M}(r)$  is defined as  $|\Lambda|r^2 + J^2/(4r^2)$ . Equation (6.78) also simplifies the null condition (6.75) as

$$2\dot{v}\dot{r} = [\mathcal{M}(r) - m(v)]\dot{v}^2. \quad (6.80)$$

The null condition above is in the same form as equation (2.67) or (3.17). In fact we can rewrite (6.79) as

$$\frac{d}{d\lambda} \left[ \frac{1}{\dot{v}} \right] = \frac{1}{2} \partial_r N(v, r) \quad (6.81)$$

which is identical to equation (2.70). The function  $N(v, r)$  in the above equation equals  $\mathcal{M}(r) - m(v)$  in this rotating 3D black hole background.

After defining a function  $R(\lambda)$  such that  $2\pi R$  is the perimeter of the ring  $S$  and another function

$$z(\lambda) \equiv \frac{2R(\lambda)}{\dot{v}(\lambda)}, \quad (6.82)$$

it is straightforward to show that (6.79), (6.80) and (6.82) give the set of equations

$$z_i(\lambda) = R(\lambda) \left[ Z_i + \int_0^\lambda \mathcal{M}'(R(\zeta)) d\zeta \right], \quad (6.83)$$

$$v_i(\lambda) = 2 \int^\lambda \frac{R(\zeta)}{z_i(\zeta)} d\zeta, \quad (6.84)$$

$$m_i(v_i(\lambda)) = \mathcal{M}(R(\lambda)) + R(\lambda) \mathcal{M}'(R(\lambda)) - \dot{z}_i(\lambda). \quad (6.85)$$

As usual the subscript  $i$  is either 1 or 2 for regions I or II respectively. The prime denotes differentiation with respect to the spatial coordinate  $R$ . By comparing the equations above with those in (2.75 - 2.77), (3.22 - 3.24) or (3.52 - 3.54), we observe that the set of equations (6.83) to (6.85) is quite different from the other sets. This can be explained by the fact that the mass  $m(v)$  in  $N(v, r)$  of the 3D black hole is isolated from the  $r$ -dependent part. That is to say  $\partial N/\partial m$  is not a function of  $r$  in this spacetime. Because of this, the computation of  $dz/d\lambda$  from (6.82) produces an  $m$ -dependent answer, which is not what one would obtain by using the other three background spacetimes. Thus isolating the mass  $m$  in the set of equations is done differently in this spacetime, thereby yielding a different looking set of matching equations.

Since the outgoing null ring is inside the black hole, its mass-energy is given by

$$\Delta m(\lambda) \equiv m_2(\lambda) - m_1(\lambda) = (Z_1 - Z_2) \dot{R}(\lambda) . \quad (6.86)$$

By using an argument similar to the one given on page 43, we conclude that  $Z_1$  must be zero. Furthermore since  $\dot{R}(\lambda)$  is expected to be negative inside the black hole, the sign of  $Z_2$  must be positive in order to have a positive  $\Delta m$  in (6.86).

Equation (6.83) can be approximated near the Cauchy horizon as

$$z_i(\lambda) \approx R(\lambda) [Z_i - 2\kappa_- \lambda] , \quad (6.87)$$

where  $\kappa_-$  is defined as

$$\kappa_- \equiv -\frac{1}{2} \mathcal{M}'(\tau_-) \quad (6.88)$$

and  $\tau_-$  is the value of  $\tau$  at the Cauchy horizon. Because the derivative of  $\mathcal{M}$  must be negative at  $\tau_-$ ,  $\kappa_-$  is positive. Once we know the approximated  $z_i$  in the neighborhood of  $\lambda = 0$ , the other function  $v_i$  becomes

$$v_i(\lambda) \approx \int^\lambda \frac{2}{Z_i - 2\kappa_- \zeta} d\zeta \quad (6.89)$$

which yields

$$v_1(\lambda) \approx -\frac{1}{\kappa_-} \ln|\lambda| , \quad (6.90)$$

$$v_2(\lambda) \approx \frac{2}{Z_2} \lambda . \quad (6.91)$$

Similar to what we did before, by using the null condition (6.80) and assuming that

$$\tilde{R}(v_1) = r_- + \epsilon(v_1) , \quad (6.92)$$

it is not difficult to show that

$$\epsilon(v_1) \approx K e^{-\kappa_- v_1} + \frac{1}{2} e^{-\kappa_- v_1} \int e^{\kappa_- v_1} \delta m(v_1) dv_1, \quad (6.93)$$

where  $K$  is an integration constant. This result, with the use of equation (6.90), implies that

$$\dot{R}(\lambda) \approx K + \frac{1}{2} \int^{v_1(\lambda)} e^{\kappa_- v} \delta m(v) dv - \frac{1}{2 \kappa_-} e^{\kappa_- v_1(\lambda)} \delta m(v_1(\lambda)). \quad (6.94)$$

The analysis in the previous section suggests that the residual mass  $\delta m(v_1)$  should be exponentially decreasing. If this decay rate is given by  $\delta m(v_1) = h \exp(-\alpha v_1)$ , then  $\dot{R}$  will be either decreasing or increasing, depending on the relative size of  $\kappa_-$  and  $\alpha$ . When  $\kappa_- > \alpha$ ,  $\dot{R}$  will diverge at a rate of  $\exp(|\kappa_- - \alpha| v_1)$  because  $v_1$  goes to infinity when the ring moves towards the Cauchy horizon. However it will deflate at a rate  $\exp(-|\alpha - \kappa_-| v_1)$  to  $K$  if  $\alpha > \kappa_-$ . The case  $\kappa_- = \alpha$  does not interest us because the two cases  $\kappa_- > \alpha$  and  $\alpha > \kappa_-$  have included the inflating and deflating scenarios; not to mention the measure zero chance of having  $\kappa_-$  equal  $\alpha$ . Rearranging equation (6.86) yields

$$m_2(\lambda) = M - Z_2 K - h e^{-\alpha v_1(\lambda)} + \frac{h \alpha Z_2}{2 \kappa_- (\kappa_- - \alpha)} e^{(\kappa_- - \alpha) v_1(\lambda)}. \quad (6.95)$$

It is obvious that when  $\alpha > \kappa_-$ , the inner mass parameter  $m_2$  is bounded from above which signifies the inhibition of mass inflation. In the case of the second dilaton black hole in Chapter 5, we have seen that the radiation attenuation can exceed the exponential growth due to the geometry at the Cauchy horizon. Since  $\alpha$  is determined by the falloff rate of the residual mass  $\delta m$  of the radiation, there is a competition between the strength of the surface gravity at the Cauchy horizon and the decay of the radiation. Unfortunately whether or not  $\kappa_-$  is greater than  $\alpha$  in this rotating 3D black hole is unclear because the conclusion of exponential decay of radiation is inferred from the use of an unrotating black hole which has

no Cauchy horizon at all. The analysis in the previous section only suggests that radiation outside a spinning black hole in three dimensions decays exponentially but the study fails to tell us the strength of the decay outside the rotating black hole. In the next section, we shall consider a special case of radiation falloff in a rotating black hole background.

### 6.3 Radiation Outside a Spinning 3D Black Hole

In section 6.1, we have seen that a conformally invariant scalar wave exponentially decays outside a static 3D black hole. When the black hole rotates, that is  $J \neq 0$ , we also find an exponential decay rate for the scalar wave, as we shall now demonstrate.

If we assume that

$$\Psi(t, r, \vartheta) = \frac{\psi(t, r)}{\sqrt{r}} . \quad (6.96)$$

that is to say there is no ‘‘spherical harmonic’’ component in the wave, the conformal scalar wave equation  $\nabla^2 \Psi = R \Psi / 8$  in the rotating 3D black hole background will also reduce to the form (4.12). The tortoise coordinate  $\rho$  is defined as (4.11) and the potential function reads

$$V_c(r) = -\frac{3|\Lambda|}{4} + \frac{1}{2r} \frac{d}{dr} N(r) - \frac{N(r)}{4r^2} . \quad (6.97)$$

Although the form of the metric (6.2) is different from the form in (4.3), the potential function (6.97) is identical to (4.7) with  $D = 2$ ,  $l = 0$  and  $\xi = 1/8$ , where  $R = 6\Lambda$  for this 3D black hole spacetime.

In the stationary case, the black hole has two horizons  $r_{\pm}$ . The function  $N(r)$  can then be written in terms of  $r_+$  and  $r_-$  as

$$N(r) = \frac{|\Lambda|}{r^2} (r^2 - r_+^2) (r^2 - r_-^2) . \quad (6.98)$$

The tortoise coordinate  $\rho$  can be expressed by using  $r_{\pm}$  as

$$\rho(r) = \frac{1}{2|\Lambda|(r_+^2 - r_-^2)} \left[ r_+ \ln \left| \frac{r - r_+}{r + r_+} \right| - r_- \ln \left| \frac{r - r_-}{r + r_-} \right| \right]. \quad (6.99)$$

The function  $\rho(r)$  has no closed form inverse but we can express the inverse in a series as [81]

$$\frac{r_+}{r(\rho)} = \frac{Y}{1 - \sigma^2} \sum_{n=0}^{\infty} a_n(\sigma) Y^{2n}. \quad (6.100)$$

where

$$\sigma = \frac{r_-}{r_+} < 1, \quad (6.101)$$

$$Y = \frac{1 - \exp(\lambda \rho)}{1 + \exp(\lambda \rho)} < 1. \quad (6.102)$$

$$\lambda = 2|\Lambda|r_+(1 - \sigma^2) > 0. \quad (6.103)$$

The coefficients  $a_n(\sigma)$  are given as

$$a_0(\sigma) = 1, \quad (6.104)$$

$$a_1(\sigma) = -\sigma^2 \frac{3 - \sigma^2}{3(1 - \sigma^2)^2}, \quad (6.105)$$

$$a_2(\sigma) = \sigma^4 \frac{25 - 17\sigma^2 + 3\sigma^4}{15(1 - \sigma^2)^4}, \quad (6.106)$$

$$a_3(\sigma) = -\sigma^6 \frac{1008 - 1039\sigma^2 + 368\sigma^4 - 45\sigma^6}{315(1 - \sigma^2)^6}, \quad (6.107)$$

⋮

which are of order  $O(\sigma^{2n})$ . If  $\sigma$  is small enough, we can employ an approximation

$$\frac{1}{r(\rho)} \approx \frac{Y}{r_+}. \quad (6.108)$$

Substituting this approximation into the potential  $V = N V_e$ , we obtain

$$\begin{aligned} V(\rho) \approx & \Lambda^2 \frac{(r_+^2 - r_-^2)(r_+^2 - 4r_-^2)}{r_+^2} \frac{\exp(\lambda \rho)}{[1 + \exp(\lambda \rho)]^2} \\ & + 12 \Lambda^2 (2r_+^2 - 3r_-^2) \frac{r_-^2}{r_+^2} \frac{\exp(2\lambda \rho)}{[1 + \exp(\lambda \rho)]^4} \\ & + 80 \Lambda^2 \frac{r_-^4}{r_+^2} \frac{\exp(3\lambda \rho)}{[1 + \exp(\lambda \rho)]^6} . \end{aligned} \quad (6.109)$$

It is obvious that the first term in the potential above has a form identical to the potential (6.34) in the static case. Since  $\lambda > 0$  but  $\rho < 0$ , the second term in the potential (6.109) is always weaker than the first one. This suggests that we may iteratively solve the wave equation, treating the first term as the lowest order potential, the second term as the first correction to this approximation, and so on.

Let us ignore the third term in the potential (6.109) for a moment. For clarity, we define the following:

$$V_0(\rho) \equiv \Lambda^2 \frac{(r_+^2 - r_-^2)(r_+^2 - 4r_-^2)}{r_+^2} \frac{\exp(\lambda \rho)}{[1 + \exp(\lambda \rho)]^2} . \quad (6.110)$$

$$V_1(\rho) \equiv 12 \Lambda^2 (2r_+^2 - 3r_-^2) \frac{r_-^2}{r_+^2} \frac{\exp(2\lambda \rho)}{[1 + \exp(\lambda \rho)]^4} . \quad (6.111)$$

$$\tilde{D} \equiv -\omega^2 - \partial_{\rho\rho} + V_0(\rho) + V_1(\rho) , \quad (6.112)$$

$$\tilde{D}_0 \equiv -\omega^2 - \partial_{\rho\rho} + V_0(\rho) . \quad (6.113)$$

When we follow the Green's function approach as was demonstrated in Section 6.1, we shall obtain the solution (6.39). The Green's function in the frequency space is given by equation (6.41), where  $\tilde{D}f(\rho; \omega) = \tilde{D}g(\rho; \omega) = 0$ . The equation  $\tilde{D}f(\rho; \omega) = 0$  has a representation

$$f(\rho; \omega) = f_0(\rho; \omega) + \int_{-\infty}^{\rho} \frac{U_+(\rho) U_-(\zeta) - U_-(\rho) U_+(\zeta)}{W(\omega; U_-, U_+)} V_1(\zeta) f(\zeta; \omega) d\zeta \quad (6.114)$$

at  $\rho = -\infty$ . The functions  $U_+(\rho)$  and  $U_-(\rho)$  satisfy the equations  $\tilde{D}_0 U_+(\rho) = 0$  and  $\tilde{D}_0 U_-(\rho) = 0$ . The other function  $f_0(\rho; \omega)$  satisfies not only the same equation

as  $U_+(\rho)$  and  $U_-(\rho)$  but also the boundary condition at  $\rho \rightarrow -\infty$ . In other words,  $f_0(\rho; \omega)$  is simply the solution (6.53) and  $U_\pm$  are  $h_\pm$  in our case with different values of  $\lambda$ ,  $\mu$  and  $\nu$ . Similarly the solution of  $\tilde{D}g(\rho; \omega) = 0$  around  $\rho = 0$  is given by

$$g(\rho; \omega) = g_0(\rho; \omega) - \int_\rho^0 \frac{U_+(\rho)U_-(\zeta) - U_-(\rho)U_+(\zeta)}{W(\omega; U_-, U_+)} V_1(\zeta) g(\zeta; \omega) d\zeta . \quad (6.115)$$

where  $g_0(\rho; \omega)$  is (6.55) if the Dirichlet condition at the spatial infinity is adopted.

We first compute the Wronskian  $W(\omega; g, f)$  for  $f(\rho; \omega)$  and  $g(\rho; \omega)$  above. Since the Wronskian is  $\rho$ -independent, the simplest way to calculate it is to evaluate the quantity at the point  $\rho = 0$ . It is not difficult to show that the expressions (6.114) and (6.115) for  $f$  and  $g$  admit the Wronskian [81]

$$W(\omega; g, f) = W(\omega; g_0, f_0) + W(\omega; g_0, f)(\rho)|_{\rho=-\infty}^{\rho=0} \quad (6.116)$$

$$= W(\omega; g_0, f_0) - W(\omega; g, f_0)(\rho)|_{\rho=-\infty}^{\rho=0} . \quad (6.117)$$

Since  $g(\rho; \omega)$  and  $f(\rho; \omega)$  satisfy a differential equation which differs from that satisfied by  $g_0(\rho; \omega)$  and  $f_0(\rho; \omega)$ , the Wronskians  $W(\omega; g_0, f)$  and  $W(\omega; g, f_0)$  are functions of  $\rho$  in general. The second term on the right side of either (6.116) or (6.117), which originates from the correction potential  $V_1$ , induces an extra ( $\rho$ -independent) term in the Wronskian  $W(\omega; g, f)$ .

Because of the presence of  $f$  (or  $g$ ) inside the integral of equation (6.114) (or (6.115)), the equation is in fact an integral equation in  $f$  (or  $g$ ). We employ the first Born approximations for  $f(\rho; \omega)$  and  $g(\rho; \omega)$  and obtain

$$\begin{aligned} f(\rho; \omega) &\approx f_1(\rho; \omega) \\ &= f_0(\rho; \omega) - i \int_{-\infty}^\rho \frac{h_+(\rho)h_-(\zeta) - h_-(\rho)h_+(\zeta)}{2\omega} V_1(\zeta) f_0(\zeta) d\zeta , \end{aligned} \quad (6.118)$$

$$\begin{aligned} g(\rho; \omega) &\approx g_1(\rho; \omega) \\ &= g_0(\rho; \omega) + i \int_\rho^0 \frac{h_+(\rho)h_-(\zeta) - h_-(\rho)h_+(\zeta)}{2\omega} V_1(\zeta) g_0(\zeta) d\zeta . \end{aligned} \quad (6.119)$$

As a result, the Wronskian  $W(\omega; g, f)$  can be approximated as

$$\begin{aligned} W(\omega; g, f) &\approx W(\omega; g_0, f_0) + W(\omega; g_0, f_1)(\rho)|_{-\infty}^0 \\ &= W(\omega; g_0, f_0) + \int_{-\infty}^0 g_0(\rho; \omega) f_0(\rho; \omega) V_1(\rho) d\rho . \end{aligned} \quad (6.120)$$

Since there are no branch cuts in either  $f_1$  or  $g_1$  but there are poles in the lower half  $\omega$ -plane in the Green's function  $\tilde{G}$  (6.41), there is an exponentially decaying wave tail in this rotating 3D black hole background.

Figure 6.5 shows the graphs of two potentials  $V$  in this stationary case with zero angular harmonics (i.e.  $l = 0$ ). One can show that when the ratio  $|\Lambda| J^2/M^2 > 16/25$ , the potential function  $V_e$  becomes negative for some  $\tau > \tau_+$ . This behavior is illustrated in one of the curve in the diagram, where  $V(\rho)$  becomes negative when  $|\rho|$  is sufficiently large. However the ratio  $|\Lambda| J^2/M^2$  cannot exceed unity for which value the black hole is extremal. In figure 6.6, we can see that the potential  $V$  in both cases vanish at an exponential rate towards the event horizon. We put a Gaussian impulse at a distance  $2\tau_+$ . The numerical response of the scalar wave over time at a distance  $4\tau_+$  is shown in figure 6.7. This diagram shows the exponentially decaying property of the wave. The shape of the falloff in the diagram differs from that of the other graphs like figures 5.2, 5.3 and 5.6 because there are no angular harmonics (i.e.  $l = 0$ ) in this case. In fact if we set  $l = 0$  in the static 3D black hole case, we shall find the shape of the falloff resembles that in figure 6.7 because the frequency (6.66) (when the Dirichlet condition is used at  $\tau = \infty$ ) or (6.70) (when the Neumann condition is used) has no real part. As a result, the Green's function (6.62) is not oscillatory.

For a rotating 3D black hole we have shown that a  $\vartheta$ -independent scalar field also has late time exponential decay. In this spacetime, one can calculate the mass inflation rate using this result. Equation (6.95) at the end of the last section

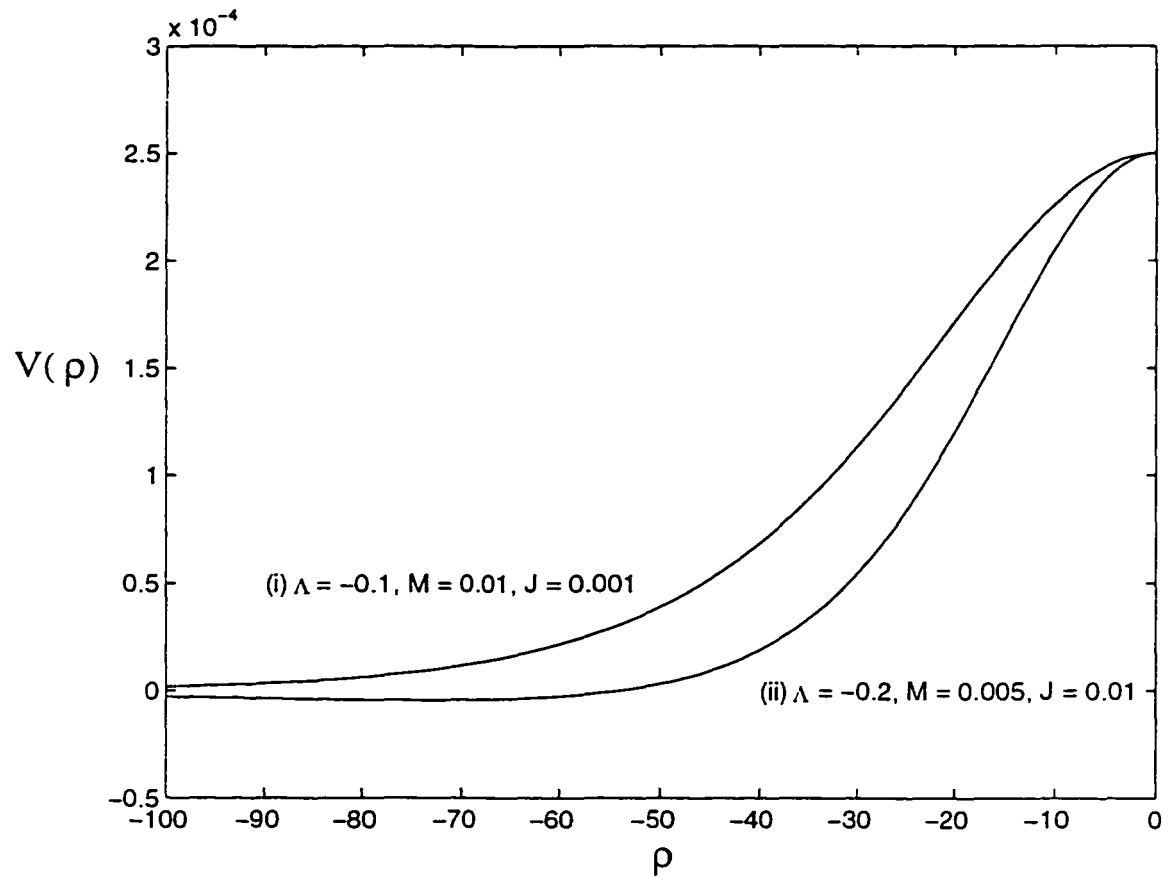


Figure 6.5: Potential function  $V(\rho)$  of two spinning 3D black hole backgrounds with (i)  $|\Lambda| J^2/M^2 = 10^{-3}$  and (ii)  $|\Lambda| J^2/M^2 = 0.8$

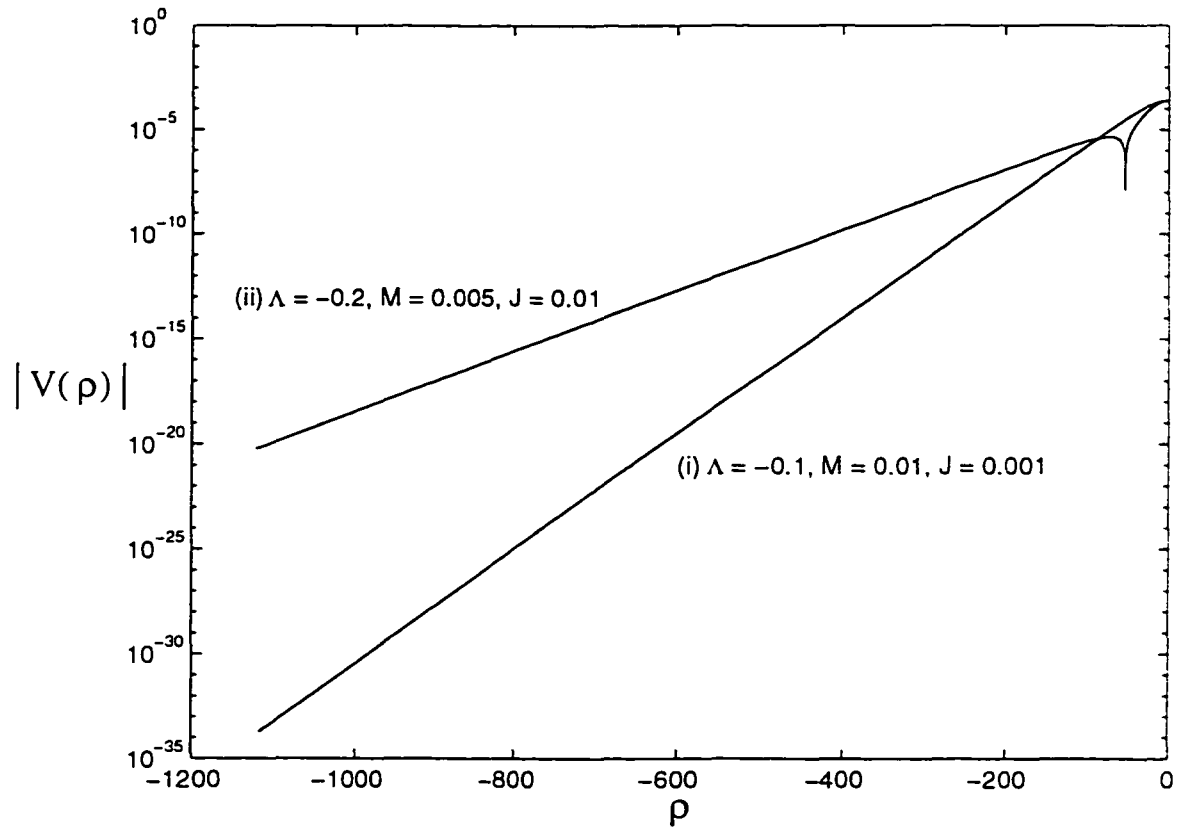


Figure 6.6: Exponentially decaying behavior of  $|V(\rho)|$  near the black hole event horizon

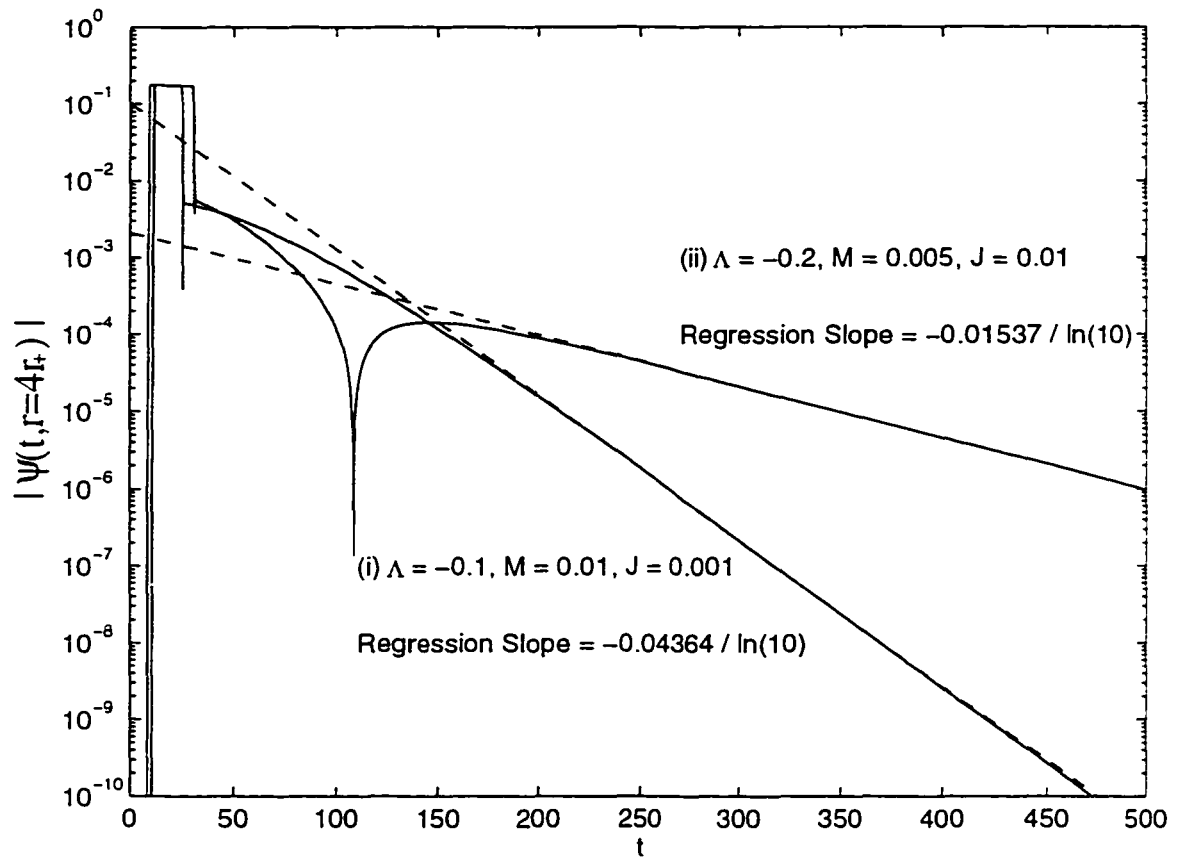


Figure 6.7: Exponential decay of the conformally invariant scalar waves in the spinning 3D black hole background.

describes how the inner mass parameter evolves. Whether mass inflation will occur or not is determined by the relative size of the surface gravity  $\kappa_-$  at the Cauchy horizon and the value of  $\alpha$  in the falloff rate  $\exp(-\alpha t)$  of the mass-energy of the ingoing radiation. For example when  $\Lambda = -0.1$ ,  $M = 0.01$  and  $J = 0.001$ , the surface gravity at the Cauchy horizon is 2.0 but the parameter  $\alpha$  is only 0.087 according to figure 6.7. Table 6.1 shows some other values of  $\alpha$  and  $\kappa$  in the rotating 3D black hole backgrounds. We find from the table that for the term  $|\Lambda| J^2/M^2$  being sufficiently small, the surface gravity  $\kappa_-$  is always larger than the radiation attenuation rate  $\alpha$ . On the other hand, when this term  $|\Lambda| J^2/M^2$  is large enough but below the extremal value, the value of  $\alpha$  becomes larger than  $\kappa_-$ . Therefore the competition between the surface gravity  $\kappa_-$  and radiation attenuation rate  $\alpha$  could turn the mass inflation either on or off.

## 6.4 A Spinoff

In this section, we turn our attention to a (3 + 1)-dimensional spacetime which is similar to the 3D black hole spacetime we have studied. This spacetime is an exact solution to a low-energy effective string theory which can be interpreted as a rotating black cosmic string [82]. On any axial plane of the black string, the geometry is identical to the spacetime of the 3D black hole. Thus mass inflation can also occur in this black string spacetime in 3 + 1 dimensions [45].

The effective (3 + 1)-dimensional action we are considering is given by [82]

$$S = \int d^4x \sqrt{-g} \left[ R - (\nabla\phi)^2 - \frac{1}{3} e^{-2\sqrt{2}\phi} H_{abc} H^{abc} + 2\Lambda e^{\sqrt{2}\phi} - 8\pi \mathcal{L}_M \right]. \quad (6.121)$$

The scalar field  $\phi$  is a dilaton field, the tensor  $H_{abc} = \partial_{[c} B_{ab]}$  is the curl of the skew-symmetric Kalb-Ramond field  $B_{ab}$  and  $\Lambda$  is a positive constant. The term  $\mathcal{L}_M$

$ \Lambda $	$M$	$J$	$ \Lambda  J^2/M^2$	$\kappa_-$	$\alpha$	$\kappa_-/\alpha$
0.1	0.5	$10^{-3}$	$4 \times 10^{-7}$	710	0.63	1100
0.1	0.1	$10^{-3}$	$10^{-5}$	63	0.28	230
1	1	0.01	$10^{-4}$	200	2.8	71
0.1	0.01	$10^{-3}$	$10^{-3}$	2.0	0.087	23
0.1	0.1	0.1	0.1	0.59	0.25	2.4
0.05	0.005	0.01	0.2	0.062	0.035	1.8
0.1	0.005	0.01	0.4	0.052	0.040	1.3
0.125	0.005	0.01	0.5	0.046	0.041	1.1
5.4	0.03	0.01	0.6	0.59	0.57	1.04
2.52	0.1	0.05	0.63	0.69	0.68	1.01
6.03	0.03	0.01	0.67	0.53	0.54	0.98
0.175	0.005	0.01	0.7	0.034	0.035	0.97
0.2	0.005	0.01	0.8	0.027	0.031	0.87

Table 6.1: The exponential falloff rate  $\alpha$ , which is found by graphical method, can be greater than the surface gravity  $\kappa_-$  in the rotating 3D black holes.

is the matter Lagrangian which is independent of the dilaton and Kalb-Ramond fields [45].

Varying the action (6.121) with respect to the fields  $\phi$ ,  $B_{ab}$  and  $g_{ab}$  gives us [45]

$$2 \nabla^2 \phi + \frac{2\sqrt{2}}{3} e^{-2\sqrt{2}\phi} H_{abc} H^{abc} + 2\sqrt{2} \Lambda e^{\sqrt{2}\phi} = 0 . \quad (6.122)$$

$$\nabla_c \left[ e^{-2\sqrt{2}\phi} H^{abc} \right] = 0 , \quad (6.123)$$

$$\begin{aligned} 8\pi T_{ab} = & G_{ab} - \Lambda e^{\sqrt{2}\phi} g_{ab} - e^{-2\sqrt{2}\phi} \left[ H_{aij} H_b{}^{ij} - \frac{1}{6} H_{ijk} H^{ijk} g_{ab} \right] \\ & - \left[ \nabla_a \phi \nabla_b \phi - \frac{1}{2} (\nabla \phi)^2 g_{ab} \right] . \end{aligned} \quad (6.124)$$

This set of equations has a stationary vacuum solution

$$\phi = \frac{1}{\sqrt{2}} \ln \left| \frac{\Lambda}{2Q^2} \right| , \quad (6.125)$$

$$H_{abc} = \frac{\Lambda^2}{4Q^3} r \epsilon_{4abc} . \quad (6.126)$$

$$ds^2 = -N(r) dt^2 + \frac{dr^2}{N(r)} + r^2 \left[ N^\vartheta(r) dt + d\vartheta \right]^2 + dz^2 . \quad (6.127)$$

where  $Q$  is an integration constant. The functions  $N$  and  $N^\vartheta$  in the metric (6.127) are given as

$$N(r) = \hat{\Lambda} r^2 - M + \frac{J^2}{4r^2} , \quad (6.128)$$

$$N^\vartheta(r) = -\frac{J}{2r^2} , \quad (6.129)$$

$$\hat{\Lambda} = \frac{\Lambda^2}{4Q^2} . \quad (6.130)$$

Because points in the  $\vartheta$ -space are identified with a period of  $2\pi$ , the spacetime manifold has a topology  $S^1 \times \mathbb{R}^3$  which represents a stationary, axially symmetric

spacetime. The metric solution is then interpretable as a straight, spinning black cosmic string of infinite length in 3 + 1 dimensions [82, 45]. The metric (6.127) is equivalent to  $ds^2 = ds_{3D}^2 + dz^2$ , where  $ds_{3D}^2$  is the 3D black hole metric we have considered on page 125. Readers are reminded that the constant  $\hat{\Lambda}$  in (6.128) is positive and  $\Lambda$  in equation (6.3) is negative. We interpret the constants of integration  $M$  and  $J$  as the mass and angular momentum per unit length of the black string respectively. The other constant  $Q$  is the charge of the axion field dual to the tensor  $H_{abc}$  [82].

Due to the similarity to the 3D black hole spacetime, it is not surprising that mass inflation can take place in this background spacetime. This can be shown by matching two Vaidya-versions of this black string spacetime along an outgoing null cylinder which is axial symmetric along the string. The rest of the calculation is similar to the one given in Section 6.2 and one will conclude that the mechanism for mass inflation in this black string spacetime is identical to the one in the 3D black hole spacetime. In other words, mass inflation could take place in this spinning black string spacetime as well [45].

The wave propagation problem in this spacetime is quite similar to that in the 3D black hole background despite the fact that the spacetime is now (3 + 1)-dimensional. One can show that the wave equation (4.2) on page 75 becomes (4.12) if we suppose

$$\Psi = \frac{\psi(t, r)}{\sqrt{r}} \cos(kz) . \quad (6.131)$$

The Ricci scalar in this black string spacetime reads

$$R = -\frac{d^2}{dr^2}N(r) - \frac{2}{r} \frac{d}{dr}N(r) + \frac{1}{2} \left[ r \frac{d}{dr}N^\theta(r) \right]^2 \quad (6.132)$$

and the potential  $V$  equals  $N V_e$  with the function

$$V_e(r) = -\xi \frac{d^2}{dr^2} N(r) + \frac{1-4\xi}{2r} \frac{d}{dr} N(r) - \frac{N(r)}{4r^2} + k^2 + \frac{\xi}{2} \left[ r \frac{d}{dr} N^\vartheta(r) \right]^2. \quad (6.133)$$

After substituting the equations (6.128) and (6.129) into (6.133), the potential function becomes

$$V_e(r) = k^2 - \frac{3\hat{\Lambda}}{4} (8\xi - 1) + \frac{M}{4r^2} - \frac{5J^2}{16r^4}. \quad (6.134)$$

It is worth noting that the parameter  $\xi$  is chosen to be  $1/8$  in the last few sections because this is the value for which the potential  $V$  is finite at spatial infinity. By choosing  $\xi = 1/8$  in (6.37),  $V \sim O(1)$  as  $r \rightarrow \infty$  and thus  $V$  is bounded there. Due to the extra degree of freedom in the  $z$  direction, this  $(3+1)$ -dimensional black string spacetime can have a finite potential at spatial infinity for any value of  $\xi$  greater than  $1/8$ , e.g.  $\xi = 1/6$ . Therefore one can remove the constant terms in (6.134) and carry out a numerical simulation for the scalar field  $\psi$ . A sample time response of the scalar field is given in figure 6.8 from which, as we expect, the field decays exponentially in a way identical to that in the rotating 3D black hole background. As a result, mass inflation can take place in a black string spacetime only if the radiation falloff rate is mild enough.

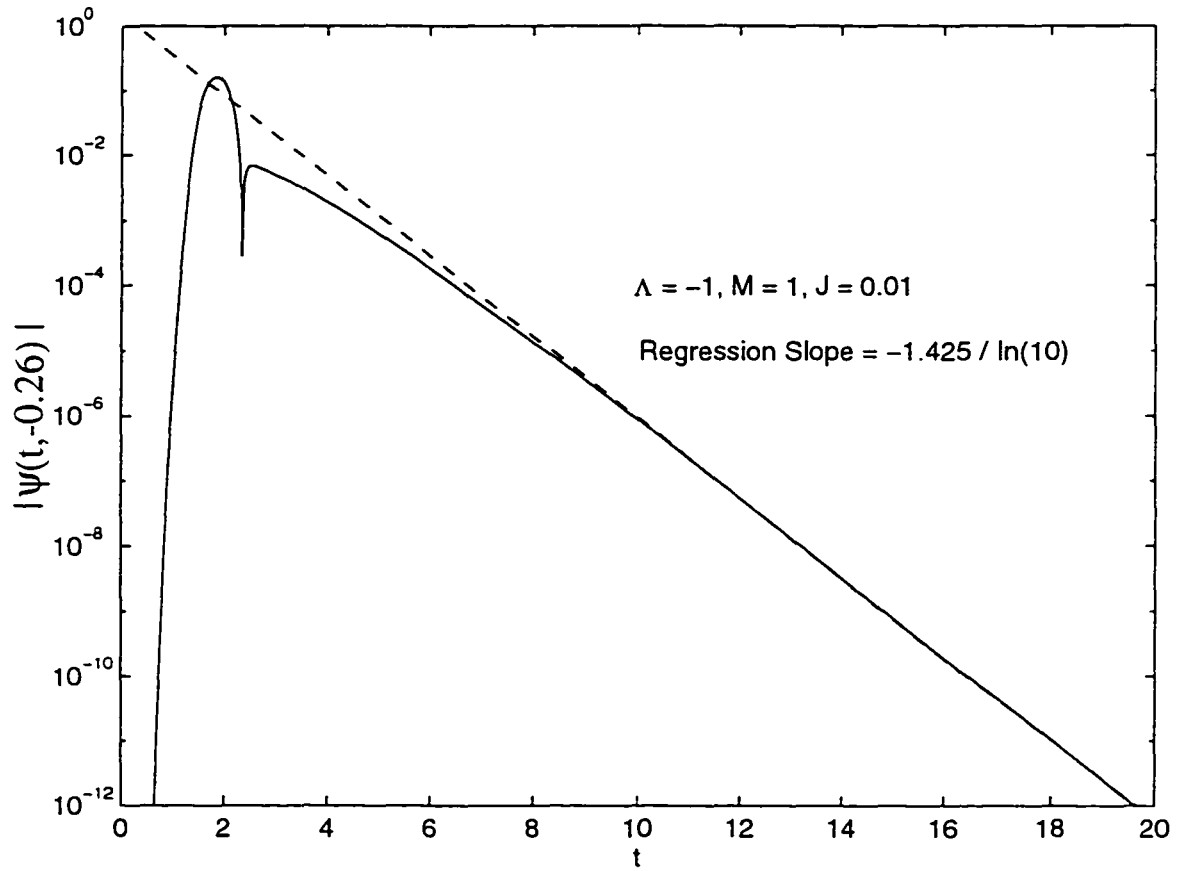


Figure 6.8: Exponentially decaying wave in the black string spacetime

# Chapter 7

## Schwarzschild-Anti-de Sitter Background

In the last few chapters, we have studied several dual-horizon and multi-horizon black hole spacetimes. Although these spacetimes have different properties, we found that the mass inflation calculations are very similar from one background to another. Whether mass inflation actually takes place in these spacetimes turns out to be determined by how the radiation dies out in these spacetimes. In this chapter we shall turn our attention to the radiation falloff problem in the Schwarzschild-anti-de Sitter (SAdS) spacetime in  $3 + 1$  dimensions. This spacetime is used to study the radiation problem because we can regard the spacetime as a relative of the Schwarzschild spacetime in which the radiation falloff property has been known since the early 1970s [20]. Moreover it is the  $(3 + 1)$ -dimensional analogue of the 3D black hole spacetime which has been studied in the last chapter. Thus the study of the radiation falloff in the SAdS black hole spacetime provides a comparison with that in the Schwarzschild spacetime and in the 3D black hole spacetime. However

we shall find that this spacetime has a completely different and unexpected radiation falloff character. Although we shall not consider mass inflation in this spacetime, any calculation of mass inflation for this case will have to take into account the results obtained in this chapter.

The Schwarzschild-anti-de Sitter (SAdS) solution is an exact solution to the vacuum Einstein's equations with a negative cosmological constant in 3 + 1 dimensions [83](p. 183), [6](p. 131). The metric of this spacetime reads

$$ds^2 = -N(r) dt^2 + \frac{dr^2}{N(r)} + r^2 \left[ d\theta^2 + \sin^2(\theta) d\phi^2 \right] . \quad (7.1)$$

$$N(r) = -\frac{\Lambda}{3} r^2 + 1 - \frac{2M}{r} , \quad (7.2)$$

where  $M$  is the mass of the black hole and the cosmological constant  $\Lambda$  is negative in this case. The lapse function (7.2) is functionally identical to the lapse function (6.3) in the 3D black hole spacetime as  $r \rightarrow \infty$ . It is not difficult to see that this is a black hole spacetime with a black hole radius  $R_b$ , defined by  $N(R_b) = 0$ . By using this radius, we can write the lapse function as

$$N(r) = \frac{|\Lambda|}{3} r^2 + 1 - \frac{R_b (3 + |\Lambda| R_b^2)}{3r} \quad (7.3)$$

which is simply

$$N(r) = \frac{|\Lambda|}{3r} (r - R_b) \left( r^2 + R_b r + R_b^2 + \frac{3}{|\Lambda|} \right) . \quad (7.4)$$

Given the metric of the form (7.1), we can reduce the scalar wave equation (4.2) into (4.12) by using the substitution (4.4). The potential  $V$  is given by equation (4.13) in which

$$V_e(r) = \frac{2|\Lambda|}{3} (1 - 6\xi) + \frac{l(l+1)}{r^2} + \frac{2M}{r^3} . \quad (7.5)$$

The tortoise coordinate (4.11) of this spacetime reads

$$\rho = \frac{R_b}{1 + |\Lambda| R_b^2} \ln \left| \frac{r - R_b}{\sqrt{r^2 + R_b r + R_b^2 + 3/|\Lambda|}} \right| + \frac{\sqrt{3}(2 + |\Lambda| R_b^2)}{\sqrt{|\Lambda|(1 + |\Lambda| R_b^2)} \sqrt{4 + |\Lambda| R_b^2}} \left[ \arctan \left( \frac{\sqrt{|\Lambda|(2r + R_b)}}{\sqrt{3} \sqrt{4 + |\Lambda| R_b^2}} \right) - \frac{\pi}{2} \right] \quad (7.6)$$

which obviously has no inverse in closed form. As a result, we cannot write the potential  $V$  in  $\rho$  explicitly.

Since the 3D black hole spacetime is an anti-de Sitter spacetime with identification, one might expect that the scalar waves in the SAdS background also have similar late time radiation falloff behavior. This view might be strengthened by comparing the potential functions (7.5) in the SAdS background and (6.31) in the 3D black hole background. One would agree that the two functions bear some resemblance. The discussion in Section 6.4 of the last chapter also fueled this belief because the black string spacetime is (3+1)-dimensional and is asymptotically anti-de Sitter in the direction perpendicular to the string axis. However waves behave differently in the SAdS background.

For the rest of this section we shall consider the case  $\xi = 1/6$  (i.e. the conformal scalar field) in the wave equation (4.2). In the conformally invariant case, the potential function  $V_c$  in equation (7.5) is identical to that for the scalar wave in the Schwarzschild background, in which the Ricci scalar vanishes. Due to the similarity between the 3D black hole spacetime and the 4D black string spacetime, we shall only compare the results in the SAdS spacetime with the results in the 3D black hole spacetime. Comparing the results in the 4D black string case should be straightforward.

The difference between the behavior of waves in the 3D black hole background and the SAdS background can be understood by examining the shape of the po-

tential  $V$ . In both cases the potentials are decreasing exponentially in  $\rho$  towards the event horizon. In the  $(2 + 1)$ -dimensional case (either rotating or static) this function attains a maximum at a distance  $r = \infty$  ( $\rho = 0$ ). This is no longer true in the SAdS background because spatial infinity (which is also given by  $\rho = 0$ ) is not the place at which  $V$  has an absolute maximum (for  $\rho \in \mathbb{R}^-$ ). As with the case in the Schwarzschild black hole background (figure 4.1), the potential  $V$  attains a maximum not far away from the event horizon. This hump just outside the black hole is a result of the use of the lapse function (7.2) which has the term  $2M/r$ . The presence of this term is responsible for the occurrence of the hump. In the SAdS case, the shape of the potential  $V$  is shown in figure 7.1. Unlike the Schwarzschild case, the tortoise coordinate  $\rho$  for the SAdS background is bounded above at zero because the leading order term in the lapse function is proportional to  $r^2$  at large distance. This has a consequence that all the outgoing waves that propagate away from the SAdS black hole will eventually return to the hole due to the boundary condition at  $\rho = 0$ . Nevertheless these returning waves will reflect off towards the spatial infinity when they come close to the right side of the hump. This is a completely different behavior from the 3D black hole case, in which the ingoing wave from spatial infinity  $\rho = 0$  continues its journey to the black hole unhindered. It is not difficult to imagine that in this SAdS background, waves bounce back and forth in the exterior region of the potential  $V$  forever.

We observe from figure 7.1 that when  $|\Lambda|$  is small (potentials (a) to (c)), the peak of the potential  $V$  moves to the left, lengthening the scalar waves' traveling time from this maximum to the spatial infinity  $\rho = 0$ . When  $l$  vanishes (cases (c) and (C)), we have  $V(0) = 0$  because the value of  $V$  at  $\rho = 0$  is  $l(l + 1)|\Lambda|/3$  in general. Therefore the potentials (a) and (b) have non-zero value at that point although this feature is not apparent on the graph due to the smallness of  $|\Lambda|$ . We

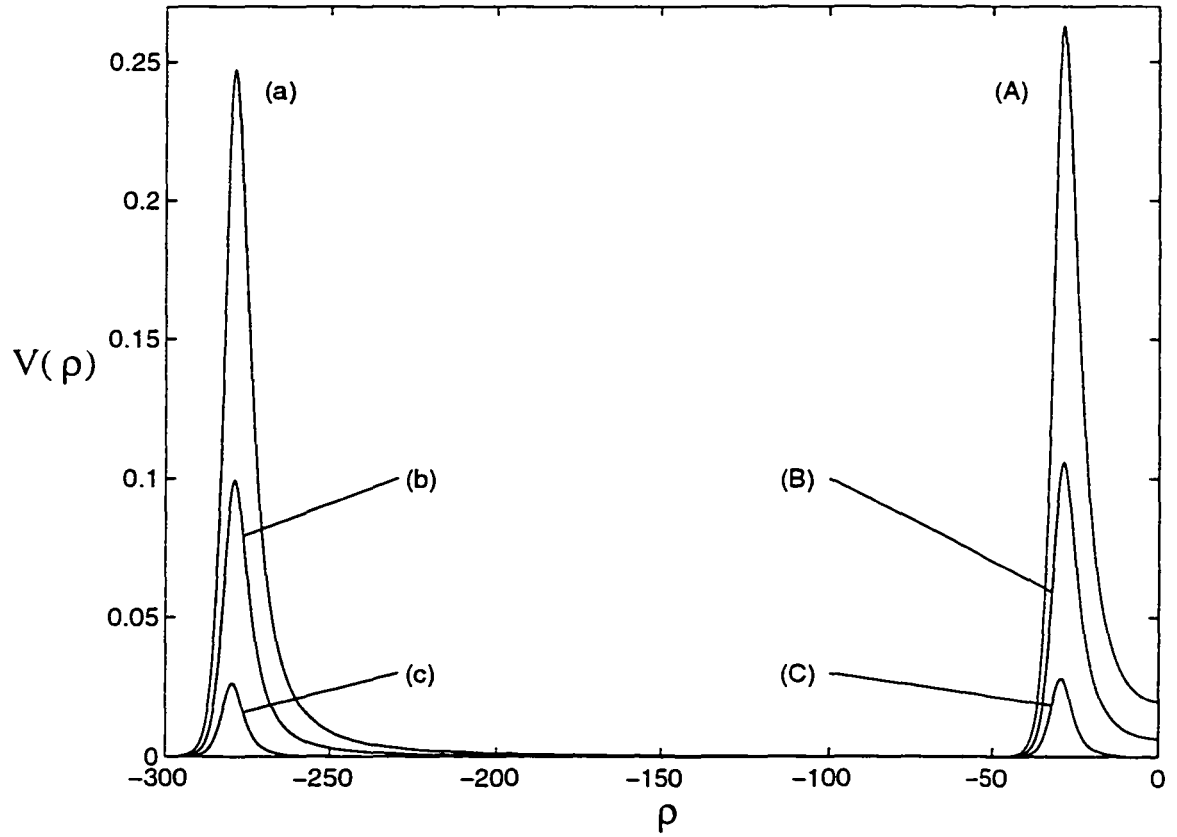


Figure 7.1: Potential  $V$  for the SAdS background. The six potentials are generated with  $R_b = 2$  and (a)  $\Lambda = -10^{-4}, l = 2$ , (b)  $\Lambda = -10^{-4}, l = 1$ , (c)  $\Lambda = -10^{-4}, l = 0$ . (A)  $\Lambda = -10^{-2}, l = 2$ , (B)  $\Lambda = -10^{-2}, l = 1$ , (C)  $\Lambda = -10^{-2}, l = 0$ .

also observe that the peak-height is considerably higher than the magnitude of  $V$  at  $\rho = 0$ . This property becomes more pronounced for large  $l$ . This causes the waves to bounce back and forth in the region outside the peak. Nevertheless, part of the waves can surmount the peak (thereby going into the black hole) because the peak-height is still finite. However it can take a long time for a significant amount of waves to leave the trapped region outside the peak.

We solve the wave equation (4.12) with (7.2) and (7.5) numerically. The results of the numerical integration are given in the next few graphs. These graphs are created so that the initial impulses are located at a distance  $r = 2 R_b$  and the time response of the waves is observed at  $r = 5 R_b$ , where  $R_b = 2$  in all cases. In figures 7.2 and 7.3, the moment of the wave is chosen to be  $l = 0$ . These diagrams show the falloff behavior of a conformal scalar wave at the distance  $\rho = -267.16$  ( $r = 5 R_b$ ). The simulation for figure 7.2 uses the Dirichlet condition (4.27) at  $\rho = 0$  but a Neumann boundary condition (4.28) is employed for figure 7.3. Since the cosmological constant  $|\Lambda|$  was chosen to be relatively small in both cases, namely  $|\Lambda| = 10^{-4} \ll 1$ , we can see on both log-log graphs that there are clearly inverse power decay behaviors. According to the graphs, this decay rate is roughly  $t^{-3}$  which agrees with the one in the Schwarzschild case. However this inverse power falloff does not last very long after the return of the outgoing wave from the spatial infinity. Both diagrams show these returning wavefronts on the far right sides of the two diagrams.

Figure 7.4 shows another simulation for scalar wave falloff in this SAdS background. In this simulation, we have  $l = 0$ ,  $\Lambda = -10^{-4}$  and the Dirichlet boundary condition is used. This is similar to the setup associated with figure 7.2. However we put the initial impulse at  $r = 5 R_b$  ( $\rho = -267.2$ ) and the observation is made at  $r = 1.000001 R_b$  ( $\rho = -305.5$ ). In other words, this is another near-horizon simu-

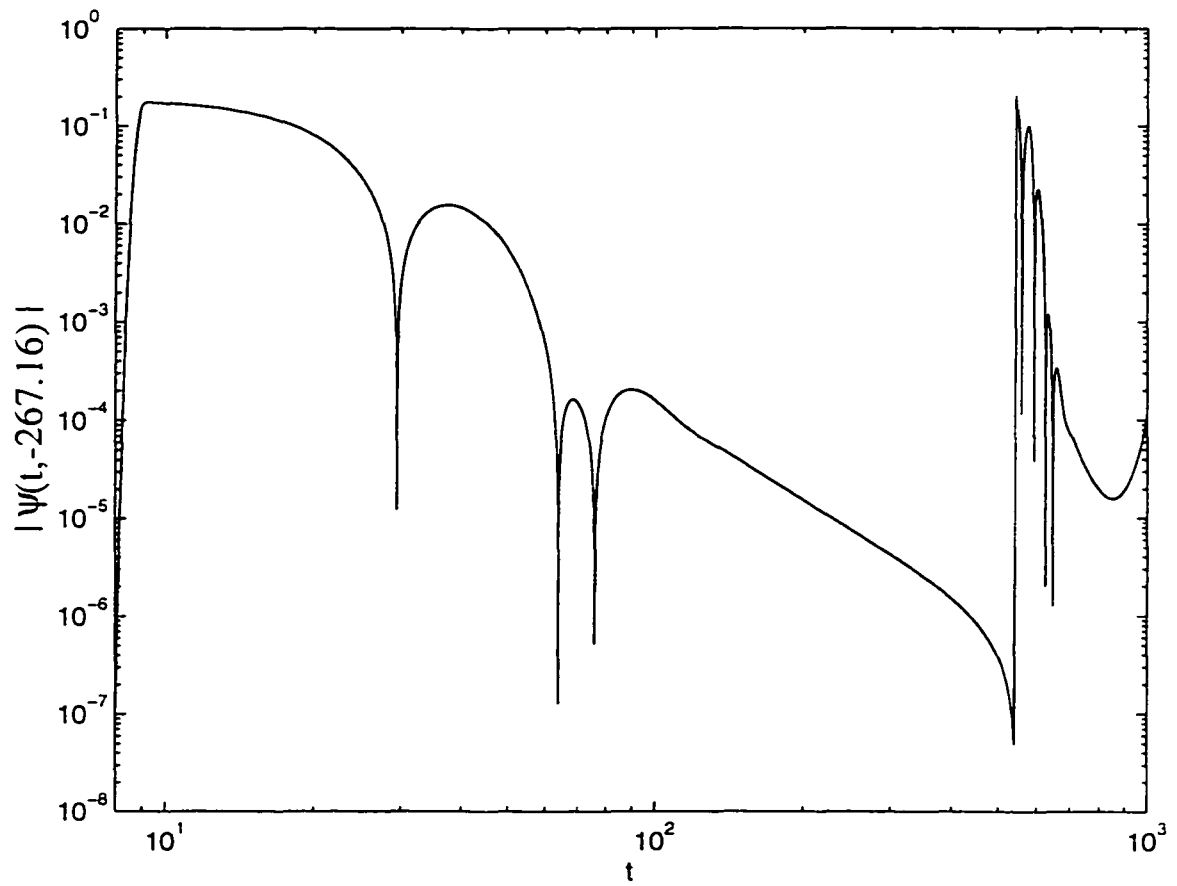


Figure 7.2: Scalar wave of  $l = 0$  decays away in the SAdS background with  $\Lambda = -10^{-4}$ . Dirichlet condition is used at  $\rho = 0$ .

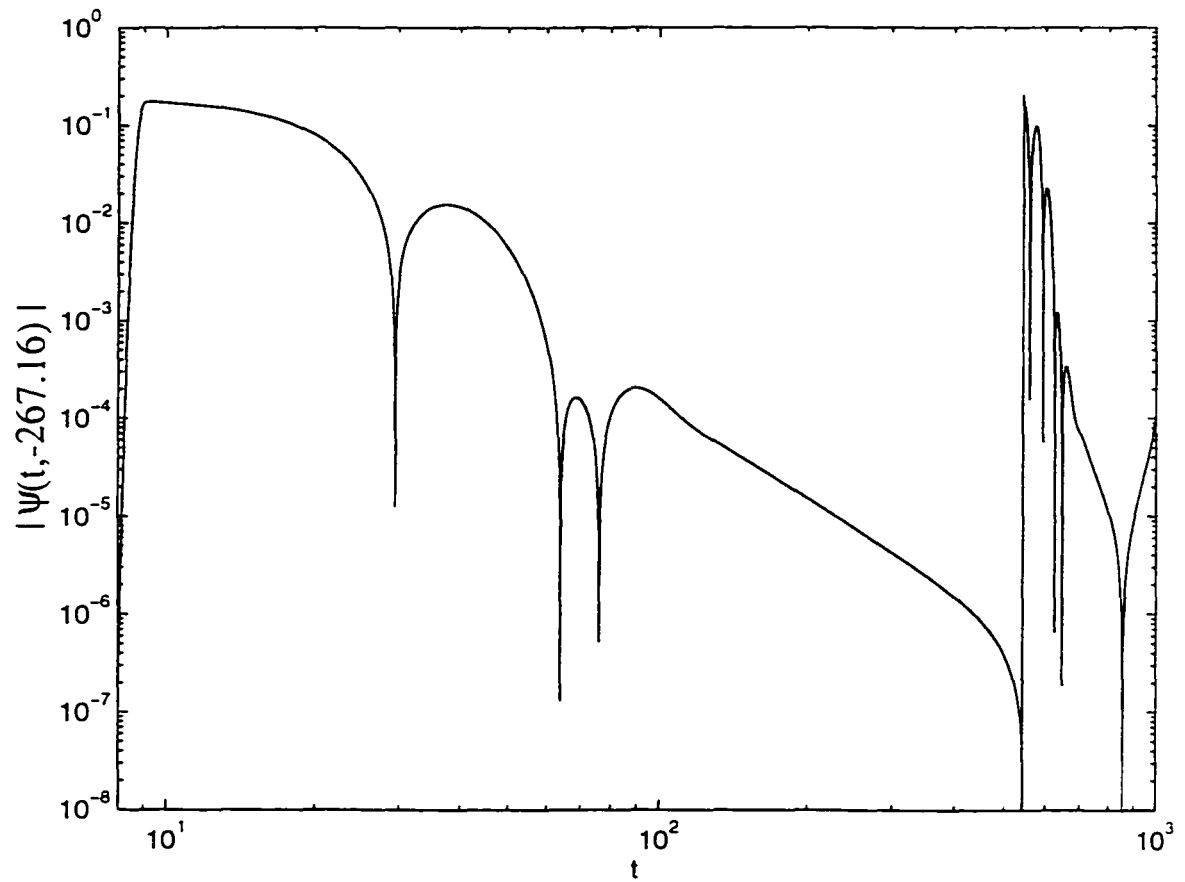


Figure 7.3: Scalar wave falloff pattern of  $l = 0$  using  $\Lambda = -10^{-4}$  and Neumann condition at  $\rho = 0$ .

lation for radiation behavior. By comparing the diagrams 7.2 and 7.4, we see that the radiation behavior is similar even if the observer is very close to the black hole.

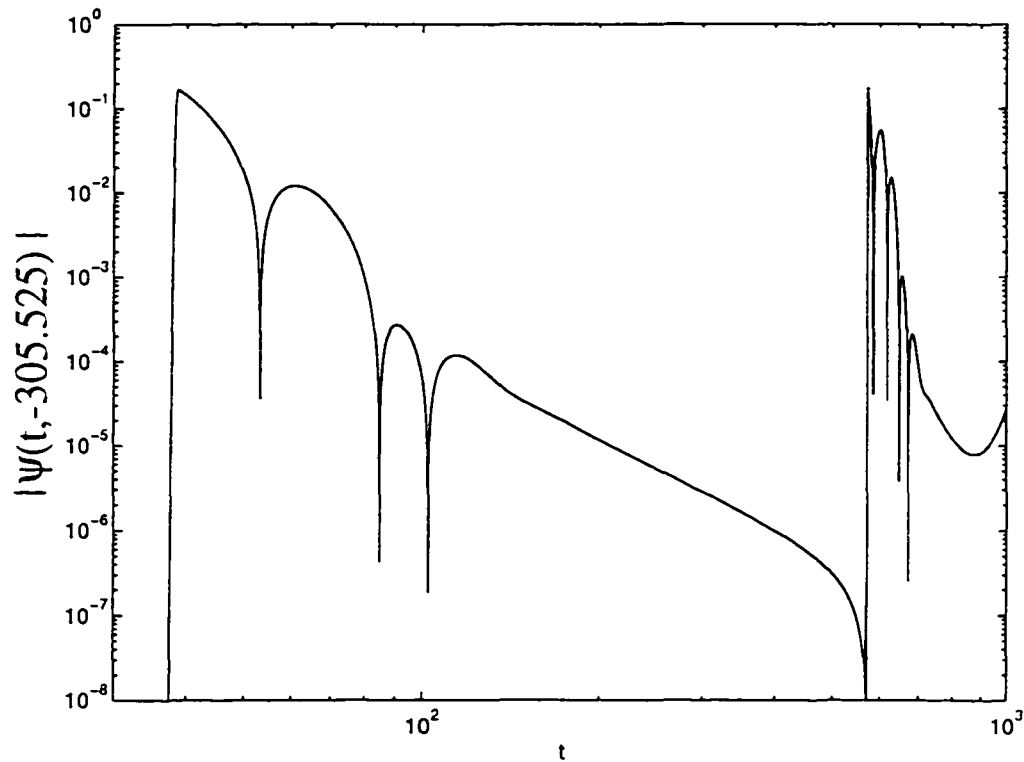


Figure 7.4: Scalar wave falloff pattern of  $l = 0$  using  $\Lambda = -10^{-4}$  and Dirichlet condition at  $\rho = 0$ . The observation in this case is close to the event horizon.

For small  $|\Lambda|$  and nonzero  $l$ , the falloff behavior resembles the case of  $l = 0$ . There is a quasi-normal oscillation initially, followed by the inverse power falloff behavior as shown in figures 7.5 and 7.6. Finally we see that some of the scalar waves arrive the observation point  $r = 5R_b$  from spatial infinity after the time  $t = 500$ .

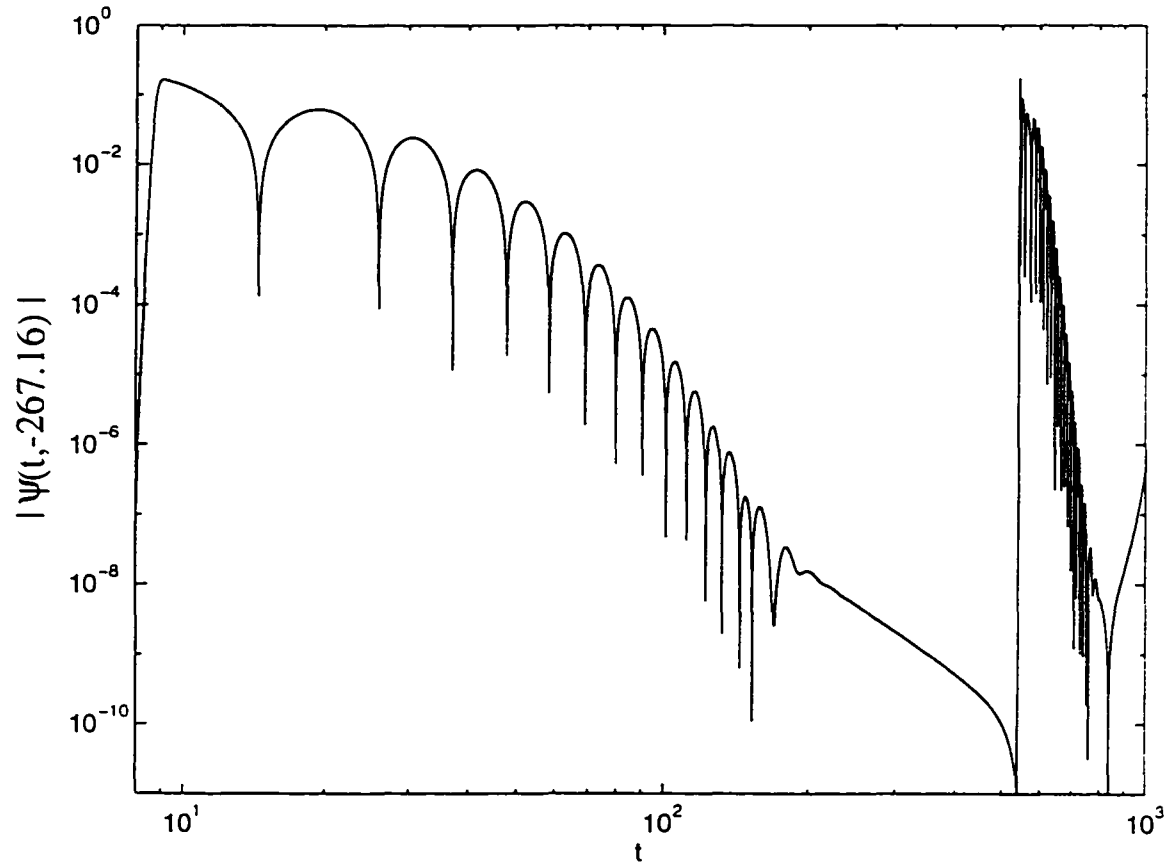


Figure 7.5: Loglog graph of the scalar wave decay behavior in the SAdS background with  $\Lambda = -10^{-4}$  and  $l = 1$ . Dirichlet condition is used in this case.

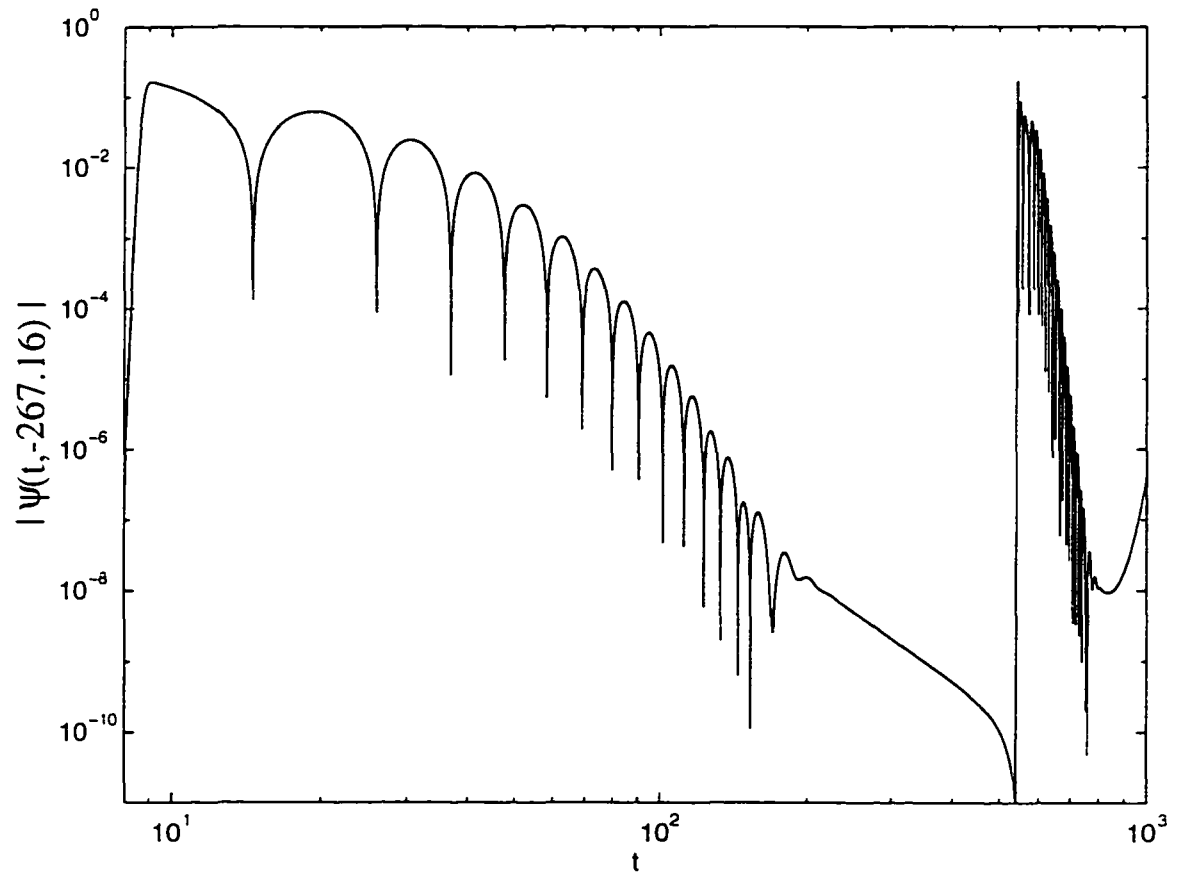


Figure 7.6: Similar graph to figure 7.5 but using the Neumann condition ( $\Lambda = -10^{-4}$  and  $l = 1$ ).

Since the finite height of the potential maximum allows the scalar waves to surmount the peak and propagate into the black hole, we expect that the peak value of the second returning wave is smaller than that of the first one. However this property is unclear from simple inspection of figures 7.2 to 7.6. Figures 7.7 to 7.10 are the numerical results we obtained using the potential functions (A) and (C) in figure 7.1. We compute the large  $|\Lambda|$  case ( $|\Lambda| = 0.01$ ) with both Dirichlet (figures 7.7 and 7.9) and Neumann (7.8 and 7.10) boundary conditions. For these large  $|\Lambda|$  cases we obtain more returning waves in a reasonable amount of CPU time. From these graphs, we can see that the scalar wave does indeed decrease but over a much larger time scale. Figures 7.7 and 7.8 indicate that the peak-height of the scalar wave has an approximate exponential falloff for  $l = 0$ . For  $l > 0$ , the peak-height has a more complicated behavior illustrated in figures 7.9 and 7.10. Over long time scales the maximum peak-height of the scalar wave has a very mild, approximately exponential falloff. From these graphs, it is clear that the radiation falloff pattern is complicated by the spherical harmonics  $l$  and the relative sizes of  $\Lambda$  and  $M$  in the background spacetime. In some cases, the decay law appears to be approximately exponential but in other cases, it is difficult to qualitatively describe the complicated falloff pattern.

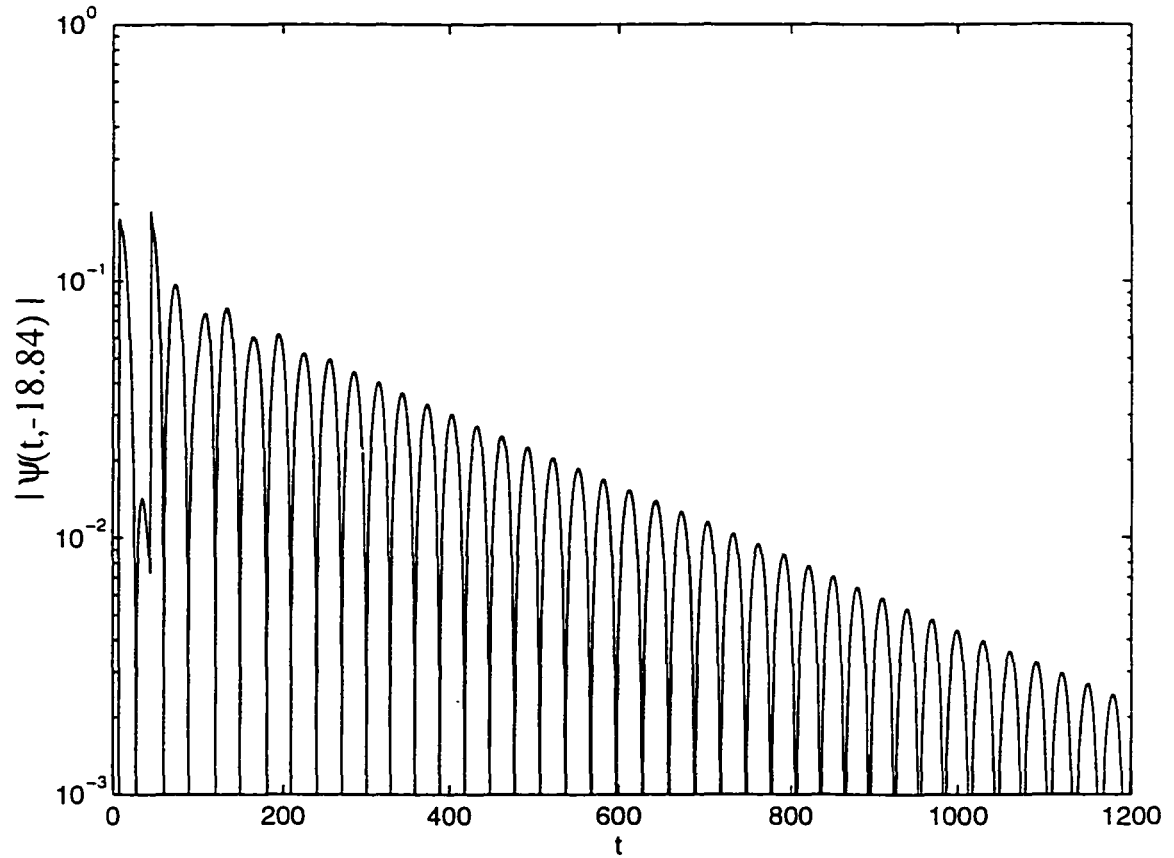


Figure 7.7: Semilog graph of the scalar wave decay behavior in the SAdS background using  $\Lambda = -10^{-2}$ ,  $l = 0$  and the Dirichlet condition.

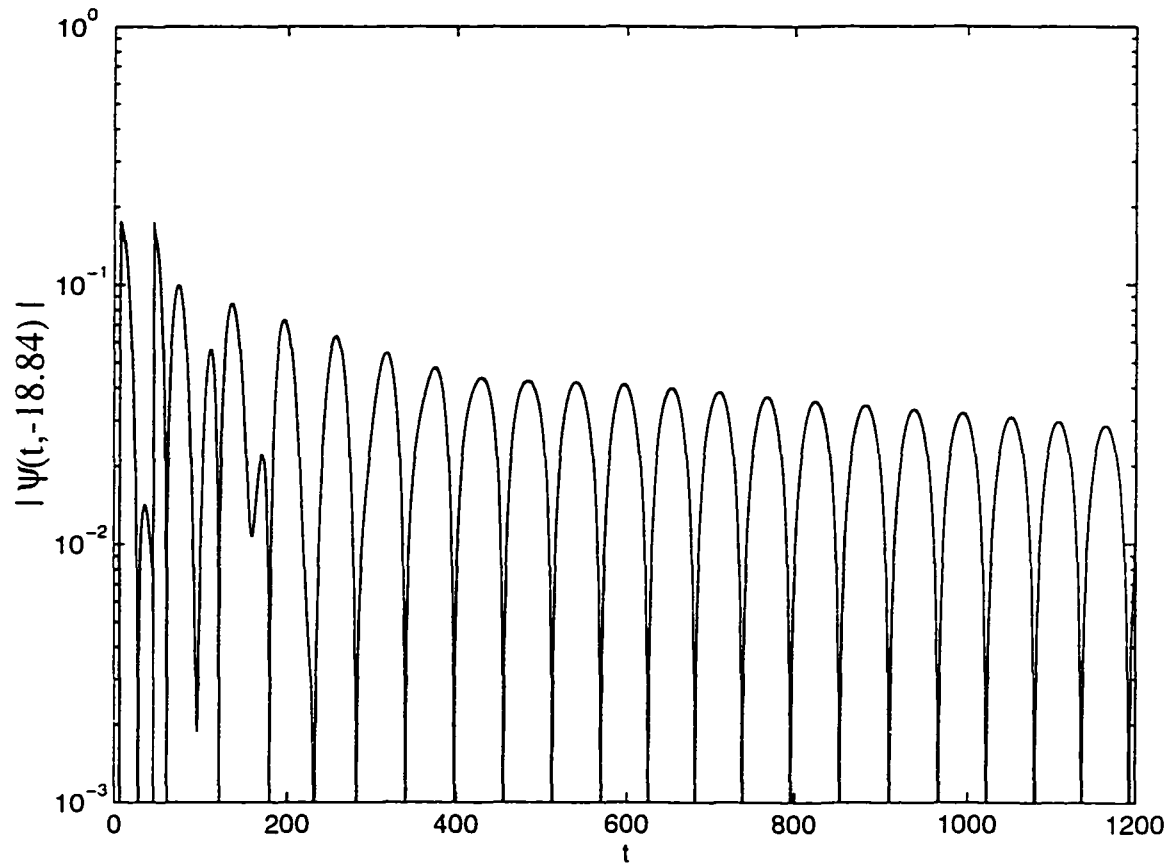


Figure 7.8: Conformally invariant scalar wave decay behavior using  $\Lambda = -10^{-2}$ ,  $l = 0$  and the Neumann condition.

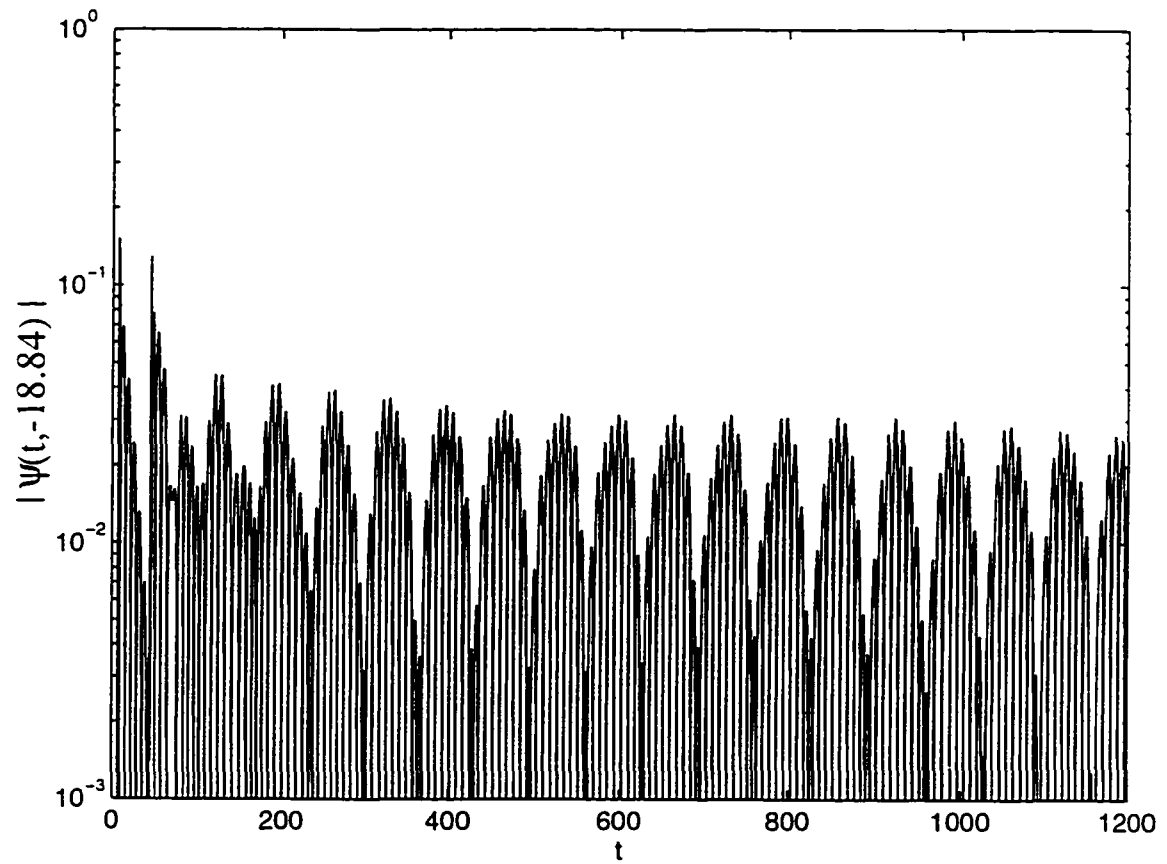


Figure 7.9: Semilog graph of the scalar wave decay behavior using  $\Lambda = -10^{-2}$ ,  $l = 2$  and the Dirichlet condition.

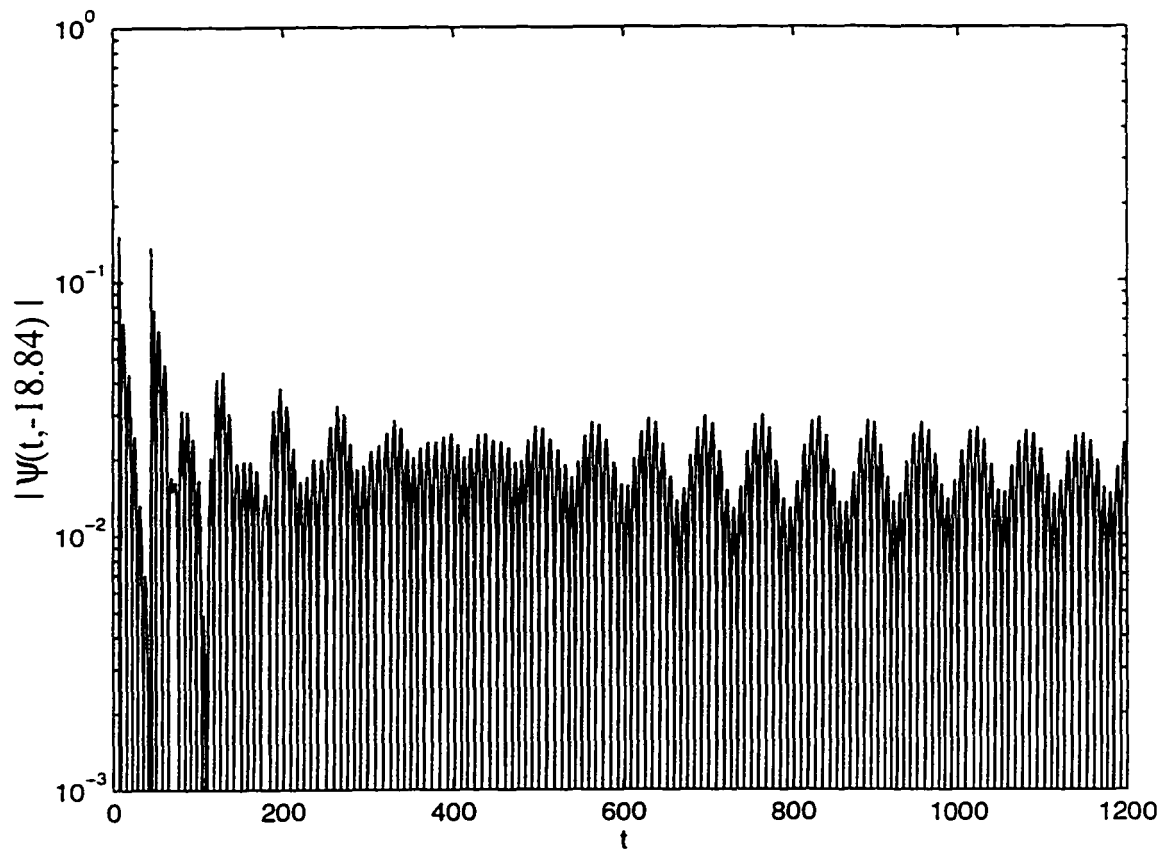


Figure 7.10: The simulation for this semilog graph uses the same inputs as the one in figure 7.9 but Neumann boundary condition replaces the Dirichlet condition in this case.

# Chapter 8

## Conclusion

The infinite blueshift of the ingoing radiation at the Cauchy horizon of the Reissner-Nordström black hole has suggested that this hypersurface is unstable since the late 1960s. The search for a spacetime singularity at the Cauchy horizon was fruitless until Poisson and Israel discovered the mass inflation phenomenon in 1989. This process is characterized by an unbounded mass parameter at the null hypersurface. This inflating mass induces a scalar curvature singularity at the Cauchy horizon, with the result that analytic continuation of the spacetime beyond the horizon might be inappropriate [28, 29]. This bizarre catastrophe inside the event horizon is expected to occur naturally and to cure the global hyperbolicity problem. Although a spherical, electrically charged collapsing star, which has a Reissner-Nordström geometry as its exterior spacetime, is a rare species in the family of collapsing stars, mass inflation is expected to be commonly found among the rotating collapsing stars which are expected to settle down to the Kerr black holes. Since the spacetime structure of the Kerr black holes is similar to that of the Reissner-Nordström black holes, theorists believe that the mass inflation process can take place inside a real

black hole [28].

This mass inflation phenomenon is triggered by the presence of radiation, both infalling and outgoing. While the presence of the outgoing radiation separates the spacetime into the inner and outer parts, the infalling stream is focused along the Cauchy horizon at which unusual energy transfer to the inner mass parameter becomes possible [28]. Because the gravitational potential energy can be arbitrarily negative, the huge gain of gravitating mass during the mass inflation process in fact comes from the abyss of the gravitational potential energy [84](p. 184).

In Chapter 2, we reviewed the phenomenon in the Reissner-Nordström background. The original scheme used by Poisson and Israel and the simpler model devised by Ori were explained. In Chapters 3 and 5, we demonstrated that mass inflation can take place in two asymptotically flat black hole spacetimes which are solutions to a  $(1 + 1)$ -dimensional dilaton theory of gravity. We have seen in Chapter 6 that the phenomenon can also occur in a rotating black hole which is a solution to the Einstein equation in  $2 + 1$  dimensions. Although it is not shown explicitly in this thesis, a rotating black cosmic string from a string theory in  $3 + 1$  dimensions also provokes the catastrophe at its Cauchy horizon [45].

We showed in those chapters that mass inflation can occur in theories other than General Relativity, in dimensions other than  $3 + 1$  and in background spacetimes other than static, asymptotically flat spacetime. In the context of Ori's method, the mass inflation calculation always produces three matching equations along an outgoing null line  $S$  which is the border of two patches of spacetime solutions. In other words, we can always find an appropriate function  $z(\lambda)$  which gives the matching equations (with the use of the Euler-Lagrange equation and the null condition.) Furthermore we observe that the mass-energy of the null shell (it is a null particle in  $1 + 1$  dimensions or a null ring in  $2 + 1$  dimensions) is always

proportional to  $\dot{R}(\lambda)$  (or  $\dot{X}(\lambda)$ ) where  $R$  (or  $X$ ) is the spatial coordinate of the null line  $S$ . In all the cases we have studied, the function  $\dot{R}(\lambda)$  has a strong dependence on the residual mass-energy of the infalling radiation  $\delta m$ . Indeed the mass inflation calculations before the involvement of  $\delta m$  in all the examples discussed in this thesis are very similar. Important differences appear after the residual mass of the infalling radiation is taken into account.

Because the qualitative behavior of the infalling radiation mass-energy  $\delta m$  varies from background to background, one cannot assume Price's radiation falloff rate in any background spacetime. In the Reissner-Nordström background, the radiation dies off outside the black hole at a rate proportional to  $1/t^p$  at late time [20], where  $p$  is some positive integer. This falloff rate also applies to the radiation behavior in the first dilaton black hole background in Section 3.1. However the second dilaton black hole background studied in Section 3.2 admits an exponential radiation falloff rate despite the fact that it is also asymptotically flat. Such a falloff rate is stronger than the inverse power one. This exponential radiation falloff rate can also be found in the background spacetimes of the rotating 3D black hole and the black string in Chapter 6. We found that if the attenuation of the radiation mass-energy is too strong, the inner mass parameter of the black hole can remain bounded. The mass diverges only when the radiation falloff is mild enough. In the calculation with non-zero surface gravity at the Cauchy horizon, we found that the inverse power radiation falloff is sufficiently weak for the occurrence of mass inflation at the Cauchy horizon, regardless of the value of  $p$  in the falloff rate  $1/t^p$ . On the other hand, when the late time radiation decays exponentially, only those spacetimes with slowly decreasing  $\delta m$  will sustain mass inflation. Thus if the background spacetime induces exponential radiation falloff, the mass inflation process quantitatively depends upon this falloff rate.

Even when the surface gravity at the Cauchy horizon vanishes, it is the function  $\delta m$  that determines whether the inner mass parameter diverges or not. As has been seen in Section 3.3, if  $\delta m$  is proportional to  $1/t^a$ , where  $a$  is a positive real number instead of an integer, there is a narrow range for  $a$  such that the phenomenon can take place. This number  $a$  is determined by how “fast” the surface gravity vanishes at the Cauchy horizon. If the lapse function  $N$  has a property  $N^{(n)}(r_-) = 0$  and  $N^{(b+1)}(r_-) = 0$  for all  $0 \leq n \leq b$ ,  $n \in \mathbb{Z}$ , where  $r_-$  denotes the location of the Cauchy horizon, mass inflation will take place when  $a = 1 + 1/b$ . If  $a$  is greater than  $1 + 1/b$ , i.e. the radiation attenuation is stronger than  $1/t^{1+1/b}$ , mass inflation cannot take place in this vanishing surface gravity case.

Determining the radiation falloff rate analytically is not always straightforward, as we have seen in Chapters 4, 5 and 6. As we saw in Chapter 7, even if numerical methods are employed, it can be difficult to describe the radiation falloff behavior. A complete mass inflation analysis must include the mass inflation calculation and the radiation falloff rate calculation. One should not underrate the importance and difficulty of the latter calculation in the analysis.

The fact that the stability of the Cauchy horizon depends upon the radiation falloff rate has been shown before [85, 86, 61]. In particular, it was shown in [85, 86] that in the Reissner-Nordström-de Sitter spacetime, the Cauchy horizon is stable only if the surface gravity at the Cauchy horizon is less than the surface gravity at the Cosmological horizon of the spacetime. However the discussion in [85, 86] is not in the context of the mass inflation process. Some of the spacetimes with mass inflation at the Cauchy horizon considered in this thesis provide further examples of this point. In fact the second dilaton spacetime in 1 + 1 dimensions with non-vanishing surface gravity at the Cauchy horizon studied in Section 3.2 and Chapter 5 is the most interesting example because the spacetime is asymptotically

flat but the radiation falloff rate is exponential. Radiation in this spacetime behaves in such a way that the stability of the Cauchy horizon depends crucially upon the radiation falloff rate.

Marković and Poisson argued that when quantum effects at the horizon are included, the Cauchy horizon of the Reissner-Nordström-de Sitter spacetime must be unstable [87]. One interesting problem for future research is to consider the stability of the Cauchy horizon in the second dilaton spacetime when such quantum effects are taken into account.

If physical spacetimes are globally hyperbolic as suggested by the strong cosmic censorship conjecture [88](p. 617), then mass inflation is of interest as a process for insuring the global hyperbolicity of the dual-horizon black holes in  $3+1$  dimensions. However this process is not a generic mechanism of sealing the Cauchy horizons, as we have seen in this thesis. It happens that either our physical  $(3+1)$ -dimensional spacetime described by General Relativity is ideal for mass inflation to occur or there exists a generic mechanism which would forbid the spacetime to extend beyond the Cauchy horizon. Thus investigation of stability of the Cauchy horizon has not been closed. Further research in this direction is necessary.

# Appendix A

## Vocabulary

$\mathcal{J}^+$  is the future null infinity. It represents the region where  $t + r \rightarrow \infty$  at finite  $t - r$ .

$\mathcal{J}^-$  is the past null infinity. It represents the region where  $t - r \rightarrow -\infty$  at finite  $t + r$ .

$i^0$  is the spacelike infinity which is defined as the intersection between  $\mathcal{J}^+$  and  $\mathcal{J}^-$ .

$i^+$  is the set of future endpoints of every timelike geodesic in the spacetime.

$i^-$  is the set of past endpoints of every timelike geodesic in the spacetime.

**Achronal set** is a subset of a spacetime manifold such that any curve lying entirely in the set is not timelike.

**Cauchy horizon** is defined as the boundary of the domain of dependence of a closed achronal set.

**Domain of dependence**  $D(S)$  of a closed achronal set  $S \subset M$  is defined as

$$D(S) = D^+(S) \cup D^-(S), \text{ where}$$

$$D^+(S) = \left\{ p \in M \left| \begin{array}{l} \text{Every past inextendible timelike} \\ \text{curve through } p \text{ intersects } S \end{array} \right. \right\} .$$

$$D^-(S) = \left\{ p \in M \left| \begin{array}{l} \text{Every future inextendible timelike} \\ \text{curve through } p \text{ intersects } S \end{array} \right. \right\} .$$

**Event horizon** is the boundary of a black hole. It is the boundary of the manifold  $M \setminus J^-(\mathcal{J}^+)$ , where  $M$  is the spacetime manifold and  $J^-(\mathcal{J}^+)$  is the causal past of the future null infinity  $\mathcal{J}^+$  of  $M$ .

**Future endpoint**  $p \in M$  of a timelike or null curve  $\gamma(t)$  in the spacetime manifold  $M$  satisfies the following condition: For every neighborhood  $O$  of  $p$ , there exists  $\tau \in \mathbb{R}$  such that for all  $t > \tau$ , we have  $\gamma(t) \in O$ .

**Future inextendible** curve is a curve without any future endpoint.

**Geodesic** is the curve that minimizes the distance between two points in a Riemannian metric space. In a Lorentzian metric space, it maximizes the distance between two points. In General Relativity, the non-spacelike geodesics of the spacetime are the world lines of freely falling bodies or the world lines of null particles.

**Lapse function**  $N$  is defined as  $N = -t^a n_a$ , where  $t^a$  is a vector field satisfying the condition  $t^a \nabla_a \tau = 1$  and  $n^a$  is a unit normal vector field to the spacelike hypersurfaces  $\Sigma_\tau$ . The set of hypersurfaces  $\Sigma_\tau$ , which are parameterized by the global time function  $\tau$ , foliates the spacetime manifold.

Surface gravity  $\kappa$  for a stationary spacetime is defined as

$$\kappa^2 \equiv -\frac{1}{2} \nabla_a \xi_b \nabla^a \xi^b ,$$

where  $\xi_a$  is a Killing vector satisfying the equation  $\xi_{[a} \nabla_b \xi_{c]} = 0$ . For a metric of the form (2.4),  $\xi^a$  can simply be  $\delta_t^a$  which gives  $\nabla_a \xi_b \nabla^a \xi^b = - [N'(r)]^2 / 2$ .

# Bibliography

- [1] K. Schwarzschild. Sitzber. Deut. Akad. Wiss. Berlin, Kl. Math.-Phys. Tech.. 189 (1916).
- [2] R. M. Wald. *General Relativity*. The University of Chicago Press, Chicago, 1984.
- [3] Sky and Telescope, **88**, 2 (1994).
- [4] R. Bender, J. Kormendy and W. Dehnen. *Astrophys. J.* **464**, L123 (1996).
- [5] R. P. Kerr. *Phys. Rev. Lett.* **11**, 237 (1963).  
E. T. Newman and A. I. Janis. *J. Math. Phys.* **6**, 915 (1965).
- [6] S. W. Hawking and G. F. R. Ellis. *The large scale structure of space-time*. Cambridge University Press, New York, 1973.
- [7] S. W. Hawking. *Commun. Math. Phys.* **43**, 199 (1975).
- [8] K. S. Thorne in *General relativity and gravitation 1992*, edited by R. J. Gleiser, C. N. Kozameh and O. M. Moreschi. IOP Publishing, Bristol, 1993.
- [9] J. N. Goldberg in *General relativity and gravitation, Vol. 1*, edited by A. Held. Plenum Press, New York, 1980.

- [10] C. J. Isham in *Quantum gravity 2*, edited by C. J. Isham, R. Penrose and D. W. Sciama. Clarendon Press, Oxford, 1981.
- [11] J. Carminati and R. G. McLenaghan. *J. Math. Phys.* **32**, 3135 (1991).
- [12] M. D. Kruskal. *Phys. Rev.* **119**, 1743 (1960).
- [13] M. Walker. *J. Math. Phys.* **11**, 2280 (1970).
- [14] J. R. Oppenheimer and H. Snyder. *Phys. Rev.* **56**, 455 (1939).
- [15] H. Stephani. *General Relativity*. Cambridge University Press, Cambridge, 1982.
- [16] H. Reissner. *Ann. Physik.* **50**, 106 (1916).  
G. Nordström. *Proc. Kon. Ned. Akad. Wet.* **20**, 1238 (1918).
- [17] E. T. Newman, E. Couch, K. Chinnapared, A. Exton, A. Prakash and R. Torrence. *J. Math. Phys.* **6**, 918 (1965).
- [18] S. W. Hawking and R. Penrose. *Proc. Roy. Soc. Lond.*, **A314**, 529 (1970).
- [19] R. Penrose in *Battelle Rencontres*, edited by C. M. DeWitt and J. A. Wheeler. Benjamin, New York, 1968.
- [20] R. H. Price. *Phys. Rev. D* **5**, 2419 (1972).
- [21] S. Weinberg. *Gravitation and cosmology*. John Wiley & Sons, New York, 1972.
- [22] M. Simpson and R. Penrose. *Int. J. Theor. Phys.* **7**, 183 (1973).
- [23] S. Chandrasekhar and J. B. Hartle. *Proc. R. Soc. Lond. A* **384**, 301 (1982).
- [24] W. A. Hiscock. *Phys. Lett. A* **83**, 110 (1981).

- [25] P. C. Vaidya. Proc. Indian Acad. Sci. A **33**, 264 (1951).  
J. Plebanski and J. Stachel. J. Math. Phys. **9**, 269 (1968). W. B. Bonnor and P. C. Vaidya. Gen. Rel. and Grav. **1**, 127 (1970).
- [26] F. J. Tipler, C. J. S. Clarke and G. F. R. Ellis in *General relativity and gravitation. Vol. 2.* edited by A. Held. Plenum Press, New York, 1980.
- [27] G. F. R. Ellis and A. R. King. Commun. Math. Phys., **38**, 119 (1974).  
A. R. King. Gen. Rel. and Grav. **10**, 1029 (1979).
- [28] E. Poisson and W. Israel. Phys. Rev. Lett. **63**, 1663 (1989).  
E. Poisson and W. Israel. Phys. Rev. D **41**, 1796 (1990).
- [29] A. Ori. Phys. Rev. Lett. **67**, 789 (1991).
- [30] U. Yurtsever. Class. Quantum Grav. **10**, L17 (1993).
- [31] M. L. Gnedin and N. Y. Gnedin. Class. Quantum Grav. **10**, 1083 (1993).
- [32] A. Bonanno, S. Droz, W. Israel and S. M. Morsink. Phys. Rev. D **50**, 7372 (1994).
- [33] P. R. Brady and J. D. Smith. Phys. Rev. Lett. **75**, 1256 (1995).
- [34] L. M. Burko and A. Ori. Preprint gr-qc/9711032.
- [35] A. Ori and É. É. Flanagan. Phys. Rev. D **53**, R1754 (1996).
- [36] S. A. Teukolsky. Astrophys. J. **185**, 635 (1973).
- [37] K. S. Thorne in *Magic without magic: John Archibald Wheeler*, edited by J. R. Klauder. W. H. Freeman and Company, San Francisco, 1972.

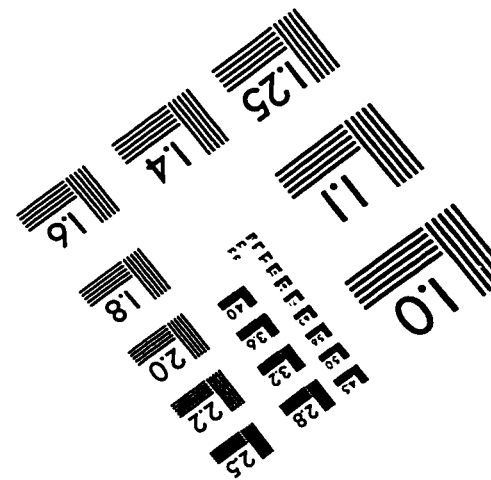
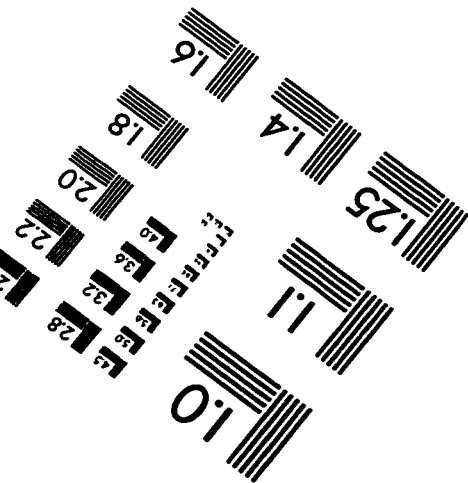
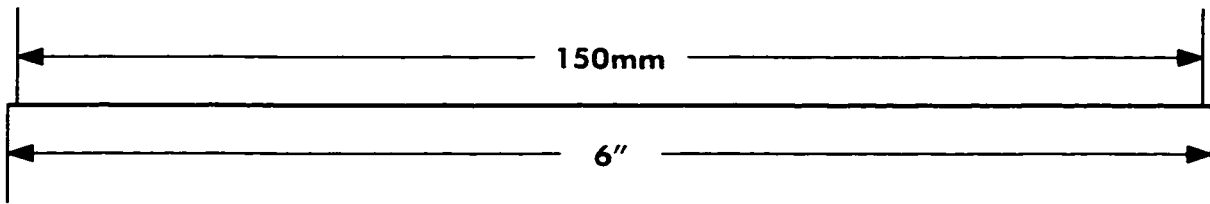
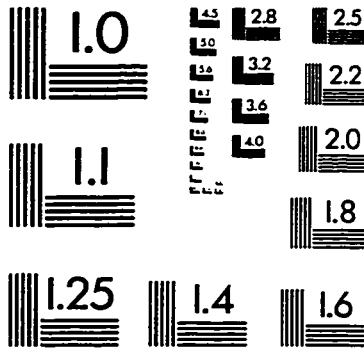
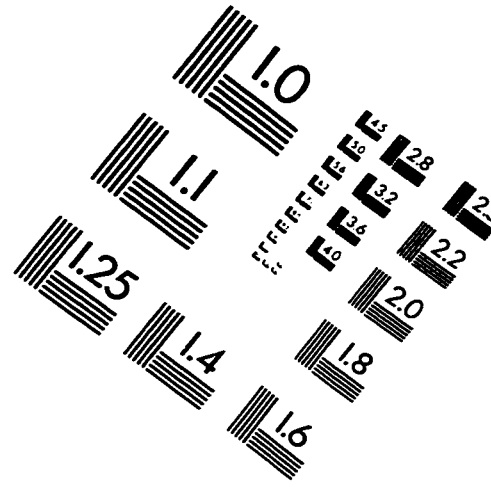
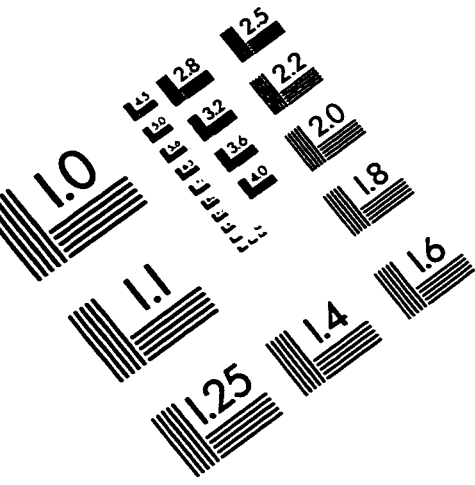
- [38] E. S. C. Ching, P. T. Leung, W. M. Suen and K. Young. *Phys. Rev. D* **52**, 2118 (1995).
- [39] R. Balbinot, P. R. Brady, W. Israel and E. Poisson. *Phys. Lett. A* **161**, 223 (1991).
- [40] P. R. Brady and C. M. Chambers. *Phys. Rev. D* **51**, 4177 (1995).
- [41] R. Balbinot and P. R. Brady. *Class. Quantum Grav.* **11**, 1763 (1994).
- [42] V. Husain. *Phys. Rev. D* **50**, R2361 (1994).
- [43] S. Droz. *Phys. Lett. A* **191**, 211 (1994).
- [44] J. S. F. Chan and R. B. Mann. *Phys. Rev. D* **50**, 7376 (1994).
- [45] J. S. F. Chan and R. B. Mann. *Phys. Rev. D* **51**, 5428 (1995).
- [46] R. G. Cai and D. F. Zhao. *Phys. Lett. A* **208**, 281 (1995).
- [47] J. S. F. Chan, K. C. K. Chan and R. B. Mann. *Phys. Rev. D* **54**, 1535 (1996).
- [48] C. W. Misner, K. S. Thorne and J. A. Wheeler. *Gravitation*. W. H. Freeman, San Francisco, 1973.
- [49] R. W. Lindquist, R. A. Schwartz and C. W. Misner. *Phys. Rev.* **137B**, 1364 (1965).
- [50] R. A. Isaacson. *Phys. Rev.* **166**, 1272 (1968).
- [51] R. B. Mann. *Gen. Rel. and Grav.* **24**, 433 (1992).
- [52] C. G. Callan, S. B. Giddings, J. A. Harvey and A. Strominger. *Phys. Rev. D* **45**, R1005 (1992).

- [53] T. Banks and M. O'Loughlin. Nucl. Phys. B, **362**, 649 (1991).
- [54] S. M. Morsink and R. B. Mann. Class. Quantum Grav., **8**, 2257 (1991).  
R. B. Mann and T. G. Steele. Class. Quantum Grav., **9**, 475 (1992).
- [55] R. B. Mann, S. M. Morsink, A. E. Sikkema and T. G. Steele. Phys. Rev. D **43**, 3948 (1991).
- [56] R. B. Mann and S. F. Ross. Phys. Rev. D **47**, 3312 (1993).
- [57] D. Christensen and R. B. Mann. Class. Quantum Grav., **9**, 1769 (1992).  
K. C. K. Chan and R. B. Mann. Class. Quantum Grav., **10**, 913 (1993).
- [58] C. R. Nappi and A. Pasquinucci. Mod. Phys. Lett. A **7**, 3337 (1992).
- [59] J. G. Russo and A. A. Tseytlin. Nucl. Phys. B **382**, 259 (1992).
- [60] R. B. Mann. Phys. Rev. D **47**, 4438 (1993).
- [61] P. R. Brady, D. Núñez and S. Sinha. Phys. Rev. D **47**, 4239 (1993).
- [62] T. Regge and J. A. Wheeler. Phys. Rev. **108**, 1063 (1957).
- [63] F. J. Zerilli. Phys. Rev. D **2**, 2141 (1970).
- [64] C. A. Hall and T. A. Porsching. *Numerical analysis of partial differential equations*. Prentice Hall, New Jersey, 1990.
- [65] K. C. K. Chan and R. B. Mann. Phys. Rev. D **50**, 6385 (1994).
- [66] K. C. K. Chan, J. H. Horne and R. B. Mann. Nucl. Phys. B **447**, 441 (1995).
- [67] G. Lifschytz and M. Ortiz. Phys. Rev. D **49**, 1929 (1994).  
S. J. Avis, C. J. Isham and D. Storey. Phys. Rev. D **18**, 3565 (1978).

- [68] C. Gundlach, R. H. Price and J. Pullin. *Phys. Rev. D* **49**, 883 (1994).
- [69] E. C. Zachmanoglou and D. W. Thoe. *Introduction to partial differential equations with application*. Dover Publications, New York, 1986.
- [70] E. S. C. Ching, P. T. Leung, W. M. Suen and K. Young. *Phys. Rev. Lett.* **74**, 2414 (1995).
- [71] *Handbook of mathematical functions*, edited by M. Abramowitz and I. A. Stegun. Dover. New York, 1972.
- [72] See page 140 to 141 of *Introduction to complex analysis*, by H. A. Priestley. Dover, New York, 1972.
- [73] F. W. J. Olver. *Asymptotics and special functions*. Academic Press. New York. 1974.
- [74] C. Barrabès, W. Israel and E. Poisson. *Class. Quantum Grav.* **7**, L273 (1990).
- [75] A. Ori. *Phys. Rev. Lett.* **68**, 2117 (1992).
- [76] A. Bonanno. *Phys. Rev. D* **53**, 7373 (1996).
- [77] M. Bañados, C. Teitelboim and J. Zanelli. *Phys. Rev. Lett.* **69**, 1849 (1992).  
M. Bañados, M. Henneaux, C. Teitelboim and J. Zanelli. *Phys. Rev. D* **48**, 1506 (1993).
- [78] K. C. K Chan. *Phys. Lett. B* **373**, 296 (1996).
- [79] J. D. Brown, J. Creighton and R. B. Mann. *Phys. Rev. D* **50**, 6394 (1994).
- [80] R. B. Mann and S. F. Ross. *Phys. Rev. D* **47**, 3319 (1993).
- [81] J. S. F. Chan and R. B. Mann. *Phys. Rev. D.* **55**, 7546 (1997).

- [82] N. Kaloper. *Phys. Rev. D.* **48**, 4658 (1993).
- [83] W. Rindler. *Essential Relativity*. Springer-Verlag, New York, 1977.
- [84] W. Israel in *Directions in General Relativity Vol. 1*, edited by B. L. Hu. M. P. Ryan and C. V. Vishveshwara. Cambridge University Press, Cambridge, 1993.
- [85] F. Mellor and I. Moss. *Phys. Rev. D* **41**, 403 (1990).  
F. Mellor and I. Moss. *Class. Quantum Grav.* **9**, L43 (1992).
- [86] P. R. Brady and E. Poisson. *Class. Quantum Grav.* **9**, 121 (1992).
- [87] D. Marković and E. Poisson. *Phys. Rev. Lett.* **74**, 1280 (1995).
- [88] R. Penrose in *General Relativity, an Einstein Centenary Survey*, edited by S. W. Hawking and W. Israel. Cambridge University Press, New York, 1979.

# IMAGE EVALUATION TEST TARGET (QA-3)



**APPLIED IMAGE, Inc**  
 1653 East Main Street  
 Rochester, NY 14609 USA  
 Phone: 716/482-0300  
 Fax: 716/288-5989

© 1993, Applied Image, Inc., All Rights Reserved